Project THEMIS
Technical Report No. 20

ON DIFFUSION FROM AN INSTANTANEOUS POINT SOURCE IN A NEUTRALLY STRATIFIED TURBULENT BOUNDARY LAYER WITH A LASER LIGHT SCATTERING PROBE

by

B. T. Yang
and
R. N. Meroney

Prepared under

Office of Naval Research
Contract No. N00014-68-A-0493-0001
Project No. NR 062-414/6-6-68 (Code 438)
U.S. Department of Defense
Washington, D.C.

Fluid Dynamics and Diffusion Laboratory
College of Engineering
Colorado State University
Fort Collins, Colorado

October 1972

CER72-73BTY-RNM-17

ABSTRACT

ON DIFFUSION FROM AN INSTANTANEOUS POINT GROUND SOURCE IN A NEUTRALLY STRATIFIED TURBULENT BOUNDARY LAYER WITH A LASER LIGHT SCATTERING PROBE

The behavior of an instantaneous point source, as it disperses in a thick, neutrally stratified, turbulent shear layer, has been examined by a laser light-scattering technique in the Meteorological Wind Tunnel. An aerosol-filled gas bubble was released in a column of water to subsequently rise and burst at the floor of the wind tunnel. This "pseudo-instantaneous" gas volume dispersed in the turbulent shear layer. Time dependent concentrations at a point were monitored by measuring the scattered light from a coherent light source by a photomultiplier-fiber optics probe. Data consisted of a series of concentration realizations downstream from the ground level source. The distribution of concentration was described by selecting coefficients empirically in a Gram-Charlier series. Puff dispersion characteristics were compared with prediction of the Lagrangian similarity diffusion theory.

Wind tunnel results were also compared with field dispersion studies conducted by Pacific Northwestern Laboratory at Hanford Reservation, Washington.

B. T. Yang
R. N. Meroney
Fluid Dynamics and Diffusion Laboratory
College of Engineering
Colorado State University
Fort Collins, Colorado 80521

ACKNOWLEDGMENTS

The authors wish to thank Professor J. E. Cermak, Professor V. A. Sandborn, Professor R. B. Kelman, and Dr. J. Peterka for their interests and valuable discussions on various aspects of this research work.

The authors are grateful to Mrs. M. L. Bates and Mrs. J. Matthews for their typing of this paper.

The partial financial support of this work provided by ONR Contract No. N00014-68-A-0493-0001 is gratefully acknowledged. Parts of the financial supports from NSF Grant No. GK 23989, and EPA Contract No. IR01-APO-1186-02 are also acknowledged.

TABLE OF CONTENTS

TABLE OF CONTENTS - Continued

LIST OF TABLES

LIST OF FIGURES

LIST OF SYMBOLS

Symbol	Definition
a	longitudinal diffusion constant (= 1.5), Sutton's diffusion constant
$\mathring{A}$	angstrom (= 10^{-10} meter)
A	constant
b	vertical diffusion constant (= 0.4)
B_i's	transformed similarity moments
c	concentration from a point source
C	Sutton's diffusion parameter
D_M	molecular diffusivity
e	exponential
E	collecting efficiency, PM tube output
E_x	excess (= flatness - 3)
f	frequency
g	gravitational acceleration, lateral diffusion constant (~1.0)
G	gamma distribution function
H_i	Hermite polynomials of degree i
i	index
I	Source strength of instantaneous sources
I_θ	Scattered light energy at angle θ
j	index
k	coagulation coefficient
K	eddy diffusivity
ℓ	mixing length
L	concentration from a line source

Symbol	Definition
m	refractive index, Sutton's diffusion parameter
n	Sutton's diffusion parameter, number concentration of aerosols
p	exponent in scattering approximation
q	viscosity
Q	mass source strength
r	radius of a bubble, radius of a aerosol particle
R_{ii}	autocorrelation function
R	probing distance in a light scattering process
s_i	random variable
sk	skewness
t	time
t_a	arrival time
t_d	departure time
T	source strength of continuous sources
u	longitudinal velocity component
u_*	shear velocity
U	mean transport velocity
v	lateral velocity component
v_f	fall velocity
v_{cf}	corrected fall velocity
V	volume of a gass bubble, volume of a aerosol particle
w	vertical velocity component
W	number particles on a unit area of a solid surface

Symbol	Definition
x,y,z	longitudinal, lateral, and vertical coordinates
z	normalized random variable
α	light scattering parameter $(2\pi r/\lambda)$
β	longitudinal similarity coordinate $(\frac{x-\bar{x}}{au_*t})$
γ	entrainment factor, parameter of a gamma distribution function
Γ	velocity gradient
Γ^i	incomplete gamma functions
δ	Dirac-delta function
η	vertical similarity coordinate $(\frac{z}{\kappa u_* t})$
θ	scattering angle
κ	Karman's constant $(= 0.4)$
λ	wavelength of the incident light, mean free path, parameter of a gamma distribution function
μ	micron $(= 10^{-6}$ meter)
ξ	spatial coordinate
ρ	density
σ	standard deviation
τ_o	shear stress at wall
ϕ	standard normal distribution
Φ	cumulant standard normal distribution
χ	concentration due to the integration of an instantaneous source

Chapter I

INTRODUCTION

Chapter I

INTRODUCTION

This study is to examine the mechanism of turbulent dispersion, from an instantaneous point source. The dispersion behavior of an instantaneous point source in a turbulent shear flow is of interest because it represents the initial building block in most point, line and volume diffusion models. A puff may also be associated with accidental breach of radioactive confinement, gas storage failure, rocket engine accident, or missile take-off. Additional examples can also be found in channel flow or rivers where tracer materials are dumped for velocity measurements. Tracers are often injected instantaneously in pipes for velocity evaluation or trouble source detection.

An instantaneous point source by definition, is a source with infinitesimally small volume but containing a finite amount of "tagged" particles which are released in a very short time period. Mathematically speaking, it is a source with a Dirac-delta function shape in both time and space coordinates. If the volume of a source is much smaller than the cube of a characteristic flow length (say, the boundary layer thickness) it can be considered a point source. If the release duration is shorter than some characteristic flow time it can be considered an instantaneous source.

The physical significance of an instantaneous point source can be seen from its definition. The species distribution due to a continuous source or even an unsteady release can be calculated by integrating the behavior of an instantaneous source in time. In the same manner, diffusion due to a volume source can be obtained by integrating in space over a distribution of point sources. For a source with an arbitrary release pattern and an arbitrary geometry the concentration distribution downstream can be constructed by proper integration (on time and space) of the result due to a distribution of instantaneous point sources. This concept is very similar to the definition of Green's function in potential theory.

Many measurements have been performed in the atmosphere to study the puff diffusion problem. The most recent field test was performed by Nichola, Ramsdell, and Ludwick (1970) in the Pacific Northwest Laboratory. The test was conducted at U. S. Atomic Commission's Hanford Reservation, Washington. The source was simply produced by crushing a quartz ampule containing Kr-85 tracer gas. Other field measurements for shell and balloon bursts and cluster behavior are tabulated in Table 1.1.

A field study, however, requires a large detecting grid system and many support personnel. The degrees of freedom of the mean wind speed, direction and thermal stratification conditions are almost infinite. To systematically survey a set of data for identical conditions is usually an exhausting process. The current study is prompted by the economics of time and resources associated with wind tunnel laboratory measurements.

The feasibility of wind tunnel simulation of atmospheric flow and its diffusion processes has been well studied (Cermak et al, 1966; McVehil et al, 1967). However, to simulate an instantaneous point source presents considerable additional difficulties.

Chandra (1967), Kesic (1966) have attempted to follow puff behavior in the laboratory with little success. Difficulties are generally associated with source generation, detection, time and space scales, and the need for many realizations to provide significant statistics.

In Chapter II, a general review of diffusion theories is found. The techniques utilized, in the present study, for source generation and detection are discussed in Chapters IV and V respectively. The details of the mathematical model will be commented upon in Chapter VIII.

Chapter II

GENERAL REVIEW ON DIFFUSION THEORIES

Chapter II

GENERAL REVIEW OF TURBULENT DIFFUSION THEORIES

The theory of turbulent diffusion, like the theory of turbulence itself, suffers from a lack of a validated physical model to act as a foundation for further insight.

Mathematically the perturbation approach, originally established by Reynolds, does not resolve physics of the fluid behavior. In fact, the additional terms (Reynolds stresses, or correlations) merely provide additional unknowns in an already complicated problem. Nevertheless, many "ad hoc" procedures have been developed to close the equations and make the solution tractable. These procedures or suggestions are generally assigned to the categories of: gradient transfer theory, statistical theory, and Lagrangian similarity theory.

2.1 Gradient-Transfer Theory

With perturbation arguments, one may express the diffusion equation as follows:

$$\frac{\partial c}{\partial t} + u_i \frac{\partial c}{\partial x_i} = -\frac{\partial}{\partial x_i} (\overline{u_i' c'}) \quad i = 1.\ 2.\ 3.$$

The terms $\overline{u_i' c'}$ which result from the averaging process are additional dependent variables. This implies that the dynamic equation is not in a closed form. The earliest attempt to overcome this difficulty was based on the assumption suggested by Taylor that

$$-\ \overline{u_i' c'} = K_i \frac{\partial c}{\partial x_i} \ .$$

The diffusion equation thus reads:

$$\frac{\partial c}{\partial t} + u_i \frac{\partial c}{\partial x_i} = \frac{\partial}{\partial x_i} (K_i \frac{\partial c}{\partial x_i}) \qquad i = 1, 2, 3.$$

Unfortunately, introducing turbulent gradient transfer coefficients K_i's does not solve the closure problem. This is because the coefficients themselves are not universal functions. The functional form of the coefficients are often based on the results of experimental observation.

Due to the analytic difficulty, the governing equations have only been solved for simple cases. For instance, in a infinite flow field, with constant wind profile and constant diffusivities assumption, the unsteady diffusion equation becomes a heat conduction equation by using the following transformation:

$$x' = x - Ut \quad .$$

This is the same as Fickian diffusion equation and has the following solution (Carslaw and Jaeger, 1971)

$$c = \frac{1}{\sqrt{2\pi}^{3/2} \sigma_x \sigma_y \sigma_z} e^{-[\frac{(x-Ut)^2}{2\sigma_x{}^2} + \frac{y^2}{2\sigma_y{}^2} + \frac{z^2}{2\sigma_z{}^2}]}$$

where $\sigma_i^2 = 2K_i t = 2K_i \frac{x}{U}$ (i = 1.2.3). Diffusion in an unbounded, two dimensional flow with constant diffusivities and constant velocity gradient Γ was solved by Novikov (Monin and Yaglom, 1970). The solution is

$$c = \frac{1}{(4\pi t)^3[(K_x + \Gamma^2 K_z t^2/12)K_y K_z]^{\frac{1}{2}}}$$

$$\cdot \exp\left\{-\frac{(x-\Gamma zt/2)^2}{4K_x t + \Gamma^2 K_z t^3/3} - \frac{y^2}{4K_y t} - \frac{z^2}{4K_z t}\right\}$$

When a reflecting boundary condition is considered, the solution for an instantaneous point source for constant diffusivities and constant velocity in the half space $(z \geq 0)$ is (Monin and Yaglom, 1970),

$$c = \frac{2}{(4\pi t)^{3/2}(K_x K_y K_z)^{\frac{1}{2}}} e^{-\left[\frac{(x-Ut)^2}{4K_x t} + \frac{y^2}{4K_y t} + \frac{z^2}{4K_z t}\right]}$$

In a shear layer, the simplified conditions such as uniform wind profile and constant diffusivities will not be valid. The special case of constant diffusivity assumption in a shear flow was examined by Van der Hegge Zijnen (Hinze, 1959). He measured the temperature profile from a heated wire placed in a horizontal plane air jet. The skewness of the measured temperature distribution was shown toward the region of large mean velocity. This experimental result disproved the validity of the constant diffusivity assumption in a shear flow since this assumption would predict the opposite behavior.

In meteorological studies, the logarithmic profile was generally accepted. However, this non-linear velocity profile presents great analytic difficulties in solving the unsteady diffusion problems.

First, the trajectory of a diffusing puff is not a linear function of time. Second, the integration of a logarithmic profile usually is difficult to obtain. These difficulties were overcome by Chatwin (1968) and Putta (1971) by applying the Lagrangian Similarity Theory. The analytic efforts will be discussed in Chapter VIII.

Another method to limit the possible functional form of transport coefficients is provided by the stipulation of dimensional consistency and coordinate transformation invariance. Donaldson et al, (1968,1971) have used this invariance technique to close the mathematical system of equations. Results are quite promising; however, a number of empirical constants remained unknown and the solution requires fairly extensive numerical computation.

2.2 Statistical Theory

In 1921, G. I. Taylor (1921) presented his famous paper "Diffusion by Continuous Movements." The statistical aspects of diffusion in a homogeneous turbulence has turned out to be a major contribution. This has been proven to be a useful analytic tool for modeling a turbulent diffusion process. A similar analysis has not yet been developed successfully for a shear flow condition. However, the statistical features of a turbulent diffusion process are appreciated.

The merit of Taylor's statistical diffusion theory is that, in certain geometrically symmetric flow, one can directly go to the physics. However, the present state of art on statistical theory is still limited in the infinite homogeneous flow. In this specific type of turbulent flow, Taylor obtained,

$$\sigma_i^2(t) = 2\,\overline{u_i'^2} \int_o^t \int_o^{t_1} R_{ii}(\xi)\, d\xi dt_1 \quad ,$$

where σ^2, $\overline{u_i'^2}$ are the variance of displacement and velocity fluctuation, $R_{ii}(\xi)$ is the auto-correlation function of velocity.

Thus the solution for a instantaneous point source in a uniform stream is

$$c = \frac{1}{\sqrt{2}\,\pi^{3/2}\,\sigma_x\sigma_y\sigma_z}\, e^{-\left[\frac{(x-Ut)^2}{2\sigma_x^2} + \frac{y^2}{2\sigma_y^2} + \frac{z^2}{2\sigma_z^2}\right]}$$

where $\sigma_i = 2\,\overline{u_i'^2} \int_o^t \int_o^{t_1} R_{ii}(\xi)\, d\xi dt_1 \quad .$

Sutton (1932) extended this theory to the atmospheric diffusion and assumed:

$$R_{ii} = \left(\frac{a}{\overline{u_i'^2}\,\xi}\right)^n$$

a, n are both constants. The final form of the solution thus becomes:

$$c = \frac{1}{\pi^{3/2}\, C^3\, (\overline{u_i'^2} t)^{3m/2}}\, e^{-\frac{y^2 + z^2 + (x-Ut)^2}{C^2 (\overline{u_i'^2} t)^m}}$$

where $m = 2-n$

and $$C^2 = \frac{4\, a^n}{(1-n)(2-n)} \quad .$$

No work has successfully extended the statistical theory to the shear flow and in the half space. This is because of lack of information on the $R_{ii}(\xi)$ variation in a half space shear flow.

2.3 Similarity Theory

This theory is based upon the "Lagrangian similarity hypothesis" which was first suggested by G. K. Batchelor in 1950.

The hypothesis suggests:

> "In the constant flux layer, the statistical properties of the velocity of a marked fluid particle, at time t after release from the ground surface, are functions of friction velocity u_* and duration time t."

The most attractive feature of this hypothesis is that it reduces the turbulent diffusion equation to a mathematically tractable form. This theory, in many ways represents a combination of the gradient-transfer theory and the statistical theory. The linear diffusivity assumption, originated from the mixing length hypothesis, falls into the category of the gradient-transfer theory. However, the Lagrangian approach to trace the statistical properties of a marked fluid particle basically is the same as the statistical theory.

Generally speaking, a Lagrangian approach is superior to an Eulerian frame in a diffusion study. This is because of the various "eddy" sizes which play the different roles in a diffusion process. In practice a Lagrangian approach usually presents extreme experimental difficulties. Analytically, however, one may apply a Lagrangian transformation to the classical Eulerian diffusion equation. The detailed mathematical description will be presented in Chapter VIII.

Chapter III

GENERAL REVIEW ON CONCENTRATION MEASURING TECHNIQUES IN A TURBULENT AIR FLOW

Chapter III

GENERAL REVIEW OF CONCENTRATION MEASURING TECHNIQUES IN A TURBULENT AIR FLOW

In turbulent diffusion studies, fluid particles are often imagined to be "tagged" such that the mixing mechanism may be carried out as if no foreign particles were present, yet the dispersive effect of the flow can be followed. Such idealistic particles are usually referred to as "passive particles."

Unfortunately, there does not seem to be any means to "tag" fluid particles without interferring with the real fluid motion. In most experimental diffusion studies, efforts have been directed to reduce the distortion due to the tagging process to a minimum.

Tracers, or "tagged" fluid particles usually provide different chemical or physical properties from ambient fluid particles. The following sections discuss briefly the possible tracers and the general measuring techniques in a turbulent air flow. Methods stated here may or may not have been used in turbulent diffusion measurements. However, the basic mechanism can always be recognized. The following table lists the basic mechanisms for particle tagging.

BASIC MECHANISMS TO TAG PARTICLES IN AN AIR FLOW

	Chemical Method	Physical Methods				
Detecting principle	Chemical reaction	Density gradient	Sub-particle and EMW emission	Heat transfer	EMW absorption or scattering	Particulates filtering

3.1 Chemical Tracers

Tracers which have different chemical properties from ambient air are classified as chemical tracers, for instance, NH_4OH, (Malhotra and Cermak, 1964; Davar, 1961), HCl, (Thompson, 1962), NO_2, (Gosline, 1972), SO_2, (Gartrell, 1964; Cramer, 1957), and the hydro-carbon family (Kitabayashi, 1967).

When chemical tracers are used for diffusion studies, concentration samples are drawn from the flow field. In order to minimize the distortion due to the presence of a sampling probe and the process of suction, the rate of drawing samples is maintained the same as the mean background velocity. In a turbulent boundary layer where the local mean velocity varies, different sucking rates are required. This sampling technique is usually referred to as "iso-kinetic sampling" (IKS).

After required chemical pretreatment, the tracer materials are presented in physically sensitive form which can be quantitatively interpreted in terms of the final colors, mass of precipitants, electrical voltages, turbidity, etc. Hydro-carbon family tracers, such as propane, can be analyzed by measuring the flame temperature of the combustion process from a drawn sample. This method can even be used to scan a diffusion plume. However, good time resolution cannot be obtained.

If concentration samples can be stored, the iso-kinetic sampling method may offer a large capacity to average point concentration distributions. In a region such as near a solid boundary, where local mean velocity is small, considerably long flushing time is required.

In a closed test environment such as a recirculating wind tunnel, a build-up concentration background may be caused by a long-time release process.

The primary drawback of chemical tracers is the time lag associated with the chemical conditioning prior to concentration evaluation. For instance, for a turbulent flow with mean free stream velocity equal to 1.5 m/sec, the time period required for the drawn sample to reach a steady value is of order 5.0 seconds. Hence the time constant of the instruments for chemical tracer measurements is of order 10 seconds. This does not include the period for chemical analysis which varies from tracer to tracer. The chemical tracers cannot be used for instantaneous puff measurement because of the long processing time constant. However, the chemical tracers and the associated processing equipments are economical in general.

3.2 Physical Tracers

Tracers which have different physical properties from ambient fluid particles, such as density, heat transfer rate, etc., can be used to detect a concentration variation. In the following sections, different physical tracers, as characterized by their detecting mechanisms, are discussed.

3.2.1 Density tracers - Gases with differing molecular weights will be called density tracers. Examples of tracers of this kind are Freon and Helium (Meroney and Yang, 1969) and etc.

The basic detecting principle is based on the difference of molecular weights between the tracer gas and the ambient gases (mainly, N_2 and O_2). The sampled gases will be ionized by a gas discharging process and then the ions are accelerated by a potential difference and allowed to enter a magnetic field. The tracer gas which has a different electron charge-to-mass ratio (e/m) from N_2 and O_2 will have a different deflection distance. (The instrument is called a mass spectrometer). A pulse circuit is used to register the number of the tracer particles after discriminating the signals from ambient air molecules.

When using density tracers, one should consider the distortion of the tracer paths due to the buoyant force. The time constant ($\geq$ 10 seconds) is also limited by the time lag found in the case of using chemical tracers. The cost of a mass spectrometer is usually higher by an order of magnitude than the device used to analyze chemical tracers.

3.2.2 Sub-particles and electromagnetic wave emitter - Naturally borne or activated sub-particles (α, β) and electromagnetic wave (γ rays, light rays) emitters are often used in concentration measurements. Examples are H-3, Kr-85 (Martin, 1965; Yang and Meroney, 1970), Ar-41 (Islitzer, 1965; Steward et al, 1954).

Sample concentrations are determined by means of an electronic counter to register the collision frequency of sub-particles, or the electromagnetic wave intensity, on the surface of a detector. High frequency Gamma rays have to be converted into a visible light spectrum in order to be counted. This method is called scintillation counting (Lapp and Andrews, 1964; Rodliffe and Fraser, 1971). The sub-particles or EMW emitters can be divided into three major categories according to different activation sequences. They are: natural emitters, pre-activated emitters, and post-activated emitters.

3.2.2.1 Natural emitters - Sub-particles or electromagnetic wave emitters which exist without a previous artificial activation process are called natural emitters. For the safety consideration, low energy, non-chemically active β-particle emitters, such as Kr-85, are preferred.

Iso-kinetic sampling techniques are usually applied to the concentration sampling in diffusion studies. Concentration samples are drawn into counter chambers such as Geiger-Mueller tubes. After a period of flushing the counter chambers by continuously drawing sample gases from a flow field a high voltage is applied across the chambers to register the collision frequency due to the emission from the sample gases.

Care should be taken when using natural emitting tracers; the half-life of the selected radioactive elements should be considerably longer than the experimental period.

Natural emitters may be used to monitor the nonstationary diffusion process: a semi-conductor detector can be exposed in an air stream to accept the direct bombarding of sub-particles or electromagnetic waves instead of drawing samples from a flow. The spatial resolution has to be considered when radioactive tracers are used. This is because of the finite travel distance of sub-particles and electromagnetic waves in an air stream. It can easily be visualized that if one exposes a semi-conductor detector to a radioactive environment, the output signal is an integrated value over a penetrable space. For instance, Kr-85 (particle maximum β energy of 0.695 Mev.) can travel almost 2 meters in air (Lapp and Andrews, 1965; Nickola, 1970). The spatial resolution may be improved by using proper blocking devices. However, the counting geometry (solid angle) is usually very poor. Consequently, a very concentrated source is needed. The time constant of analyzing natural emitter tracers depends on the techniques used. When isokinetic sampling is used, the period required for transferring sample and flushing a counter chamber is of order 1 minute. The electronic counting device costs in the order of $1,000. When a semi-conductor is used as a detector, the time for converting the concentration to electric signal output is almost instantaneous if proper block technique is used.

3.2.2.2 Pre-activated emitters - These kinds of tracers can be considered when the safety of handling radioactive materials is concerned during nonexperimental periods. Many elements can be radioactively activated by using fast deutron or neutron striking. By proper designing, this method may be considered as an ideal "tagging" in diffusion studies. However, to activate a "passively" radioactive element, usually, is not a simple process, it requires a linear accelerator or a special research reactor to carry out the activation process.

Fluorescent powders can also be used to serve the same purpose. They can be premixed thoroughly with a air flow and activated to emit visible light by shooting an ultra-violet light beam.

For diffusion studies, the pre-activated emitters are rarely used due to the cost and the complication of the activation processes. When radioactive emitters are used, the cost of facilities is very high. When fluorescent powders are used, a completely dark experimental environment is required. The time constant for concentration analysis is the same as that in Section 3.2.1.

3.2.2.3 Post-activated emitters - Often, for safety and publicity reasons, tracers used in studying diffusion in a residential area have to be harmless and not significantly visible. In addition, in order to distinguish a studied source from other sources, a specially selected source has to be used. For instance, to study urban diffusion problems, NO_2 or SO_2 will not be proper tracers because one may not be able to distinguish the tracers from the background environment. Colbolt sulphate ($CoSo_4 7H_{20}$) was often used for this specific purpose (Islitzer and Slade, 1968). The collected samples can be evaluated by a neutron activation process. Fluorescent particles and zinc cadmium (Smith and Hay, 1961) are also used in a similar manner at night with an ultra-violet activation analysis.

Another application of post-emitting tracers is to improve the spatial resolution which is present when using a natural emitter. For instance, a concentrated neutron beam can be used to activate the flow only in a well confined region. An ultra-violet laser beam can also be applied to the premixed fluorescent air flow.

In addition to being easily distinguished, the post-activated emitters can offer a very fine concentration resolution, i.e., small concentration is easy to be identified. Because of its special purpose, the relatively long time constant of this method is not generally concerned. The cost of the system depends on the complication of the activation process.

3.2.3 Heat transfer tracers - Gases, such as He (Ruff and Gelhar, 1970; Exall, 1970), which have significantly different heat transfer coefficients from air can be used as concentration measurements. Local mean concentration can be detected by using a calibrated hot-wire probe. This method has not been widely used because of the difficulties in separating the concentration signals from the signals due to convection. A similar operation can be achieved by releasing a pre-heated gas tracer (Kesic, 1966) and using a cold wire as receiver. The local concentration is associated with the local temperature in a mixing process. The buoyancy force should be considered. Due to the limitation of heating temperature, this technique can only be used in a very short downstream distance. The time constant of heat transfer tracer measurements is of the order 10^{-3} seconds. However, using a hot wire to detect Helium concentration usually suffers a "historical effect" which distorts the hot-wire output signals. This was described by Way and Libby (1971).

The thermal conductivity cell type gas chromatograph (Meroney, 1963) also belongs to this category. Time constant of using gas chromatograph is limited by the period of drawing samples from a flow field (~10 sec.). Costs for heat transfer tracer measurements depend on the degree of complication and the resolution of the devices.

3.2.4 Electromagnetic wave (EMW) absorption or scattering tracers - The presence of solid or liquid particles in an air flow causes EMW (such as radio waves, light rays) to diffract, reflect, refract, and extinct. These properties can be used to probe the local number concentration of the particulates.

Two major categories of these methods can be specified as absorption and scattering measurement. First, the EMW intensity extincts in a negative exponential manner when it passes through a uniformly distributed particle-present environment. This phenomenon is referred to as absorption. For instance, by measuring the decreased intensity from a laser beam, one may evaluate an integrated concentration over the light path. This can be used to monitor the aerosol pollutants level over an urban area (Melngailis, 1971). This prospective concentration measurement technique has not yet been used in laboratory measurements. Second, the scattering phenomenon, which is a combination of diffraction, refraction, and reflection of EMW, can be used to evaluate a turbulent diffusion process. This specific method will be discussed in Chapter V.

The main application of using the EMW absorption or scattering properly for concentration measurements is remote sensing. This technique has been most popular since the invention of laser. Due to the extremely high transmitting velocity of EMW, the time constant of this type of measurement is of the order 10^{-6} seconds. The cost of instrumentation also depends on the sophistication of the overall system.

3.2.5 Particulate filtering tracers - Particulates which have larger physical dimensions than air molecules can be used as tracers. Samples can be drawn through selected filter paper and analyzed. Usually, the filtering process is combined with another prescribed technique.

3.3 Tracers and Boundary Conditions

The boundary condition at the ground level is defined as a reflection condition, i.e., $\partial c/\partial z = 0$. This condition implies no mass transport across the floor boundary, and no deposition on the floor. When gaseous tracers are used, this condition is clearly true. When oil droplets or solid particles are used, the deposition of the tracer particles should be considered. This is especially important when release is conducted at the ground level where the highest concentration is located.

In the field tests, for instance, with fluorescent particles as tracers, the deposition will be very significant. This is the same as the settling phenomena in a river bed. The main cause of deposition is due to the impaction of airborne particulates on a solid surface. The impactions are determined by the following factors:

1. Local turbulent intensity.
2. Fall velocity, which depends on the density and the size of particles.
3. The adhesive force of the particle to the solid surface.

These imperfect reflection boundary conditions for non-reactive tracers may be generalized as:

$$K_z \frac{\partial c}{\partial z} + E\, V_f\, C + \gamma\, W = 0 \quad .$$

E is collecting efficiency which indicates the percentage of number particles striking the surface, V_f is the fall velocity, γ is an entrainment factor, and W is the number of particles on a unit area of solid surface. It can be seen that when $E = W = 0$, one has a perfect reflection condition.

Chapter IV

SOURCES OF DIFFUSION

Chapter IV

SOURCES OF DIFFUSION

4.1 Classification of Diffusion Sources

In this section, the initial conditions utilized for different diffusion processes are classified according to the release periods of the source. The time dependent turbulent diffusion equation can be written as:

$$\frac{\partial c}{\partial t} + u_j \frac{\partial c}{\partial x_j} = \frac{\partial}{\partial x_j} (- \overline{c' u_j'}) \quad \text{in which} \quad j = 1,2,3.$$

Boussinesq suggested that the correlation terms may be replaced by eddy diffusivities, K_j's:

$$\frac{\partial c}{\partial t} + u_j \frac{\partial c}{\partial x_j} = \frac{\partial}{\partial x_j} (K_j \frac{\partial c}{\partial x_j}) \quad .$$

Usually, eddy transport coefficients are assumed to be only functions of coordinates and turbulent structure parameters. Thus, the form of a turbulent diffusion equation is a non-vectoral, 4-dimensional, 2nd order of sum of 7, linear, non-homogeneous partial differential equation. If the diffusion process is time-independent, i.e., $\partial c/\partial t = 0$, the only conditions needed to solve the equation (of elliptic form) are closed boundary conditions. The problem thus becomes a boundary value problem. For a time-dependent process, this equation takes parabolic form; an initial condition is required to solve the equation. The detailed classification due to different release periods and geometrical form will be discussed in the following sections.

4.1.1 Instantaneous Sources - The mathematical descriptions for various source geometries are as follows:

a. Point source:

$$t = 0, \quad c = I_p \ \delta(0,0,0,0)$$

in which δ is a Dirac-delta function, the source is at the origin of the coordinates, and

$$I_p = \int_V c(x,y,z,t_o)d\vec{r} \qquad \text{at} \quad t = t_o > 0,$$

where $\int_V d\vec{r} = \int_{-\infty}^{\infty} \int_{-\infty}^{\infty} \int_{-\infty}^{\infty} dx\ dy\ dz$.

b. Line source: (cross wind)

$$t = 0, \quad c = I_\ell \ \delta(0,\ y,\ 0,\ 0)$$

I_ℓ: concentration per unit length at y-direction,

or

$$I_\ell = \int_{-\infty}^{\infty} \int_{y_o}^{y_o+1} \int_{-\infty}^{\infty} c(x,y,z,t_o)dx\ dy\ dz \quad \text{at} \quad t = t_o \geq 0 \ .$$

c. Volume source:

$$t = 0, \quad c = I_v \ \delta(x,y,z,o)$$

$I_v(x,y,z,t)$ is the initial concentration distribution over a 3-dimensional space,

or

$$I_v = \int_V c(x,y,z,t_o)d\vec{r} \quad \text{at} \quad t = t_o \geq 0 \ .$$

As mentioned in Chapter I, there are actually no real instantaneous sources. For practical purposes, if a release time is relatively short compared with an appropriate characteristic time, we may consider it as an instantaneous release. In a similar manner, if a release exit is relatively smaller than characteristic dimensions in a flow, it may be considered as a point release. Thus, we may claim that the blast of a bomb in the atmosphere may be an instantaneous point source. The crosswind jet-trail may be an instantaneous line source. A large scale explosion, such as an atomic cloud, may be an instantaneous volume source.

4.1.2 Continuous sources - As we have stated at the beginning of this chapter, this is not an initial value problem due to $\partial c/\partial t = 0$. The mass conservation and boundary conditions are the only conditions to be considered:

a. Point source:

$$c(0, 0, 0, t) \to T_p$$

T_p is the source strength (mass/unit time)

$$\int_V c \, d\vec{r} = \int_o^{t_o} T_p \, dt = T_p \, t_o \quad \text{at} \quad t = t_o >> 0.$$

Usually, the mass conservation is written as:

$$T_p = \int_{-\infty}^{\infty} \int_{-\infty}^{\infty} u \, c(x_o, y, z) dy \, dz$$

in which x is the mean convective direction, u is the local mean convective velocity in the x-direction.

b. Line source: (cross wind)

$$c(0, y, 0, t) \to T_\ell$$

T_ℓ is source strength per unit length at y-axis

$$\int_{-\infty}^{\infty} \int_{y_o}^{y_o+1} \int_{\infty}^{\infty} c(x,y,z) d\vec{r} = T_\ell \, t_o \quad \text{at} \quad t = t_o >> 0$$

or

$$T_\ell = \int_{\infty}^{\infty} \int_{y_o}^{y_o+1} u\, c(x_o,y,z)dy\, dz \ .$$

c. Volume source:

The boundary condition for a volume source cannot be specified in a simple mathematical form. This is because, for a given point where a source is located, the local concentration is the sum of the local source strength and the concentration transport from the upstream source. The transport of concentration is due to the convective motion and diffusion. These kinds of problems may often be overcome by the superposition of point sources.

An appropriate example of a continuous point source is a continuous release from an isolated factory stack. A crosswind highway at the rush hour is an example of a continuous line source. Water vapor over a sizeable lake or the forest fire provides a good example of a volume source. The solution of a continuous volume source can be obtained by integrating many instantaneous point sources over time and space.

Examples of non-stationary sources exist in daily life. Non-stationary release at factory stacks, crosswind highways, and urban regions would be good examples of point, line, and volume sources, respectively.

4.2 The Laboratory Instantaneous (Point) Source

Considerable difficulties have been found when producing a laboratory scale instantaneous (point) source. Again, it is not possible to produce a Dirac-delta function source in both time and space, yet the tracer materials should be enough to be detected reasonably far downstream in a dispersion process.

4.2.1 Criteria of producing a laboratory instantaneous point source - The criteria of producing a laboratory instantaneous point source are described as follows:

a. Disturbance - Any mechanical device inserted into the flow field to produce an instantaneous point source appears to generate mechanical turbulence or vortex shedding. If the disturbance scale is much larger than the original source dimension, the "point" source picture may be destroyed right after release. A short cylindrical container has been tested (see Fig. 4.1) to produce an instantaneous source. Unfortunately, significant vortex shedding occurred behind the container.

b. Source strength - The source strength of an instantaneous point source should be sufficient to provide detectable signals at a desired downstream distance.

c. Release duration - The duration between the first tracer particle released and the last tracer particle released into a flow should be small in order to meet the criteria of an "instantaneous" condition.

d. Shape - Few experiments have been conducted to study instantaneous point sources. Usually fast injection of tracer materials was used without considering the original source shapes (Chandra, 1967, Exall, 1970). The actual resulting puff shapes are considered to be mostly elliptical or long cylindrical. It is true that one cannot conceivably find a perfect instantaneous point source to meet every requirement. However, one may conclude from the linearity of the diffusion equation that a spherical source is better than other shapes. This can be argued in the following manner: concentration at a downwind distance is the sum of the contribution due to each instantaneous source. From the linearity of the diffusion equation, one can claim that the concentration distribution due to an instantaneous sphere (not very sizeable, of course) is proportional to the concentration due to an instantaneous source further upstream. In addition, the isotropic diffusing pattern of a cloud in the downstream will not be confused with the initial isotropic (circular) distribution.

e. Concentration distribution - For the same reason, as stated in d., the concentration distribution in an instantaneous "point source" should be nearly uniform. The fast injection type release will cause an initially turbulent jet mixing.

f. Repeatability - In order to obtain a statistically significant ensemble mean of a diffusion behavior, the source has to be produced repeatedly.

4.2.2 Possible means of producing a laboratory instantaneous point source - The first laboratory instantaneous plane source was due to G. I. Taylor in 1954. Salt water was just "dumped" into a fully developed pipe flow as a plane source. Concentration samples were picked up by a conductance gauge. This was the first attempt to produce a laboratory instantaneous source.

In the air flow, only a few attempts have been made. In a field test, one can simply apply a small scale explosion as an instantaneous point source.

There have been two laboratory scale measurements conducted at Colorado State University. Kesic (1966) used a hot wire to generate an instantaneous point thermal puff by pulse heating. The maximum measuring distance (centerline) was four inches. The short measuring distance and the buoyancy effects limited the experiments significance. Chandra (1967) used a bypass control to release a jet-like Helium source. The samples were picked up by an iso-kinetic sampling probe. The maximum detecting distance was four feet. With a mean free stream velocity of 20 ft/sec, the source was only allowed to diffuse in the order of 0.1 sec. It is questionable if the iso-kinetic sampling method had sufficient resolution; it is also doubtful if turbulent jet effects were still significant over the measuring distance.

There are advantages and shortcomings to different techniques in generating a laboratory scale instantaneous point source. The writer has summarized the following methods:

a. Neutron activation - A pulse neutron activation process may offer a reasonable laboratory scale instantaneous point source.

b. Pulse UV illuminance - When a fluorescent particle has been pre-mixed thoroughly in a (darkened) air flow, a pulse ultra-violet laser beam can produce a well-defined instantaneous point source. This needs a small light blockage device to limit the illuminance distance in order to assume a point source instead of a line source.

c. Pulse heating - A pulse voltage can be applied to a hot wire to produce a thermal puff. The limitation of this method is a short measuring distance.

d. Bubble bursting - An aerosol filled gas bubble can be used as an instantaneous source at the instant of bursting. This method was used in this experiment.

4.2.3 Bursting of a tracer-containing, rising gas bubble as an instantaneous point source - An aerosol filled gas bubble bursting at ground level has been adopted as an instantaneous source. Various aspects of this idea will be discussed later.

a. Zero mechanical blockage - There need be almost no mechanical device above the floor of the wind tunnel. This implies that no mechanical disturbance will be introduced. A hot-wire probe was used to measure the momentum injection due to the bursting process. There was no appreciable added upward velocity to be observed when the probe was only 5 cm above the bursting location. This is probably due to intense turbulent motion near the floor and the strong vertical shear which actually suppresses the bursting near ground level.

b. Source strength - With a laser light scattering method (will be described in Chapter V), the maximum measuring distance in this experiment is extended to 4 m from the source.

c. Instantaneousness - To the authors' knowledge, there is no literature to be found on the bursting process of a rising gas bubble at the surface of a liquid. An estimate of vertical velocity of an injected puff has been made by a hot-wire probe when there was no convective velocity above the water surface. A hot-wire probe was set 2 cm above the water surface. When a gas bubble bursted, a sudden rise from the hot-wire anemometer could be seen on an oscilloscope screen. The magnitude of the signal fell into the range of 10 miliseconds. In the presence of a shear flow, no significant signals could be observed due to the high fluctuation near the wall.

4.2.3.1 The mechanics of gas bubbles rising through water - The rise of gas bubbles in liquids was first studied by Allen in 1900. But most studies deal with very small bubbles (<10 cm^3) which do not behave similarly to large ones. Davies and Taylor (1950) were the first to investigate large bubbles which varied from 1.5 to 200 cm^3 in volume. (The original study was related to the phenomenon of submarine explosion). Davies and Taylor's work also motivates the design of the bubble generator which is used to produce the "pseudo-instantaneous" point source.

The bubble generator utilized in this experiment is shown in Figure 4.2. It consisted of a plexiglass cylindrical tank, a plastic cup and a manual rotating mechanical device. The basic procedure of producing a single large bubble is as follows: An upside-down cup was set to accommodate a gas-aerosol mixture which entered from the bottom glass valve. The cup was filled with aerosol cloud by displacing water. The cup was suddenly pivoted to expel the aerosol cloud. It has been found that tilting the containing cup to a right angle was sufficient to displace all the gas out of the cup. An angular speed of 1/2 cycle per second would offer enough acceleration to form a single bubble without disturbing the water. Several cup shapes were tried, and it can be concluded that the original shape of the container, whether semi-spherical, short cylindrical or beaker-like was not critical. Figure 4.3 plots the consecutive movement of a bubble rising in the water.

In order to measure the mean rise velocity and monitor the arrival of a gas bubble two wires were mounted in the bubble generator to form a capacitance gauge. Two wires were placed at different distances beneath the water surface. As gas bubbles pass each wire, the capacitance shifts between the two wires and can be determined from the output of a capacitance meter. Since the distance between the two wires is predetermined (10 cm), the rising velocity can be easily found:

$$U_R = \frac{10\ \text{cm}}{\Delta t}$$

Δt is the time (sec) between the peaks of the capacitance variation due to the passing bubble.

The results from 150 samples are plotted in Figure 4.4. The mean velocity from the 150 samples is 57.2 cm/sec. This result can be compared with Davies and Taylor's (1950) empirical formula:

$$U_R = 24.8\ V^{1/6}$$

in which U_R is rise velocity and V is volume of the bubble. From a graduated glass cylinder, the volume of the bubble used in this experiment is 157 cm^3. Davies and Taylor thus predicted:

$$U_R = 24.8 \times (157)^{1/6} = 56.9\ \text{cm/sec.}$$

The consistency appears excellent.

The radius of the upper surface of the rising bubble can also be obtained from the semi-empirical formulas by Davies and Taylor:

$$U_R = 2/3\ (g\ r)^{1/2}$$

in which g is gravitational acceleration, and r is the radius of the surface of the upper part of a bubble. Therefore, the radius r of a bubble while reaching the water surface is:

$$r = \frac{9}{4}\ \frac{U_R^2}{g} = \frac{9}{4}\ \frac{(57.2)^2}{980} = 7.5\ \text{cm.}$$

This is very close to the observed size of the rising bubbles. Thus, the initial shape and behavior of this laboratory scale instantaneous point source was approximately defined.

4.2.3.2 <u>Experimental observation on bursting of a gas bubble</u> - A shadowgraph was made from a laser Schlieren system (Fig. 4.5). Due to the limited light field, only a burst due to a smaller size gas bubble was observed (see Fig. 4.6). The observed shape of the burst was almost semi-spherical when there was no flow over the water surface. There was no observation made when there was flow present due to the fact that the optical system could not be moved.

The light-scattering probe (Chapter V) was set 5 cm above the water surface to measure the instantaneous injection at the bursting instance. When there was no flow over the water surface, one could clearly observe a sharp output signal at the moment of bursting. When there was a flow, no significant signal could be seen; hence, all aerosols passed beneath the probe. The strong shear evidently suppresses the upward movement during the bursting.

Therefore, the characteristics of the source may be summarized as follows:

(1) It was a ground level source because the upward momentum was suppressed by the shear flow. This was very similar to the phenomenon of a short smoke stack: if an injection rate was small compared to the local mean flow, the plume had only a small tendency to rise. The free stream velocity used was 1.17 m/sec. The rising velocity of the gas bubble has been shown to be 0.57 m/sec. If the bursting speed is isotropic over the water surface, a value less than 0.57 m/sec was expected. (This was due to the kinetic energy lost against surface tension during the bursting process). Thus, it is reasonable to assume it behaved as a ground source.

(2) The shape was circular at the ground level. This was due to the original circular shape of the gas bubble.

(3) It was instantaneous. From the hot-wire signal, the bursting process was in the order of 10 milliseconds (measured when no mean wind was present).

Chapter V

LASER LIGHT-SCATTERING PROBE
(L.L.S.P.)

Chapter V

LASER LIGHT-SCATTERING PROBE (L.L.S.P.)

Due to the time-dependent characteristics of an instantaneous puff diffusion measurement, a unique laser light-scattering probe was developed. The following sections describe the theory, construction, and response of the instrument.

In physical science one of the most important achievements in the later 19th century was Maxwell's electromagnetic theory of light. Based on this theory, optical scattering and EMW scattering could be linked together into one coherent theory. The classical problem of light scattering from a homogeneous sphere has been treated by many great mathematical physicists such as Poisson, Cauchy, Green, Stokes and Rayleigh. However, electromagnetic wave scattering theories did not draw much attention in applied physics until the recent development of the quantum theory. Until advances were made in the scattering theories the systematic design of a light-scattering probe was difficult if not impossible.

The history of using light scattering for concentration measurement is rather short. Rosensweig, Hottel and Williams (1961) were the first to use scattered light as a dynamic concentration measurement. This study of air free jet mixing was conducted in the Massachusetts Institute of Technology. The basic experimental arrangement is shown in Figure 5.1. It is interesting to note that in this experiment the positions of the turbulent jet were adjusted rather than adjusting the optical system. This was due to the large dimension and the clumsy nature of optical devices.

Subsequently, work was also done in the same facility at M.I.T. to study a confined jet (Becker _et al_., 1963). In 1966, Becker, Rosensweig and Gwozdz applied the method in studying turbulent mixing in a pipe. In the study, a fully developed situation was assumed. Therefore, diffusion source positions could be translated along the pipe instead of moving the optical probe. Later the same facility was again used to study the mixing mechanism of a turbulent flame by Gurnitz (1966). A general discussion of the prescribed measurement techniques can be found in the paper by Becker _et al_, (1967).

Due to its clumsy nature, the light-scatter equipment developed by Becker _et al_, is not suitable for concentration measurements in a wind-tunnel or in a confined flow field. Liu (1972) built a compact probe by using two pieces of long fiber optics as both incident and scattered-light transmitters. The schematic arrangements of Liu's probe is shown in Figure 5.2. Liu was the first to map an entire plume for both local mean and fluctuating concentrations for an elevated continuous source over a wind-generated water wave.

All light sources used in the measurements described above provided chromatic light. In classical optical theories, monochromatic and plane waves are usually assumed. Before the birth of the laser (first ruby laser built by T. H. Maiman, Hughes Aircraft Co., 1960) many classical light scattering experiments based on the assumption of monochromaticity were difficult to perform. In 1964, Yeh and Cummins used laser light scattering for velocity measurements. This technique is usually referred to as the "Laser Doppler Velocimeter" (LDV). In LDV measurements, the frequency shift (Doppler principle) due to the scattered light was of primary interest. The particulates which cause the light scattering can be either naturally borne or artificially fed. When an optimum signal to noise level is desired, the latter technique is used (Rolfe et al, 1968; Witte et al, 1972). To the authors' knowledge, there has been no laboratory concentration measurement by using laser light-scattering method.

5.1 Summary of Light-Scattering Theories

The basic assumptions of all classical light scattering theories are as follows:

a. The incident light is a plane, monochromatic (temporally coherent) and a spatially coherent electromagnetic wave; hence, the advantage of a laser as a light scattering source.

b. The scattering light has the same frequency as the incident wave; hence, the choice of an optical filter if discriminating other frequencies from the scattering wave is necessary.

c. When a light wave travels in a perfectly homogeneous medium, it will not be scattered; thus when a light beam traverses a "clean" standard composition of air, there will not be any scattered light. A light scatterer is thus defined as matter with a different refractive index from standard air.

d. Scatterers are homogeneous spherical particles, which is true when particulates are liquid aerosol particles instead of solid particulates.

e. The total scattered energy is the sum of the scattered energy due to each particle; this is called independent scattering. Thus the scattered light waves due to different particles are incoherent. No scattered waves will be enhanced or destroyed due to phase lags.

This assumption implies that if the number concentrations of the present aerosol particles are small, no significant second order scattering will occur. A crude estimation has shown that a mutual separation distance of three times the radius of aerosol particles is a sufficient condition for independent scattering. The linear calibration curve discussed in Chapter VI has shown that independent scattering conditions did exist in the experiments discussed herein.

The phenomenon of radiation scattering is actually a consequence of the interaction between electromagnetic waves and electrons within the matter. When the size of scatterers is greater than the incident wavelength, the macroscopic arguments, such as the refractive boundary conditions, are adequate to describe the scattering phenomena.

There are two major categories in scattering theories, namely, Rayleigh scattering and Mie scattering. Rayleigh scattering theory was derived by L. Rayleigh in 1871. In this theory the light wave is treated as charges of a linearly oscillating dipole or arrays of dipoles. Mie scattering was first derived by G. Mie in 1908 based on electromagnetic wave theory. The latter is the most general thoery for scattering phenomena.

5.1.1 Rayleigh scattering - The result of Rayleigh's law of scattering states:

$$I_\theta = I_o \frac{9\pi^2 V^2}{2\ R^2 \lambda 4} \left(\frac{m^2-1}{m^2+2}\right)^2 (1 + \cos^2 \theta)$$

in which I_o = incident light intensity

I_θ = scattered intensity in the direction θ

V = volume of a dielectric sphere

R = distance between the sphere center and point of observation

λ = wave length of incident light

m = refractive index of the sphere.

This scattering theory only applies to the situation where the scatterer is relatively small compared to the incident wavelength. The effect of this limitation has been evaluated by Holl in 1948 (Green and Lane, 1964). The upper size limit of the scatterers is 0.06 micron diameter for the visible light range, i.e., the size of a scatterer is at least one order smaller than the incident wavelength. This type of scattering has very limited effect on signal strength for the scattering experiments studied herein. This is because the scattered energy would be on the same order as instrumentational noise. However, this theory laid the foundation for the more general Mie theory.

5.1.2 Mie scattering - The Mie theory is the most complete analytic solution for the general scattering theory. Corresponding to Rayleigh's law, the Mie theory can be stated as:

$$I_\theta = \frac{\lambda^2}{8\pi^2 R^2} (i_1^2 + i_2^2)\ I_o$$

in which i_1 = scattered light perpendicular to the plane of observation and i_2 = scattered light parallel to the plane of observation. i_1 and i_2 are defined in terms of coefficients of electric and magnetic waves, namely, a_n and b_n (n is arbitrary integral). a_n and b_n are usually expressed in a complicated infinite series involving Bessel, Hankel and Legendre functions and parameters α and m. (α is the ratio of the scattered circumference to the incident wavelength, viz., $\alpha = 2\pi r/\lambda$, m is the refractive index of the scatterer).

Until the invention of the high speed computer, the Mie theory did not receive much attention since when $\lambda < r$, the series converges extremely slowly. Many efforts have been made to find an approximate solution. For instance, one investigator assumed the scattered energy was to correlate with the diameter in the following form:

$$I_{scattered} \propto \alpha^p$$

by keeping other variables constant. Such methods have failed due to the strong fluctuation of the exponent p (Von de Hulst, 1957). Especially, when an incident light is chromatic, the i_2 component will vary its maxima and minima due to different wavelengths. Standard tables (Denman et al., 1966) are available to evaluate the coefficients a_n's and b_n's for different length parameter α and refractive index m. For $\alpha \geq 20$, the results of Mie theory can be shown by the classical ray optics (see Figure 5.5), i.e., the scattering process is the consequence of reflection, refraction and diffraction processes. The detailed Mie theory and discussion can be found in Von de Hulst's (1957) "Light Scattering by Small Particles." This is a standard reference book on light scattering theories. The results of the Mie scattering theory as they apply to the laser scattering probe design will be discussed in their appropriate following sections.

5.2 Light Scattering Probe

The following table summarizes the light scattering system. Each part will be discussed separately.

L.L.S.P. Components

Name	Function	Remarks
	a. Incident light system	
Laser	Light source	5 m w. Spectral Physics model 120, 6328Å, polarized, Model 256 exciter.
Reflecting mirror	Light deflector	12^{mm} dia., 0.15^{mm} thickness, front-surfaced
	b. Aerosol particles	
Di-octyle phthalate particles	Light scatterer	Cumulative mass = 98%, $d < 10\mu$ atomization principle: air blast
	c. Receiving system	
Optical aperture	Increase spatial resolution	Scattering angle $\theta \cong 1\ 2^{o}$
Fiber optics	Scattered light transmitter	Transmission 4000 A ~ 8000 A, Dolan-Jenner Industries, BXL-36 3 ft long
Photo-multiplier	Light sensor	RCA 7265, 14 stages operating voltage: 2800 VDC S - 20 response: 3000 A to 8000 A

5.2.1 Incident light source: 5MW, He-Ne Laser - The important parameters of an incident light source for scattering purposes are amplitude, polarization, coherence, and frequency. The amplitude is an indication of total power per unit area. Polarization determines the orientation of the electric-field vector as a function of time in a plane perpendicular to the direction of propagation. This implies that a polarized wave forms a straight line lissajous figure on the plane. This can be done by passing unpolarized light waves through a Brewster's window.

The most important characteristics of a laser light source are its coherence and limited frequency range signal. This is the same as saying spatial coherence and temporal coherence. Spatial coherence allows the laser to be radiated in an extremely narrow beam. In the light scattering theories, this spatial coherence, which causes a perfect plane wave, is highly desired. The monochromaticity of the laser makes the scattering easy to evaluate. Actually, laser output can be composed of several discrete frequencies depending on the optical cavity length and power output. These are called the modes. In most lasers, many axial cavity modes may exist so that the overall output consists of radiation at a number of closely spaced frequencies. Due to the extremely close spacing, the total output can be considered as a monochromatic light source. (For instance, the laser electromagnetic wave is of order 10^{14} Hz, the axial mode spacing is of order 10^{8} Hz). Generally, random variations of the laser medium together with non-linear effects cause the modes to change in an unpredictable manner. (An acousto-optic mode-locker has been recently developed for stabilizing this mode shifting). The consequence of modes shifting is a change of overall power.

The dimensions of the Spectra-Physics Model 120 and the Model 256 exciter are shown in Figure 5.4. The manufacturer's description is found in Table 5.1. The maximum total power variation of the laser, after 40 minutes' warming up, is about 5%. Due to the imperfection of the hemispherical resonator, a diffraction pattern is always found. This diffraction for the laser is shown in Figure 5.5. This picture was taken by blocking the main laser beam with a 1 cm wide black strip. A focal plane shutter was used after removing the lens system in front of a Polaroid camera. In this wind tunnel diffusion experiment, the diffracted light was used as a monitor of the stationarity of the incident light intensity.

5.2.2 Light deflector: the mirror - Currently, a front surfaced mirror is the only means to direct a laser light beam without suffering loss of coherence. Theoretically, a coherent light could be directed by 2 layers of constantly flowing fluids which have different refractive indexes (Hellman, 1969). At the present time, the deflection of a coherent light beam relies on a front surface mirror.

In this light probe, a 12mm diameter front aluminum surfaced mirror was used to deflect the laser beam to the desired degree. The thickness of the mirror was 0.15^{mm}. The possible distortion on upstream flow due to the mirror is thus negligible. By proper construction of coating and incident angle, a mirror may reflect more than 95% of the incident energy. (The reflectivity of this mirror, however, is about 70%).

5.2.3 Light scatterers: DOP aerosols - Desirable characteristics of aerosol are as follows: First, the size of the aerosol particles will be large enough (compared with the incident light wavelength 6328 Å) to provide detectable scattering light. Second, the size should be small enough that the aerosol does not settle significantly. Third, the aerosol should be monodispersible, easily generated, and repeatable in preparation.

The aerosol substance used throughout this experiment was di-octyle phthalate (DOP, $C_6 H_4$ -1, 2 - $\left[CO_2 (C H_2)_7 C H_3\right]_2$, Aldrich Chemical Co., Milwaukee, Wisconsin, refractive index = 1.44, molecular weight =

390.56, specific density = 1.48). The aerosol generator utilized is a type of "Collison atomizer." A Collison type atomizer (see Figure 5.6) is actually a conventional air-blast atomizer. The difference is that a collison atomizer has a baffle to remove most of the coarse aerosol particles. Air-blast atomization is a very complex process. The mechanism of generating droplets from the bulk liquid has not been fully understood. A possible conceptual procedure may be as follows: First, small disturbances on the liquid surface are initiated from the air-liquid interaction when compressed air is applied. The strong shear due to the turbulent jet thus drags out fine ligaments from the bulk liquid stream. The ligaments finally collapse into droplets under surface tension.

There is no information on the real size distribution of these DOP particles. However, the same type atomizer was used on a similar aerosol liquid DBP (Di-butyle phthalate) with total pressure of 30 psi. The cumulative size distribution is shown in Figure 5.7 in both linear and logarithmic scales. One can see that almost 80% of the total aerosol particles range from 1.5 to 5 microns. In the aerosol industry, this type of distribution can be considered as monodisperse in aerosols. (The mean diameter is about 2.7μ). The operating pressure in this experiment is 10 psi which may cause a slightly larger mean droplet diameter. However, the characteristic size distribution may still remain the same. A mean diameter of 4μ will be used in subsequent calculations. In Appendix C, the aerosol size distribution is examined under a photographic microscope, the aerosol particles show a remarkably uniform distribution. The average size is about 4μ in diameter.

The fall velocity V_f of these aerosols in still air may be estimated by applying Stoke's law for falling spheres, i.e.,

$$V_f = \frac{(\rho - \rho') \ gd}{18q}$$

$$= \frac{1.48 \times 980 \times (4 \times 10^{-4})^{-2}}{18 \times 1.91 \times 10^{-4}}$$

$$= 6.96 \times 10^{-2} \text{ cm/sec}$$

where ρ = density of the DOP (1.48)

ρ' = density of the air (negligible compared to DOP)

g = gravitational acceleration

q = viscosity of air at 20^o C.

This relation is limited to those conditions where the ratio of inertia to viscous force parameter $Re(V_f \rho' d/\mu)$ is < 0.05 or $d \leq 1.96\mu$. For a particle size comparable to the mean free path of air, the aerosol fall velocity will be underestimated by using Stoke's law. This phenomenon is due to the "slip" of the aerosols between the air molecules. Cuningham (Green and Lane, 1964) has introduced a formula for the fall velocity correction. The corrected fall velocity is

$$V_{fc} = V_f \times (1 + \frac{2A\lambda}{d})$$

A = constant approximately equal to 1,

λ = mean free path of air for standard atmosphere 6.53×10^{-6} cm.

Thus, the corrected fall velocity for a 4μ diameter particle is estimated to be

$$V_{fc} = 6.96 \ (1 + 2 \times \frac{6.53}{400}) = 7.18 \times 10^{-2} \text{ cm/sec.}$$

The maximum total travel time is about seven seconds. The above calculation implies the maximum mean fall displacement will be 0.5 cm.

Another characteristic property of the aerosol particles is their "mobility" in a turbulent flow. This can be evaluated (Becker, et al., 1967) by assuming an aerosol "riding" on a sinusoidal motion with frequency (Becker, et al., 1967) and the rms value u'. Then the following relationship can be found:

$$\left(\frac{u'}{u}\right)^2 = \frac{1}{(1 + 2\pi f v_{cf}/g^2)}$$

or $\quad f = \sqrt{\left(\frac{u}{u'}\right)^2 - 1} \; \frac{g}{2\pi v_{cf}} \quad$, if $\quad \frac{u'}{u} = 0.9, \quad f \cong 1050$ cps.

The calculation indicates that the aerosols can follow 90% fluctuation amplitude up to 1050 cycles per second.

In practice, coagulation, sedimentation, and absorption of aerosols on the wall are complicating factors. DOP is a physically nonvolatile substance, thus it will persist for a long time in a state of non-equilibrium of vapor pressure between aerosols and the ambient. Therefore, the variation of aerosol sizes by change of phase is very slow.

Aerosol particles may be lost after generation when they are transported through channels or tubes. The effects are due to two factors; namely, diffusion and sedimentation. The combined effects have not yet been treated simultaneously. Such a loss of aerosol can be estimated by assuming that the deposition of particles is due to the collision of aerosols with the tube wall (Green and Lane, 1964).

$$n/n_o = 4 \left[0.1952 \exp \left(-7.313 \frac{K\ell}{2r^2 v}\right) + 0.243 \exp \left(-44.5 \frac{K\ell}{2r^2 v}\right) + \cdots \right]$$

where K is the diffusivity and ℓ is the radius of the tube, V is the mean velocity and r is the diameter of the aerosols. When $V^2 \gg K\ell$, the loss due to such deposition is negligible. In this experiment, V^2 approximately exceeds $K\ell$ by the order of 2.

Coagulation of aerosols may be the most important aerosol sink in practice. When particles strike each other and stick together, the average size will gradually increase with time. A useful method to estimate the rate of coagulation is as follows:

$$\frac{dn}{dt} = kn^2 \quad .$$

k is called the coagulation coefficient which varies with the aerosol. Usually, for small particle concentration, k is very small ($\sim 7 \times 10^{-8}$ cm^3/min). Thus, a decrease in number concentration takes several minutes to reduce by one order. In these experiments, the maximum duration of the diffusion process is less than 8 seconds. Thus, the number of particles may be assumed to be constant.

5.2.4 <u>Optical aperture</u> - An optical aperture was mounted at the very end of the fiber optics. The main purpose of the optical aperture was to increase the spatial resolution of the sample volume. The real dimension is shown in Figure 5.8.

The inside surface of this optical aperture was coated with a least-reflective black paint (optical black paints, Edmund Scientific

Company, No. 606 08) to minimize the undesired light. This also maximized the solid angle for the given sample volume.

5.2.5 Scattered light transmitter: fiber optics - The combination of optical aperture and fiber optics is equivalent to a lens-aperture system as shown in Figure 5.9. The advantage of using fiber optics is its flexibility and light weight. The light conducting property offers a prospective future for constructing a compact light detection probe.

The transmission of the scattered light is based on the internal reflection in each glass or plastic fiber (diameter is of order 10^{-3} inch). Like any other light transmitter, fiber optic transmission also involves transmission losses which are always frequency dependent. This loss in light transmission efficiency may be attributed to end losses and line losses:

a. End losses - These are due to the Fresnel losses from reflection at both entrance and exit faces. Other losses at both ends are due to the voids between fibers. Thirty percent of the incident light is unavailable as a result of such end losses. (Fresnel losses may be reduced by a special optical coating).

b. Line losses (or line attenuation) - These losses are due to absorption during the process of transmission through the fibers. The fiber optics used herein are shown in Figure 5.10. Figure 5.11 shows the light transmission characteristics versus wavelength. The percentage transmission for this fiber optics at 6328Å is about 50%.

5.2.6 Scattered light sensor: RCA photomultiplier tube 7265 - A light sensor is a device to convert light energy to electrically measurable signals such as resistance drop or current variation. A photomultiplier is actually a combination of a light sensor and a low-noise amplifier. The energy conversion is from photon kinetic energy to an electrical current. A load resistor is usually applied to convert current into a voltage mode.

An RCA - 7265, 14-stage photomultiplier was used to probe the scattered light after transmission through the fiber optics. Figures 5.12 and 5.13 show the dimension outline and basing diagram. Figures 5.14 and 5.15 show the typical spectral response characteristics and sensitivity diagram. The sensitivity A and B in Figure 5.15 are due to the two typical circuitries which serve as voltage-divider arrangements. These are shown in Figures 5.16 and 5.17. The circuitry in Figure 5.16 was used in this experiment. Arrangement B is essentially for "low" light level experiments incorporating photon counting. The operating voltages in this experiment were 2,000, 2,500 and 2,800 VDC.

5.2.7 The overall system

a. Overall system construction - Total probe configuration is shown in Figures 5.18 and 5.19. The laser was stored in a 7.6 x 10.2 x 71.1 cm wooden box. The main scattering probe was mounted on the laser with a 2.54 cm x 32-in thread adapter. The supporting frame was made of 1.27 cm - OD and 0.63 cm - OD brass tubes. The 12^{mm} diameter mirror was carefully glued on the gradually tapered end of the brass-tube truss.

The relative position between the reflecting mirror and the optical aperture was so constructed that the scattering angle was small ($\sim 12^{o}$). Only a small fraction of the diffracting light was allowed to enter the fiber optics receiver. This small portion of diffracting light was used to monitor the stability of the laser light.

Since the laser output was vertically polarized, the scattered energy was maximum on the plane perpendicular to the polarized plane. The sample volume was slightly in front of the system so that the blockage effect would be minimal. In Liu's probe (1972) the ¼" gap between two fiber optics might have a significant blocking effect.

The RCA - 7265 pM tube was covered by a dielectric magnetic shield (Millen, No. 80802E, J. Millen Co., 150 Exchange St., Malden 48, Mass.). The shield was directly connected to the metal collar which is at a high negative potential, (~2500V). The major purpose of the shield was to prevent the path of the secondary electrons from deviating due to the presence of any external electromagnetic fields. High caution is needed in handling the magnetic shield because of the high negative potential.

In this experiment, the shield was well insulated. The shield also served as a support to mount the pM tube to the wooden case in which the laser was located. In front of the pM tube, a blackened plexiglass cap was mounted on the magnetic shield (see Figure 5.21). A guide tube was used to position the outlet of the fiber optics. This forced all the transmitted scattered light to fall uniformly on the cathode surface. The whole system was thus in a compact, movable, and rigid state.

b. Spatial resolution - The spatial resolution was examined by injecting aerosols through a small diffuser (~0.07 cm I.D.) into the laser beam. The result was shown in Figure 5.21. The cross section of the laser beam was ~2 mm (from instruction manual). The sample volume was slightly greater than that of conventional hot-wire probes. However, the real sample volume is not critical since concentration is a scalar quantity.

c. Overall frequency response - The time constant of the pM tube (with a 30 ft operation signal cord 4659, of capacitance about 10 pf/ft) was calibrated by using a strobe light and a pulse light input and shown to be 0.8 m sec or 8 x 10^{-4} sec.

Another characteristic of a scattering probe is frequency response. For a high frequency square wave input, a probe may not be able to record the peak value. This was examined by passing a laser beam through holes on a fast rotating plate as shown in Figure 5.22. The maximum peak values for a given frequency were recorded and plotted in Figure 5.23.

The overall-system frequency response is the minimum between the optical system frequency response and the frequency response of the aerosols. For aerosols with diameter greater than 1 micron, the overall system frequency is usually dominated by the aerosol frequency response. This has been shown to be about 1050 cycles per second in section 5.2.3.

5.2.8 The possibility of measuring $\overline{u_i'c'}$ - The undefined term $\overline{u_i'c'}$ in Reynold's diffusion equation has been very difficult to measure in the laboratory. Using Boussinesq's assumption, one usually assumes the correlation term is directly proportional to the mean concentration gradient, but the need for measuring the actual correlation is apparent.

Way and Libby (1971) were the first to conduct such a measurement in a turbulent helium jet. They used a hot film and a hot wire delicately precalibrated for various concentrations and velocities. Since in certain concentration ranges the hot film is relatively insensitive to the velocity variation. The velocity signals from the hot wire could thus be separated by using the referenced concentration signals from the hot film. The process was carried out with a cubic-spline fitting of the calibration curve and separating the concentration output from velocity signals by a digital computation.

A complication of the hot wire experiment is that both velocity and concentration signals are due to heat transfer. It is more desirable that velocity and concentration signals be due to different mechanisms. It is proposed that the term $\overline{u_i'c'}$ can be measured by an optical system. A laser Doppler velocimeter may be developed to detect instantaneous velocity variation, but before the signals enter the signal processor, the DC variation actually indicates concentration variation. Typical Doppler frequency shifts are greater than 10 k Hz. The concentration fluctuation is usually below 3k Hz. The signals cannot be confused due to the different frequency ranges. To obtain the quantity $\overline{u_i'c'}$, one can simply correlate the signal directly from the pM tube and the signal frequency tracker.

Another relatively simple technique is to use the present laser light-scattering probe coupled with a conventional hot wire probe. Of course, the spatial resolution will be crucial. If a hot wire is placed very close to the sample volume and does not reflect the light, the local velocity fluctuating signals can be directly correlated with the concentration output. Using this method, one has to assume that the presence of aerosol particles will not distort the real velocity signals. Extremely high frequency signals may be detected from the velocity signals due to the aerosol impaction on a hot wire. However, these high frequency spikes can be discriminated by using a low-pass electronic filter (Sandborn, 1972).

Chapter VI

EXPERIMENTAL EQUIPMENT CALIBRATION AND LABORATORY TECHNIQUE

Chapter VI

EXPERIMENTAL EQUIPMENT CALIBRATION AND LABORATORY TECHNIQUE

The experimental measurements were carried out in the Meteorological Wind Tunnel at the Fluid Dynamics and Diffusion Laboratory, Colorado State University. The primary purpose was to determine time and space variation in a concentration field produced by ground released, instantaneous point source releases in a neutral turbulent shear layer. The calibration of the measuring apparatus and the experimental procedures are discussed in this chapter. A description of the light scattering probe and the puff release mechanism can be found in Chapter IV and Chapter V, respectively.

6.1 Calibration Procedure

Critical to the use of the light scattering probe as a quantitative measuring device is the assumption of a linear voltage output with respect to the number concentration. In Chapter V, it was proposed that for a relatively low aerosol concentration the scattered light energy is linearly proportional to the number concentration (for a fixed scattered angle and relative distance, of course). In the following calibration process, we verify this linear relationship.

6.1.1 The linearity of photomultiplier output versus input light energy - The linearity of the photomultiplier tube response was checked by using a set of 3.67 x 3.67 cm precise optical filters. These variable band-pass interference filters were supplied by Optics Technology, Inc., Palo Alto, California. The principle of checking the linearity is based on two known factors. First, the output light beam is monochromatic (λ = 6328 Å). Second, the laser is a light source of constant power. The transmission percentage for each optical filter is known versus wavelength. The filters were of multilayer dielectric design; they reflect rather than absorb. Of course, the light intensity of the laser beam was much too high to shoot directly into a photomultiplier tube. A double scattering from two pieces of photograph black paper was so adjusted that the input light intensity would not saturate the pM tube (maximum current = 1 ma). The output was plotted in Figure 6.1. Based on the results of these measurements, we confirmed the linear relationship between light energy and output voltage.

6.1.2 <u>Linearity of pM output versus concentration</u> - The next step was to examine the aerosol concentration versus pM output. These calibration processes were carried out in a 14 cm I.D. cast iron pipe. The pipe was 14 m long through which air was driven by a 1 hp fan. The experimental arrangement is shown in Figure 6.2. The DOP aerosols were injected into the far inlet. A set of screens (grid sizes >> aerosol sizes) were used to encourage mixing. The principle of this calibration is based on the mass conservation law, measured velocity profiles, and the same aerosol emission rate:

$$Q = 2\pi \int_0^{r_o} r \cdot \overline{C}(r)\, \overline{V}(r) dr, \quad r_o = 14 \text{ cm}.$$

After a perfect mixing process,

$$\overline{C}(r) = C_o;$$

hence,

$$C_o = \frac{Q}{2\pi \int_0^{r_o} r \cdot \overline{V}(r) dr} .$$

Since the emission of the aerosol was constant when applied pressure (10 psi) was constant, from the mass conservation law, one could simply change the total flow rate in order to change the diluted aerosol concentrations.

Figure 6.3 displays plots of $E - E_o$ vs. $1/V_{max}$. The upper part of the figure shows the corresponding operating voltages of the motor and the mean velocities. The results show the excellent linear correlation between the pM output and the concentration.

6.1.3 <u>Various applied voltage calibration</u> - Different levels of aerosol concentrations can be measured by varying the applied voltage of the photomultiplier tube. The voltage may be varied within the limitation that the maximum yield of current from the pM tube is 1 ma. If the input light, or the concentration in the sample volume, produces more than 1 ma, the tube will be "saturated."

The pM (photomultiplier) tube was calibrated for three applied voltages; namely, 2.0, 2.5 and 2.8 KDV. These results are shown in Figure 6.3. Because the mean velocity could only be adjusted over one order of magnitude, only one data point was taken for the case where applied voltage is equal to 2.0 KDV. The data shows the following relationship:

$$(E - E_o)\Big|_{2.0\ \text{KDV}} = 13.3\ (E - E_o)\Big|_{2.8\ \text{KDV}}$$

$$(E - E_o)\Big|_{2.5\ \text{KDV}} = 2.59\ (E - E_o)\Big|_{2.8\ \text{KDV}}$$

The results could also be obtained approximately from Figure 5.15.

6.2 Measurements

6.2.1 Wind tunnel - The Meteorological Wind Tunnel (Figure 6.4) at the Fluid Dynamics and Diffusion Laboratory, Colorado State University, was primarily designed to simulate atmospheric shear flows. A 25 m long test section provides a well-developed turbulent boundary layer. The pressure gradient along the test section can be controlled by a height adjustable ceiling. The air speed can be regulated to values from -2 to 35 m/sec. The source location was set 1.0 m from the aluminum plate or 11 m from the entrance contraction.

6.2.2 Velocity - To provide maximum diffusion time, the free stream velocity was set at the small value of 1.17 m/sec. A hot-wire anemometer was used to measure the mean and rms values in the fully developed turbulent boundary layer. The mean velocity profile plotted on semi-log paper suggested that the values of roughness parameter z_o, and shear velocity $u*$ in

$$\frac{u}{u_*} = \frac{1}{\kappa} \ln \left(\frac{z}{z_o}\right)$$

are 0.94×10^{-5} m, and 0.0582 m/sec, respectively. Figure 6.5 displays the mean velocity, rms velocity, and turbulent intensity in the boundary layer region utilized.

Velocity measurement was taken at 4 meters from the source. The boundary thickness (~28 cm) growth in this region is relatively small. In this study, the flow is assumed to be fully developed and stationary.

6.2.3 Puff measurements - Puffs were produced from the bubble generator (see Chapter IV). The applied pressure of compressed air was maintained as 10 psi. The first T-valve was used to exhaust the aerosol cloud to the ambient. The sequence of test operations was:

1. Flipped the cup in the bubble generator face upward.
2. Switched on the glass valve and exhausted the aerosol for 3 seconds.
3. Flipped the cup upside-down.
4. Filled the cup with aerosol cloud.
5. Waited for approximately 5 seconds to assure that all the exhausted aerosol passed downstream, then started the FM tape recorder. Flipped the cup about 90° to release the aerosol cloud.
6. The capacitance gauge output, which indicated bubble passage was examined on the screen of the oscilloscope to make certain that the bubble released uniformly. Six releases were recorded for each station.
7. Moved the L.L.S.P. to the next station.
8. Repeated the entire process.

The measuring stations were:

x(m) = 0.5, 1.0, 1.5, 2.0, 2.5, 3.0, 3.5, 4.0 m

y(cm) = 0, 5, 10, 15, 20, -10, -20

z(cm) = 0, 7, 14, 23.

A schematic diagram of the experimental arrangement is shown in Figure 6.6.

6.2.4 <u>Short period plume measurements</u> - The schematic diagram for the short period plume measurements is shown in Figure 6.7. Time triggering was controlled by a 1-volt power supply monitored by an Ortec - 482 electromechanical timer.

The sequence of operations were as follows:

1. The aerosol cloud was exhausted to the ambient through the T-valve.
2. The FM tape recorder was started.
3. The T-valve was opened to pass aerosol from the source and the timer set. Tape recorder Channel 1 recorded a square-wave signal of 1 volt. Channel 2 recorded the concentration signal for a given station.
4. After 1 minute, the timer shut off the square wave to Channel 1. Simultaneously, the aerosol supply was turned off.

Note that all operations, except the automatic shut off done in step 4 by the electromagnetic timer, were manual. The time lag due to human reflex is in the order of 0.1 sec. In step 3, for instance, to switch on the aerosol supply and set the time, the accuracy in time lag is adequate, compared with the delaying and decaying period. These periods were in the order of seconds. The measuring stations were:

a. $y = z \cong 0$

   $x(m) = 0.5, 1.0, 1.5, 2.0, 2.5, 3.0, 4.0, 4.5, 5.0, 5.5.$

b. $x = 4.0^m$

   $y(cm) = 0, 5, 10, 20.$

   $z(cm) = 0, 7, 14, 23, 30.$

At the stations $(y = z = 0)$ $x = 0.5^m$ and $x = 1.0^m$, due to the higher concentration, the applied voltage used was 2.5^{KDV}. At the station $(y = z = 0)$ $x = 1.5^m$, the applied voltage was 2.5^{KDV} at all other stations, 2.8^{KDV} was applied.

Chapter VII

METHOD OF DATA AVERAGING

Chapter VII

METHOD OF DATA AVERAGING

7.1 Problems of Analyzing Puff Data

Since the purpose of this study is to obtain the mean puff shape with time and space, only the "instantaneous mean" is of interest. As a result of the inherent randomness of turbulent processes we found that for a given flow condition and measuring location the sample outputs did not fall onto an identical trace. Hence, one must rationalize a data averaging process.

One may take a given signal trace as a realization of a random process for each defined $t = t_o$. If a large amount of data is available, i.e., when the amount of data approaches infinity, all of the traces at the defined time $t = t_o$ should converge to the local ensemble mean. For a small amount of data, however, we may not perform the same process of ensemble averaging. One must avoid smoothing to the point of losing information of the characteristic shape of the output signals. This problem frequently occurs in the construction of a hydrogram which indicates the time dependent discharge of a reservoir (see Figure 7.1). Since the number of these records is generally few, the averaging process conventionally applied is to take the "analog" average of the average peak p and the average peak arrival time t_p. The final output still contains the mean values of the important parameters of the hydrogram, i.e., p and t_p.

Important parameters which describe the character of a diffusion process are the moments. The author has investigated various possible frequency distributions to approximate the puff dispersion output traces. An optimum distribution function should contain the following properties.

a. An integrated dosage which is equal to the estimated mean integrated dosage,

b. An average arrival time, which is equal to the estimated mean value, and

c. Characteristic shape factors, which are represented by the estimated mean shape factors.

We shall use the concept of statistical estimation from given samples. The difference between this situation and the usual statistic is that one does not perform an estimation on data which belongs to the same process. On the contrary, we are estimating six groups of distribution curves. We are weighing six groups of continuous distribution functions instead of weighing numerous discrete data points. From the prescribed three conditions, we shall attempt to construct a unique representative curve from the estimated mean statistical moments. If we examine the commonly utilized skewed distribution curves, such as gamma, beta, etc., we find it difficult to satisfy the mutually-correlated statistical parameters. Hence, one seeks a generalized distribution function which has independent statistical moments.

7.2 Curve Fitting by Gram-Charlier Distribution

Most distribution functions are unimodal, i.e., the derivative vanishes only at one point. These types of curves may be fitted by various methods; namely, power series, Fourier series, Hermite polynomials, etc. These are so composed that the coefficients may be found by using the relationship between orthonormal sets. In this situation we intend to retain primarily the statistical moments of a concentration profile, hence, a Gram-Charlier series is the proper choice. In the past it has been the general practice, in diffusion investigations, to find only the second moment of concentration distribution. The skewed shape of a plume has been of concern only when the diffusion process was in a flow where strong shear was present. Since the diffusing aerosol studied herein underwent strong shear, one must calculate higher order moments. Characteristics of such distribution functions are discussed in the following paragraphs.

If one starts with a random variable $s = \sum_{n=1}^{n} s_i$ where the s_i's are sets of independent random variables, then for each set s_i with the mean m_i and standard deviation σ_i, we can obtain the similar expression

$$m = \sum_{i=1}^{n} m_i$$

$$\sigma^2 = \sum_{i=1}^{n} \sigma_i^2 \ .$$

De Moivre's theorem (Cramer) stated that if s_i's have the same distribution, the asymptotic trend of the distribution function $f(s-m/\sigma)$ approaches a standard normal, i.e.,

$$\lim_{i\to\infty} f\left(\frac{s-m}{\sigma}\right) \to \frac{1}{\sqrt{2\pi}} e^{-1/2 \left(\frac{s-m}{\sigma}\right)2} = \phi\left(\frac{s-m}{\sigma}\right) \ .$$

This result can also be obtained by using the central limit theorem.

If we use the "standardized variable" $z = s-m/\sigma$, then any distribution function can be written as the sum of a standard normal plus a perturbed function or residual $r(z)$, i.e., for $z \varepsilon C^2$

any $f(z) = f\left(\frac{s-m}{\sigma}\right) = \phi(z) + r(z)$.

We can extend this idea to the statistical distribution families, i.e., any standarized distribution function, can be approximated as perturbed normal distribution functions. Thus, we may write the approximated function as

$$f(z) = \sum_{i=1}^{\infty} \frac{a_i \phi^{(i)}(z)}{i!} .$$

Note that there is an identity which plays an essential role in this error function-like series, namely

$$\phi^{(i)}(z) = (-1)^i H_i(z)\, \phi(z)$$

where $H_i(z)$ is the Hermite polynomial of degree i. The first six terms are:

$$H_0 = 1$$
$$H_1 = z$$
$$H_2 = z^2 - 1$$
$$H_3 = z^3 - 3z$$
$$H_4 = z^4 - 6z^2 + 3$$
$$H_5 = z^5 - 10z^3 + 15z$$
$$H_6 = z^6 - 15z^4 + 45z - 15.$$

The orthogonal relationship of Hermite polynomials is

$$\int_{-\infty}^{\infty} H_m H_n \,\phi(z)dz = \begin{cases} n! & \text{for } m = n \\ 0 & \text{for } m \neq n \end{cases} .$$

Using this identity, one can find the coefficients

$a_o = 1$ from the definition of a distribution function

$$\left.\begin{aligned} a_1 &= 0 \\ a_2 &= 0 \end{aligned}\right\}$$ from the normalization

$$a_3 = - \int_{-\infty}^{\infty} f(z)\, z^3\, dz = - \text{ skewness (sk)}$$

$$a_4 = + \int_{-\infty}^{\infty} f(z) z^4 dz - 3 = \text{Flatness} - 3 = \text{Excess (Ex)}$$

$$a_5 = - \int_{-\infty}^{\infty} f(z) z^5 dz + 10 \text{ sk}$$

$$a_6 = + \int_{-\infty}^{\infty} f(z) z^6 dz - 15 \text{ Ex} + 15.$$

Therefore, one finally obtains the following expression

$$f(z) = \phi(z) + \frac{sk}{3!} \phi^{(3)}(z) + \frac{Ex}{4!} \phi^{(4)}(z)$$

The cumulant function can thus be written as

$$F(z) = \Phi(z) + \frac{sk}{3!} \Phi^{(3)}(z) + \frac{Ex}{4!} \Phi^{(4)}(z)$$

Φ is the cumulant function of ϕ. The explicit form is obtained by using the identity,

$$\phi^{(i)} = (-1)^i H_i(z)\, \phi(z) \quad ,$$

and one obtains $f(z) = (z)\left(1 + \frac{sk}{6} H_3(z) + \frac{Ex}{24} H_4 + \cdots\right)$

The convergence of this series is also discussed by Cramer (1957). If the integral

$$\int_{-\infty}^{\infty} e^{z^2/4}\, dF(z)$$

or

$$\int_{-\infty}^{\infty} e^{z^2/4} f(z) dz$$

is convergent, the series is always convergent. As a matter of fact, only a very small class of functions do not converge. In the general practice the convergence property of the expansion will not cause any serious difficulty. This is because it is usually sufficient to use only a few terms to give a good approximation.

The order of magnitude of the terms of the Gram-Charlier series is not steadily decreasing as i increases. That is,

i =	3	(4,6)	(5,7,9)	(8,10,12)	(11,13,15)
order of magnitude	$n^{-1/2}$	n^{-1}	$n^{-3/2}$	n^{-2}	$n^{-5/2}$

where n is the number of data points.
The power series can thus be arranged in a manner so that terms with the same order of magnitude are grouped. (This type of expansion was also given by Edgeworthe.) The expansion of the order n^{-1} reads:

$$f(z) = \phi(z)\left[1 + \frac{sk}{6} H_3 + \frac{Ex}{24} H_4 + \frac{1}{120} \; sk^2 \; H_6\right] .$$

The average number of digitized data points for each concentration trace is in the order of 50. Thus, one can obtain the following estimation:

$$0 \; (n^{-1/2}) \sim 0.15$$

$$0 \; (n^{-1}) \sim 0.01 \qquad .$$

In order to express characteristics of the time-dependent signal, the first 4 moments have been listed for each location in Table 7.1. There were 6 tests for each station. The mean and the variances for each moment for each station were also calculated. The integration of the total signal was listed under MO which indicated the 0^{th}

moment. k1, k2, k3, k4 are called the first four cumulants. The cumulants are directly related to the estimated moments, i.e.,

$$k1 = \int_0^\infty c(t)\ t\ dt$$

$$k2 = \int_0^\infty c(t)\ (t-k1)^2\ dt$$

$$k3 = \int_0^\infty c(t)\ (t-k1)^3\ dt$$

$$k4 = \int_0^\infty c(t)\ (t-k1)^4\ dt\ .$$

The mean values of MO, mean, sigma, skewness and flatness can be used to reproduce the original analog signals. Typical examples for the puff distribution are shown in Figure 7.1 through Figure 7.3 for ground level concentrations on the center line. Note that the measurable "ground level" was about 8^{mm} above the wind tunnel floor due to the physical limitations of the probe. a, b, c, d, e, f indicate the digitized points for the six different tests.

In order to examine the correctness of the computed moments, a standard normal together with the given moments,

Mean = 0.0

$\sigma = 1$

Skewness = 0

Flatness = 3. (Ex = 0.)

was used to confirm the moments computation. The explicit form of the computation formula is:

$$f(z) = \frac{1}{\sqrt{2\pi}}\ e^{-z^2/2}\ \left(1 + \frac{1}{6}\ sk\ H_3 + \frac{Ex}{24}\ H_4 + \frac{1}{72}\ sk^2\ H_6\right)\ .$$

In other words, the formula which is used to "reproduce" the original output would be:

$$f(\tau) = \frac{MO}{\sqrt{2\pi}} \quad e^{-\tau/2} \left[1 + \frac{1}{6} \text{ sk } H_3(\tau) + \frac{Ex}{24} H_4 \; (\tau) \right.$$

$$\left. + \frac{1}{72} \; sk^2 \; H_6 \; (\tau) \right]$$

where $\tau = \frac{t-t \text{ mean}}{6}$.

7.3 Illustrative Examples

A computer program was used to verify the "goodness of fit" of the Gram-Charlier series for a given standard distribution. Obviously, for a standard normal, where

$$\phi(z) = \frac{1}{\sqrt{2\pi}} \quad e^{-z^2/2}$$

with the skewness = 0 and the Excess = 0, then the Gram-Charlier series is identical to the exact functional form of $\phi(z)$. (Here we only consider the accuracy up to the order of n^{-1}.)

Table 7.2 provides a listing of computer program (CHARLI) and its results. Consider the three curves in Figures 7.4 and 7.5. The solid curve represents the exact form of a given gamma distribution, i.e.,

$$f(x) \;=\; \Big[f \; (x, \; r, \; \lambda) \Big] \;=\; \frac{\lambda}{\Gamma(r)} \;\; (\lambda z)^{r-1} \;\; e^{-\lambda z}$$

where $\Gamma(r) = \int_0^\infty x^{r-1} \; e^{-z} \, dx$. The dashed line indicates the Gram-Charlier series of 3 degrees of Hermite polynomials, or to the order of $n^{-1/2}$. The curve indicated with the dots provides the result from the Gram-Charlier series of the order of n^{-1}.

One can see that even in the order of $n^{-1/2}$, the fitting curve is very close to the true gamma distribution. For the order of n^{-1}, the fitting is slightly better. Note the comparison was carried out in the original coordinate x instead of the normalized coordinate. This was done by applying the transformation pair:

$$\begin{cases} z = \dfrac{x-m}{\sigma} \\ x = z\sigma + m . \end{cases}$$

Chapter VIII

MATHEMATICAL ANALYSIS OF TURBULENT DIFFUSION FROM AN INSTANTANEOUS POINT SOURCE

Chapter VIII

MATHEMATICAL ANALYSIS OF TURBULENT DIFFUSION FROM AN INSTANTANEOUS POINT SOURCE

From the law of mass conservation and the incompressibility condition, the diffusion equation in a convective flow field reads:

$$\frac{\partial c}{\partial t} + u_i \frac{\partial c}{\partial x_i} = \frac{\partial}{\partial x_i} D_M \frac{\partial c}{\partial x_i} \qquad i = 1.\ 2.\ 3.$$

in which D_M is molecular diffusivity. In a turbulent flow, when a perturbation theory is used to represent the turbulent behaviors, one obtains:

$$c = \overline{c} + c'$$

$$u_i = \overline{u}_i + u_i' \quad .$$

After applying Reynold's averaging process, the equation becomes:

$$\frac{\partial \overline{c}}{\partial t} + \overline{u}_i \frac{\partial \overline{c}}{\partial x_i} = \frac{\partial}{\partial x_i} \overline{c'u_i'} + \frac{\partial}{\partial x_i} (D_M \frac{\partial \overline{c}}{\partial x_i}) \quad .$$

Based on the observation, that the molecular diffusion is at least three orders less than the turbulent diffusion terms;

$$\frac{\partial}{\partial x_i} D_M \frac{\partial \overline{c}}{\partial x} << \frac{\partial}{\partial x_i} \overline{c'u_i'}$$

the molecular diffusion terms can thus be neglected. By means of the same order-of-magnitude analysis, the longitudinal diffusion is at least 2 orders less than the convective term:

$$\frac{\partial}{\partial x} \overline{c'u'} << u \frac{\partial \overline{c}}{\partial x}$$

and the longitudinal diffusion term can also be neglected. (This is true for both continuous plume and instantaneous puffs.) In a fully developed turbulent flow, $\overline{u}_2 = \overline{u}_3 = 0$. The final equation utilized for diffusion in a turbulent field is:

$$\frac{\partial \overline{c}}{\partial t} + \overline{u}_i \frac{\partial \overline{c}}{\partial x_i} = \frac{\partial}{\partial x_2} \overline{c'u_2'} + \frac{\partial}{\partial x_3} \overline{c'u_3'} .$$

For the sake of clarity, the bars which indicate the averaged quantities will not be used hereafter; thus in meteorological coordinates, the governing equation is:

$$\frac{\partial c}{\partial t} + u \frac{\partial c}{\partial x} = \frac{\partial}{\partial y} \overline{c'v'} + \frac{\partial}{\partial z} \overline{c'w'} \tag{8.1}$$

If one introduces the eddy diffusivities concept, i.e.,

$$K_y \frac{\partial c}{\partial y} = \overline{c'v'} \quad , \quad K_z \frac{\partial c}{\partial z} = \overline{c'w'}$$

equation (8.1) can be written as:

$$\frac{\partial c}{\partial t} + u \frac{\partial c}{\partial t} = \frac{\partial}{\partial y} (K_y \frac{\partial c}{\partial y}) + \frac{\partial}{\partial z} (K_z \frac{\partial c}{\partial z}) . \tag{8.2}$$

The justification of introducing eddy diffusivities has been briefly discussed in Chapter V.

The functional form of the mean velocity profile in a turbulent boundary layer was discussed by Prandtl in 1925. He introduced the concept of "mixing length," ℓ, and assumed ℓ is proportional to the distance from the wall, i.e.,

$$\ell = \kappa z ,$$

where κ is Von Karman's constant. The turbulent stress $\overline{\rho u'w'}$ thus becomes:

$$\rho\overline{u'w'} = \rho\, \ell^2 \left(\frac{\partial u}{\partial z}\right)^2 = \rho\, k^2\, z^2 \left(\frac{\partial u}{\partial z}\right)^2 \quad .$$

Prandtl, again, assumed a constant shearing stress across the boundary layer, i.e.,

$$\frac{1}{k} \sqrt{\frac{\tau_o}{\rho}} = - \frac{u_*}{\kappa} = \text{constant}$$

where κ is Von Karman's constant and is equal to 0.4 in the air flow, u_* is the shearing velocity. After all these assumptions, the famous logarithmic profile is obtained. In a neutrally stratified turbulent flow, the turbulent Schmidt number Sc may be assumed equal to unity. Thus, the diffusivity in the z direction K_z can be written as:

$$K_z = \kappa\, u_*\, z \quad .$$

This was suggested by Ellison (1959) and confirmed by Pasquill (1966).

The functional form of K_y is still not known. There have been many hypotheses. The most common ones are to assume a simple constant relationship (Rao, Nee, and Yang, 1971):

$$K_y \propto K_z \quad \text{or,} \quad K_y = \text{const.}\ K_z$$

Another suggestion (Davies, 1951) was to use a power law form; i.e.,

$$K_y = A\, u^{1-n}\, z^m \, .$$

For most applications, instead of seeking the functional form of K_y and K_z the variations of standard deviations, σ_y and σ_z are mainly concerned.

8.1 Prior Solutions for the Statistical Behavior of Instantaneous Line Sources

An analytical solution for line puffs (with linear diffusivity and a logarithmic velocity profile) was first examined by Chatwin in 1968. He applied the Lagrangian similarity theory and Aris' moment transformation to the instantaneous line-puff analysis. The exact solution for the first moment was found by Chatwin. Putta (1971) performed a complicated analysis to obtain the second moment of the two-dimensional diffusing cloud, and he estimated the 3rd moment of the cloud concentration at the ground level. Note that all the previous mathematical solutions are only for instantaneous line source. The results will be summarized as follows:

The governing partial differential equation for the diffusion process from a two-dimensional, ground released, instantaneous line source is:

$$\frac{\partial L}{\partial t} + \left(\frac{u_*}{\kappa} \; \ln \frac{z}{z_o}\right) \frac{\partial L}{\partial x} = \frac{\partial}{\partial z} \left(\kappa \; u_* \; z \frac{\partial L}{\partial z}\right) . \tag{8.3}$$

(Note: It is essentially the same as integrating equation (8.1) over y domain.)

Initial condition: $L = \delta \; (t, \; x = z = 0)$

Boundary conditions: $K_z \left.\frac{\partial L}{\partial z}\right|_{z=0} = 0$

$$L, \quad \nabla L \to 0 \quad \text{as} \quad \begin{array}{l} x \to \pm\infty \\ y \to \pm\infty \\ z \to \infty \end{array} .$$

By integrating equation (8.3) over x and substituting the proper boundary conditions, one can reduce the sum of the orders of the differential equation by one:

Let

$$L\ (x,\ z,\ t) = L_*\ (z,t)\ f\ (x|z,t)$$

then,

$$L_*(z,t) = \int_{-\infty}^{\infty} L(x,z,t)dx\ . \tag{8.4}$$

Equation (8.3) thus becomes:

$$\frac{\partial L_*}{\partial t} = \frac{\partial}{\partial z}\ (\kappa\ u_*\ z\ \frac{\partial L_*}{\partial z})\ .$$

In statistical terms, L_* is called "marginal concentration distribution." One thus readily obtains the following solution (Carslaw and Jaeger, 1959) for L_*:

$$L_*(z,t) = \frac{1}{\kappa u_* t}\ \exp\ (-\ \frac{z}{\kappa u_* t})\ .$$

The next step is to seek the concentration distribution in the x-direction $f(x|z,t)$ which is lost in the integration process (8.4). At this point the Lagrangian similarity theory is involved. The concentration distribution L is assumed to be dependent upon two similarity parameters as suggested by Batchelor (1957); namely,

$$\beta = \frac{x-\bar{x}}{a u_* t}\ ,\quad \eta = \frac{z}{\kappa u_* t} \tag{8.5}$$

and

$$\sigma_x,\ \sigma_y,\ \sigma_z \propto u_* t \tag{8.6}$$

therefore,

$$L\ (x,z,t) = \frac{1}{a\kappa (u_* t)^2}\ F\ (\beta,\eta)\ . \tag{8.7}$$

By using the similarity theory, the sum of the order of the governing differential equation was reduced by one.

The trajectory of the center of gravity of the cloud is obtained by taking the first moment of equation (8.3) and substituting the result into L_*. The result reads:

$$\frac{d\overline{x}}{dt} = \frac{u_*}{\kappa} \int_0^\infty \ell n \left(\frac{z}{z_o}\right) \frac{1}{u_* t} e^{-\frac{z}{\kappa u_* t}} dz = \frac{u_*}{\kappa} \ell n \frac{\kappa u_* t}{z_o e^\gamma}$$

where $\overline{x} = \int_{-\infty}^{\infty} x \cdot L(x, z = \text{const.}, t) dx$

where γ(Euler's constant) = $0.5772 \cdots$

and

$$\overline{x} = \frac{u_* t}{\kappa} \left[\ell n \frac{u_* t}{z_o e^\gamma} - 1\right] \quad . \tag{8.8}$$

The height of the center of gravity of the cloud $\overline{z}$ can be obtained in the similar manner. It reads:

$$\overline{z} \left(\ell n \frac{\overline{z}}{z_o} - \gamma - 1\right) = \kappa^2 \, \overline{x} = \kappa u_* \, \ell n \frac{\kappa u_* t}{z_o e^\gamma} \quad . \tag{8.9}$$

Thus the trajectory of a puff can be described as:

$$\overline{x} = \frac{\overline{z}}{\kappa^2} \left[\ell n \frac{\overline{z}}{z_o \; e^{\gamma+1}}\right] \quad . \tag{8.10}$$

Using the given trajectory, one proceeds to seek the functional form of $F(\beta, \eta)$. The partial differential equation in β-η space is:

$$\eta \frac{\partial^2 F}{\partial \eta^2} + (\eta+1) \frac{\partial F}{\partial \eta} + \left(\beta - \frac{1}{a\kappa} \ell n \; \eta \; e^\gamma\right) \frac{\partial F}{\partial \beta} + 2F = 0 \tag{8.11}$$

Aris' moments method is now used to evaluate the moments from the transformed dynamic equation (8.11) instead of seeking an exact solution form. The sum of the orders in equation (8.11) is, again, reduced to one less order in the integration process. This is demonstrated as follows:

$$\text{let} \qquad B_n(\eta) = \int_{-\infty}^{\infty} \beta^n \cdot F(\beta,\eta) d\beta$$

which is the nth moment about the c.g. of the cloud in the transformed x-direction β. The transformed boundary conditions are

$$B_n(\eta) \to 0 \quad , \quad \text{for} \quad \eta \to \infty$$

and

$$F(\beta,\eta) \to 0 \quad \text{as} \quad \beta,\eta \to \infty$$

$$\eta \frac{dB\eta}{d\eta} \to 0 \quad \text{as} \quad \eta \to 0 \; .$$

A series of ordinary differential equations can be obtained by taking moments from equation (8.11) together with the assumption of similarity:

$$n = 0 \qquad \eta \frac{d^2 B_o}{d\eta^2} + (\eta+1) \frac{dB_o}{d\eta} + B_o = 0$$

$$n = 1 \qquad \eta \frac{d^2 B_1}{d\eta^2} + (\eta+1) \frac{dB_1}{d\eta} = - \frac{B_o}{a\kappa} \ell n \; \eta \; e^{\gamma}$$

$$n = 2 \qquad \eta \frac{d^2 B_2}{d\eta^2} + (\eta+1) \frac{dB_2}{d\eta} - B_2 = - \frac{2B_1}{a\kappa} \ell n \; \eta \; e^{\gamma}$$

$$n = k \qquad \eta \frac{d^2 B_k}{d\eta^k} + (\eta+1) \frac{dB_k}{d\eta} - (\eta-1) \; B_k = \frac{-kB_{k-1}}{a\kappa} \ell n \; \eta \; e^{\gamma} \; .$$

Applying integration by parts, Chatwin obtained $B_o(\eta) = e^{-\eta}$ and

$$B_1(\eta) = \frac{e^{-\eta}}{a\kappa} (\ell n \; \eta + \gamma - 1) + \frac{E_1(\eta)}{a\kappa} \tag{8.12}$$

where $E_1(\eta) = \int_\eta^\infty \frac{e^{-\eta}}{\eta} d\eta$. The function $E_1(\eta)$ can be found in a standard integration table.

The difficulty of solving the set of differential equations increases as η increases. Numerical integration is made difficult by the singularity at the ground level. Putta (1971) performed a tedious integration by using the identity:

$$\lim_{\eta \to o} E_1(\eta) + e^{-\eta} \ell n (\eta e^\gamma) \to 0 \ .$$

He obtained the vertical distribution of the standard deviation of the cloud. It reads:

$$B_2(\eta) = \frac{1}{a^2\kappa^2} \quad 2E_1(\eta) \ 1 + \ell^2 e^{-\eta} (\eta+2) - 2\eta E_1(\eta)$$

$$+ 3 e^{-\eta} - (\eta+1)\Gamma''(1,\eta) + 2\gamma\Gamma'(1,\eta) + \gamma^2 e^{-\eta} \tag{8.13}$$

where $\Gamma''(a,\eta) = \frac{\partial^2\Gamma}{\partial a^2}(a,\eta) \int_o^\infty (\ell n \ t)^\eta e^t t^{a-1} dt$

(incomplete gamma function)

$\ell = \ell n (\eta e^{-\gamma})$. The predicted variation of the standard deviation is so small in the vertical that it may be approximated by a constant. Putta also investigated the value of the third moment at the ground level, $B_3(\eta = 0) \cong -\frac{2.267}{a^3\kappa^3}$. The normalized third moment, i.e., the skewness, is about -1.02.

8.2 Present Contribution

8.2.1 The gamma distribution approximation - Three moments of the concentration distribution are sufficient to approximate a distribution.

Following the same arguments as found in Chapter VII, the Gram-Charlier distribution is appropriate. The distribution in the x-direction thus reads:

$$f(\beta) = \frac{e^{-\frac{\beta^2}{2}}}{\sqrt{2\pi}} \left[1 + \frac{1}{6} \lambda_3 \; H_3 \; (\beta) + \cdots\right] .$$

Therefore, if one used the calculated three moments, one may approximate the distribution function at the ground level as:

$$f(\beta) = \frac{1}{\sqrt{2\pi}} \left[1 - 1.02 \; H_3(\beta)\right] \; e^{-\frac{\beta^2}{2}}$$

$$= \frac{1}{\sqrt{2\pi}} \left[1 - \frac{1.02}{6} \; (\beta^3 - 3\beta)\right] \; e^{-\frac{\beta^2}{2}} . \qquad (8.14)$$

Putta has indicated that the variation of σ_x is not sensitive to height z and neither is λ_3. One may thus claim that the overall distribution is,

$$F(\beta,\eta) = \frac{1}{\kappa u_* t \; \sqrt{2\pi}} \left[1 - \frac{1.02}{6} \; (\beta^3 - 3\beta)\right] \; e^{-\frac{\beta^2}{2} - \eta} \qquad (8.15)$$

where η is a normalized variable in z-direction defined as $z/\kappa u_* t$.

The distribution is plotted (dashed line) in Figure 8.1. One may ask if the distribution could be classified as a specific standard distribution since the Gram-Charlier distribution only gives a general form. There are several advantages to the use of a standard distribution function. First, one can obtain a better functional feeling for the behavior of the distribution curve. Second, the moments are always available and defined. Third, the negative exponent is reduced to the first order. Fourth, the intermittent "negative concentration" can be avoided.

To approximate a distribution function is a problem of estimation in statistics. For a distribution which does not show great skewness, a moment estimate method is appropriate (Kendall and Sturt, 1963). Several things must be considered in selecting a standard distribution function:

1. In the normalized coordinate system, β and η, the standard deviation should be one.
2. The definite termination trend for the measured puff is one-sided. One can see the trend of termination is definite for positive β but not for negative β. The long tail in the downstream side was due to the presence of strong shear. The upstream side has a definite trend toward termination because of the finite convective velocity and finite diffusion transport.

A gamma distribution has been selected to approximate this function. Its choice is based on the above two arguments.

Now let one examine the basic gamma distribution:

$$G(x) = \frac{\lambda}{\Gamma(\gamma)} (\lambda x)^{\gamma-1} \; e^{-\lambda x} \qquad 0 < x < \infty \tag{8.16}$$

where $\Gamma(\gamma) = \int_0^\infty z^{\gamma-1} \; e^{-z} \, dz$. From the moment generating function $(\lambda/\lambda-\tau)^\gamma$ we can obtain the first three normalized moments, namely:

$$\text{mean} = \frac{\gamma}{\lambda}$$

$$\text{standard deviation} = \frac{\sqrt{\gamma}}{\lambda}$$

$$\text{skewness} = \frac{1}{\gamma^{1/2}} \; .$$

Examining the general shape of a gamma distribution, one has to apply the following transformation:

$$x' = \text{mean} - x$$

in order to fit the longitudinal distribution. This is actually an inverse gamma distribution. From Figure 8.1 the value of the positive termination is about 2.3. Therefore we have three equations to be satisfied:

$$\text{mean} \qquad \frac{\gamma}{\lambda} = 2.3$$

$$\text{standard deviation} \qquad \frac{\sqrt{\gamma}}{\lambda} = 1$$

$$\text{skewness} \qquad \frac{2}{\gamma^{1/2}} = 1 \; .$$

If we have three equations with two unknowns, one is dealing with an overdetermined system. (If there is no equation linearly dependent of any others, we may also call it inconsistent.) Since not all of these equations are linear equations, we cannot apply linear programming techniques to seek the optimum point. However, a least-square principle can still be used.

Now we are seeking a point (γ_o, λ_o) in the set (see Figure 8.2) $\left[\gamma < 2.3\lambda, \;\; \delta > \lambda^2, \;\; \gamma > 4\right]$ which satisfies the following condition that $E = (\gamma_o - 2.3\,\lambda_o)^2 + (\gamma_o - \lambda_o^2)^2 + (\gamma_o - 4)^2 = \text{minimum}$, i.e.,

$$\frac{\partial E}{\partial \gamma_o} = 0 \quad ; \quad 6\gamma_o - 2\lambda_o^2 - 4.6\lambda_o - 8 = 0$$

or

$$3\gamma_o - \lambda_o^2 - 2.3\ \lambda_o - 4 = 0 \quad , \tag{8.17}$$

$$\frac{\partial E}{\partial \lambda} = 0\ ; \quad 2.3(\delta_o - 2.3\ \lambda_o) + (\delta_o - \lambda_o^2)2\lambda = 0 \quad , \tag{8.18}$$

so

$$\gamma_o = \frac{\lambda_o^2}{3} + \frac{2.3}{3}\lambda_o + \frac{4}{3} \quad . \tag{8.19}$$

Substituting equation (8.19) into equation (8.17), one obtains

$$\lambda_o^3 - 1.73\lambda_o^2 + 0.63\lambda_o - 2.3 = 0 \quad .$$

The only real root of this cubic equation was calculated by using IBM's Subroutine POLRY. (IBM's scientific subroutine package.) The root is:

$$\lambda_o = 1.9859 \quad \text{and} \quad \gamma_o = 4.1704 \ .$$

The result of the inverse gamma distribution is shown (solid line) in Figure 8.1. The author has chosen to use the values:

$$\lambda_o = 2.0$$

$$\gamma_o = 4.0$$

for convenience. The inverse gamma distribution was plotted in Figure 8.3. The similarity profile was plotted as a dashed line.

Note that one cannot justify which distribution, the Gram-Charlier series, or inverse gamma, is a better estimate of the exact cloud concentration distribution, unless higher moments are obtained. The reasons for choosing the inverse gamma distribution have been stated at the beginning of this section. In addition, one may claim that the solution is in a closed form if a standard distribution is used. By "closed form", we mean the integrated value is exactly unity (definition of a distribution function).

Using the chosen values ($\lambda_o = 2$, $\gamma_o = 4$), one can immediately write down the similarity profile as:

$$G(\beta) = \frac{2.0}{\Gamma(4)} \left[2 \cdot (2-\beta)^{(4-1)}\right] e^{-2(2-\beta)} \qquad (\beta=-\infty,2) \qquad (8.20)$$

where $\Gamma(4) = 3 \times 2 \times 1 = 6$

$$G(\beta) = \frac{8}{3} (2-\beta)^3 \; e^{-2(2-\beta)} \quad .$$

If we use the explicit form, the function will read:

$$G(x,t|z) = \frac{8}{3}\left[2 - \frac{x-\bar{x}}{au^* t}\right]^3 \; e^{-2\left[2 - (\frac{x-\bar{x}}{au^* t})\right]} \qquad (\beta=-\infty,2) \qquad (8.21)$$

where $\bar{x} = \frac{u_* t}{\kappa} \left[\ell n \frac{\kappa u_* t}{z_o e^{\gamma}} - 1\right]$.

Hence, the complete approximate solution for a ground released, instantaneous line source must be

$$L(x,z,t) = \frac{8}{3} (2 - \frac{x-\bar{x}}{au_* t})^3 \; e^{-2(2 - \frac{x-\bar{x}}{au_* t})} \cdot \frac{1}{\kappa u_* t} \cdot e^{-(\frac{z}{\kappa u_* t})} \qquad (8.22)$$

8.2.2 <u>Instantaneous point source</u> - In Monin and Yaglom's book (p. 641), "Statistical Fluid Mechanics," it is stated that

> "No single explicit analytical solution of a non-stationary diffusion problem in a half-space $Z>0$, from an instantaneous point source, has apparently yet been obtained in any case of a wind velocity which varies with height."

Here we shall use the consequence of similarity theory and Hermite polynomials to approximate the solution. In section 8.2.1 we have already obtained the approximate analytical form of $L(x)$. The information concerning lateral dispersion from an instantaneous point source has been lost due to the integration:

$$L(x,z,t) = \int_{-\infty}^{\infty} c(x,y,z,t)dy \quad .$$

Using the concept of separation of variables, we may assume an infinite series solution, i.e.,

$$c(x,y,z,t) = L(x,z,t) \cdot \sum_{i=0}^{\infty} p_i w_i \left(\frac{y-\overline{y}}{gu_* t}\right) \tag{8.23}$$

If we again use the normalized coordinate $(y-\overline{y})/gu_*t$ (as a consequence of similarity theory) as the variable in the Gram-Charlier series for the expression of w_i, then the approximate solution reads:

$$c(x,y,z,t) = L(x,z,t)\ \phi \left(\frac{y-\overline{y}}{gu_* t}\right) \left(1 + \lambda_3 H_3 \left(\frac{y-\overline{y}}{gu_* t}\right) + \cdots\right) \tag{8.24}$$

(g is an unknown constant).

From the symmetric flow condition and plane homogeneity, the mean coordinate $\overline{y}$ equals zero and the skewness (of the concentration profile on x-y plane) vanishes. This is equivalent to a normal distribution.

$$c(x,y,z,t) = L(x,z,t)\ \frac{1}{\sqrt{2\pi}\ gu_* t}\ e^{-\left(\frac{y}{gu_* t}\right)^2/2} \quad . \tag{8.25}$$

From turbulence measurements over a flat plate, the turbulent quantities tend to have the following relation:

$$\overline{u'} > \overline{v'} > \overline{w'} \ .$$

Therefore, one can estimate, the magnitude g should be:

$$(0.4)\ k < g < a\ (1.5)\ .$$

In this study, g-value would be estimated from the measurements and is suggested to be ~1.

Chapter IX

EXPERIMENTAL RESULTS

Chapter IX

EXPERIMENTAL RESULTS

9.1 Puffs

9.1.1 Mean arrival time of puffs - Figure 9.1 shows the arrival time of the center of gravity of the puffs at the ground level. The standard deviation of the arrival time for a measuring station is also plotted. The delay time between the triggered signals (the peak of the second pulse from the capacitance gauge output) and the actual probable starting instant was about 0.3 seconds. The mean transport velocity is about 0.9 m/sec (regression coefficient = 0.994).

The arrival time based on the Lagrangian similarity theory has also been plotted, that is

$$\bar{x} = \frac{u_* t}{\kappa} \left[\ell n \frac{\kappa u_* t}{z_o e^{\gamma}} - 1 \right] \tag{9.1}$$

in which $\kappa = 0.4$ and $\gamma = 0.577$. In the measurements, $u_* = 0.0582$ m/sec and $z_o = 0.94 \times 10^{-5}$ m.

One then obtains

$$\bar{x} = 0.14t \ \ell n \ t + 0.9075t$$

and for

$$t = 0.5, \quad \bar{x} = 0.048 + 0.4537$$

while

$$t = 4 \text{ sec}, \ \bar{x} = 0.77 + 3.63.$$

One can see that the second term, i.e., the linear term is actually the dominant term in the computation. One can conclude that for a short release period the mean arrival time of puffs can be approximated by using the local mean convective velocity.

Figures 9.2 and 9.3 plot all the arrival times for different stations. Figure 9.3 shows the significance of a slightly higher transport velocity when the measuring stations are off the ground level.

9.1.2 <u>First arrival time and departure time of puffs</u> - Due to the finite transport velocity aerosol puffs will not be detected by the L.L.S.P. for an initial time lag. The time delay between release and the first detectable concentration is called "the first arrival time of a puff."

The first arrival time can be estimated by using the similarity profile. From the inverse-gamma profile there should be a definite time where the concentration becomes detectable, i.e., $(x-\overline{x})/au_*t = 2$. Therefore, for a certain downwind distance X_o, the first arrival time is the root of the following equation:

$$X_o - \frac{u_*t}{\kappa}\left[\ell n \frac{\kappa u_* t}{z_o e^\gamma} - 1\right] = 2au_*t$$

or

$$\frac{X_o}{t} - \frac{u_*}{\kappa} \ell n\ t - \left(\frac{u_*}{\kappa} \ell n \frac{\kappa u_*}{z_o e^\gamma} - \frac{u_*}{\kappa} + 2au_*\right) = 0 \ . \tag{9.2}$$

Apparently, the exact root of t cannot be expressed explicitly. The numerical solution was obtained by means of Newton's iteration method, (S.S.P., p. 226 subroutine RTNI). The numerical equation in this experiment is:

$$\frac{X_o}{t} - 0.145\ \ell n\ t - 1.0821 = 0 \ . \tag{9.3}$$

The accuracies of the roots are 0.0001. The results are plotted in Figure 9.4.

The departure time in this problem is defined as the time when the puff concentration drops to a negligible level after the puff passes a measuring station. From Figure 9.4 one can see that when $(x-\bar{x})/au_*t \leq -6$ the concentration will not be significant. The numerical values have also been obtained by applying Newton's iteration method. In Figure 9.4, departure time (I) indicates the roots of $(x-\bar{x})/au_*t \leq -6$, departure time (II) indicated the roots of $(x-\bar{x})/au_*t \leq -10$. The observed first arrival time and departure time can also be seen in Figure 9.4. The discrepancy between measurements and predicted behavior is most likely due to the fact that the sources were not perfect point sources.

9.1.3 <u>The statistical moments of puffs in the longitudinal direction</u> - The longitudinal standard deviation σ_x and the skewness of the aerosol puffs has been estimated analytically by Putta (1971). The predictions are

$$\left.\begin{aligned} \sigma_x &= au_*t = 1.5\, u_*t \\ \text{skewness} &= -1 \end{aligned}\right\} \text{ at the ground level .}$$

Since the variations of both σ_x and skewness for different heights are small, the data for the different heights can be compared against the prediction. Only the data within 8 cm from the wall was used because of the strong intermittency in light scattering signals beyond 8 cm. Figure 9.5 displays the σ_x's for different coordinate locations. An extrapolation indicates a non-zero value at $t=0$. This must be due to the fact that the source was not a "point" source.

Because of the relatively small diffusion rate compared to the mean convective velocity the puffs can be considered as "frozen" in pattern when passing through a measuring station. For a longer diffusion time, the frozen pattern will no longer exist. This will be discussed further in section 9.3.3. Thus at the ground level σ_x can be transformed (for short time periods) into the following form:

$$\sigma_x = au_* t = au_* \frac{\bar{x}}{\frac{u_*}{\kappa}\left[\ell n \frac{\kappa u_*}{z_o e^{\gamma}} - 1\right]} .$$

Figure 9.5 plots the measured σ_x's. The regressional line shown in Figure 9.5 shows the predicted a-value of 1.5 as being excellent (the regressional coefficient is 0.614). This is the first time that the a-value was ever examined in the laboratory.

The skewness estimated by Putta (1971) for such puffs is -1. In time domain, the skewness must then be +1. Figure 9.6 plots the skewness for the measured concentration distribution.

The predicted skewness appears to be slightly greater than the observed values. This may be because of the finite resolution of the L.L.S.P. Due to the presence of the strong shear near the ground level, the analytic concentration distribution tends to have an extremely long tail. This long tail with its small concentrations may not be detectable. However, this long tail will contribute a greater amount to the skewness than the standard deviation. (If one assumes a truncation of the signal to 1/50 of the local maximum, the adjusted predicted value would be 0.65 which is very close to the observed values.)

Figure 9.7 plots the measured flatness value from the concentration signals. The data suggests a quite constant value with time.

Note that the higher the calculated moments are, the larger the errors are due to both truncation and the limitation of concentration resolution.

Figure 9.8 plots the dimensions of λ_y and λ_z. These values were obtained from the representative curves at $t = t_{mean}$. The values λ_y and λ_z have been defined as in the distance between c_{max} and $\frac{1}{2}c_{max}$.

9.2 Plumes

In the short period release study, the arrival time of a plume has been defined as the period between the release time and the time when the L.L.S.P. detected ten percent of the local mean concentration value. The departure time is defined as the period between the shut-off time and the time when the L.L.S.P. detected ten percent of the local mean concentration.

Figure 9.9 shows the plots of the arrival time and the departure time. One can see that the longer departure time also results from the growth pattern due to the longitudinal shear.

Figures 9.10 and 9.11 display the local mean concentration values and concentration iso-pleths at $x = 4.0$ m. These results show similar patterns to those detected by Chaudhry and Meroney (1969). Figure 9.12 shows the arrival time of the plume at the y-z plane for $x = 4.0$ m.

9.3 The Upper Limit Condition of a Puff - Continuous Source

For a fixed point in a stationary flow field, the integrated concentration rates due to a puff through time t should be equal to the local mean concentration for a continuous source. This relationship exists when the initial source geometries are identical. Malhotra and Cermak (1964) have demonstrated that $c_{max} \propto x^{-1.4}$ for a continuous ground released source. However, the experiment was conducted in a somewhat thinner boundary layer still undergoing relatively rapid growth.

Chaudhry and Meroney (1969) obtained

$$c_{max} \propto x^{-1.78} \quad \text{(for neutral case)}$$

for ground released continuous sources in the same wind tunnel used herein. The results for the integrated puff outputs and the continuous plume releases are plotted in Figure 9.13. This is probably the first experimental evidence to prove the long accepted integration relationship between an instantaneous puff and a continuous release.

9.3.1 Numerical integration of the similar puff profile - The numerical integration of the proposed similarity profile has been accomplished on a CDC 6400 digital computer. The equations integrated are

$$\chi_{\text{continuous line source}} = \int_{t_a}^{t_d} L(x,z,t)\,dt \tag{9.4}$$

$$= \int_{t_a}^{t_d} \frac{8}{3}\left(2 - \frac{x-\bar{x}}{au_*t}\right)^3 e^{-2\left(2 - \frac{x-\bar{x}}{au_*t}\right)} \frac{1}{\kappa u_* t}\, dt \tag{9.5}$$

$$\chi_{\text{continuous point source}} = \int_{t_a}^{t_d} c(x,y,t)dt \quad .$$

The numerical values for the experimental conditions studied herein have been substituted under the integral. The resulting expressions are:

$$\chi_{\substack{\text{continuous line} \\ \text{source at ground} \\ \text{level}}} = \int_{t_a}^{t_d} \frac{8}{3} \left(2 - \frac{x-\overline{x}}{0.873t}\right)^3 e^{-2\left(2 - \frac{x-\overline{x}}{0.873t}\right)} \frac{1}{0.0233t} dt \tag{9.6}$$

$$\chi_{\substack{\text{continuous point source} \\ \text{at ground level}}} = \int_{t_a}^{t_d} \frac{1}{\sqrt{2\pi}} \frac{1}{u_* t} \cdot L(x,z=0,t)dt \tag{9.7}$$

in which $\overline{x}$, arrival time t_a, and departure time t_d can be obtained by Newton's iteration method described in section 9.1. Figure 9.14 shows the integrated curve and a comparison with previous measurements of continuous sources. The results are summarized in the following tabulated form:

	Continuous Line Source	Continuous Point Source
Malhotra & Cermak (1964)	$c_{max} \sim x^{-0.85}$	$c_{max} \sim x^{-1.4}$
Chaudhry & Meroney (1969)	$c_{max} \sim x^{-0.75}$	$c_{max} \sim x^{-1.78}$
Integrated value from similar profile	$c_{max} \sim x^{-0.80}$	$c_{max} \sim x^{-1.63}$

9.3.2 <u>Determination of the lateral diffusion constant g</u> - One of the most important assumptions in the similarity theory is that the puff dimensions, in terms of plume standard deviations σ_x, σ_y, σ_z are linearly proportional to the products of shear velocity u_*, and travel time t , i.e.,

$$\sigma_x = ay_*t$$

$$\sigma_z = bu_*t$$

$$\sigma_y = gu_*t \ .$$

The values of a and b have been estimated analytically. For the logarithmic velocity profile and linear diffusivity profile, the estimated values are 1.5 and 0.4 respectively. The lateral diffusion constant g has not yet been evaluated. This section will be devoted to this investigation.

As we suggested in Chapter V, the complete solution for a ground released puff is equation (8.25). A sensible estimation for g might be $b < g < a$. This is suggested since the lateral spread of a puff is usually greater than the vertical spread. The large longitudinal spread is due to the dominant shear effects. Since the constant g will not change the slope of a $\log c_{max}$ vs. $\log x$ plot, the only means to estimate its value is to examine the value of a local measured concentration relative to a given source strength Q.

A convenient set of experimental data is the work of Chaudhry and Meroney (1969) for a ground released, continuous point source where

$$Q = 20 \ \mu c_i/\text{c.c.}$$

$$c_{x=1m} = 3\text{x } 10^3 \ pc_i/\text{c.c.} \quad \text{at} \quad y = z = 0 \ .$$

From equation (8.25), we obtain:

$$\left.\frac{Q}{g}\right|_{x=1m} = \frac{20 \times 126.7}{g} = 3 \times 10^3$$

so

$$g \sim 0.854 \sim 1.0 \; .$$

Figure 9.8 shows the good agreement of the puff data with the value of $g = 1.0$.

9.3.3 The Eulerian-Lagrangian relationship in puff measurements - An identifying feature on Lagrangian similarity theory is that one conceptually follows the center of gravity of a puff. Experimentally, more than one probe would be necessary to find the relationship between the Lagrangian mode of the puffs behavior and the Eulerian signals of our measuring devices. However, if only one probe is available, there is need to find the transformation which relates a Eulerian output with Lagrangian behavior.

In the experiment the actual signal outputs appear in the time domain (from the realization records). The obvious question to ask is, "If one obtains a standard deviation from a concentration signal measured at a fixed distance, what can one say about the spatial dimensions of a puff at a time t_o?" In Appendix A, a computer experiment has been developed to demonstrate the characteristic signal distributions caused by measuring at a fixed point in time. A simple forced diffusion model was chosen: isotropic growth of a one-dimensional puff in a homogeneous flow. In the space domain, the functional form of C is designed to always have a Gaussian distribution. However, in the time domain, the signals will be skew (dependent upon the rate of diffusion). In other words, after a long diffusion period, a linear time-space transformation may introduce errors.

It is of interest to recreate the L.L.S.P. signals by means of a similarity model. We shall assume that: the descriptive function

$$\overline{x}(u_*,t) = \frac{u_* t}{\kappa} \left(\ln \frac{\kappa u_* t}{z_o e^{\gamma}} - 1\right)$$

is correct. For this study, the description function is

$$\overline{x}(t) = 0.14t \ln t + 0.90t \quad .$$

We must also assume the descriptive function of concentration, equation (8.25), is correct.

As a consequence, then the descriptive function $\{c(x,y,z,t)$ and $\overline{x}(t)\}$ is correct, which implies finally: for $y = z = 0$, the transformation $t = h(x,c)$ is correct. From the syllogism, the relation $t = f(x)$ could be obtained from the function $c(t,x) = 0$.

In order to compare the outputs for standard deviation and skewness, the process of numerical integration has been performed by using a CDC 6400 digital computer. Thus, the explicit form of $f(x)$ is not essential. The predicted functions in time space are shown in Figures 9.15 and 9.16. The calculated standard deviation (in terms of seconds) and skewness are shown in Figure 9.17. These figures show a very important result, i.e., for a short travel distance (corresponding a short travel time), the distribution space and time can be transformed according to Taylor's hypothesis: $X = Ut$ without risking great errors. When the dimension of a puff is small, the period required for a puff to pass a fixed point is short. In a short period, the diffusion is negligible compared to the mean convective motion. However, for a longer travel distance, the standard deviation in time space should not follow a simple linear transformation.

In Appendix A, the equivalent situation is to increase the diffusion velocity a. This effect must be considered in interpreting field data where the dimensions of puffs are usually large. For instance, in the study at Hanford Reservation, Washington (Nickola, 1971), the total period for a puff to pass a measuring station is of the order of 100 seconds. The direct transformation

$$\sigma_{x\ (\mathrm{space})} = U_{\mathrm{local}} \times \sigma_{x\ (\mathrm{time})}$$

should overestimate the real spatial standard deviation by a factor of two. This type of transformation was also used in evaluating the mass dispersion in an open-channel flow by Sayre (1968). The transport period of order 90 seconds also makes the direct transformation doubtful in the latter case.

9.4 Comparison with Field Data

The most recent field study for instantaneous puff behavior is reported by Nickola (1970, 1971). He used 64 Geiger-Müller tube sensors to measure the concentration profiles of a Krypton-85 puff at distances of 200 m and 800 m from the release point. Only those releases under neutral or near neutral stratification conditions, i.e., Run No. P_3, P_5, and P_6, have been selected for comparison. Values of u_* for these conditions were not reported. However, the vegetation is reported to be primarily sagebrush and steppe grasses; hence, z_o is assumed to be 5 cm (Pasquill, 1962). From the provided velocity profiles the friction velocity u_* for each case is estimated to be

Run No. P_3 ; $u_* = 0.364$ m/sec

Run No. P_5 ; $u_* = 0.690$ m/sec

Run No. P_6 ; $u_* = 0.625$ m/sec.

The mean arrival times are computed by using the mean transport velocities at 1.5 m as reported by Nickola.

Standard deviation values predicted by similarity theory and the field data are plotted in Figure 9.18. One can see that the standard deviation increases at a similar rate to the prediction. Figure 9.19 plots the ratios of λ_y to λ_z. The predicted value of 0.66 is apparently too high as compared with the observed data. This may be because the test grid did not fully cover the full dimensions of the puffs. Figure 9.20 displays the integrated concentration (or dosage) due to puffs. The slopes predicted by numerical integration (see section 9.3.1) are also plotted. The comparison appears reasonable.

Chapter X

CONCLUSIONS

Chapter X

CONCLUSIONS

The behavior of an instantaneous point source, as it disperses in a thick, neutrally stratified turbulent shear layer, has been examined by a laser light-scattering technique in the Meteorological Wind Tunnel at Colorado State University. An aerosol filled gas bubble was released in a column of water to subsequently rise and burst at floor level of the wind tunnel. This "pseudo instantaneous source" was proposed as a means to obtain optimum source geometry, repeatability, and avoid mechanical blockage to the flow field.

Time dependent concentrations at a point were monitored by measuring the scattered light from a coherent light source by a photomultiplier-fiber optics probe. This lightweight mobile probe provided extremely fast response to a rapidly changing signal. Future modification to permit concentration flux measurements are very promising.

Data consists of a series of six concentration realizations per point tested downstream from the ground level source. The distributions have been described by selecting appropriate moments of a Gram-Charlier series by using analog averages. Puff dispersion characteristics have been compared with predictions of the Lagrangian Similarity Diffusion Theory. It has been demonstrated that the inverse-gamma distribution demonstrates all the significant behavior variations of the measured plume or puff. Substitution of this standard distribution function for the functionally more complicated Gram-Charlier series may provide a major simplification to future statistical analysis.

The Eulerian-Lagrangian relationship in a time-dependent convective diffusion process was examined. It was shown that for a laboratory scale diffusion process (<7 seconds), the error of assuming a frozen puff is insignificant. However, in the field study, this error usually is appreciable. The spatial geometric shape distortion in a time record was demonstrated in a simple computer experiment.

The field data collected by Pacific Northwestern Laboratory at Hanford Reservation, Washington have been compared with the similarity solution and found to be of the same order.

The theoretical analysis and the experimental results discussed earlier lead to the following significant conclusions:

1. The Lagrangian Similarity Theory provides a good approximation to the behavior of an instantaneous puff diffusing in a shear layer from a ground level.

2. The coefficients c and a suggested by Chatwin and Putta through integration of the diffusion equations are substantially supported by experimental measurements. Data suggests $b = 0.4 \pm 0.1$, and $a = 1.3 \pm 0.4$.

3. The lateral dispersion constant, heretofore unpredicted or measured was found to be $g = 1.0 \pm 0.1$.

4. Similarity Theory has been used to predict mean arrival time, first arrival time, and departure time. Puff behavior in the laboratory was essentially identical.

5. Integrated puff concentration measurements do agree with the results for continuous releases previously prepared.

TL 501
A38

BIBLIOGRAPHY

1. Batchelor, G. K., "An Introduction to Fluid Dynamics," Cambridge Press, 1967.

2. Batchelor, G. K., "Application of the Similarity Theory of Turbulence to Atmospheric Diffusion," Quart. J. of Royal Meteo. Society, Vol. 76, No. 328, pp. 133-140, 1950.

3. Becker, H. A., Hottel, H. C. and Williams, G. C., "Mixing and Flow in Ducted Turbulent Jets," Ninth International Symposium on Combustion, pp. 7-20, 1963.

4. Becker, H. A., Rosensweig, R. E. and Gwozdz, J. R., "Turbulent Dispersion in a Pipe Flow," A. I. Ch. Eng. J., Vol. 12, pp. 964-972, 1966.

5. Becker, H. A., Hottel, H. C. and Williams, G. C., "On the Light-Scatter Technique for the Study of Turbulent Mixing," J. Fluid Mech., Vol. 30, part 2, pp. 259-283, 1967.

6. Blifford, I. H., Jr., editor, "Particulate Models: Their Validity and Application," NCAR Technical Notes, NCAR-TN/PROC-68, August, 1971.

7. Brown, G. L. and Rebollo, M. R., "A Small, Fast-response Probe to Measure Composition of a Binary Mixture," AIAA Journal, Vol. 10, No. 5, pp. 649-652, 1972.

8. Carslaw, H. S. and Jaeger, J. C., "Conduction of Heat in Solids," Oxford at the Clarendon Press, 1971.

9. Cermak, J. E. and Arya, S. P. S., "Problem of Atmospheric Shear Flows and Their Laboratory Simulation," Boundary-Layer Meteorology, Vol. 1, pp. 40-60, 1960.

10. Cermak, J. E., "Lagrangian Similarity Hypothesis Applied to Diffusion in Turbulent Shear Flow," J. of Fluid Mechanics, Vol. 15, Part 1, pp. 49-64, 1963.

11. Cermak, J. E. et al., "Simulation of Atmospheric Motion by Wind Tunnel Flows," Colorado State University Technical Report CER66JEC-VAS-EJP-RNM-GJB-HC-SI-17.

12. Chandra, S., "Diffusion from an Instantaneous Point Source into a Turbulent Boundary Layer," Technical Report, CER-67-68SC7, Colorado State University, 1967.

13. Chatwin, P. C., "The Dispersion of a Puff of Passive Contaminant in a Constant Stress Region," Quart. J. Royal Meteo. Society, Vol. 94, No. 401, pp. 555-562, 1968.

14. Chaudhry, F. H. and Meroney, R. N., "Turbulent Diffusion in a Stably Stratified Shear Layer," Technical Report, CER69-70 HC-RNM12, Colorado State University, 1969.

15. Cramer, H. G., "A Practical Method for Estimating the Dispersal of Atmospheric Contaminants," Proceedings of the 1st National Conference on Applied Meteorology, pp. C-33 to C-55, American Meteorological Society, Hartford, Conn., October, 1957.

16. Cramer, H. G., "Mathematical Methods of Statistics," Princeton Press, 1957.

17. Davar, K. S., "Diffusion from a Point Source with a Turbulent Boundary Layer," Ph.D. dissertation, Colorado State University, 1961.

18. Davies, R. M. and Taylor, G. I., "The Mechanics of Large Bubbles Rising Through Extended Liquids and Through Liquids in Tubes," Proc. Royal Society, A200, No. 375, pp. 375-390, 1950.

19. Davies, D. R., "Three Dimensional Turbulence and Evaporation in Lower Atmosphere," I. Quart. Journal of Mechanics and Applied Mathematics, Vol. 3, pp. 51-63, 1951.

20. Denman, H. H., Heller, W. and Pangonis, W. J., "Angular Scattering Functions for Spheres," Wayne State University Press, Detroit, 1966.

21. Donaldson, C. duP. and Rosenbaum, H., "Calculation of Turbulent Shear Flow Through Closure of the Reynolds Equation by Invariant Modeling," A.R.A.P. Report 162, Dec., 1968.

22. Donaldson, C. duP. and Hilst, G. R., "Computing Dispersal of Atmospheric Pollutants Near Airports," Aeronautical Research Associates of Princeton, Inc., Report NASA, CR-111962, July, 1971.

23. Drake, R. L., "The Scalar Transport Equation of Coalescence Theory: Moments and Kernels," J. of the Atmospheric Sciences, Vol. 29, No. 3, pp. 537-547, April, 1972.

24. Egan, B. A. and Mehoney, J. R., "Numerical Modeling of Advection and Diffusion of Urban Area Source Pollutants," J. of Applied Meteorology, Vol. 11, No. 2, pp. 312-322, March, 1972.

25. Ellison, T. H., "Turbulent Transport of Heat and Momentum from an Infinite Plane," J. of Fluid Mech., Vol. 2, Part 5, pp. 456-466, 1957.

26. Exall, D. I., "A Study of the Use of Statistical Turbulence Parameters in Correlating Axial Dispersion Data in the Central Core of Air Flowing in a Pipe," Ph.D. dissertation, Dept. of Chemical Engineering at University of Natal, Durban, October, 1970.

27. Gartrell, F. G., Thomas, F. W., Carpenter, S. B., Pooler, F. U., Turner, B. B. and Leavitt, J. M., "Full Scale Study of Dispersion of Stack Gases," A Summary Report, Tennessee Valley Authority and Public Health Service, Chattanooga. Tennessee, 1964.

28. Gosline, C. A., "Dispersion from Short Stacks," Chemical Eng. Progr., Vol. 48, pp. 165-172, 1972.

29. Green, H. L. and Lane, W. R., "Particulate Cloud: Dust, Smokes and Mists," 2nd edition, Van Nostrand Company, Inc. 1964.

30. Gurnitz, R. N., "Development and Application of a Light Scattering Techniques for the Study of Premixed Turbulent Flames," Sc.D. thesis, Department of Chemical Engineering, Massachusetts Institute of Technology, Cambridge, Mass., 1966.

31. Harlow, F. H. and Amsedn, A. A., "Fluid Dynamics, A LASL Monograph," Los Alamos Scientific Laboratory of University of California, LA-4700, June, 1971.

32. Hellman, H., "Laser," USAEC, Division of Technical Information, 1969.

33. Herman, B. M., Browing, S. R. and Reagan, J. A., "Determination of Aerosol Size Distribution from Lidar Measurements," J. of the Atmospheric Sciences, Vol. 28, No. 5, pp. 763-771, July, 1971.

34. Hidy, G. M., "On Atmospheric Simulation: A Colloquium," NCAR Technical Notes, NCAR-TN-22, November, 1966.

35. Hino, M., "Computer Experiment on Smoke Diffusion over a Complicated Topograph," Atmospheric Environment, Vol. 2, pp. 543-558, 1968.

36. Hino, M., et al., "Relationship Among Meteorological Factors Affecting Concentration Distribution of Smoke," Technical Report No. 65049, CRIEPI (in Japanese), 1966.

37. Hinze, J. O., "Turbulence," McGraw-Hill Book Co., Inc., 1959.

38. Islitzer, N. F., "Aerodynamic Effects of Large Reactor Complexes Upon Atmospheric Turbulence and Diffusion," U.S. Weather Bureau, National Reactor Testing Station, Technical Report IDO-12041, Idaho Falls, Idaho, May, 1965.

39. Islitzer, N. F. and Slade, D. H., "Diffusion and Transport Experiments," Meteorology and Atomic Energy, USAGC, Division of Technical Information, pp. 117-197, 1968.

40. Kendall, M. G. and Sturt, A., "The Advanced Theory of Statistics," Vol. 1, Charles Griffin and Company Limited, 1963.

41. Kesic, D. M., "Diffusion of Heat from an Instantaneous Point Source in a Turbulent Boundary Layer," Technical Report CER66-67-DK45, Colorado State University, 1966.

42. Kitabayashi, K., "Turbulence Structure and Diffusion in Wind Tunnel Boundary Layer," Technical Report, Resources Research Institute, Tokyo, Japan, 1967.

43. Lapp, R. E. and Andrews, H. L., "Nuclear Radiation Physics," 3rd edition, Prentice-Hall, Inc., 1964.

44. Liu, Peter, H. T., "Mass Diffusion over Wind Waves," Ph. D. dissertation, College of Engineering, Colorado State University, February, 1972.

45. Malhotra, R. C. and Cermak, J. E., "Mass Diffusion in Neutral and Unstably Stratified Boundary-Layer Flows," Int. J. Heat Mass Transfer, Vol. 7, pp. 169-186, Pergamon Press, 1964.

46. Martin, J. G., "The Correlation of Wind Tunnel and Field Measurements of Gas Diffusion Using Krypton-85 as a Tracer," Ph. D. dissertation, University of Michigan, 1965.

47. McVehil, G. E., Ludwig, G. R. and Sundaram, T. R., "On the Feasibility of Modeling Small Scale Atmospheric Motions," Cornell Aeronautical Laboratory, Technical Report CAL Report No. ZB-2328-P-1, April, 1967.

48. Melngailis, I., "The Use of Lasers in Pollution Monitoring," Inst. Elec. Electron. Engrs., Trans. Geosci. Electron., Vol. 10, No. 1, pp. 7-17, January, 1971.

49. Meroney, R. N., "Experimental Investigation of the Effects of Transpiration Cooling on a Partially Dissociated Turbulent Boundary Layer," M.S. Thesis, Mechanical Engineering Department, University of California at Berkeley, 1963.

50. Meroney, R. N. and Yang, B. T., "Wind Tunnel Studies of the Air Flow and Gaseous Plume Diffusion in the Leading Edge and Downstream Region of a Model Forest," Technical Report ECOM #6, Colorado State University, November, 1969.

51. Monin, A. S. and Yaglom, A. M., "Statistical Fluid Mechanics," M.I.T. Press, 1970.

52. Monin, A. S., "Smoke Propagation in the Surface Layer of the Atmosphere," Atmospheric Diffusion and Air Pollution, edited by F. N. Frenkiel and P. A. Sheppard, Advance in Geophysics, Vol. 6, pp. 331-345, 1959.

53. Nee, V. W. and Kovasznay, "The Calculation of the Incompressible Turbulent Boundary Layers by a Simple Theory, Proc. Computations of Turbulent Boundary Layers," AFUSR-IFP-Stanford Conference, Vol. 1, pp. 300-319, 1968.

54. Nickola, P. W. and Ramsdell, J. V., Jr. and Ludwick, J. D., "Detailed Time-Histories of Concentrations Resulting from Puff and Short-Period Releases of an Inert Radioactive Gas: A Volume of Atmospheric Diffusion Data," Battelle Memorial Institute, Pacific Northwest Laboratories, Technical Report BNWL-1272, UC-53, February, 1970.

55. Nickola, P. W., "Measurements of the Movement, Concentration and Dimensions of Clouds Resulting from Instantaneous Point Sources," J. Applied Meteorology, Vol. 10, No. 5, pp. 962-973, October, 1971.

56. Orgill, M. M., Cermak, J. E. and Grant, L. O., "Laboratory Simulation and Field Estimates of Atmospheric Transport-Dispersion Over Mountainous Terrain," Technical Report CER70-71MMO-JEC-LOG40, Colorado State University, May, 1971.

57. Pasquill, F., "Atmospheric Diffusion," D. Van Nostrand Co., 1962.

58. Pasquill, F., "Atmospheric Dispersion of Pollution," Presidential Address delivered before the Royal Meteorological Society, April 21, 1971, Quart. J. Royal Meteo. Society, Vol. 97, No. 414, pp. 369-395, October, 1971.

59. Pasquill, F., "Lagrangian Similarity and Vertical Diffusion from a Source at Ground Level." Quart. J. Royal Meteo. Society, Vol. 92, pp. 185-195, 1966.

60. Putta, S. N., "Mass Dispersion from an Instantaneous Line Source in a Turbulent Shear Flow," Ph.D. dissertation, Colorado State University, June, 1971.

61. Rodliffe, R. S. and Fraser, A. J., "Measurements on the Release of Gaseous Activity from a Short Stack," Atmospheric Environment, Vol. 5, pp. 193-208, 1971.

62. Rolfe, E., Silk, J. K., Booth, S., Meister, K. and Young, R. M., "Laser Doppler Velocity Instrument," NASA Contractor Report NASA CR-1199, December, 1968.

63. Ruff, J. F. and Gelhar, L. W., "Porous Boundary Effects in Turbulent Shear Flow," Water Resources and Hydrodynamics Laboratory, Report No. 126, M.I.T., July, 1970.

64. Rosensweig, R. E., Hottel, H. C. and Williams, G. C., "Smoke-Scattered Light, Measurement of Turbulent Concentration Fluctuation," Chem. Eng. Science, Vol. 15, pp. 111-121, 1961.

65. Sandborn, V. A., "Resistance Temperature Transducers," Metrology Press, Fort Collins, Colorado, 1972.

66. Sayre, W. W., "Dispersion of Mass in Open-Channel Flow," Hydraulics Paper No. 3, Colorado State University, 1968.

67. Schlichting, H., "Boundary Layer Theory," McGraw-Hill Co., 1960.

68. Shih, C., "Continuous Point Source Diffusion in a Turbulent Shear Layer," M.S. Thesis, Colorado State University, 1966.

69. Sklarew, R. C., Fabrick, A. J. and Prager, J. E., "A Particle-in-Cell Method for Numerical Solution of the Atmospheric Diffusion Equation and Application to Air Pollution Problems," System, Science and Software Report, 3SR-844-I, November, 1971, (PB 209-290).

70. Slade, D. H., "Meteorology and Atomic Energy," USAEC, Division of Technical Information, 1968.

71. Smith, F. B. and Hay, J. S., "The Expansion of Clusters of Particles in the Atmosphere," Quart. J. of Royal Meteo. Society, Vol. 87, pp. 82-101, 1961.

72. Stewart, N. G., Gale, H. J. and Crook, R. N., "The Atmospheric Diffusion of Gaseous Discharges from the Chimney of the Harwell Pile (BGPO)," British Report AERE HP/P-1452, 1954.

73. Sutton, O. G., "A Theory of Eddy Diffusion in the Atmosphere," The Proceedings of the Royal Society, Series A., Vol. 135, pp. 143-165, 1932.

74. Taylor, G. I., "Diffusion by Continuous Movements," The Proceedings of the London Mathematical Society, Vol. 20, pp. 196-212, 1921.

75. Thiebaux, M. L., "Wiener-Hermite Expansion Applied to Passive Scalar Dispersion in a Non-Uniform Turbulent Flow," J. of the Atmospheric Sciences, Vol. 29, No. 3, pp. 510-516, April, 1972.

76. Thompson, N., "Short-Range Vertical Diffusion in Stable Condition," Quart. J. of Royal Meteo. Society, Vol. 91, pp. 175-184, 1962.

77. Turner, D. B., "Work-Book of Atmospheric Dispersion Estimates," U.S. Department of Health, Education and Welfare, Public Health Service, 1969.

78. Van De Hulst, H. C., "Light Scattering by Small Particles," John Wiley and Sons, Inc., New York, 1957.

79. Van Pelt et al., "A Review of Selected Bioeffects Thresholds for Various Spectral Ranges of Light," Laser Regulatory Standards (Drafts), Bureau of Radiological Health, U.S. Public Health Service, January, 1972.

80. Way, J. and Libby, P. A., "Application of Hot-Wire Anemometry and Digital Techniques to Measurements in a Turbulent Helium Jet," AIAA Journal, Vol. 9, No. 8, pp. 1507-1573, August, 1971.

81. Witte, A. B., Fox, J. and Rungaldier, H., "Localized Measurements of Wake Density Fluctuation Using Pulsed Laser Holographic Interferometry," AIAA Journal, Vol. 10, No. 4, pp. 481-488, April, 1972.

82. Yang, B. T. and Meroney, R. N., "Gaseous Dispersion into Stratified Building Wakes," Colorado State University Technical Report, CER70-71BTY-RNM8, August, 1970.

APPENDIX A

A Simple Stochastic Model for Describing the Functional Form of a Time-Dependent Diffusion Process in a Convective Field

From the typical skewed output curves in this experiment, one is able to deduce that the long tail of the curve in the time coordinate is due to the longer diffusion time and the presence of strong shear. The following analysis is to demonstrate the characteristic signal behavior which results from the difference in various diffusion times.

We shall assume the cloud from a one-dimensional instantaneous source grows in such a manner that the standard deviation of concentration distribution is a linear function of time t, i.e., $\sigma = at$. This assumption is consistent with the suggestion that the diffusion occurs in a constant flux layer. (Taylor, (1921) proved that σ is proportional to the $\sqrt{t}$ for long dispersion time in a homogeneous turbulence).

Next a simple model of isotropic diffusion is assumed, i.e., the spatial distribution is a normal distribution function. Thus we obtain:

$$C(t,x) = \frac{V}{\sqrt{2\pi}\, at} \exp\left(- \frac{X}{2a^2t^2}\right) .$$

Notice that when

$$X \neq 0, \quad C(t,x_o) = 0$$

$$X = 0 \quad \lim_{t\to 0} C(t,0) \to \infty \quad .$$

In a homogeneous flow field, the distance between a measuring point and the center of the cloud can be obtained by a simple coordinate transformation such as $X = X_o - Vt$. Where X_o is the original probing distance, V is the mean convective velocity. Thus the observed concentration at any instant t reads:

$$C(t) = \frac{V}{\sqrt{2\pi}\ at} \exp\left(\frac{(X_o-Vt)^2}{2a^2t^2}\right) \tag{A.1}$$

The mathematical properties of this distribution are described as follows:

(1) $X_o \neq Vt$, $\lim_{t\to 0} C(t) = 0$

(2) $X_o = Vt$, $\lim_{t\to 0} C(t) = \infty$,

0: otherwise.

The distribution reaches its maximum value when,

$$\frac{dc}{dt} = 0$$

or

$$t = \frac{X_o}{\sqrt{V^2+2a^2}} < \frac{X_o}{V} .$$

This delay time is due to diffusion effects.

If $V = 0$, the concentration distribution may be transformed by using

$$\xi = \frac{1}{t^2}$$

$$C(\xi,X_o) = \frac{V}{a\sqrt{2\pi}} \xi^{1/2} e^{-\frac{X_o}{2a^2}\xi} . \tag{A.2}$$

Notice that a standard gamma distribution has the form of $\frac{\lambda}{\Gamma(\gamma)} (\lambda x)^{\gamma-1} e^{-\lambda x}$. Thus the concentration distribution in a stagnant flow is a gamma distribution with two degrees of freedom (3/2 and $X_o/2a^2$) (Parzen, 1967). For $V \neq 0$, or in a convective flow field, the statistical properties of the concentration distribution cannot be obtained in closed functional form.

The zeroth moment, or the total observed mass is:

$$\frac{V}{a\sqrt{2\pi}} \int_o^\infty t^{-1} e^{-\frac{(X_o - Vt)}{2a^2t^2}} dt .$$

The result is expected to approach unity when $a \lll V$ (due to the conservation of mass), i.e.,

$$\int_o^\infty \frac{V}{a\sqrt{2\pi}} \frac{1}{t} e^{-\frac{(X_o - Vt)^2}{2a^2t^2}} dt \to 1 \ (a \ll V)$$

or

$$\int_o^\infty \frac{V}{a\sqrt{2\pi}} \frac{1}{t} e^{-\left[\frac{(V - X_o/t)}{\sqrt{2}a}\right]^2} dt \to 1 .$$

If we use the following transformation:

$$\xi = \frac{1}{\sqrt{2}a} \left(\frac{X_o}{t} - V\right) . \tag{A.3}$$

then the transformed boundary conditions will be:

$$t = 0, \quad \xi \to + \infty$$

$$t = \infty, \quad \xi \to - \frac{V}{\sqrt{2}a} .$$

From the transformation (A.3), one obtains

$$- \frac{dt}{t^2} = \frac{\sqrt{2a}}{X_o} \; \xi$$

$$dt = \frac{X_o}{(\sqrt{2a}\;\xi + V)^2} \times \frac{-\sqrt{2a}}{X_o} \; d\xi = \frac{-\sqrt{2a}\; X_o}{(\sqrt{2a}\;\xi+V)^2} \; d\xi$$

so

$$\int_o^{\infty} \frac{1}{a\sqrt{2\pi}} \; \frac{1}{t} \; e^{-\frac{(X_o - Vt)}{2a^2t^2}} \; dt$$

$$= \int_{\infty}^{-V/\sqrt{2a}} \frac{1}{\sqrt{2\pi a}} \; \frac{(\sqrt{2a}\;\xi+V)^2}{X_o} \; e^{-\xi^2} \; \frac{-\sqrt{2a}\; X_o}{(\sqrt{2a}\;\xi+V)^2} \; d\xi$$

$$= \frac{V}{\sqrt{\pi}} \int_{-V/\sqrt{2a}}^{\infty} \frac{e^{-\xi^2}}{V + \sqrt{\ a}\;\xi} \; d\xi$$

$$= \frac{V}{\sqrt{\pi}} \int_{-V/\sqrt{2a}}^{\infty} \frac{e^{-\xi^2}}{V + \sqrt{2a}\;\xi} \; d\xi + \frac{1}{\sqrt{\pi}} \int_o^{\infty} \frac{e^{-\xi^2}}{V + \sqrt{2a}\;\xi} \; d\xi$$

$$\rightarrow 1 \quad (a << V) \quad .$$

We thus obtain the identity:

$$1 - \frac{V}{\sqrt{\pi}} \int_o^{\infty} \frac{e^{-\xi^2}}{V+\sqrt{2a}\;\xi} \; d\xi = \int_o^{V/\sqrt{2a}} \frac{1}{\sqrt{\pi}} \; \frac{e^{-\xi^2}}{V+\sqrt{2a}\;\xi} \; d\xi \qquad \text{(A.4)}$$

The second term in equation (A.4) can be evaluated as follows:

$$V \int_{0}^{\infty} \frac{e^{-\xi^2}}{V + \sqrt{2a}\ \xi}\ d\xi$$

$$= \int_{0}^{\infty} \frac{e^{-\xi^2}}{1 + \frac{\sqrt{2a}}{V}\ \xi}\ d\xi$$

$$= \int_{0}^{\infty} e^{-\xi^2}\ (1 - A\xi + A^2\xi^2 - A^3\xi^3 + \cdots)d\xi \tag{A.5}$$

where $A = \frac{\sqrt{2a}}{V}$.

The following identities are used to evaluate equation (A.5)

$$\int_{0}^{\infty} e^{-\xi^2}\ d\xi = \frac{\sqrt{\pi}}{2}$$

$$\int_{0}^{\infty} z^{2n}\ e^{-z^2}\ dz = \frac{1\cdot 3\cdot 5\ \cdots\ (2n-1)}{2^{n+1}}\ \sqrt{\pi}$$

$$\int_{0}^{\infty} z^{2n+1}\ e^{-z^2}\ dz = \frac{n!}{2} .$$

Therefore, equation (A.5) becomes:

$$(\frac{\sqrt{\pi}}{2} - \frac{A}{2} + \frac{A^2}{4} \qquad - \cdots\cdot)$$

$$= \sqrt{\pi} \left[\sum_{n=0}^{\infty} A^{2n}\ \frac{1\cdot 3\cdot 5\cdots\ 2n-1}{2\ n+1} \right] + \sum_{n=0}^{\infty} \frac{n!}{2}\ A^{2n+1} .$$

The identity (A.4) thus reads:

for $a << V$,

$$\int_{o}^{V/\sqrt{2a}} \frac{e^{-\xi^2}}{V + \sqrt{2a}} \, d\xi$$

$$= \sqrt{\pi} - \sqrt{\pi} \sum_{n=0}^{\infty} \left(\frac{1 \cdot 3 \cdot 5 \cdots 2n-1}{2^{n+1}} - \sum_{n=0}^{\infty} \frac{1}{2V} \left(\frac{2a}{V}\right)^{2n+1} n! \right) \quad (A.6)$$

The next step is to seek the moments for this distribution. First we try the moment generating function:

$$m(t) = E\{e^{\tau t}\}$$

$$= \frac{V}{a\sqrt{2\pi}} \int_{o}^{\infty} e^{\tau t} \frac{1}{t} e^{-\frac{(X_o - Vt)^2}{2a^2 t^2}} dt$$

$$= \frac{1}{a\sqrt{2\pi}} \int_{o}^{\infty} e^{-\frac{1}{2a^2}\left(\frac{X_o}{t^2} - \frac{2VX_o}{t} + V^2 + 2a^2 \tau t\right)} dt \, .$$

Thus the nth moment with respect to $t = 0$ is equal to

$$\left. \frac{d^n m(\tau)}{d\tau^n} \right|_{\tau=0} \qquad (\tau \text{ is a dummy variable.})$$

Since the moment generating function is a complicated form, the exact integral is not available. A table has been obtained by using numerical integration. In Table A.1 the computer program TREVA is listed. In Table A.2, the maximum concentration value and its corresponding time t, together with the first four statistical moments are also listed.

The authors have named this particular function (A.1) the C-distribution. The C-distribution is a three parameter family, namely, X_o, V and a. When the ratio of diffusion to the mean convective motion is small, i.e., $a/V \ll 1$, the integration over time space approaches unity. Physically, this implies that: if $V \gg a$, all the diffusion matter will be detected by the observer. If $a \sim V$, part of the matter will be "permanently missing."

Figure A.1 indicates that for a long diffusion time (or a large diffusion velocity) the spatial distribution of a puff will not be the same as that of the realization at the measuring point. For instance, when $a/V > 0.1$, the realization curve indicates a significant skewness; however, the spatial distribution is always Gaussian.

APPENDIX B

Averaging Time Scale for Time-Dependent Concentration Measurements

In an unsteady diffusion process, problems arise as to what the minimum averaging time scale should be in defining the "instantaneous mean concentration." This is to say that a minimum characteristic time interval Δt is such that

$$\bar{c} = \int_{t_1}^{t_1+\Delta t} c\,dt$$

represents the instantaneous mean.

From the output signals (Fig. A.2), one can see that there exists a significant increase of D-C trend. Obviously, if one defines Δt as being of the order of 1 second, the averaged concentration will lose its significance; this implies that if the averaging time is of the same order as the time period for a puff to pass through a measuring point, the information contained will be distorted.

The definition of Δt can also be interpreted as follows: for any Δt_i such that

$$E\left[(\bar{c}_i \Delta t_i) t_i^n\right] \rightarrow \int_0^{\infty} c t^n \, dt$$

Δt_i is sufficiently long to avoid misrepresenting the local mean signal. This is equivalent to many stochastic processes where it is required that

$$E^n\left[\{E\ f(t)\right]\} \rightarrow E^n\{f(t)\} \quad ,$$

where E is the averaging function. A similar argument was used by

Sayre (1968) in defining the instantaneous concentration distribution from an instantaneous plane source in an open channel flow

In the experiment discussed herein Δt is chosen to be of the order of 0.1 sec. This is based on the arguments that Δt must be sufficiently large compared to the local Eulerian time scale T_E. T_E is defined as

$$T_E = \int_0^\infty R_{11}(\tau)\, d\tau \quad .$$

$R_{11}(\tau)$ is the autocorrelation function of u component. In a wind tunnel, the Eulerian time scale in a boundary layer is of the order 10^{-2} seconds or less (Baldwin and Johnson, unpublished paper, 1968). There are two major reasons why this time scale was chosen. First, the Eulerian time scale can be taken as a "snap-shot" of an "average eddy" passing through as measuring point. Second, this is a measurable quantity in any point of a turbulent flow. Since the average time of Δt is much greater than T_E, the average concentration is thus well defined.

APPENDIX C

Average Aerosol Size Determined by An Impingement Method

The size distribution of aerosol particles can be determined by various methods, namely, light scattering, filtering, electro-magnetic field chamber, etc. The more precise methods use the physics of light scattering because the scatterer size is a sensitive parameter of scattered light intensity (Van de Hulst, 1957).

In the present case, the authors chose to use available facilities to determine the approximate aerosol sizes. The procedure was to impinge the aerosol jet (mass jet) upon a clear glass plate. Only a few aerosol particles stayed on the glass plate after a period of five seconds. (This confirms the arguments in section 5.2.3 that zero deposition may be assumed.) The sample glass plate was then examined under a microscope (160x).

Figure A.3 displays a typical picture against a calibrated scale of 10μ. The sizes appear excellently uniform and close to the estimated mean aerosol size of four microns.

APPENDIX D

The Possibility of Constructing a Finite Lateral Concentration Distribution

In heat transfer and diffusion problems for the infinite boundary situations, solutions usually have distributions of exponential decay or error function. This suggests the anomalous idea that, instantaneously, at a finite distance from an instantaneous source, the temperature or mass concentration should always be finite. For instance, a normal distribution has a value of 1/4000th of the peak value at the distance of four standard deviations.

In a turbulent mixing motion, the local mean mass concentration is actually equivalent to the probability for a particle to reach a measuring point. The movement of a particle, at any instant, should still be constrained by the law of motion. This infinite diffusion velocity cannot be accepted as a realistic model.

The above prescribed problem has been discussed by Monin (1959). He assumed a maximum diffusion velocity and transformed the diffusion equation (parabolic form) into a hyperbolic form. This was a conceptual means to constrain the possibility of infinite velocity. Because of analytic difficulties, the solution was only obtained for a two-dimensional flow with a constant mean wind profile. Another apparent difficulty is the lack of information on the "maximum diffusion velocity." This is essentially the same as questioning the Hay-Pasquill coefficient which correlates the measurable Eulerian information with the Lagrangian behavior.

A compromise between the well-established parabolic diffusion equation and the hyperbolic equation is to take the results from the parabolic solution and to use a curve fitting technique to confine the distribution to a finite domain. The following example is used to describe the concept.

One of the standard Pearson distribution family with only a finite sample space is the beta distribution. The beta distribution has the following form:

$$f(x,a,b) = \frac{1}{\beta(a,b)} x^{a-1} (1-x)^{b-1} I_{(0,1)}$$

where $\beta(a,b) = \int_0^1 x^{a-1} (1-x)^{b-1} dx$. The sample space in this particular distribution is confined in the values between $x = 0$ and $x = 1$. The beta distribution may also be transformed into an arbitrary finite space by using $x' = d(x-e)$. If we wish to use the beta distribution to approximate the lateral concentration distribution (y-direction), the following constraints are needed to determine the two parameters a and b:

i) The profile is symmetric with respect to $y = 0$. This implies that $a = b$.

ii) This condition also indicates $e = 0.5$. The standard deviation of $f(x,a,b)$ is $\sigma_y = u_* t$, i.e.,

$$\sigma = \sqrt{\frac{ab}{(a+b+1)(a+b)^2}} = \frac{1}{2\sqrt{2a+1}} = u_* t \quad .$$

Note that there are still two constants d and a to be determined. The authors have chosen the following criteria to define d and a:

$$\left|\frac{f(x = 0.5)}{f(x = \sigma)}\right| + \left|\frac{f(x = 0.5)}{f(x = 2\sigma)}\right| = \text{minimum.}$$

This has been done by the trial and error technique. The final values chosen are $a = 4$, $d = 6$. Hence, the distribution is:

$$\frac{1}{\beta(4,4)} \left(\frac{9-x'}{36}\right)^3 \quad \text{or} \quad 140 \left(\frac{9-x'}{36}\right)^3$$

where $x' = y/u_*t$.

In Figure A.4, both the suggested beta distribution and the standard normal have been plotted. The chosen constraint $d = 6$ implies that the resulting maximum diffusion velocity is $3u_*$. The error involved in using the beta distribution to approximate a normal is that it predicts lower concentration in the center, and higher concentration off the centerline. This may not be an ideal way to confine diffusion rates because of the apparent difference in functional behavior between the two distributions. However, it does eliminate the anomaly of infinite diffusion velocity.

Table 1.1 Summary of Recent Quasi-Instantaneous-Source Experiments

Experiment	Location of experiment	Number of releases and maximum sampling distance	Sampled material and sampling method	Height of release and release duration	Type of terrain	Initial source size and temperature	Parameters directly measured
(Smith and Hay, 1961)	Porton Downs, England	10 releases; 300 m	Lycopodium spores; impaction on adhesive cylinders	Surface; 1 sec	Downland	1 to 4 m; ambient	Surface dosage distribution
Sand Storm (Taylor, 1965)	Edwards AFB, Calif.	43 releases; 2400 m	Beryllium powder in rocket propellant; aspirated filters	Surface (plus initial height of rise); 2 to 8 sec	Flat desert	Diameter of 15 to 45 m; above ambient	Surface dosage distribution
(Högström, 1964)	Agesta and Studsvik, Sweden	430 releases; $\approx$5000 m	Oil fog;photography from position upwind of source	24 to 87 m; 30 sec	Low hills	Small; close to ambient	Puff width and puff depth
Dugway (Cramer et al, 1964)	Dugway Proving Grounds, Utah	33 releases; 1100 m maximum used here	BW and CW gases and particulates	Surface; 3 and 26 sec	Flat desert	Finite but accounted for by authors; near ambient	Surface dosage distribution and limited measurements of vertical distribution
Point Arguello (Smith et al., 1964)	Naval Missile Facility,Pt. Arguello, Calif.	17 releases; $\approx 10^4$m	Zinc cadmium sulfide; rotorods and aspirated filters	Surface; 1 min	Rugges coastline	Small; ambient	Dosage along irregular arcs
Reactor Destruction Test (Islitzer and Markee, 1964)	National Reactor Testing Station, Idaho Falls, Idaho	4 releases; 6100 m	Fission products aspirated filters	Surface;<30 sec	Flat desert	10 meters; above ambient	Surface dosage distribution
Texas (MacCready, Smith, and Wolf, 1961)	Dallas TV tower, Cedar Hill, Tex.	37 releases; $\approx 10^4$m	Zinc cadmium sulfide;aspirated filters on tower	110 to 320 m; small(aircraft-released line source upwind of tower)	Rolling terrain	Finite but accounted for by authors; ambient	Vertical dosage distribution on tower
Hanford Reservation (Nickola, Ramsdell, Jr., and Ludwick, 1970)	Washington	13 releases;	Kr-85 gas (radio isotopes) GM tubes to analyz local concentration	Surface: instantaneous and finite releases <20 min.	Flat desert	<30 cm; ambient	Surface and vertical instantaneous concentration

Table 5.1 The General Description of the Laser.

Model 120 Specifications

Output	Wavelength: 632.8 nm. (Visible red.) Power: >5.0 mW Transverse mode: TEM_{00}
Beam Characteristics	Beam diameter: 0.65 mm at $1/e^2$ points Beam divergence: 1.7 milliradians Degree of polarization: Linear to better than 1 part per thousand Angle of polarization: Adjustable, vertical ±20°
Resonator Characteristics	Resonator configuration: Long radius Resonator length: 39 cm Axial mode spacing: 385 MHz Plasma excitation: direct current self-starting
Amplitude Stability	Beam amplitude noise (1–100 KHz): <0.5% rms Beam amplitude ripple (120 Hz): <0.2% rms Long term power drift: <5% Warm-up time: >3 mW at turn-on >5 mW 3 minutes after turn-on
Environmental Capability	Operating temperature: 10 to 40° C Altitude: Sea level to 10,000 feet Humidity: 90% relative humidity
Physical Characteristics	Weight: Laser—7½ lbs. Exciter—7½ lbs. Cable Length (Exciter to Laser): 8 feet (Extension sections available)
Power Requirements	Voltage: 115/230 V Frequency: 50 to 400 Hz Volt-Amps: 50 VA

*From "Model 120 Stabilite Gas Laser with Model 256 Exciter" instruction manual, Spectral-Physics, Inc., 1970.

Table 7.1 Experimental Data for Puff Measurements.

STATION X=0.5M,Y=00 CM,Z=00CM.

	MO	K1	K2	K3	K4	MEAN (SEC.)	SIGMA (SEC.)	SKEWNESS	FLATNESS
	.7849	.9236	.0417	.0057	.0087	.9236	.2041	.6674	4.9874
	1.0263	1.0623	.0792	.0158	.0199	1.0623	.2814	.6212	3.1714
	1.3468	1.0121	.1071	.0300	.0435	1.0121	.3273	.8552	3.7932
	.9773	.9671	.0767	.0284	.0347	.9671	.2769	1.3379	5.0984
	.9876	.7525	.0615	.0139	.0155	.7525	.2479	.9136	4.1023
	.8770	.7670	.0658	.0185	.0194	.7670	.2565	1.0851	4.4816
MEAN=	1.0000	.9141	.0720	.0185	.0236	.9141	.2657	.9154	4.4057
SIGMA=	.17465	.11706	.01989	.00854	.01182	.11706	.03733	.24460	.87207

STATION X=1.0M,Y=00 CM,Z=00CM.

	MO	K1	K2	K3	K4	MEAN (SEC.)	SIGMA (SEC.)	SKEWNESS	FLATNESS
	.8389	1.1510	.0546	.0129	.0158	1.1510	.2336	1.0132	4.6306
	.7116	1.2526	.0432	.0080	.0081	1.2526	.2078	.8896	4.3624
	.6781	1.2461	.0473	.0124	.0123	1.2461	.2174	1.2046	5.5138
	.6419	1.1752	.0484	.0076	.0084	1.1752	.2201	.7110	3.5766
	.7442	1.1162	.0575	.0069	.0093	1.1162	.2398	.5010	2.7987
	.6225	1.1230	.0392	.0016	.0059	1.1230	.1979	.2064	3.8247
MEAN=	.7062	1.1773	.0484	.0082	.0096	1.1773	.2194	.7543	4.1178
SIGMA=	.07189	.05444	.00625	.00377	.00266	.05444	.01425	.33024	.85542

STATION X=1.5M,Y=00 CM,Z=00CM.

	MO	K1	K2	K3	K4	MEAN (SEC.)	SIGMA (SEC.)	SKEWNESS	FLATNESS
	.6641	2.2238	.1851	.0534	.1060	2.2238	.4302	.6712	3.0941
	.5299	2.0378	.1304	.0754	.0990	2.0378	.3611	1.6017	5.8268
	.4292	2.0598	.1464	.0638	.0841	2.0598	.3826	1.1380	3.9222
	.5248	2.1064	.2486	.1148	.1992	2.1064	.4986	.9260	3.2228
	.4098	1.9409	.1044	.0425	.0520	1.9409	.3232	1.2596	4.7666
	.4074	1.9877	.1116	.0402	.0495	1.9877	.3341	1.0777	3.9765
MEAN=	.4609	2.0594	.1544	.0650	.0983	2.0594	.3883	1.1124	4.1348
SIGMA=	.10724	.09026	.04965	.02532	.04995	.09026	.06037	.28646	.93516

STATION X=2.0M,Y=00 CM,Z=00CM.

	MO	K1	K2	K3	K4	MEAN (SEC.)	SIGMA (SEC.)	SKEWNESS	FLATNESS
	.2246	2.5308	.2336	.1536	.2433	2.5308	.4833	1.3608	4.4582
	.3683	2.7114	.2190	.1090	.1985	2.7114	.4680	1.0634	4.1391
	.2561	2.3903	.1369	.0676	.1066	2.3903	.3700	1.3333	5.6872
	.3976	2.6809	.2166	.0715	.1647	2.6809	.4654	.7091	3.5113
	.2855	2.6818	.1702	.0539	.1170	2.6818	.4126	.7672	4.0382
	.1975	2.5387	.0931	.0387	.0552	2.5387	.3052	1.3608	6.3677
MEAN=	.2883	2.5890	.1782	.0824	.1475	2.5890	.4174	1.0991	4.7003
SIGMA=	.07261	.11361	.05037	.03838	.06218	.11361	.06333	.27549	.99832

Table 7.1 Experimental Data for Puff Measurements (Continued).

STATION, X=2.5M, Y=00 CM, Z=00CM.

	MO	K1	K2	K3	K4	MEAN (SEC.)	SIGMA (SEC.)	SKEWNESS	FLATNESS
	.2977	2.9562	.1642	.0498	.0965	2.9562	.4055	.7400	3.5715
	.2589	2.7577	.1544	.0486	.0812	2.7577	.3950	.8010	3.4042
	.2938	2.7257	.1940	.0693	.1245	2.7257	.4404	.8109	3.3088
	.2986	2.8745	.1901	.0729	.1258	2.8745	.4561	.8787	3.4803
	.2463	2.9547	.2542	.1418	.2411	2.9547	.5042	1.1366	3.7313
	.2798	2.6896	.1694	.0645	.1259	2.6896	.4115	.9257	4.3187
MEAN=	.2642	2.8194	.1877	.0745	.1321	2.8194	.4517	.8785	3.6558
SIGMA=	.03077	.10625	.03282	.03146	.05151	.10625	.03641	.11601	.33275

STATION, X=3.0M, Y=00 CM, Z=00CM.

	MO	K1	K2	K3	K4	MEAN (SEC.)	SIGMA (SEC.)	SKEWNESS	FLATNESS
	.2106	3.2648	.4535	.3277	.7270	3.2648	.6754	1.0731	3.3344
	.1057	3.8146	.3358	.1683	.4560	3.8146	.5965	.7950	3.4443
	.1361	3.4917	.3446	.1256	.3897	3.4917	.5871	.6207	3.2806
	.1947	3.5098	.4250	.2989	.6678	3.5098	.6519	1.0791	3.6978
	.1271	3.5075	.5625	.2754	.8508	3.5075	.7499	.6483	2.6274
	.1954	3.7856	.4965	.0902	.6025	3.7856	.7047	.2577	2.4428
MEAN=	.1763	3.5620	.4596	.2140	.6309	3.5620	.6606	.7453	3.1712
SIGMA=	.03322	.18792	.07610	.09027	.15526	.18792	.05726	.28597	.46941

STATION, X=3.5M, Y=00 CM, Z=00CM.

	MO	K1	K2	K3	K4	MEAN (SEC.)	SIGMA (SEC.)	SKEWNESS	FLATNESS
	.1063	4.4406	.2805	.1086	.2656	4.4406	.5296	.7511	3.3751
	.1017	4.2789	.3399	-.0067	.3761	4.2789	.5899	-.0309	2.9041
	.0848	4.3792	.3515	.0244	.3440	4.3792	.5927	.1174	2.7881
	.1047	4.1101	.4070	.1010	.4429	4.1101	.6379	.3890	2.6746
	.0846	4.3893	.3330	.0541	.2777	4.3893	.5771	.2814	2.5056
	.1113	4.1358	.4186	.0948	.4275	4.1358	.6470	.3499	2.4396
MEAN=	.0989	4.2890	.3584	.0627	.3556	4.2890	.5974	.3063	2.7808
SIGMA=	.01044	.12699	.04610	.04274	.06772	.12699	.03902	.25777	.30903

STATION, X=4.0M, Y=00 CM, Z=00CM.

	MO	K1	K2	K3	K4	MEAN (SEC.)	SIGMA (SEC.)	SKEWNESS	FLATNESS
	.0784	4.5093	.4142	.2340	.5680	4.5093	.6436	.8777	3.3105
	.0738	4.6800	.5559	.2784	.9588	4.6800	.7321	.7095	3.3306
	.1426	4.5504	.5832	.3142	1.0127	4.5504	.7637	.7354	2.9774
	.0822	4.6949	.6676	.4167	1.2252	4.6949	.8171	.7659	2.7489
	.0856	4.6509	.4798	.2631	.7123	4.6509	.6927	.7916	3.0852
	.0940	4.6021	.7259	.3635	1.5359	4.6021	.8520	.5878	2.9109
MEAN=	.0934	4.6279	.5678	.3116	1.0015	4.6279	.7502	.7393	3.0619
SIGMA=	.02301	.05147	.10611	.06221	.31857	.05147	.07073	.08856	.21287

Table 7.1 Experimental Data for Puff Measurements (Continued).

STATION X=0.5M,Y=05 CM,Z=00CM.

	MO	K1	K2	K3	K4	MEAN (SEC.)	SIGMA (SEC.)	SKEWNESS	FLATNESS
	.5276	.6987	.0327	.0006	.0031	.6987	.1808	.0976	2.9162
	.6056	.7490	.0441	.0015	.0048	.7490	.2101	.1428	2.4811
	.5454	.7497	.0306	.0017	.0025	.7497	.1748	.5193	2.7129
	.5024	.7742	.0655	.0109	.0132	.7742	.2563	.6524	3.0785
	.6447	.7711	.0487	.0042	.0067	.7711	.2206	.3915	2.8590
	.5362	.7862	.0497	.0074	.0076	.7862	.2250	.6692	3.0598
MEAN=	.5603	.7540	.0452	.0043	.0063	.7540	.2109	.3788	2.8479
SIGMA=	.04900	.02859	.01166	.00371	.00357	.02859	.02734	.22273	.20639

STATION X=1.0M,Y=05 CM,Z=00CM.

	MO	K1	K2	K3	K4	MEAN (SEC.)	SIGMA (SEC.)	SKEWNESS	FLATNESS
	.3722	1.3695	.0600	.0105	.0116	1.3695	.2450	.7016	3.2301
	.5285	1.4762	.0627	.0090	.0113	1.4762	.2503	.5754	2.8679
	.3988	1.4569	.0725	.0101	.0141	1.4569	.2693	.5184	2.6775
	.2685	1.4790	.0567	.0097	.0098	1.4790	.2381	.7204	3.0523
	.2802	1.5161	.0969	.0072	.0226	1.5161	.3113	.2572	2.4047
	.1739	1.2128	.1214	.0223	.0368	1.2128	.3485	.5263	2.4935
MEAN=	.3370	1.4184	.0784	.0114	.0177	1.4184	.2771	.5465	2.7877
SIGMA=	.11274	.10223	.02339	.00497	.00951	.10223	.04030	.15916	.29373

STATION X=1.5M,Y=05 CM,Z=00CM.

	MO	K1	K2	K3	K4	MEAN (SEC.)	SIGMA (SEC.)	SKEWNESS	FLATNESS
	.2199	2.1011	.1554	.0405	.0620	2.1011	.3843	.6616	2.5657
	.3945	2.1555	.1904	.0590	.0993	2.1555	.4363	.7106	2.7394
	.2743	2.0740	.2055	.0693	.1070	2.0740	.4534	.7442	2.5332
	.2142	2.1300	.1615	.0322	.0587	2.1300	.4019	.4961	2.2482
	.3725	2.0715	.2242	.0937	.1640	2.0715	.4735	.8826	3.2635
	.3372	1.9929	.1664	.0417	.0734	1.9929	.4079	.6147	2.6498
MEAN=	.3021	2.0875	.1839	.0561	.0941	2.0875	.4279	.6850	2.6666
SIGMA=	.07069	.05164	.02501	.02089	.03634	.05164	.02888	.11859	.30684

STATION X=2.0M,Y=05 CM,Z=00CM.

	MO	K1	K2	K3	K4	MEAN (SEC.)	SIGMA (SEC.)	SKEWNESS	FLATNESS
	.2985	2.4907	.1526	.0312	.0617	2.4907	.3906	.5242	2.6485
	.1948	2.5745	.2128	.0505	.1006	2.5745	.4613	.5953	2.3969
	.1915	2.4599	.1761	.0501	.0859	2.4599	.4196	.6785	2.7718
	.0964	2.5722	.1616	.0206	.0375	2.5722	.4019	.3166	2.2028
	.3126	2.5049	.1996	.0358	.0893	2.5049	.4471	.3775	2.2335
	.2758	2.4484	.1524	.0293	.0471	2.4484	.3659	.6069	2.6847
MEAN=	.2203	2.4751	.1726	.0372	.0750	2.4751	.4141	.5165	2.4897
SIGMA=	.07547	.06003	.02742	.01295	.02127	.06003	.03309	.12908	.22338

Table 7.1 Experimental Data for Puff Measurements (Continued).

STATION X=2.5M,Y=05 CM,Z=00CM.

	MO	K1	K2	K3	K4	MEAN (SEC.)	SIGMA (SEC.)	SKEWNESS	FLATNESS
	.2156	2.9295	.1598	.0120	.0535	2.9295	.3998	.1879	2.0928
	.2490	2.8826	.1999	.0607	.1076	2.8826	.4471	.6788	2.6935
	.2558	2.9680	.1693	.0583	.0727	2.9680	.4115	.5503	2.5351
	.2831	3.0453	.2044	.0446	.0967	3.0453	.4522	.4829	2.3145
	.1753	3.1376	.1290	.0186	.0340	3.1376	.3592	.4009	2.0446
	.2277	3.0546	.1178	.0129	.0301	3.0546	.3432	.3182	2.1715
MEAN=	.2344	3.0029	.1634	.0312	.0658	3.0029	.4022	.4365	2.3087
SIGMA=	.03400	.08534	.03246	.01809	.02940	.08534	.04070	.15858	.23613

STATION X=0.5M,Y=10 CM,Z=00CM.

	MO	K1	K2	K3	K4	MEAN (SEC.)	SIGMA (SEC.)	SKEWNESS	FLATNESS
	.2068	1.2122	.1047	.0714	.1089	1.2122	.4298	.0996	3.1911
	.2236	1.1802	.1618	.0467	.0679	1.1802	.4022	.7174	2.5951
	.4251	1.1489	.1081	.0185	.0317	1.1489	.3288	.5136	2.7155
	.2807	1.0693	.0796	.0060	.0177	1.0693	.2821	.2686	2.7886
	.0666	1.1289	.1156	.0135	.0284	1.1289	.3401	.3442	2.1272
	.2043	1.0665	.0789	.0062	.0170	1.0665	.2809	.2804	2.7355
MEAN=	.2478	1.1343	.1214	.0270	.0453	1.1343	.3440	.5040	2.6922
SIGMA=	.10750	.05360	.03959	.02412	.03314	.05360	.03599	.25561	.31339

STATION X=1.0M,Y=10 CM,Z=00CM.

	MO	K1	K2	K3	K4	MEAN (SEC.)	SIGMA (SEC.)	SKEWNESS	FLATNESS
	.3609	1.7142	.1273	.0267	.0447	1.7142	.3568	.5883	2.7592
	.2276	1.6325	.0678	.0111	.0133	1.6325	.2604	.6300	2.9023
	.2677	1.7939	.0967	.0178	.0267	1.7939	.3109	.5908	2.8580
	.3556	1.7132	.1261	.0315	.0478	1.7132	.3552	.7024	3.0062
	.2491	1.5749	.1302	.0493	.0580	1.5749	.3608	1.0506	3.4219
	.4014	1.7339	.1293	.0311	.0465	1.7339	.3598	.6668	2.7761
MEAN=	.3104	1.6938	.1129	.0279	.0395	1.6938	.3340	.7048	2.9539
SIGMA=	.06494	.07108	.02528	.01202	.01495	.07108	.03720	.15979	.22477

STATION X=1.5M,Y=10 CM,Z=00CM.

	MO	K1	K2	K3	K4	MEAN (SEC.)	SIGMA (SEC.)	SKEWNESS	FLATNESS
	.2741	2.1212	.1604	.0520	.0857	2.1212	.4005	.8092	3.3320
	.2765	2.1407	.1638	.0515	.0795	2.1407	.4048	.7741	2.9636
	.1913	2.1740	.1658	.0540	.0810	2.1740	.4072	.7990	2.9459
	.5507	2.2567	.2857	.0756	.1987	2.2567	.5326	.5005	2.4696
	.3339	2.1122	.2426	.0941	.1065	2.1122	.4925	.7880	3.1697
	.1841	1.9319	.1144	.0346	.0490	1.9319	.3383	.8943	3.7395
MEAN=	.3018	2.1194	.1884	.0603	.1134	2.1194	.4293	.7608	3.1034
SIGMA=	.12279	.09346	.05686	.01926	.05735	.09346	.06437	.12268	.38887

Table 7.1 Experimental Data for Puff Measurements (Continued).

STATION X=2.0M, Y=10 CM, Z=00CM.

	MO	K1	K2	K3	K4	MEAN (SEC.)	SIGMA (SEC.)	SKEWNESS	FLATNESS
	.3019	2.4945	.3295	.1271	.2089	2.4945	.5741	.6719	2.6606
	.2111	2.7081	.4557	.2260	.5157	2.7081	.6751	.7545	2.4831
	.4100	2.6715	.3461	.1540	.3725	2.6715	.5885	.7561	3.1075
	.1913	2.4149	.1912	.0701	.1215	2.4149	.4373	.8380	3.3215
	.1515	2.4752	.3048	.1240	.2377	2.4752	.5521	.7367	2.5509
	.1546	2.5817	.2606	.0595	.1841	2.5817	.5105	.4471	2.7108
MEAN=	.2367	2.5573	.3146	.1268	.2867	2.5573	.5562	.6974	2.8071
SIGMA=	.09221	.10620	.08100	.05528	.12909	.10620	.07272	.12209	.30336

STATION X=2.5M, Y=10 CM, Z=00CM.

	MO	K1	K2	K3	K4	MEAN (SEC.)	SIGMA (SEC.)	SKEWNESS	FLATNESS
	.1765	3.0462	.2153	.0575	.1269	3.0462	.4619	.5840	2.7898
	.1485	2.7874	.3069	.1337	.2760	2.7874	.5540	.7864	2.9306
	.1465	2.6108	.1927	.0442	.0894	2.6108	.4390	.5229	2.4057
	.1421	2.8357	.3442	.0777	.2552	2.8357	.5067	.3850	2.1573
	.1274	2.8154	.3172	.0656	.2080	2.8154	.5632	.3671	2.0677
	.1668	3.2070	.3548	.0666	.2494	3.2070	.5786	.3458	2.2255
MEAN=	.1513	2.8857	.2848	.0742	.2005	2.8857	.5306	.4982	2.4261
SIGMA=	.01614	.19220	.05959	.02847	.06914	.19220	.05798	.15539	.32642

STATION X=3.0M, Y=10 CM, Z=00CM.

	MO	K1	K2	K3	K4	MEAN (SEC.)	SIGMA (SEC.)	SKEWNESS	FLATNESS
	.1455	3.5723	.3709	.1179	.3056	3.5723	.6090	.5222	2.2217
	.1473	3.6746	.2773	.0557	.1670	3.6746	.5266	.3814	2.1725
	.1105	3.5474	.2860	.0668	.1887	3.5474	.5347	.4366	2.3078
	.2164	3.6666	.3505	.0257	.2579	3.6666	.5820	.1237	2.0992
	.1254	3.5537	.2549	.0280	.1406	3.5537	.5049	.2177	2.1637
	.1263	3.6045	.2657	.0315	.1601	3.6045	.5155	.2296	2.2674
MEAN=	.1452	3.6032	.3009	.0543	.2033	3.6032	.5471	.3185	2.2054
SIGMA=	.03422	.05105	.04577	.03225	.05884	.05105	.03916	.15869	.06916

STATION X=1.5M, Y=20 CM, Z=00CM.

	MO	K1	K2	K3	K4	MEAN (SEC.)	SIGMA (SEC.)	SKEWNESS	FLATNESS
	.1399	2.1685	.2044	.0075	.1523	2.1685	.5333	.0495	1.8819
	.0998	2.2190	.1602	.0163	.0612	2.2190	.4002	.2547	2.3864
	.1172	2.0389	.1540	.0301	.0510	2.0389	.5660	.6128	2.8415
	.2167	2.0424	.1882	.0241	.0851	2.0424	.4339	.2951	2.4017
	.1106	1.9631	.1693	.0263	.0656	1.9631	.4115	.3774	2.2873
	.1365	1.7617	.1646	.0710	.0922	1.7617	.4057	1.0627	3.4042
MEAN=	.1368	2.0323	.1834	.0292	.0846	2.0323	.4251	.4420	2.5338
SIGMA=	.03857	.14808	.04788	.02008	.03336	.14808	.05237	.32587	.47912

Table 7.1 Experimental Data for Puff Measurements (Continued).

STATION X=2.0M,Y=20 CM,Z=00CM.

	MO	K1	K2	K3	K4	MEAN (SEC.)	SIGMA (SEC.)	SKEWNESS	FLATNESS
	.0940	2.3804	.1382	.0111	.0526	2.3804	.3718	.2156	2.7535
	.1535	2.4801	.1405	.0314	.0604	2.4801	.3748	.5969	3.0506
	.0422	2.2508	.0913	.0114	.0257	2.2508	.3022	.4139	3.0833
	.3428	2.2641	.1918	.0805	.1353	2.2641	.4579	.0892	3.6264
	.1656	2.3399	.1818	.0175	.0775	2.3399	.4264	.2258	2.3386
	.2966	1.9699	.1543	.0795	.1142	1.9699	.3828	1.3123	4.7967
MEAN=	.1791	2.2809	.1496	.0386	.0772	2.2809	.3843	.6206	3.2763
SIGMA=	.10714	.15862	.03279	.03006	.03664	.15862	.04417	.39914	.78220

STATION X=2.5M,Y=20 CM,Z=00CM.

	MO	K1	K2	K3	K4	MEAN (SEC.)	SIGMA (SEC.)	SKEWNESS	FLATNESS
	.1285	2.7202	.1404	.0499	.0646	2.7202	.3747	.9487	3.2776
	.0139	2.6366	.0870	.0094	.0204	2.6366	.2980	.3644	2.7005
	.0380	2.6868	.0752	.0106	.0176	2.6868	.2743	.5122	3.1117
	.2225	2.8128	.1726	.0607	.0962	2.8128	.4154	.0461	3.2504
	.1329	3.0152	.2373	.0102	.1467	3.0152	.3072	.0782	2.2161
	.0980	2.6209	.2040	.0673	.1134	2.6209	.4317	.7329	2.7238
MEAN=	.1047	2.7487	.1561	.0347	.0765	2.7487	.3864	.3804	2.8767
SIGMA=	.06874	.13458	.06374	.02518	.04732	.13458	.08242	.29805	.37255

STATION X=3.0M,Y=20 CM,Z=00CM.

	MO	K1	K2	K3	K4	MEAN (SEC.)	SIGMA (SEC.)	SKEWNESS	FLATNESS
	.1088	3.2571	.2126	.0633	.1201	3.2571	.4611	.6452	2.6566
	.1322	3.2882	.3174	.0938	.2176	3.2882	.3633	.5245	2.1609
	.1380	3.3383	.2775	.0082	.1675	3.3383	.5267	.0562	2.1754
		NO SIGNAL OBSERVED							
		NO SIGNAL OBSERVED							
		NO SIGNAL OBSERVED							
MEAN=	.0626	3.2935	.2692	.0551	.1684	3.2935	.5170	.4086	2.3310
SIGMA=	.06341	.03215	.04319	.03542	.03981	.03215	.04228	.25403	.23035

STATION X=3.5M,Y=20 CM,Z=00CM.

	MO	K1	K2	K3	K4	MEAN (SEC.)	SIGMA (SEC.)	SKEWNESS	FLATNESS
	.1465	3.3577	.2064	.0520	.1285	3.3577	.4545	.3548	3.0130
	.0427	3.4893	.2874	.0907	.2121	3.4893	.3361	.5886	2.5678
	.0660	3.6823	.1958	.0745	.1177	3.6823	.4419	.0631	3.0872
	.3598	3.8019	.3062	-.0171	.2817	3.8019	.5534	-.1007	3.0047
	.3908	3.7925	.1840	.0093	.0768	3.7925	.4289	.1174	2.2695
	.3718	4.4574	.6948	.2677	.9879	4.4574	.8335	.4615	2.0463
MEAN=	.3795	3.7635	.3125	.0794	.3007	3.7635	.5413	.4141	2.6648
SIGMA=	.05320	.34887	.17717	.09162	.31456	.34887	.13085	.31818	.40066

Table 7.1 Experimental Data for Puff Measurements (Continued).

STATION X=4.0M,Y=20 CM,Z=00CM.

	MO	K1	K2	K3	K4	MEAN (SEC.)	SIGMA (SEC.)	SKEWNESS	FLATNESS
	.0494	4.2796	.8447	.5363	1.5292	4.2796	.9191	.6907	2.1429
	.0715	4.1955	.6645	.4151	1.0345	4.1955	.8152	.7664	2.3431
	.1075	4.4748	.4059	.2474	.6604	4.4748	.6571	.9567	4.0078
	.0510	4.1251	.3601	.2425	.4239	4.1251	.6000	1.1226	3.2697
	.0602	4.1878	.3647	.1974	.4357	4.1878	.6039	.8959	3.2747
	.0040	.5885	.0001	0.0000	0.0000	.5885	.0112	.4806	3.4057
MEAN=	.0573	3.6412	.4400	.2731	.6806	3.6412	.5977	.8188	3.0736
SIGMA=	.03077	1.36976	.26486	.16899	.48902	1.36976	.28757	.20445	.64057

STATION X=1.0M,Y=-20CM,Z=00CM.

	MO	K1	K2	K3	K4	MEAN (SEC.)	SIGMA (SEC.)	SKEWNESS	FLATNESS
	.0544	1.2207	.0916	.0181	.0176	1.2207	.3027	.6539	2.1030
	.0893	1.2619	.0546	.0044	.0059	1.2619	.2337	.3442	1.9730
	.0698	1.3159	.0172	.0004	.0008	1.3159	.1310	.1880	2.6189
	.0151	1.3940	.0340	.0021	.0023	1.3940	.1843	.3294	1.9829
	.0227	1.2655	.0247	.0024	.0013	1.2655	.1570	.6180	2.1719
	.0492	1.3962	.0496	.0042	.0052	1.3962	.2227	.3806	2.0949
MEAN=	.0500	1.3090	.0453	.0053	.0055	1.3090	.2052	.4190	2.1574
SIGMA=	.02554	.06681	.02446	.00590	.00572	.06681	.05611	.16494	.21776

STATION X=1.5M,Y=-20CM,Z=00CM.

	MO	K1	K2	K3	K4	MEAN (SEC.)	SIGMA (SEC.)	SKEWNESS	FLATNESS
	.0287	2.5364	.0517	-.0002	.0055	2.5364	.2273	-.0168	2.0451
	.0473	2.4869	.0433	.0022	.0040	2.4869	.2082	.2475	2.1516
	.0736	2.5502	.0642	.0045	.0099	2.5502	.2555	.2777	2.3916
	NO SIGNAL OBSERVED								
	NO SIGNAL OBSERVED								
	NO SIGNAL OBSERVED								
MEAN=	.0249	2.5245	.0531	.0022	.0065	2.5245	.2297	.1695	2.1961
SIGMA=	.02815	.02718	.00859	.00192	.00250	.02718	.01857	.15229	.14492

STATION X=2.0M,Y=-20CM,Z=00CM.

	MO	K1	K2	K3	K4	MEAN (SEC.)	SIGMA (SEC.)	SKEWNESS	FLATNESS
	.0545	2.2521	.1056	.0102	.0258	2.2521	.3249	.2960	2.1345
	.1118	2.3150	.0685	.0151	.0127	2.3150	.2618	.7305	2.7107
	.3035	2.7392	.2522	.1211	.1954	2.7392	.5022	.9565	3.0734
	.0641	2.5770	.1267	.0188	.0351	2.5770	.3560	.4164	2.1845
	.0615	2.4521	.1718	.0296	.0645	2.4521	.4145	.4155	2.1843
	.1003	2.2355	.0550	.0105	.0086	2.2355	.2303	.8594	3.0626
MEAN=	.1159	2.4285	.1296	.0339	.0567	2.4285	.3483	.6124	2.5583
SIGMA=	.08640	.18275	.06708	.03956	.06467	.18275	.09136	.24855	.40867

Table 7.1 Experimental Data for Puff Measurements (Continued).

STATION X=2.5M,Y=-20CM,Z=00CM.

	MO	K1	K2	K3	K4	MEAN (SEC.)	SIGMA (SEC.)	SKEWNESS	FLATNESS
	.1018	2.9719	.1805	.0404	.0745	2.9719	.4248	.5268	2.2873
	.0847	2.9457	.1495	.0194	.0459	2.9457	.3867	.3360	2.0511
	.0970	2.8579	.0891	.0269	.0284	2.8579	.2984	1.0125	3.5849
	.2440	3.1136	.1515	.0398	.0693	3.1136	.3890	.6762	3.0243
	.1906	3.1601	.1322	.0210	.0434	3.1601	.3635	.4365	2.4874
	.1547	3.2584	.1872	.0001	.0800	3.2584	.4326	.0016	2.2844
MEAN=	.1455	3.0479	.1485	.0246	.0569	3.0479	.3825	.4982	2.6199
SIGMA=	.05740	.14232	.03247	.01570	.01876	.14232	.04433	.30917	.52584

STATION X=3.0M,Y=-20CM,Z=00CM.

	MO	K1	K2	K3	K4	MEAN (SEC.)	SIGMA (SEC.)	SKEWNESS	FLATNESS
	.0959	3.5224	.1817	.0423	.0905	3.5224	.4263	.5465	2.7412
	.0824	3.3384	.1643	.0391	.0694	3.3384	.4054	.5866	2.5717
	.1109	3.4440	.1488	.0496	.0733	3.4440	.3858	.8636	3.3115
	.0975	3.3155	.1951	.0655	.1089	3.3155	.4417	.7608	2.8630
	.0738	3.6442	.2146	.0509	.1196	3.6442	.4632	.5123	2.5975
	.0857	3.3930	.0958	.0175	.0291	3.3930	.3096	.5915	3.1667
MEAN=	.0907	3.4429	.1667	.0441	.0818	3.4429	.4053	.6435	2.8753
SIGMA=	.01215	.11290	.03803	.01455	.02956	.11290	.04943	.12568	.27769

STATION X=3.5M,Y=-20CM,Z=00CM.

	MO	K1	K2	K3	K4	MEAN (SEC.)	SIGMA (SEC.)	SKEWNESS	FLATNESS
	.0611	4.0319	.3947	.1403	.3585	4.0319	.6283	.5660	2.3009
	.1573	4.1473	.3475	.0318	.2786	4.1473	.5895	.1552	2.3071
	.0733	4.0849	.2875	.0552	.1952	4.0849	.5362	.2283	2.3628
	.0437	3.8746	.3594	.1743	.3414	3.8746	.5995	.8091	2.6426
	.0597	3.8759	.2223	.0502	.1534	3.8759	.4715	.4791	2.6990
	.0589	3.9010	.1785	.0413	.1109	3.9010	.4225	.5475	3.4813
MEAN=	.0723	3.9859	.2983	.0788	.2363	3.9859	.5412	.4642	2.6325
SIGMA=	.03028	.10775	.07715	.05662	.09641	.10775	.07336	.21094	.41101

STATION X=4.0M,Y=-20CM,Z=00CM.

	MO	K1	K2	K3	K4	MEAN (SEC.)	SIGMA (SEC.)	SKEWNESS	FLATNESS
	.0488	4.0152	.1416	.0295	.0502	4.0152	.3763	.5539	2.5012
	.0460	4.1960	.0977	.0009	.0195	4.1960	.3125	.0290	2.0482
	.0885	4.2590	.1502	.0088	.0476	4.2590	.3876	.1518	2.1082
	.0592	4.2924	.2286	-.0141	.1119	4.2924	.4782	-.1293	2.1407
	.0781	4.2541	.1654	-.0190	.0685	4.2541	.4067	-.2818	2.5033
	.1479	4.2551	.1740	.0057	.0734	4.2551	.4171	.0785	2.4230
MEAN=	.0781	4.2085	.1596	.0020	.0618	4.2085	.3964	.0670	2.2874
SIGMA=	.03471	.09190	.03926	.01590	.02833	.09190	.04958	.26014	.19216

Table 7.1 Experimental Data for Puff Measurements (Continued).

STATION X=0.5M,Y=00 CM,Z=00CM.

	MO	K1	K2	K3	K4	MEAN (SEC.)	SIGMA (SEC.)	SKEWNESS	FLATNESS
	.0482	.7667	.0783	.0174	.0157	.7667	.2799	.7919	2.5601
	.0071	.7008	.0042	.0003	.0001	.7008	.0646	.9933	5.2124
	NO SIGNAL OBSERVED								
	NO SIGNAL OBSERVED								
	NO SIGNAL OBSERVED								
	NO SIGNAL OBSERVED								
MEAN=	.0092	.7338	.0413	.0088	.0079	.7338	.1722	.8926	3.8863
SIGMA=	.01764	.03295	.03705	.00855	.00780	.03295	.10765	.10070	1.32615

STATION X=1.0M,Y=00 CM,Z=00CM.

	MO	K1	K2	K3	K4	MEAN (SEC.)	SIGMA (SEC.)	SKEWNESS	FLATNESS
	.0075	.9059	.0027	0.0000	0.0000	.9059	.0516	.0846	2.7365
	.0327	.9722	.0142	.0020	.0007	.9722	.1194	1.1629	3.6753
	.0046	.8705	.0025	0.0000	0.0000	.8705	.0503	.2002	1.6580
	.0152	.9106	.0097	.0004	.0002	.9106	.0983	.4254	2.0478
	.2196	1.8279	.0961	.0156	.0229	1.8279	.3100	.5246	2.4745
	NO SIGNAL OBSERVED								
MEAN=	.0465	1.0974	.0250	.0036	.0048	1.0974	.1259	.4795	2.5184
SIGMA=	.07820	.36670	.03580	.00605	.00907	.36670	.09585	.37575	.68552

STATION X=1.5M,Y=00 CM,Z=00CM.

	MO	K1	K2	K3	K4	MEAN (SEC.)	SIGMA (SEC.)	SKEWNESS	FLATNESS
	.4697	1.8560	.1075	.0294	.0349	1.8560	.3278	.8349	3.0242
	.3893	1.6925	.0499	.0079	.0072	1.6925	.2235	.7111	2.8786
	.5152	1.7213	.0653	.0116	.0118	1.7213	.2585	.6954	2.7634
	.5869	1.6702	.1052	.0230	.0291	1.6702	.3244	.6724	2.6312
	.4886	1.6799	.1251	.0279	.0399	1.6799	.3536	.6310	2.5502
	.3399	1.9450	.0552	.0106	.0095	1.9450	.2550	.8146	3.1274
MEAN=	.4649	1.7565	.0847	.0184	.0221	1.7565	.2866	.7266	2.8292
SIGMA=	.08096	.10121	.02895	.00866	.01302	.10121	.05042	.07590	.20444

STATION X=2.0M,Y=00 CM,Z=00CM.

	MO	K1	K2	K3	K4	MEAN (SEC.)	SIGMA (SEC.)	SKEWNESS	FLATNESS
	.4567	1.9985	.0814	.0110	.0199	1.9985	.2855	.4729	2.9988
	.2303	1.8419	.0421	.0080	.0072	1.8419	.2053	.9261	4.0444
	.2406	2.1209	.1992	.0539	.0996	2.1209	.4464	.6061	2.5104
	.3711	2.0445	.1428	.0254	.0498	2.0445	.3779	.4717	2.4420
	.4877	2.2160	.1818	.0568	.0855	2.2160	.4264	.4750	2.5197
	.0613	2.3704	.0628	.0105	.0106	2.3704	.2506	.6665	2.6913
MEAN=	.3080	2.0987	.1185	.0243	.0451	2.0987	.3320	.6050	2.8678
SIGMA=	.14710	.16685	.05976	.01667	.03585	.16685	.09034	.16278	.55721

Table 7.1 Experimental Data for Puff Measurements (Continued).

STATION X=2.5M,Y=00 CM,Z=00CM.

	MO	K1	K2	K3	K4	MEAN (SEC.)	SIGMA (SEC.)	SKEWNESS	FLATNESS
	.1315	2.3981	.1283	.0513	.0659	2.3981	.3582	1.1173	4.0038
	.3396	2.4992	.1417	.0413	.0602	2.4992	.3764	.7747	2.9979
	.1817	2.4652	.1417	.0409	.0600	2.4652	.3764	.7660	2.9887
	.1695	2.3191	.1046	.0141	.0359	2.3191	.3235	.4169	3.2798
	.1330	2.3045	.1266	.0367	.0459	2.3045	.3558	.8144	2.8618
	.0695	3.0075	.1225	.0026	.0344	3.0075	.3500	.0597	2.2931
MEAN=	.1708	2.4989	.1276	.0311	.0504	2.4989	.3567	.6582	3.0708
SIGMA=	.08352	.23808	.01261	.01705	.01235	.23808	.01792	.33586	.51230

STATION X=3.0M,Y=00 CM,Z=00CM.

	MO	K1	K2	K3	K4	MEAN (SEC.)	SIGMA (SEC.)	SKEWNESS	FLATNESS
	.0778	2.8878	.0961	.0105	.0216	2.8878	.3101	.3526	2.3389
	.2161	2.9253	.1431	.0301	.0764	2.9253	.3783	.3564	3.7311
	.1060	2.8201	.1875	.0662	.1008	2.8201	.4330	.8149	2.8651
	.1262	2.7345	.0555	.0066	.0076	2.7345	.2356	.5086	2.4601
	.2215	2.7216	.0947	.0132	.0235	2.7216	.3078	.4535	2.6160
	.1482	3.3318	.1047	.0209	.0364	3.3318	.3236	.6166	3.3223
MEAN=	.1493	2.9035	.1136	.0246	.0444	2.9035	.3314	.5504	2.8889
SIGMA=	.05355	.20525	.04173	.02011	.03312	.20525	.06161	.14413	.49304

STATION X=3.5M,Y=00 CM,Z=00CM.

	MO	K1	K2	K3	K4	MEAN (SEC.)	SIGMA (SEC.)	SKEWNESS	FLATNESS
	.2195	3.3890	.1494	.0287	.0637	3.3890	.3865	.4968	2.8550
	.0267	3.1649	.1085	-.0084	.0270	3.1649	.3293	-.2345	2.2968
	.1028	3.5406	.2171	.0310	.1068	3.5406	.4659	.3063	2.2670
	.0759	3.4043	.1791	.0193	.0711	3.4043	.4232	.2545	2.2174
	.0649	3.3807	.1192	.0192	.0359	3.3807	.3453	.4666	2.5261
	.2025	4.2221	.1991	.0512	.1293	4.2221	.4462	.5759	3.2638
MEAN=	.1154	3.5169	.1621	.0235	.0723	3.5169	.3994	.3109	2.5710
SIGMA=	.07138	.33401	.03991	.01782	.03627	.33401	.05031	.26761	.37755

STATION X=4.0M,Y=00 CM,Z=00CM.

	MO	K1	K2	K3	K4	MEAN (SEC.)	SIGMA (SEC.)	SKEWNESS	FLATNESS
	.0216	3.7950	.1427	.0493	.0680	3.7950	.3777	.9149	3.3395
	.0349	3.8979	.2071	.0544	.1064	3.8979	.4550	.5770	2.4809
	.0596	3.8006	.2073	.0673	.1137	3.8006	.4553	.7136	2.6464
	.0368	3.8352	.1223	.0190	.0366	3.8352	.3496	.4436	2.4472
	.0506	3.7943	.1174	.0094	.0364	3.7943	.3427	.2334	2.6403
	.0006	1.1888	.0071	.0001	.0001	1.1888	.0845	.2090	1.9748
MEAN=	.0340	3.3853	.1340	.0332	.0602	3.3853	.3441	.5152	2.5882
SIGMA=	.01918	.98297	.06746	.02495	.04040	.98297	.12464	.25207	.40378

Table 7.1 Experimental Data for Puff Measurements (Continued).

STATION X=1.5M,Y=05 CM,Z=00CM.

	MO	K1	K2	K3	K4	MEAN (SEC.)	SIGMA (SEC.)	SKEWNESS	FLATNESS
	.4050	1.6491	.1677	.0503	.0815	1.6491	.4095	.7324	2.8974
	.2363	1.5473	.1025	.0278	.0297	1.5473	.3202	.8466	2.8265
	.2047	1.5209	.0558	.0092	.0098	1.5209	.2362	.6980	3.1548
	.2517	1.6029	.0502	.0039	.0066	1.6029	.2241	.3496	2.6194
	.2195	1.5860	.0503	.0066	.0074	1.5860	.2243	.5843	2.9414
	.2514	1.6361	.0421	.0060	.0063	1.6361	.2053	.6948	3.5335
MEAN=	.2614	1.5904	.0781	.0173	.0235	1.5904	.2699	.6509	2.9955
SIGMA=	.06636	.04546	.04466	.01677	.02717	.04546	.07246	.15508	.28792

STATION X=2.0M,Y=05 CM,Z=00CM.

	MO	K1	K2	K3	K4	MEAN (SEC.)	SIGMA (SEC.)	SKEWNESS	FLATNESS
	.1272	2.3599	.1248	.0255	.0433	2.3599	.3532	.5789	2.7850
	.1636	2.2096	.1602	.0415	.0765	2.2096	.4003	.6477	2.9808
	.2123	2.1680	.1282	.0217	.0451	2.1680	.3581	.4728	2.7445
	.2261	2.3679	.0978	.0147	.0269	2.3679	.3128	.4818	2.8079
	.2515	2.2172	.0941	.0271	.0370	2.2172	.3067	.9392	4.1771
	.2675	2.2839	.0681	.0015	.0119	2.2839	.2609	.0867	2.5749
MEAN=	.2080	2.2677	.1122	.0220	.0401	2.2677	.3320	.5345	3.0114
SIGMA=	.04879	.07601	.02944	.01219	.01975	.07601	.04446	.25353	.53466

STATION X=2.5M,Y=05 CM,Z=00CM.

	MO	K1	K2	K3	K4	MEAN (SEC.)	SIGMA (SEC.)	SKEWNESS	FLATNESS
	.1323	2.9049	.1748	.0382	.0856	2.9049	.4181	.5222	2.8008
	.1887	2.8647	.2735	.1200	.2382	2.8647	.5230	.8391	3.1844
	.0978	2.9136	.1840	.0629	.0989	2.9136	.4289	.7972	2.9229
	.1201	2.7674	.1504	.0511	.0791	2.7674	.3878	.8759	3.5002
	.1165	2.7901	.1118	.0243	.0391	2.7901	.3343	.6491	3.1335
	.1248	2.6615	.1252	.0463	.0611	2.6615	.3538	1.0449	3.8982
MEAN=	.1300	2.8170	.1699	.0571	.1003	2.8170	.4076	.7881	3.2400
SIGMA=	.02828	.08822	.05277	.03048	.06451	.08822	.06129	.16651	.36715

STATION X=3.0M,Y=05 CM,Z=00CM.

	MO	K1	K2	K3	K4	MEAN (SEC.)	SIGMA (SEC.)	SKEWNESS	FLATNESS
	.0407	3.0639	.2440	.0728	.1463	3.0639	.4939	.6042	2.4573
	.0191	3.0651	.3092	.1000	.2061	3.0651	.5561	.5817	2.1549
	.0513	3.1194	.2158	.1048	.1691	3.1194	.4646	1.0453	3.6302
	.0700	2.9907	.1641	.0534	.0891	2.9907	.4051	.8036	3.3083
	.0542	3.1389	.1355	.0374	.0647	3.1389	.3681	.7499	3.5221
	.0528	3.1605	.1226	.0281	.0482	3.1605	.3501	.6549	3.2087
MEAN=	.0480	3.0897	.1985	.0661	.1206	3.0897	.4396	.7399	3.0469
SIGMA=	.01552	.05684	.06524	.02921	.05727	.05684	.07241	.15711	.54831

Table 7.1 Experimental Data for Puff Measurements (Continued).

STATION X=3.5M,Y=05 CM,Z=00CM.

	MO	K1	K2	K3	K4	MEAN (SEC.)	SIGMA (SEC.)	SKEWNESS	FLATNESS
	.1158	3.6814	.3197	.1177	.2765	3.6814	.5654	.6512	2.7057
	.0742	3.5803	.1992	.0753	.1164	3.5803	.4463	.8470	2.9548
	.0759	3.7739	.2876	.0519	.1744	3.7739	.5563	.5562	2.1081
	.0979	3.4254	.1281	.0555	.0564	3.4254	.3579	.7740	3.4552
	.1641	3.7228	.2676	.1158	.2182	3.7228	.5173	.8567	3.0484
	.0711	3.4368	.1292	.0458	.0561	3.4368	.3594	.9858	3.5641
MEAN=	.0998	3.6054	.2219	.0757	.1496	3.6054	.4658	.7585	2.9524
SIGMA=	.05277	.15502	.07514	.03272	.08155	.15502	.08252	.20547	.44430

STATION X=4.0M,Y=05 CM,Z=00CM.

	MO	K1	K2	K3	K4	MEAN (SEC.)	SIGMA (SEC.)	SKEWNESS	FLATNESS
	.1058	4.0072	.2244	.0815	.1462	4.0072	.4757	.7646	2.9054
	.0919	3.9285	.1306	.0444	.0615	3.9285	.3614	.9415	3.5905
	.0862	4.1028	.1481	.0157	.0515	4.1028	.3848	.2750	2.3491
	.0611	3.8960	.1523	.0132	.0591	3.8960	.3902	.2218	2.5503
	.0241	3.8845	.1317	.0277	.0447	3.8845	.3629	.5794	2.5782
	.0654	3.9048	.1700	.0396	.0681	3.9048	.4125	.5653	2.3562
MEAN=	.0724	3.9559	.1598	.0370	.0718	3.9559	.3975	.5579	2.7213
SIGMA=	.02645	.07772	.03192	.02284	.05408	.07772	.03817	.25273	.45016

STATION X=3.5M,Y=-20CM,Z=00CM.

	MO	K1	K2	K3	K4	MEAN (SEC.)	SIGMA (SEC.)	SKEWNESS	FLATNESS
	.0965	3.3785	.0913	.0109	.0188	3.3785	.3022	.3958	2.2575
	.0191	3.2085	.0553	.0022	.0029	3.2085	.1879	.3292	2.2956
	.0480	3.0917	.0563	.0013	.0070	3.0917	.2572	.0952	2.1968
	.0655	3.2585	.1612	.0054	.0504	3.2585	.4015	.0840	1.9387
	.0351	3.4437	.1169	-.0054	.0293	3.4437	.3418	-.1341	2.1422
	.0952	3.7058	.1564	.0310	.0557	3.7058	.3955	.5014	2.2789
MEAN=	.0599	3.3477	.1029	.0076	.0275	3.3477	.3110	.2119	2.1846
SIGMA=	.02099	.19655	.04714	.01156	.02010	.19655	.07848	.21644	.12145

STATION X=4.0M,Y=-20CM,Z=00CM.

	MO	K1	K2	K3	K4	MEAN (SEC.)	SIGMA (SEC.)	SKEWNESS	FLATNESS
	.0404	3.9742	.0798	.0006	.0125	3.9742	.2824	.0265	1.9624
	.0696	3.8075	.1345	.0141	.0422	3.8075	.3667	.2060	2.3525
	.0594	3.7209	.0855	.0066	.0167	3.7209	.2924	.2626	2.2829
	.0295	3.9358	.0457	.0008	.0047	3.9358	.2139	.0809	2.2372
	NO SIGNAL OBSERVED								
	NO SIGNAL OBSERVED								
MEAN=	.0331	3.8790	.0864	.0055	.0190	3.8790	.2889	.1640	2.2057
SIGMA=	.02670	.09635	.03168	.00551	.01406	.09635	.05416	.11227	.14332

Table 7.1 Experimental Data for Puff Measurements (Continued).

STATION X=1.5M,Y=00 CM,Z=16CM.

	MO	K1	K2	K3	K4	MEAN (SEC.)	SIGMA (SEC.)	SKEWNESS	FLATNESS
	.0419	1.4085	.0607	.0001	.0071	1.4085	.2465	.0092	1.9525
	.1500	1.3893	.0357	.0067	.0047	1.3893	.1888	.9925	3.6736
	.0198	1.4841	.0091	.0004	.0002	1.4841	.0954	.4303	2.2896
	.0509	1.4037	.0109	-.0002	.0007	1.4037	.1576	-.0825	2.0338
	.0512	1.3805	.0171	.0009	.0007	1.3805	.1508	.4157	2.3649
	.0746	1.8995	.0699	.0127	.0127	1.8995	.2645	.6876	2.5825
MEAN=	.0614	1.4945	.0352	.0054	.0043	1.4945	.1772	.4085	2.4811
SIGMA=	.04315	.18452	.02204	.00477	.00450	.18452	.06179	.36968	.57528

STATION X=2.0M,Y=00 CM,Z=16CM.

	MO	K1	K2	K3	K4	MEAN (SEC.)	SIGMA (SEC.)	SKEWNESS	FLATNESS
	.1291	1.9885	.1339	.0486	.0501	1.9885	.3660	.9906	2.7913
	.2445	1.8730	.0703	.0154	.0149	1.8730	.2651	.7188	3.0154
	.1246	2.0335	.1181	.0019	.0289	2.0335	.3436	.0480	2.0720
	.0769	2.0415	.0487	.0017	.0053	2.0415	.2207	.1584	2.2277
	.0659	1.9590	.0645	.0062	.0093	1.9590	.2540	.3811	2.2408
	.1724	2.5495	.1476	.0493	.0655	2.5495	.3842	.8683	3.0050
MEAN=	.1356	2.0742	.0972	.0202	.0290	2.0742	.3756	.5275	2.5587
SIGMA=	.06011	.21975	.03757	.02071	.02208	.21975	.06162	.35468	.38931

STATION X=2.5M,Y=00 CM,Z=16CM.

	MO	K1	K2	K3	K4	MEAN (SEC.)	SIGMA (SEC.)	SKEWNESS	FLATNESS
	.0655	2.6436	.1625	.0210	.0574	2.6436	.4028	.5209	2.1782
	.0942	2.7978	.3663	.1106	.3005	2.7978	.6052	.4989	2.2581
	.0425	2.5606	.1167	.0142	.0275	2.5606	.3416	.3560	2.0053
	.0621	2.5997	.0808	.0198	.0215	2.5997	.2843	.8619	3.2682
	.0557	2.7427	.1064	.0202	.0285	2.7427	.3261	.5829	2.5205
	.1950	2.9832	.1186	.0345	.0502	2.9832	.3445	.8450	3.5697
MEAN=	.0858	2.7213	.1585	.0367	.0808	2.7213	.3840	.5776	2.6297
SIGMA=	.05126	.14233	.09599	.03361	.09900	.14233	.10484	.21552	.58492

STATION X=3.0M,Y=00 CM,Z=16CM.

	MO	K1	K2	K3	K4	MEAN (SEC.)	SIGMA (SEC.)	SKEWNESS	FLATNESS
	.0688	3.1207	.2228	.0422	.1154	3.1207	.4720	.4011	2.2855
	.0536	2.9967	.1718	.0243	.0678	2.9967	.4145	.3418	2.2955
	.0528	2.9379	.1153	.0179	.0361	2.9379	.3396	.4577	2.7160
	.0557	2.8687	.0744	.0124	.0146	2.8687	.2727	.6126	2.6448
	.0266	2.8966	.0839	.0079	.0165	2.8966	.2897	.3234	2.3146
	.1624	3.7984	.1967	.0507	.1025	3.7984	.4435	.5810	2.6430
MEAN=	.0700	3.1032	.1441	.0259	.0584	3.1032	.3720	.4529	2.4832
SIGMA=	.04319	.32144	.05633	.01556	.03922	.32144	.07594	.11086	.18645

Table 7.1 Experimental Data for Puff Measurements (Continued).

STATION X=3.5M,Y=00 CM,Z=16CM.

	MO	K1	K2	K3	K4	MEAN (SEC.)	SIGMA (SEC.)	SKEWNESS	FLATNESS
	.0141	3.8909	.2045	.0658	.1238	3.8909	.4522	.7117	2.8804
	.0109	3.8986	.2856	.0321	.1011	3.8986	.5344	.2101	2.2210
	.0155	3.4464	.1429	.0247	.0551	3.4464	.3701	.4573	2.6993
	.0053	3.0665	.1630	.0148	.0551	3.0665	.4038	.2250	2.0727
	.0064	3.0761	.1406	.0104	.0463	3.0761	.3749	.1979	2.5283
	.2015	4.0890	.4244	-.0059	.5208	4.0890	.6515	-.0159	1.7812
MEAN=	.0419	3.5779	.2268	.0240	.1298	3.5779	.4658	.2980	2.3318
SIGMA=	.07154	.40675	.10128	.02184	.09779	.40675	.09931	.22981	.37136

STATION X=4.0M,Y=00 CM,Z=16CM.

	MO	K1	K2	K3	K4	MEAN (SEC.)	SIGMA (SEC.)	SKEWNESS	FLATNESS
	.0060	3.9675	.2134	.0097	.0922	3.9675	.4620	.0988	2.0239
	.0119	4.0328	.2920	.0387	.1932	4.0328	.5403	.2450	2.2659
	.0056	4.2200	.1679	.0159	.0626	4.2200	.4097	.2505	2.2211
	.0259	4.2002	.1637	.0287	.0643	4.2002	.4046	.4329	2.3999
	.0047	4.1479	.1518	.0067	.0465	4.1479	.3896	.1128	2.0193
	.0021	1.9738	.0527	-.0014	.0043	1.9738	.2297	-.1147	1.5631
MEAN=	.0090	3.7570	.1736	.0164	.0772	3.7570	.4060	.1675	2.0822
SIGMA=	.00728	.80247	.07168	.01357	.05819	.80247	.09358	.16721	.26795

STATION X=2.0M,Y=05 CM,Z=16CM.

	MO	K1	K2	K3	K4	MEAN (SEC.)	SIGMA (SEC.)	SKEWNESS	FLATNESS
	.0801	2.0817	.0483	.0032	.0059	2.0817	.2197	.3016	2.5460
	.0685	2.2347	.0818	.0136	.0155	2.2347	.2860	.5825	2.3207
	.0995	2.1624	.1798	.0582	.0835	2.1624	.4241	.7625	2.5813
	.0764	2.1672	.0808	.0160	.0181	2.1672	.2843	.6957	2.7684
	.1018	2.1004	.0907	.0092	.0227	2.1004	.3011	.3359	2.7606
	.1402	2.2946	.1393	.0559	.0665	2.2946	.3732	1.0743	3.4290
MEAN=	.0944	2.1735	.1034	.0260	.0354	2.1735	.3147	.6254	2.7343
SIGMA=	.02371	.07342	.04340	.02231	.02889	.07342	.06627	.26325	.34506

STATION X=2.5M,Y=05 CM,Z=16CM.

	MO	K1	K2	K3	K4	MEAN (SEC.)	SIGMA (SEC.)	SKEWNESS	FLATNESS
	.1567	2.3472	.1303	.0219	.0450	2.3472	.3610	.4663	2.6517
	.1745	2.3993	.1037	.0248	.0319	2.3993	.3221	.7426	2.9673
	.1144	2.2508	.0523	.0079	.0079	2.2508	.2286	.6610	2.0832
	.0643	2.1801	.0375	.0048	.0037	2.1801	.1937	.6612	2.6493
	.0360	2.3464	.0938	.0223	.0205	2.3464	.3063	.7768	2.3255
	.1233	2.9587	.1927	.0406	.0963	2.9587	.4390	.4802	2.5914
MEAN=	.1115	2.4151	.1017	.0204	.0342	2.4151	.3084	.6313	2.6781
SIGMA=	.04845	.25322	.05120	.01178	.03106	.25322	.08118	.11930	.20780

Table 7.1 Experimental Data for Puff Measurements (Continued).

STATION X=3.0M, Y=05 CM, Z=16CM.

	MO	K1	K2	K3	K4	MEAN (SEC.)	SIGMA (SEC.)	SKEWNESS	FLATNESS
	.1708	2.9184	.1042	.0174	.0285	2.9184	.3227	.5175	2.6248
	.1881	3.1157	.1964	.0217	.0925	3.1157	.4452	.2494	2.3977
	.1176	2.8413	.1770	.0760	.1062	2.8413	.4207	1.0201	3.3903
	.1131	3.0455	.2265	.0450	.1554	3.0455	.4759	.4173	2.6385
	.1169	3.0168	.1944	.0254	.0796	3.0168	.4410	.2960	2.1062
	.1262	3.4423	.1451	.0284	.0603	3.4423	.3809	.5134	2.8635
MEAN=	.1388	3.0630	.1739	.0356	.0857	3.0630	.4141	.5023	2.6702
SIGMA=	.02946	.19102	.03956	.02000	.03385	.19102	.04982	.25239	.39819

STATION X=3.5M, Y=05 CM, Z=16CM.

	MO	K1	K2	K3	K4	MEAN (SEC.)	SIGMA (SEC.)	SKEWNESS	FLATNESS
	.0635	3.5316	.1457	.0371	.0550	3.5316	.3818	.6674	2.5888
	.0498	3.4405	.1082	.0119	.0267	3.4405	.3290	.3342	2.2768
	.0453	3.3336	.2139	.0288	.1205	3.3336	.4625	.2911	2.6332
	.0716	3.4276	.3754	-.0417	.3374	3.4276	.6127	-.1812	2.3941
	.0568	3.5280	.1626	.0161	.0659	3.5280	.4032	.2455	2.4949
	.0872	3.9631	.1327	.0150	.0418	3.9631	.3643	.3094	2.3758
MEAN=	.0624	3.5374	.1897	.0112	.1079	3.5374	.4256	.2777	2.4606
SIGMA=	.01403	.20179	.08910	.02523	.10673	.20179	.09299	.24761	.12456

STATION X=4.0M, Y=05 CM, Z=16CM.

	MO	K1	K2	K3	K4	MEAN (SEC.)	SIGMA (SEC.)	SKEWNESS	FLATNESS
	.0718	3.9187	.2140	.0526	.1074	3.9187	.4625	.3291	2.3461
	.1067	4.0486	.1830	.0571	.0939	4.0486	.4278	.7297	2.8025
	.0233	3.7127	.1411	-.0122	.0442	3.7127	.3757	-.2299	2.2184
	.0369	3.5407	.1564	.0078	.0493	3.5407	.3954	.1258	2.0154
	.0398	3.8915	.1750	.0271	.0602	3.8915	.4184	.3700	1.9633
	.0133	.6139	.0103	.0003	.0003	.6139	.1016	.3151	2.5965
MEAN=	.0486	3.2877	.1466	.0188	.0592	3.2877	.3636	.2733	2.3257
SIGMA=	.03165	1.20662	.06504	.02291	.03493	1.20662	.12021	.28795	.30005

STATION X=1.5M, Y=10 CM, Z=16CM.

	MO	K1	K2	K3	K4	MEAN (SEC.)	SIGMA (SEC.)	SKEWNESS	FLATNESS
	.0386	.5031	.0039	.0003	.0001	1.4489	.0621	1.3818	4.2328
	.0321	.6215	.0099	.0002	.0003	1.7899	.0996	.2128	2.6142
	.0225	.5128	.0035	-.0002	0.0000	1.4769	.0595	-.0820	2.4499
	.0250	.4474	.0029	0.0000	0.0000	1.2885	.0535	.2852	2.5280
	.0192	.4381	.0018	.0001	0.0000	1.2617	.0421	.9824	2.8482
	.0740	.6964	.0081	.0005	.0002	2.0056	.0902	.6735	3.0977
MEAN=	.0352	.5365	.0050	.0001	.0001	1.5453	.0678	.4423	2.9618
SIGMA=	.01846	.09318	.00294	.00022	.00012	.26835	.02033	.71402	.60798

Table 7.1 Experimental Data for Puff Measurements (Continued).

STATION X=2.0M,Y=10 CM,Z=16CM.

	MO	K1	K2	K3	K4	MEAN (SEC.)	SIGMA (SEC.)	SKEWNESS	FLATNESS
	.0704	.7160	.0046	-.0002	.0001	2.2769	.0677	-.5542	3.1175
	.0559	.6585	.0057	.0003	.0001	2.0504	.0755	.8101	2.7693
	.0165	.6114	.0031	.0001	0.0000	1.9443	.0556	.6877	2.5065
	.0519	.5674	.0052	.0002	0.0000	1.8043	.0569	.8711	3.0925
	.0097	.5813	.0001	0.0000	0.0000	1.8485	.0098	1.7962	8.7975
	.1259	.8474	.0077	-0.0000	.0002	2.6947	.0878	-.0623	2.5705
MEAN=	.0484	.6603	.0041	.0001	.0001	2.0999	.0589	.5914	3.8090
SIGMA=	.03966	.09648	.00237	.00016	.00007	.30680	.02454	.74460	2.24306

STATION X=2.5M,Y=10 CM,Z=16CM.

	MO	K1	K2	K3	K4	MEAN (SEC.)	SIGMA (SEC.)	SKEWNESS	FLATNESS
	.0231	.9423	.0066	0.0000	.0001	3.1567	.0810	.0474	2.4429
	.0251	.8572	.0054	.0002	.0001	2.8716	.0795	.5012	2.5151
	.0590	.9055	.0156	-.0001	.0006	3.0334	.1249	-.0618	2.2685
	.0574	.7299	.0107	.0002	.0002	2.4452	.1033	.1752	2.1806
	.0666	.7739	.0159	.0008	.0006	2.5926	.1262	.3993	2.2950
	.1658	.8940	.0144	.0015	.0007	2.9949	.1198	.8985	3.5713
MEAN=	.0661	.8505	.0114	.0004	.0004	2.8491	.1048	.3263	2.5456
SIGMA=	.04759	.07506	.00421	.00056	.00025	.25144	.02096	.32020	.47194

STATION X=3.0M,Y=10 CM,Z=16CM.

	MO	K1	K2	K3	K4	MEAN (SEC.)	SIGMA (SEC.)	SKEWNESS	FLATNESS
	.1353	.8794	.0157	.0010	.0005	2.8756	.1169	.6199	2.7167
	.0929	.8585	.0120	.0010	.0005	2.8073	.1094	.7703	3.3196
	.0460	.8832	.0082	.0003	.0002	2.8881	.0908	.3938	2.2852
	.0515	.8430	.0082	.0004	.0002	2.7566	.0907	.5744	2.7571
	.1100	.9522	.0090	-0.0000	.0002	3.1137	.0947	-.0261	2.5244
	.0857	.9108	.0150	.0010	.0005	2.9783	.1225	.5524	2.3848
MEAN=	.0866	.8878	.0110	.0006	.0003	2.9033	.1042	.4774	2.6646
SIGMA=	.03124	.03567	.00271	.00040	.00015	.11664	.01275	.25134	.33719

STATION X=3.5M,Y=10 CM,Z=16CM.

	MO	K1	K2	K3	K4	MEAN (SEC.)	SIGMA (SEC.)	SKEWNESS	FLATNESS
	.0658	.9313	.0117	.0004	.0003	3.6134	.1080	.2908	2.0361
	.0392	.9237	.0142	.0007	.0004	3.5840	.1192	.4430	2.1173
	.1184	.9207	.0130	.0006	.0004	3.5723	.1140	.4220	2.5096
	.1248	.9383	.0084	.0004	.0002	3.6406	.0918	.5556	3.1788
	.0324	.9533	.0078	.0002	.0001	3.6988	.0881	.2663	2.1954
	.0586	.9924	.0133	.0002	.0004	3.8505	.1153	.1249	1.9930
MEAN=	.0732	.9453	.0114	.0004	.0003	3.6599	.1061	.3504	2.3384
SIGMA=	.03605	.02441	.00245	.00019	.00012	.09471	.01191	.13981	.41142

Table 7.1 Experimental Data for Puff Measurements (Continued).

STATION X=4.0M,Y=10 CM,Z=16CM.

	MO	K1	K2	K3	K4	MEAN (SEC.)	SIGMA (SEC.)	SKEWNESS	FLATNESS
	.0376	.9639	.0130	.0004	.0004	3.9809	.1142	.2658	2.2134
	.0272	1.0107	.0124	-.0006	.0004	4.1742	.1113	-.4705	2.4384
	.0216	.9344	.0050	-0.0000	.0001	3.8591	.0705	-.0121	2.1505
	.0157	.9517	.0063	.0001	.0001	3.9305	.0793	.1335	2.3057
	.0410	.9421	.0071	.0004	.0001	3.8909	.0841	.6444	2.7794
	NO SIGNAL OBSERVED								
MEAN=	.0238	.9606	.0088	.0001	.0002	3.9671	.0919	.1122	2.3775
SIGMA=	.01375	.02694	.00329	.00037	.00015	.11126	.01761	.36380	.22309

STATION X=2.5M,Y=20 CM,Z=16CM.

	MO	K1	K2	K3	K4	MEAN (SEC.)	SIGMA (SEC.)	SKEWNESS	FLATNESS
	.0034	.6157	.0007	0.0000	0.0000	2.5367	.0262	.0920	2.1456
	.0143	.6124	.0019	0.0000	0.0000	2.5231	.0431	.3610	2.2107
	.0100	.7177	.0028	0.0000	0.0000	2.9569	.0527	.2186	1.8274
	.0162	.6409	.0016	0.0000	0.0000	2.6735	.0404	.4679	2.3621
	.0264	.6124	.0020	0.0000	0.0000	2.5231	.0449	.4624	2.9890
	NO SIGNAL OBSERVED								
MEAN=	.0117	.6414	.0018	0.0000	0.0000	2.6427	.0415	.3204	2.3070
SIGMA=	.00868	.04055	.00068	0.00000	0.00000	.16705	.00866	.14567	.38501

STATION X=3.0M,Y=20 CM,Z=16CM.

	MO	K1	K2	K3	K4	MEAN (SEC.)	SIGMA (SEC.)	SKEWNESS	FLATNESS
	.0070	.7023	.0037	0.0000	0.0000	3.1744	.0611	.0774	1.7513
	.0245	.7785	.0129	.0009	.0004	3.5179	.1138	.6050	2.2779
	.0095	.7011	.0035	.0001	0.0000	3.1690	.0585	.3449	2.3365
	.0116	.6371	.0020	0.0000	0.0000	2.8797	.0446	.5203	2.5026
	.0140	.8520	.0066	-0.0000	.0001	3.8510	.0812	-.0872	2.2499
	NO SIGNAL OBSERVED								
MEAN=	.0111	.7342	.0057	.0002	.0001	3.3184	.0720	.2921	2.2236
SIGMA=	.00742	.07398	.00388	.00035	.00015	.33438	.02391	.26181	.25191

STATION X=3.5M,Y=20 CM,Z=16CM.

	MO	K1	K2	K3	K4	MEAN (SEC.)	SIGMA (SEC.)	SKEWNESS	FLATNESS
	.0175	.7595	.0043	.0001	0.0000	3.5385	.0653	.1810	1.9909
	.0041	.8417	.0016	0.0000	0.0000	3.9225	.0400	.3798	2.1347
	.0146	.8476	.0050	.0001	.0001	3.9498	.0710	.2825	2.0509
	.0204	.8006	.0027	.0001	0.0000	3.7308	.0520	.6964	2.9021
	.0190	.7976	.0027	.0001	0.0000	3.7168	.0516	.7888	3.0763
	.0165	.9062	.0057	-0.0000	0.0000	4.2229	.0606	-.1846	2.4622
MEAN=	.0154	.8255	.0035	.0001	.0000	3.8468	.0567	.3573	2.4362
SIGMA=	.00534	.04663	.00115	.00005	.00004	.21728	.01017	.32456	.42133

Table 7.1 Experimental Data for Puff Measurements (Continued).

STATION X=4.0M, Y=20 CM, Z=16CM.

	MO	K1	K2	K3	K4	MEAN (SEC.)	SIGMA (SEC.)	SKEWNESS	FLATNESS
	.0524	.8845	.0084	.0001	.0001	4.7144	.0918	.0806	2.0904
	.0444	.8547	.0078	.0001	.0001	4.4490	.0880	.0868	2.1296
	.0133	.9415	.0043	-0.0000	0.0000	5.0182	.0655	-.1653	2.2179
	.0318	.9502	.0157	0.0000	.0004	5.0646	.1171	.0118	2.0301
	.0309	.9285	.0121	-.0002	.0003	4.9489	.1099	-.1458	1.9966
	NO SIGNAL OBSERVED								
MEAN=	.0255	.9079	.0093	0.0000	.0002	4.8390	.0945	-.0264	2.0929
SIGMA=	.01455	.04501	.00332	.00011	.00015	.22923	.01810	.10888	.07771

STATION X=3.0M, Y=-20CM, Z=16CM.

	MO	K1	K2	K3	K4	MEAN (SEC.)	SIGMA (SEC.)	SKEWNESS	FLATNESS
	0.0000	0.0000	-0.0000	-0.0000	-0.0000	0.0000	-0.0000	-0.0000	-3.0000
	.0105	.7412	.0019	0.0000	0.0000	4.5732	.0440	.1297	1.9730
	.0286	.7382	.0039	0.0000	0.0000	4.5847	.0622	.1582	2.8804
	.0144	.7204	.0029	-0.0000	0.0000	4.4449	.0536	-.0408	2.4847
	.0218	.7021	.0051	.0001	.0001	4.3320	.0714	.1961	2.0009
	NO SIGNAL OBSERVED								
MEAN=	.0145	.5804	.0028	.0000	.0000	3.5809	.0462	.0888	1.2678
SIGMA=	.00900	.29053	.00174	.00004	.00004	1.79256	.02484	.09255	2.16010

STATION X=3.5M, Y=-20CM, Z=16CM.

	MO	K1	K2	K3	K4	MEAN (SEC.)	SIGMA (SEC.)	SKEWNESS	FLATNESS
	.0112	.7460	.0018	0.0000	0.0000	3.4092	.0426	.4231	2.7756
	.0446	.8175	.0075	.0003	.0001	3.7960	.0885	.4670	2.4432
	.0233	.8626	.0064	.0002	.0001	3.9421	.0802	.4049	2.2778
	.0306	.8703	.0055	.0001	.0001	3.9773	.0740	.2795	2.0888
	.0177	.8032	.0021	.0001	0.0000	3.6706	.0457	1.0765	2.9951
	.0370	.8728	.0075	.0001	.0001	3.9887	.0867	.1553	2.3049
MEAN=	.0274	.8287	.0051	.0001	.0001	3.7873	.0693	.4677	2.4809
SIGMA=	.01152	.04553	.00255	.00009	.00005	.20809	.01830	.29143	.31055

STATION X=4.0M, Y=-20CM, Z=16CM.

	MO	K1	K2	K3	K4	MEAN (SEC.)	SIGMA (SEC.)	SKEWNESS	FLATNESS
	.0392	.7956	.0178	.0006	.0006	2.5857	.1333	.2431	2.0050
	.0063	1.0015	.0042	-0.0000	0.0000	3.2549	.0647	-.1017	1.9861
	.0035	.8079	.0011	0.0000	0.0000	2.6257	.0528	.7390	2.9687
	.0217	.8644	.0100	0.0000	.0002	2.8093	.1000	.0019	2.0684
	.0077	.8798	.0052	0.0000	0.0000	2.8593	.0567	.2206	2.2892
	.1712	3.0508	.1396	.0438	.0609	9.9151	.3737	.8387	3.1245
MEAN=	.0416	1.2333	.0293	.0074	.0103	4.0083	.1269	.3256	2.4070
SIGMA=	.05923	.81554	.04963	.01628	.02264	2.65051	.11498	.35103	.46504

Table 7.2 Program CHARLI

```
      PROGRAM CHARLI
     1(INPUT,OUTPUT,TAPE5=INPUT,TAPE6=OUTPUT,FILMPL)
C       THIS PROGRAM IS TO TEST THE GRAM-CHARLIE DISTRIBUTION
      DIMENSION GX(4)
      DIMENSION S1GA(4),S2GA(4),SKEWGA(4),FLATGA(4),XX(200),YY(200)
      DIMENSION R(4),RAMDA(4)
      DIMENSION Y(200)
      COMMON X(200)
      DIMENSION LABT(4),LA(2),LAA(2),LAAA(2)
      DATA S1SN/0.0/,S2SN/1./,SKEWSN/0./,FLATSN/3./,X0/-8./
      READ(5,40) LABT    ,LA    ,LAA    ,LAAA
   40 FORMAT(4A10,/,2A10,/,2A10,/,2A10)
      DO 1 I=1,160
      X(I)=X0+0.1*FLOAT(I)
      Y(I)=0.399*EXP(-(X(I)**2)/2.)
    1 CONTINUE
      WRITE(6,2)
    2 FORMAT(1H1,*    STANDARD NORMAL   *)
      WRITE(6,3)   (X(I),Y(I),I=1,160)
    3 FORMAT(/    ,8(F6.2,2X,F 5.2))
      CALL GRAM (S1SN,S2SN,SKEWSN,FLATSN)
C       SSP PP. 361 FOR GAMMA DISTRIBUTION (FUNCTION) CALCULATION
C       THE FIRST TWO CASES ARE R=1, WHICH ARE EXPONENTIAL DISTRIBUTION
      DATA  (R(I),I=1,4)/4.0,4.0,4.0,4.0/
      DATA  (RAMDA(I),I=1,4)/  1.6,1.75,1.8,2.0/
      DO 21 I=1,4
      S1GA(I)=R(I)/RAMDA(I)
      S2GA(I)=R(I)**0.5/RAMDA(I)
      SKEWGA(I)=2./R(I)**0.5
      FLATGA(I)=(6.+3.*R(I))/R(I)
      DO 31 J=1,160
      XX(J)=FLOAT(J)*0.05
      X(J)=XX(J)
      CALL GMMMA(R(I),GX(I),IER)
      YY(J)=RAMDA(I)/GX(I)*(RAMDA(I)*XX(J))**(R(I)-1.)*EXP(-1.*RAMDA(I)*
     1XX(J))
   31 CONTINUE
      WRITE(6,32)(XX(K),YY(K),K=1,160)
   32 FORMAT(/    ,8(F6.2,2X,F 5.2))
      CALL FRAME
      CALL SET(0.2,0.8,0.1,0.9,0.,8.,0.0,0.5,1)
      CALL GRDFMT(6H(F6.2),6H(F6.3))
      CALL PERIML(8,10,5,10)
      CALL CURVE(XX,YY,160)
      CALL PSYM(XX(90),YY(90),1HG,2,0,1)
      CALL PSYM(XX(10),YY(10),1HG,2,0,1)
      CALL PWRT(250,950,LABT,40,1,0)
      CALL PWRT(500,850,LA,20,1,0)
      CALL PWRT(500,800,LAA,20,1,0)
      CALL PWRT(500,750,LAAA,20,1,0)
      CALL GRAM (S1GA(I),S2GA(I),SKEWGA(I),FLATGA(I) )
   21 CONTINUE
      END
```

Table 7.2 Program CHARLI (Continued).

```
      SUBROUTINE GRAM (S1,S2,SKEW,FLAT)
      DIMENSION XX(200),YY(200),H3(200),H4(200),H6(200),H7(200),H8(200)
      COMMON X(200)
      EX=FLAT-3.
      DO 1 I=1,160
      XX(I)=(X(I)-S1)/S2
      H3(I)=XX(I)**3-3.*XX(I)
      H4(I)=XX(I)**4-6.*XX(I)**2+3.
      H6(I)=XX(I)**6-15.*XX(I)**4+45.*XX(I)**2-15.
      H7(I)=XX(I)**7-21.*XX(I)**5+105.*XX(I)**3-105.*XX(I)
      H8(I)=XX(I)**8-28.*XX(I)**6+210.*XX(I)**4-420.*XX(I)**2+105.
      YY(I)=(0.399/S2)*(1.+0.1666*SKEW*H3(I)      )*EXP(-0.5*XX(I)**2)
    1 CONTINUE
C     3RD POLYNOMIAL
      CALL CURVE(X,YY,160)
      CALL PSYM(X(35),YY(35),1HT,2,0,1)
      CALL PSYM(X(95),YY(95),1HT,2,0,1)
      WRITE(6,2) S1,S2,SKEW,FLAT
    2 FORMAT(//,*  MEAN=* F6.2 ,* VARIANCE =  *,F6.3,*   SKEWNESS=  *
     1,F6.3,*     FLATNESS=    *,F6.2)
      WRITE(6,3)   (XX(I),YY(I),I=1,160)
    3 FORMAT(/    ,8(F6.2,2X,F 5.2))
C     4TH POLYNOMIAL
      DO 4 I=1,160
      YY(I)=YY(I)+(0.399/S2)*(0.0416*EX*H4(I)+0.0138*(SKEW**2)*H6(I))
     1*EXP(-0.5*XX(I)**2)
    4 CONTINUE
      WRITE(6,5)(XX(I),YY(I),I=1,160)
    5 FORMAT( /     ,8(F6.2,2X,F5.2))
      CALL CURVE(X,YY,160)
      CALL PSYM(X(05),YY(05),1HF,2,0,1)
      CALL PSYM(X(99),YY(99),1HF,2,0,1)
      RETURN
      END
```

Table A.1 Program TREVA

```
*FORTRAN
      PROGRAM TREVA
C   ---THIS PROGRAM IS TO EVALUATE THE C-DISTRIBUTION BY USING
C      NUMERICAL INTERGRATION TO FIND THE FIRST FIVE MOMENTS.
C     C-DISTRIBUTION IS  A REPRESENTATIVE DISTRIBUTION CURVE FOR A
C      ONE-DIMENSIONAL CONVECTIVE DIFFUSION .
C     THERE ARE  3 PARAMETERS , NAMELY XO,A, AND V
C    XO STANSS FOR THE INITIAL MEASIRING POSITION, A IS THE RATE OF
C      DIFFUSION, V IS THE  MEAN CONVECTIVE VELOSITY

      DIMENSION LABT(3)
      DIMENSION UBO(3),       XO(5),       T(5001),F(5001),LABX(4)
      DIMENSION LABY(4),ANS(6),V(5)
      DIMENSION CH(10),A(10)
      DATA (UBO(I),I=1,3) /0.0,0.02,100./
      DATA (XO(I),I=1,5)/1.0,2.0,3.0,4.0,5.0/
      DATA (V(J),J=1,5)/+0.25,0.3,0.4,0.5,0.6/
      DATA (A(K),K=1,10)/+0.01,0.02,0.03,0.04,0.05,0.06,0.07,0.08
     1,0.1,0.2/
      F(1)=0.0


      DO 10 L=2,5001
   10 T(L)=FLOAT(L-1)*0.02
      T(1)=0.
      READ (5,20) LABX,LABY,LABT
   20 FORMAT (15X,4A10,/,14X,4A10,/,3A10)
      READ (5,22) (CH(K),K=1,10)
   22 FORMAT(10A1)
      DO 1 I=1,5
      WRITE (6,1000)XO(I)
 1000 FORMAT (1H1,40X,* MATHEMATICAL  PROPERTIES  OF  C-DISTRIBUTION  *,
     1 /,55X,* XO=*,F5.2,/,25X,* 0TH MOMENT      C-MAX      T (CMAX)  MEAN
     1          SIGMA           SKEWNESS       FLATNESS*)
      DO 2 J=1,5
      WRITE (6,1001) V(J)
 1001 FORMAT (10X,*V=*,F5.3)
      PUNCH 2000,XO(I),V(J)
 2000 FORMAT( * XO=*,F5.2,5X,*V=*,F5.3)
      DO 21 K=1,10
      DO 3 L=2,5001
      F(L)=(0.399* V(J))/(A(K)*T(L))
     1 *EXP(-0.5*((XO(I)-V(J)*T(L))/ (A(K)*T(L)))**2)
    3 CONTINUE

C     SEARCH THE MAX. F-VALUE
      DO 331 LL=2,5001
      IF(F(LL).LT.F(LL-1)) GO TO 431
  331 CONTINUE
  431 MAXT=LL-1
      TMAX=FLOAT (MAXT)*0.02
      IF(K .EQ.1) GO TO 30
      GO TO 31
   30 CONTINUE
C      FMX AND IFMX ARE SET UP FOR PLOTTING
      FMX=IFIX(F(MAXT))+1
      IFMX=FMX

   31 CONTINUE
C      SSP

C     REVISED IBM SSP SUBROUTINE MOMEN
```

Table A.1 Program TREVA (Continued).

```
      CALL MOMEN (F,UBO,5,ANS,FSUM)
      FSUM=FSUM*0.02
      SIGMA=ANS(2)**0.5
      SKEW= ANS(3)/ANS(2)**1.5
      FLAT= ANS(4)/ ANS(2)**2
      WRITE (6,1003) A(K),
     1               FSUM,F(MAXT),TMAX,ANS(1),SIGMA,SKEW,FLAT
 1003 FORMAT (13X,*A=*,F6.4,2X,F10.6,2X,F8.3,4X,F8.4,2X,F5.2,
     15X,F8.4,5X,E9.2,5X,E13.3)
      PUNCH 2001,A(K),F(MAXT),TMAX,ANS(1),SIGMA,SKEW,FLAT
 2001 FORMAT(*A=*,F5.3, 4F7.4,2E13.3)
   21 CONTINUE
    2 CONTINUE
    1 CONTINUE
      END

      SUBROUTINE MOMEN (F,UBO,NOP,ANS,T)
      DIMENSION F(1),UBO(1),ANS(1)
C
      DO 100 I=1,4
  100 ANS(I)=0.0
C
C     CALCULATE THE NUMBER OF CLASS INTERVALS
C
      N=(UBO(3)-UBO(1))/UBO(2)+0.5
C
C     CALCULATE TOTAL FREQUENCY
C
      T=0.0
      DO 110 I=1,N
  110 T=T+F(I)
C
      IF(NOP-5) 130, 120, 115
  115 NOP=5
  120 JUMP=1
      GO TO 150
  130 JUMP=2
C
C        FIRST MOMENT
C
  150 DO 160 I=1,N
      FI=I
  160 ANS(1)=ANS(1)+F(I)*(UBO(1)+(FI-0.5)*UBO(2))
      ANS(1)=ANS(1)/T
C
      GO TO (350,200,250,300,200), NOP
C
C        SECOND MOMENT
C
  200 DO 210 I=1,N
      FI=I
  210 ANS(2)=ANS(2)+F(I)*(UBO(1)+(FI-0.5)*UBO(2)-ANS(1))**2
      ANS(2)=ANS(2)/T
      GO TO (250,350), JUMP
C
C        THIRD MOMENT
C
  250 DO 260 I=1,N
      FI=I
  260 ANS(3)=ANS(3)+F(I)*(UBO(1)+(FI-0.5)*UBO(2)-ANS(1))**3
      ANS(3)=ANS(3)/T
      GO TO (300,350), JUMP
C
C        FOURTH MOMENT
C
  300 DO 310 I=1,N
      FI=I
  310 ANS(4)=ANS(4)+F(I)*(UBO(1)+(FI-0.5)*UBO(2)-ANS(1))**4
      ANS(4)=ANS(4)/T
  350 RETURN
      END
```

Table A.2 Mathematical Properties of C-Distribution.

XO= 1.00

	0TH MOMENT	C-MAX	T (CMAX)	MEAN	SIGMA	SKEWNESS	FLATNESS
V= .250							
A= .0100	1.001753	2.494	4.0200	4.02	.1617	2.44E-01	3.119E+00
A= .0200	1.006673	1.251	4.0000	4.06	.3342	5.12E-01	3.537E+00
A= .0300	1.015219	.837	3.9600	4.13	.5324	8.47E-01	4.552E+00
A= .0400	1.028027	.631	3.9200	4.25	.7859	1.46E+00	1.182E+01
A= .0500	1.046366	.508	3.8800	4.43	1.2366	6.59E+00	2.405E+02
A= .0600	1.072902	.427	3.8200	4.77	2.5324	1.27E+01	3.008E+02
A= .0700	1.111068	.369	3.7400	5.48	5.0494	9.21E+00	1.202E+02
A= .0800	1.161124	.327	3.6800	6.66	8.1974	6.25E+00	5.156E+01
A= .1000	1.275854	.267	3.5200	9.96	13.9557	3.66E+00	1.774E+01
A= .2000	1.396821	.154	2.8000	19.68	23.0425	1.69E+00	5.050E+00
V= .300							
A= .0100	1.001260	3.579	3.3400	3.35	.1119	2.02E-01	3.082E+00
A= .0200	1.004650	1.799	3.3400	3.37	.2289	4.18E-01	3.355E+00
A= .0300	1.010462	1.203	3.3200	3.41	.3573	6.66E-01	3.929E+00
A= .0400	1.018970	.906	3.3000	3.47	.5070	9.92E-01	5.220E+00
A= .0500	1.030649	.728	3.2600	3.56	.6990	1.74E+00	2.568E+01
A= .0600	1.046369	.610	3.2200	3.69	1.0423	8.27E+00	3.907E+02
A= .0700	1.067812	.526	3.1800	3.92	1.9709	1.57E+01	4.976E+02
A= .0800	1.097328	.464	3.1400	4.36	3.7998	1.20E+01	2.105E+02
A= .1000	1.183089	.378	3.0400	6.21	8.9452	5.98E+00	4.581E+01
A= .2000	1.475294	.211	2.5200	16.98	21.7267	1.96E+00	6.141E+00
V= .400							
A= .0100	1.000771	6.384	2.5200	2.51	.0628	1.51E-01	3.046E+00
A= .0200	1.002664	3.192	2.5200	2.52	.1271	3.07E-01	3.190E+00
A= .0300	1.005868	2.133	2.5000	2.54	.1947	4.76E-01	3.465E+00
A= .0400	1.010462	1.604	2.5000	2.56	.2680	6.66E-01	3.929E+00
A= .0500	1.016569	1.287	2.4800	2.60	.3501	8.98E-01	4.768E+00
A= .0600	1.024372	1.076	2.4600	2.64	.4464	1.23E+00	8.226E+00
A= .0700	1.034153	.925	2.4400	2.69	.5714	2.78E+00	1.231E+02
A= .0800	1.046374	.813	2.4200	2.77	.8004	1.26E+01	8.782E+02
A= .1000	1.081672	.657	2.3800	3.10	2.4344	1.83E+01	5.058E+02
A= .2000	1.445019	.354	2.1000	11.51	18.0295	2.76E+00	1.051E+01
V= .500							
A= .0100	1.000545	9.975	2.0200	2.01	.0401	1.20E-01	3.029E+00
A= .0200	1.001753	4.987	2.0200	2.02	.0808	2.44E-01	3.119E+00
A= .0300	1.003785	3.325	2.0200	2.02	.1229	3.73E-01	3.281E+00
A= .0400	1.006673	2.499	2.0000	2.04	.1671	5.12E-01	3.537E+00
A= .0500	1.010462	2.005	2.0000	2.05	.2144	6.66E-01	3.929E+00
A= .0600	1.015219	1.673	2.0000	2.07	.2662	8.47E-01	4.552E+00
A= .0700	1.021032	1.439	1.9800	2.10	.3245	1.08E+00	5.885E+00
A= .0800	1.028027	1.262	1.9800	2.13	.3931	1.55E+00	3.043E+01
A= .1000	1.046377	1.017	1.9400	2.22	.6566	1.82E+01	1.676E+03
A= .2000	1.312160	.535	1.7800	6.83	13.1370	4.24E+00	2.260E+01
V= .600							
A= .0100	1.000423	14.009	1.6800	1.68	.0278	1.00E-01	3.020E+00
A= .0200	1.001260	7.159	1.6800	1.68	.0560	2.02E-01	3.082E+00
A= .0300	1.002664	4.792	1.6800	1.69	.0847	3.07E-01	3.190E+00
A= .0400	1.004650	3.599	1.6800	1.69	.1145	4.18E-01	3.355E+00
A= .0500	1.007240	2.881	1.6800	1.70	.1456	5.36E-01	3.591E+00
A= .0600	1.010462	2.402	1.6800	1.71	.1787	6.66E-01	3.929E+00
A= .0700	1.014356	2.065	1.6600	1.73	.2143	8.14E-01	4.425E+00
A= .0800	1.018970	1.811	1.6600	1.74	.2535	9.92E-01	5.251E+00
A= .1000	1.030649	1.456	1.6400	1.79	.3499	2.22E+00	1.322E+02
A= .2000	1.194513	.755	1.5400	3.76	8.1325	7.21E+00	6.307E+01

Table A.2 Mathematical Properties of C-Distribution (Cont'd.)

XO= 2.00

	0TH MOMENT	C-MAX	T (CMAX)	MEAN	SIGMA	SKEWNESS	FLATNESS
V= .250							
A= .0100	1.001753	1.248	8.0000	8.04	.3254	2.44E-01	3.119E+00
A= .0200	1.006673	.625	7.9600	8.12	.6684	5.12E-01	3.537E+00
A= .0300	1.015219	.419	7.9000	8.26	1.0648	8.47E-01	4.582E+00
A= .0400	1.028026	.316	7.8200	8.49	1.5716	1.45E+00	9.067E+00
A= .0500	1.046344	.254	7.7200	8.85	2.4005	3.62E+00	5.261E+01
A= .0600	1.072375	.214	7.6000	9.47	4.1286	6.13E+00	7.958E+01
A= .0700	1.107607	.185	7.4800	10.54	6.8770	5.52E+00	4.811E+01
A= .0800	1.149750	.165	7.3400	12.05	9.9917	4.32E+00	2.705E+01
A= .1000	1.232650	.134	7.0400	15.62	15.2912	2.87E+00	1.204E+01
A= .2000	1.224052	.077	5.5600	24.61	23.4575	1.44E+00	4.179E+00
V= .300							
A= .0100	1.001260	1.796	6.6800	6.69	.2238	2.02E-01	3.082E+00
A= .0200	1.004650	.900	6.6600	6.74	.4579	4.18E-01	3.358E+00
A= .0300	1.010462	.601	6.6200	6.82	.7147	6.66E-01	3.929E+00
A= .0400	1.018970	.453	6.5800	6.94	1.0139	9.92E-01	5.215E+00
A= .0500	1.030649	.364	6.5200	7.11	1.3971	1.62E+00	1.286E+01
A= .0600	1.046352	.305	6.4400	7.37	2.0137	4.10E+00	7.419E+01
A= .0700	1.067520	.263	6.3600	7.80	3.2520	7.19E+00	1.185E+02
A= .0800	1.095541	.232	6.2800	8.49	5.2998	6.92E+00	7.857E+01
A= .1000	1.168985	.189	6.0800	10.84	10.4484	4.42E+00	2.719E+01
A= .2000	1.325594	.106	5.0200	21.55	22.2411	1.69E+00	5.085E+00
V= .400							
A= .0100	1.000771	3.192	5.0200	5.02	.1256	1.51E-01	3.046E+00
A= .0200	1.002664	1.597	5.0000	5.04	.2542	3.07E-01	3.190E+00
A= .0300	1.005868	1.067	5.0000	5.07	.3895	4.76E-01	3.463E+00
A= .0400	1.010462	.802	4.9800	5.12	.5360	6.66E-01	3.929E+00
A= .0500	1.016563	.643	4.9400	5.18	.7001	8.98E-01	4.768E+00
A= .0600	1.024372	.538	4.9200	5.27	.8928	1.25E+00	7.028E+00
A= .0700	1.034152	.463	4.8800	5.38	1.1395	2.08E+00	2.896E+01
A= .0800	1.046361	.407	4.8400	5.53	1.5283	5.21E+00	1.387E+02
A= .1000	1.081014	.329	4.7400	6.11	3.4840	9.78E+00	1.706E+02
A= .2000	1.358742	.177	4.1600	15.37	18.7234	2.41E+00	8.576E+00
V= .500							
A= .0100	1.000545	4.987	4.0200	4.01	.0802	1.20E-01	3.029E+00
A= .0200	1.001753	2.494	4.0200	4.02	.1617	2.44E-01	3.119E+00
A= .0300	1.003785	1.665	4.0000	4.04	.2458	3.75E-01	3.281E+00
A= .0400	1.006673	1.251	4.0000	4.06	.3342	5.12E-01	3.537E+00
A= .0500	1.010462	1.002	3.9800	4.09	.4288	6.66E-01	3.929E+00
A= .0600	1.015219	.837	3.9600	4.13	.5324	8.47E-01	4.582E+00
A= .0700	1.021032	.719	3.9400	4.18	.6490	1.08E+00	5.726E+00
A= .0800	1.028027	.631	3.9200	4.25	.7859	1.46E+00	1.182E+01
A= .1000	1.046366	.508	3.8800	4.43	1.2366	6.59E+00	2.405E+02
A= .2000	1.275854	.267	3.5200	9.96	13.9557	3.66E+00	1.774E+01
V= .600							
A= .0100	1.000423	7.116	3.3600	3.35	.0557	1.00E-01	3.020E+00
A= .0200	1.001260	3.579	3.3400	3.35	.1119	2.02E-01	3.082E+00
A= .0300	1.002664	2.396	3.3400	3.36	.1694	3.07E-01	3.190E+00
A= .0400	1.004650	1.799	3.3400	3.37	.2289	4.18E-01	3.358E+00
A= .0500	1.007240	1.440	3.3400	3.39	.2912	5.36E-01	3.591E+00
A= .0600	1.010462	1.203	3.3200	3.41	.3573	6.66E-01	3.929E+00
A= .0700	1.014356	1.033	3.3000	3.44	.4286	8.14E-01	.428E+00
A= .0800	1.018970	.906	3.3000	3.47	.5070	9.92E-01	5.220E+00
A= .1000	1.030649	.728	3.2600	3.56	.6990	1.74E+00	2.568E+01
A= .2000	1.183089	.378	3.0400	6.21	8.9452	5.98E+00	4.981E+01

Table A.2 Mathematical Properties of C-Distribution (Cont'd.)

	0TH MOMENT	C-MAX	T (CMAX)	MEAN	SIGMA	SKEWNESS	FLATNESS
			XO= 3.00				
V= .250							
A= .0100	1.001753	.832	12.0000	12.05	.4851	2.44E-01	3.119E+00
A= .0200	1.006673	.417	11.9400	12.17	1.0026	5.12E-01	3.537E+00
A= .0300	1.015219	.279	11.8600	12.38	1.5972	8.47E-01	4.552E+00
A= .0400	1.028026	.210	11.7200	12.72	2.3570	1.41E+00	8.477E+00
A= .0500	1.046312	.169	11.5800	13.26	3.5509	2.90E+00	2.793E+01
A= .0600	1.071783	.142	11.4000	14.15	5.6556	4.20E+00	3.704E+01
A= .0700	1.104334	.123	11.2000	15.49	8.5414	3.94E+00	2.606E+01
A= .0800	1.140135	.109	11.0000	17.20	11.5405	3.28E+00	1.690E+01
A= .1000	1.200659	.089	10.5400	20.79	16.3329	2.35E+00	8.880E+00
A= .2000	1.116850	.051	8.3400	28.63	23.5738	1.26E+00	3.662E+00
V= .300							
A= .0100	1.001260	1.197	10.0000	10.03	.3358	2.02E-01	3.082E+00
A= .0200	1.004650	.600	9.9800	10.10	.6868	4.18E-01	3.355E+00
A= .0300	1.010462	.401	9.9200	10.22	1.0720	6.66E-01	3.929E+00
A= .0400	1.018970	.302	9.8400	10.40	1.5209	9.92E-01	5.213E+00
A= .0500	1.030649	.243	9.7600	10.67	2.0949	1.59E+00	1.086E+01
A= .0600	1.046330	.203	9.6400	11.05	2.9778	3.19E+00	3.640E+01
A= .0700	1.067213	.175	9.5200	11.66	4.5064	4.83E+00	5.295E+01
A= .0800	1.093904	.155	9.4000	12.57	6.7270	4.84E+00	4.063E+01
A= .1000	1.157993	.126	9.1000	15.25	11.7686	3.48E+00	1.816E+01
A= .2000	1.231511	.070	7.5200	25.39	22.4848	1.49E+00	4.416E+00
V= .400							
A= .0100	1.000771	2.128	7.5200	7.52	.1883	1.51E-01	3.046E+00
A= .0200	1.002664	1.065	7.5000	7.55	.3812	3.07E-01	3.190E+00
A= .0300	1.005868	.711	7.4800	7.60	.5842	4.76E-01	3.463E+00
A= .0400	1.010462	.535	7.4400	7.67	.8040	6.66E-01	3.929E+00
A= .0500	1.016569	.429	7.4000	7.77	1.0502	8.98E-01	4.768E+00
A= .0600	1.024372	.359	7.3600	7.89	1.3391	1.23E+00	6.846E+00
A= .0700	1.034152	.309	7.3000	8.06	1.7072	1.94E+00	1.841E+01
A= .0800	1.046347	.271	7.2400	8.29	2.2556	3.78E+00	5.914E+01
A= .1000	1.080446	.219	7.1000	9.10	4.5332	6.58E+00	8.177E+01
A= .2000	1.303114	.118	6.2400	18.79	19.2249	2.14E+00	7.272E+00
V= .500							
A= .0100	1.000545	3.325	6.0200	6.01	.1203	1.20E-01	3.029E+00
A= .0200	1.001753	1.662	6.0200	6.03	.2425	2.44E-01	3.119E+00
A= .0300	1.003785	1.110	6.0000	6.05	.3687	3.73E-01	3.281E+00
A= .0400	1.006673	.834	5.9800	6.09	.5013	5.12E-01	3.537E+00
A= .0500	1.010462	.668	5.9600	6.14	.6432	6.66E-01	3.929E+00
A= .0600	1.015219	.558	5.9400	6.20	.7986	8.47E-01	4.552E+00
A= .0700	1.021032	.480	5.9000	6.27	.9735	1.08E+00	5.704E+00
A= .0800	1.028027	.421	5.8800	6.37	1.1788	1.44E+00	9.749E+00
A= .1000	1.046356	.339	5.8000	6.64	1.8197	4.44E+00	9.220E+01
A= .2000	1.251837	.178	5.2800	12.87	14.6652	3.22E+00	1.443E+01
V= .600							
A= .0100	1.000423	4.788	5.0200	5.01	.0835	1.00E-01	3.020E+00
A= .0200	1.001260	2.394	5.0200	5.02	.1679	2.02E-01	3.082E+00
A= .0300	1.002664	1.597	5.0000	5.04	.2542	3.07E-01	3.190E+00
A= .0400	1.004650	1.200	5.0000	5.06	.3434	4.18E-01	3.355E+00
A= .0500	1.007240	.961	4.9800	5.08	.4368	5.36E-01	3.591E+00
A= .0600	1.010462	.802	4.9800	5.12	.5360	6.66E-01	3.929E+00
A= .0700	1.014356	.689	4.9600	5.16	.6429	8.14E-01	4.425E+00
A= .0800	1.018970	.604	4.9400	5.21	.7604	9.92E-01	5.216E+00
A= .1000	1.030649	.485	4.8800	5.34	1.0480	1.66E+00	1.569E+01
A= .2000	1.175337	.252	4.5600	8.56	9.7191	5.09E+00	3.468E+01

Table A.2 Mathematical Properties of C-Distribution (Cont'd.)

XO= 4.00

	0TH MOMENT	C-MAX	T (CMAX)	MEAN	SIGMA	SKEWNESS	FLATNESS
V= .250							
A= .0100	1.001753	.624	16.0000	16.06	.6469	2.44E-01	3.119E+00
A= .0200	1.006673	.313	15.9200	16.22	1.3367	5.12E-01	3.537E+00
A= .0300	1.015219	.209	15.8000	16.51	2.1295	8.47E-01	4.552E+00
A= .0400	1.028026	.158	15.6400	16.96	3.1421	1.40E+00	8.137E+00
A= .0500	1.046256	.127	15.4200	17.67	4.6820	2.55E+00	1.928E+01
A= .0600	1.071004	.107	15.2000	18.79	7.0870	3.26E+00	2.236E+01
A= .0700	1.100679	.092	14.9400	20.34	10.0193	3.07E+00	1.667E+01
A= .0800	1.130481	.082	14.6600	22.14	12.8492	2.65E+00	1.174E+01
A= .1000	1.172312	.067	14.0600	25.60	17.1361	1.97E+00	6.921E+00
A= .2000	1.036440	.039	11.1000	32.16	23.5520	1.12E+00	3.298E+00
V= .300							
A= .0100	1.001260	.898	13.3400	13.37	.4477	2.02E-01	3.082E+00
A= .0200	1.004650	.450	13.3000	13.46	.9157	4.18E-01	3.355E+00
A= .0300	1.010462	.301	13.2200	13.62	1.4293	6.66E-01	3.929E+00
A= .0400	1.018970	.226	13.1200	13.87	2.0278	9.92E-01	5.211E+00
A= .0500	1.030648	.182	13.0000	14.22	2.7922	1.57E+00	9.981E+00
A= .0600	1.046297	.153	12.8600	14.73	3.9303	2.76E+00	2.426E+01
A= .0700	1.066833	.132	12.7000	15.50	5.7103	3.75E+00	3.129E+01
A= .0800	1.092127	.116	12.5200	16.60	8.0489	3.75E+00	2.525E+01
A= .1000	1.147749	.094	12.1400	19.48	12.9097	2.86E+00	1.313E+01
A= .2000	1.160044	.053	10.0200	28.81	22.5942	1.34E+00	3.934E+00
V= .400							
A= .0100	1.000771	1.596	10.0200	10.02	.2510	1.51E-01	3.046E+00
A= .0200	1.002664	.799	10.0000	10.06	.5083	3.07E-01	3.190E+00
A= .0300	1.005868	.533	9.9600	10.13	.7790	4.76E-01	3.463E+00
A= .0400	1.010462	.401	9.9200	10.22	1.0720	6.66E-01	3.929E+00
A= .0500	1.016569	.322	9.8600	10.35	1.4003	8.98E-01	4.768E+00
A= .0600	1.024372	.269	9.8000	10.52	1.7855	1.22E+00	6.766E+00
A= .0700	1.034151	.231	9.7400	10.75	2.2744	1.86E+00	1.494E+01
A= .0800	1.046330	.203	9.6400	11.05	2.9778	3.19E+00	3.640E+01
A= .1000	1.079861	.164	9.4600	12.07	5.5478	5.01E+00	4.836E+01
A= .2000	1.259778	.088	8.3000	21.93	19.6113	1.93E+00	6.312E+00
V= .500							
A= .0100	1.000545	2.494	8.0200	8.02	.1604	1.20E-01	3.029E+00
A= .0200	1.001753	1.248	8.0000	8.04	.3234	2.44E-01	3.119E+00
A= .0300	1.003785	.833	8.0000	8.07	.4916	3.73E-01	3.281E+00
A= .0400	1.006673	.625	7.9600	8.12	.6684	5.12E-01	3.537E+00
A= .0500	1.010462	.501	7.9400	8.18	.8576	6.66E-01	3.929E+00
A= .0600	1.015219	.419	7.9000	8.26	1.0648	8.47E-01	4.552E+00
A= .0700	1.021032	.360	7.8600	8.36	1.2980	1.08E+00	5.694E+00
A= .0800	1.028026	.316	7.8200	8.49	1.5716	1.43E+00	9.067E+00
A= .1000	1.046344	.254	7.7200	8.85	2.4005	3.62E+00	5.261E+01
A= .2000	1.232650	.134	7.0400	15.62	15.2912	2.87E+00	1.204E+01
V= .600							
A= .0100	1.000423	3.588	6.6800	6.68	.1113	1.00E-01	3.020E+00
A= .0200	1.001260	1.796	6.6800	6.69	.2238	2.02E-01	3.082E+00
A= .0300	1.002664	1.198	6.6800	6.71	.3389	3.07E-01	3.190E+00
A= .0400	1.004650	.900	6.6600	6.74	.4579	4.18E-01	3.355E+00
A= .0500	1.007240	.721	6.6400	6.77	.5824	5.36E-01	3.591E+00
A= .0600	1.010462	.601	6.6200	6.82	.7147	6.66E-01	3.929E+00
A= .0700	1.014356	.516	6.6000	6.87	.8573	8.14E-01	4.425E+00
A= .0800	1.018970	.453	6.5800	6.94	1.0139	9.92E-01	5.215E+00
A= .1000	1.030649	.364	6.5200	7.11	1.3971	1.62E+00	1.286E+01
A= .2000	1.168985	.189	6.0800	10.84	10.4484	4.42E+00	2.719E+01

Table A.2 Mathematical Properties of C-Distribution (Cont'd.)

			XO= 5.00				
	0TH MOMENT	C-MAX	T (CMAX)	MEAN	SIGMA	SKEWNESS	FLATNESS
V= .250							
A= .0100	1.001753	.499	19.9800	20.07	.8084	2.44E-01	3.119E+00
A= .0200	1.006673	.250	19.9000	20.27	1.6709	5.12E-01	3.557E+00
A= .0300	1.015219	.167	19.7400	20.65	2.6619	8.47E-01	4.552E+00
A= .0400	1.028025	.126	19.5400	21.20	3.9266	1.39E+00	7.851E+00
A= .0500	1.046155	.102	19.2800	22.08	5.7879	2.28E+00	1.476E+01
A= .0600	1.069920	.085	18.9800	23.39	8.4117	2.69E+00	1.556E+01
A= .0700	1.096318	.074	18.6600	25.08	11.3100	2.50E+00	1.176E+01
A= .0800	1.120068	.065	18.3000	26.90	13.9342	2.18E+00	8.741E+00
A= .1000	1.145153	.053	17.5600	30.11	17.7373	1.68E+00	5.615E+00
A= .2000	.970685	.031	13.8800	35.33	23.4456	1.00E+00	3.024E+00
V= .300							
A= .0100	1.001260	.719	16.6600	16.71	.5596	2.02E-01	3.082E+00
A= .0200	1.004650	.360	16.6200	16.83	1.1446	4.18E-01	3.355E+00
A= .0300	1.010462	.241	16.5200	17.03	1.7867	6.66E-01	3.929E+00
A= .0400	1.018970	.181	16.4000	17.33	2.5348	9.92E-01	5.210E+00
A= .0500	1.030647	.146	16.2400	17.77	3.4888	1.55E+00	9.397E+00
A= .0600	1.046243	.122	16.0600	18.41	4.8683	2.49E+00	1.835E+01
A= .0700	1.066332	.105	15.8600	19.33	6.8858	3.12E+00	2.135E+01
A= .0800	1.090053	.093	15.6400	20.57	9.2587	3.07E+00	1.750E+01
A= .1000	1.137430	.076	15.1600	23.56	13.8857	2.42E+00	1.004E+01
A= .2000	1.100864	.042	12.5200	31.93	22.6156	1.20E+00	3.566E+00
V= .400							
A= .0100	1.000771	1.277	12.5200	12.53	.3138	1.51E-01	3.046E+00
A= .0200	1.002664	.639	12.4800	12.57	.6354	3.07E-01	3.190E+00
A= .0300	1.005868	.427	12.4600	12.65	.9737	4.76E-01	3.463E+00
A= .0400	1.010462	.321	12.4000	12.77	1.3400	6.66E-01	3.929E+00
A= .0500	1.016569	.257	12.3400	12.94	1.7504	8.98E-01	4.767E+00
A= .0600	1.024372	.215	12.2600	13.15	2.2319	1.22E+00	6.712E+00
A= .0700	1.034149	.185	12.1600	13.43	2.8409	1.82E+00	1.317E+01
A= .0800	1.046307	.163	12.0600	13.81	3.6934	2.85E+00	2.642E+01
A= .1000	1.079209	.131	11.8200	15.03	6.5186	4.08E+00	3.248E+01
A= .2000	1.222979	.071	10.3800	24.87	19.9114	1.75E+00	5.572E+00
V= .500							
A= .0100	1.000545	1.995	10.0200	10.02	.2005	1.20E-01	3.029E+00
A= .0200	1.001753	.998	10.0000	10.04	.4042	2.44E-01	3.119E+00
A= .0300	1.003785	.666	9.9800	10.08	.6145	3.73E-01	3.281E+00
A= .0400	1.006673	.500	9.9600	10.14	.8355	5.12E-01	3.557E+00
A= .0500	1.010462	.401	9.9200	10.22	1.0720	6.66E-01	3.929E+00
A= .0600	1.015219	.335	9.8800	10.32	1.3310	8.47E-01	4.552E+00
A= .0700	1.021032	.288	9.8400	10.45	1.6225	1.08E+00	5.688E+00
A= .0800	1.028026	.253	9.7800	10.60	1.9643	1.42E+00	8.713E+00
A= .1000	1.046330	.203	9.6400	11.05	2.9778	3.19E+00	3.640E+01
A= .2000	1.215942	.107	8.7800	18.26	15.8446	2.59E+00	1.026E+01
V= .600							
A= .0100	1.000423	2.867	8.3600	8.35	.1391	1.00E-01	3.020E+00
A= .0200	1.001260	1.437	8.3400	8.36	.2798	2.02E-01	3.082E+00
A= .0300	1.002664	.959	8.3400	8.39	.4236	3.07E-01	3.190E+00
A= .0400	1.004650	.720	8.3200	8.42	.5723	4.18E-01	3.355E+00
A= .0500	1.007240	.577	8.3000	8.46	.7280	5.36E-01	3.591E+00
A= .0600	1.010462	.481	8.2800	8.52	.8933	6.66E-01	3.929E+00
A= .0700	1.014356	.413	8.2400	8.59	1.0716	8.14E-01	4.425E+00
A= .0800	1.018970	.362	8.2200	8.67	1.2674	9.92E-01	5.214E+00
A= .1000	1.030649	.291	8.1400	8.89	1.7460	1.60E+00	1.160E+01
A= .2000	1.163313	.151	7.5800	13.07	11.1315	3.90E+00	2.196E+01

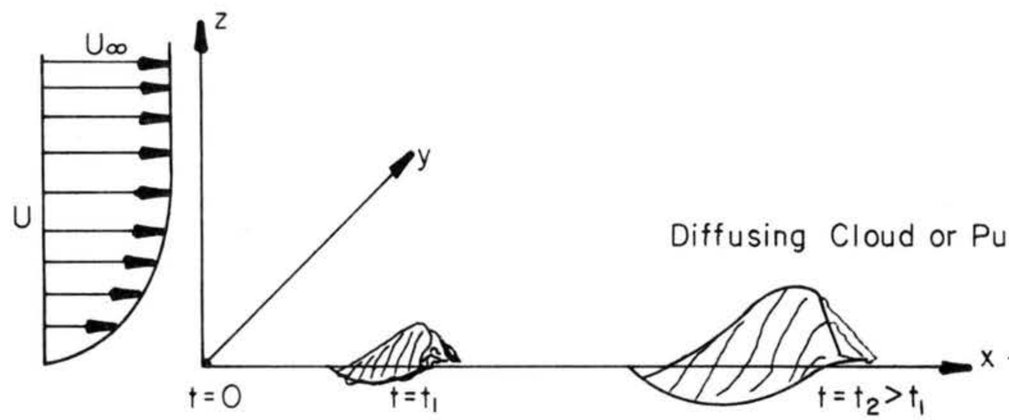

Fig. 1.1 Diffusion from a ground released instantaneous puff.

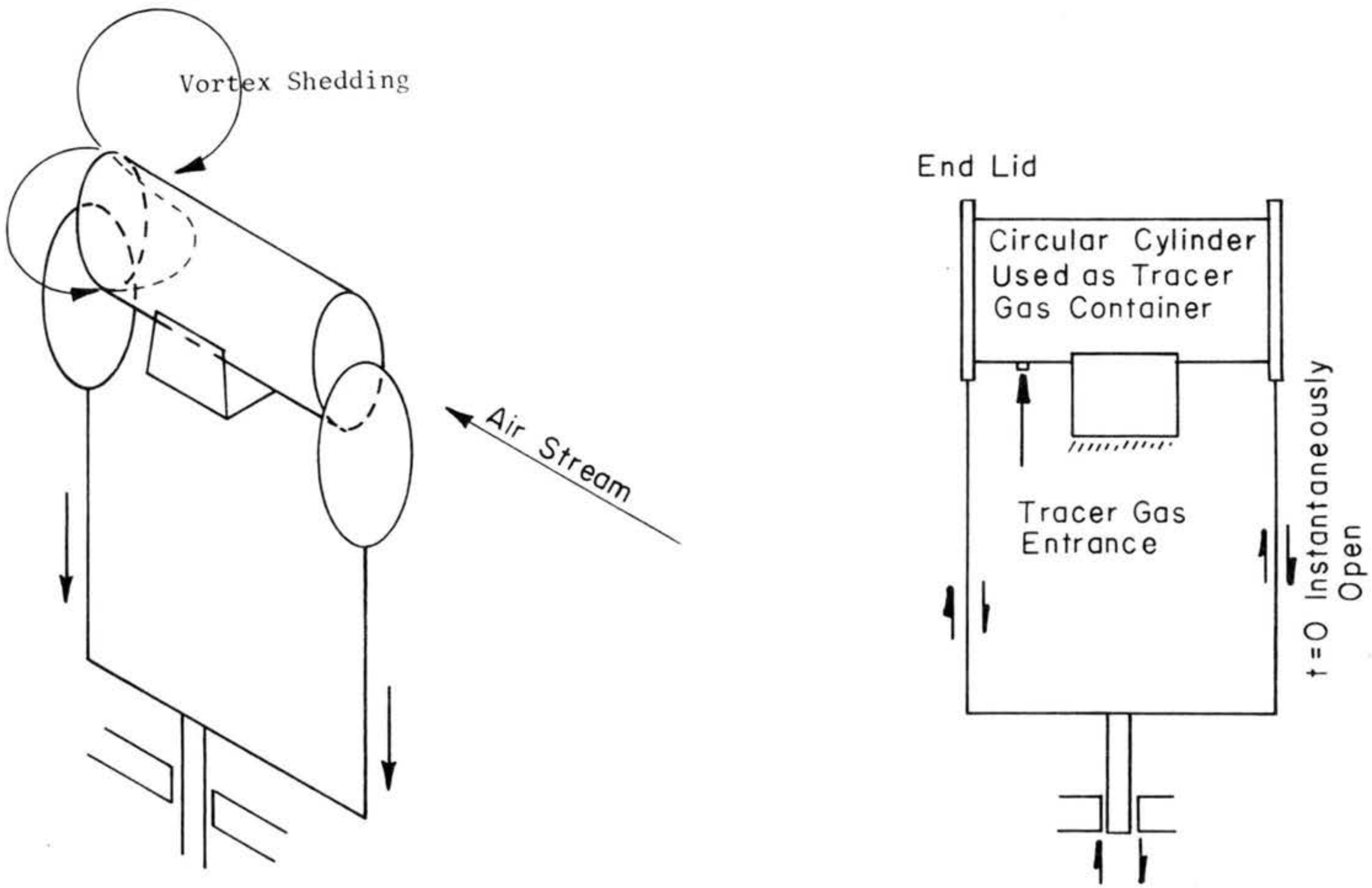

Fig. 4.1 Mechanical device for the release of an instantaneous source.

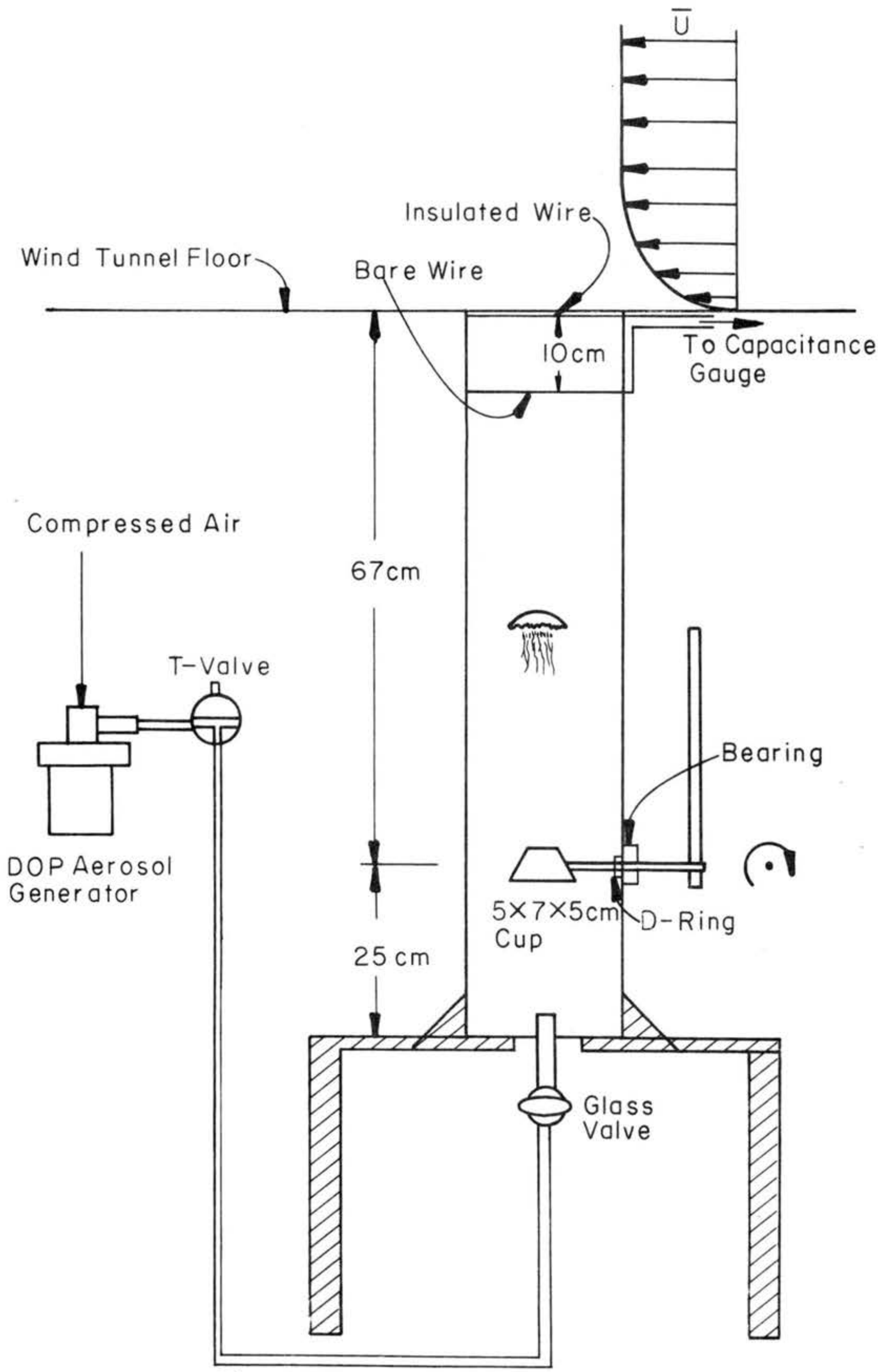

Fig. 4.2 Instantaneous puff generator.

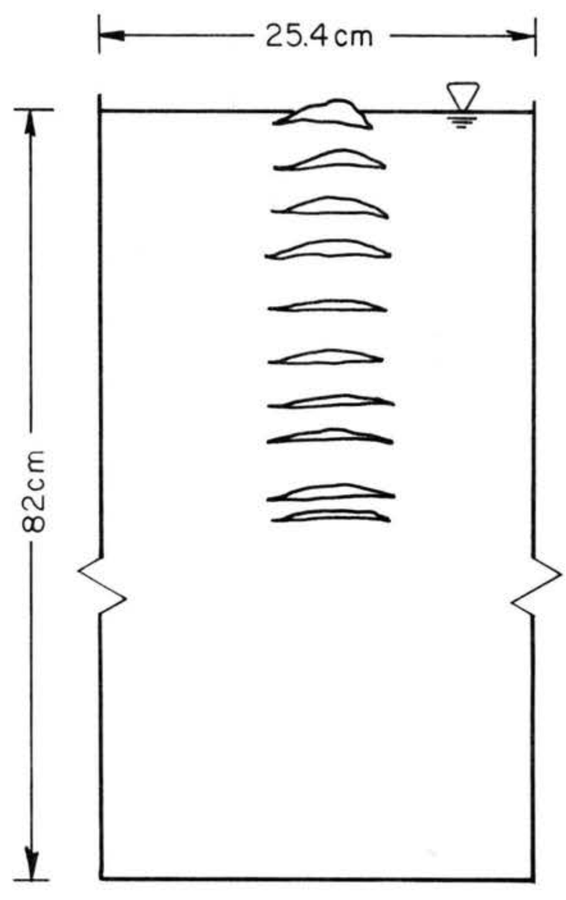

Fig. 4.3 Consecutive pictures of rising bubble in the water (3/64 second per picture).

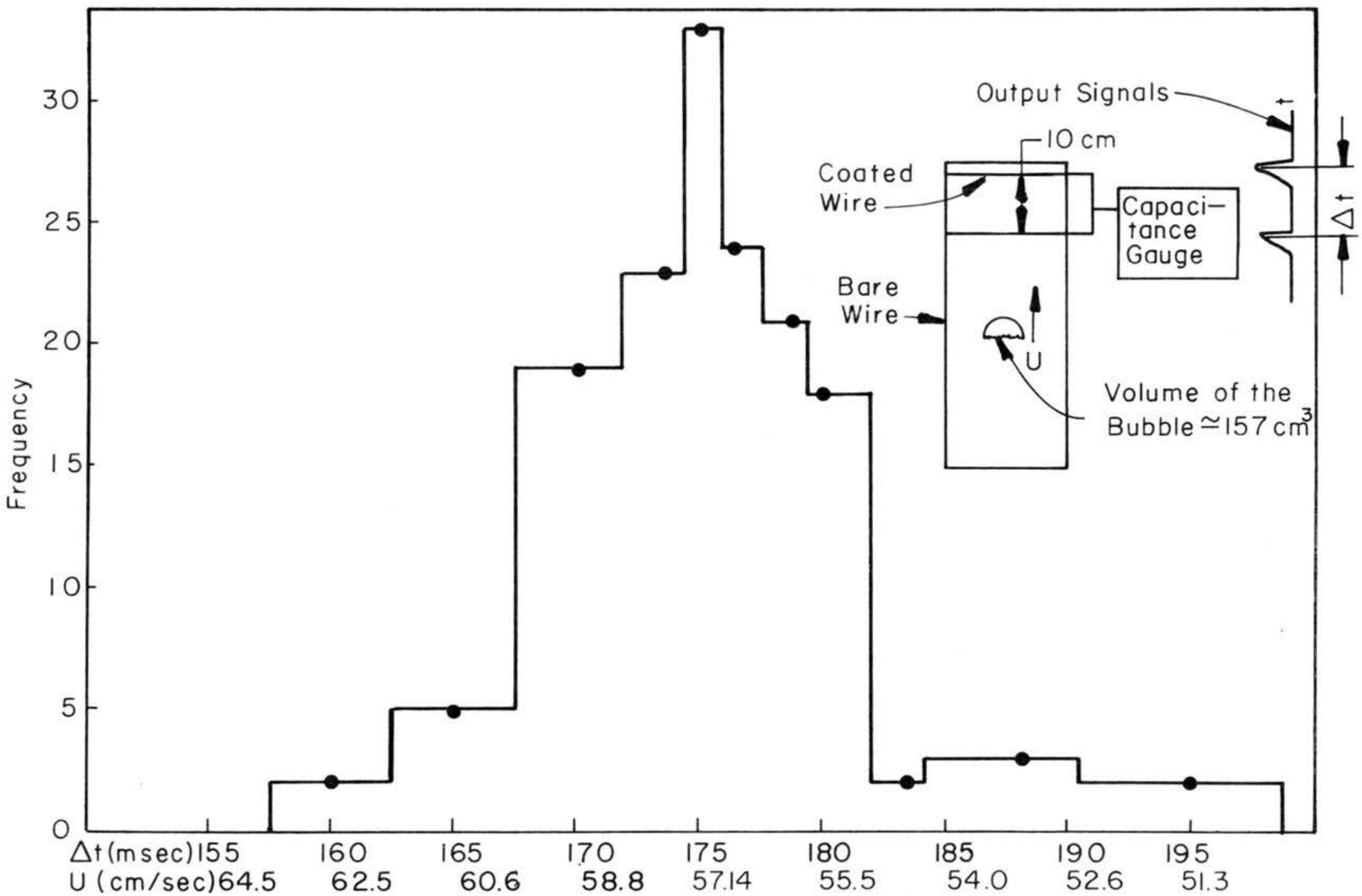

Fig. 4.4 Velocity distribution of rising gas bubbles.

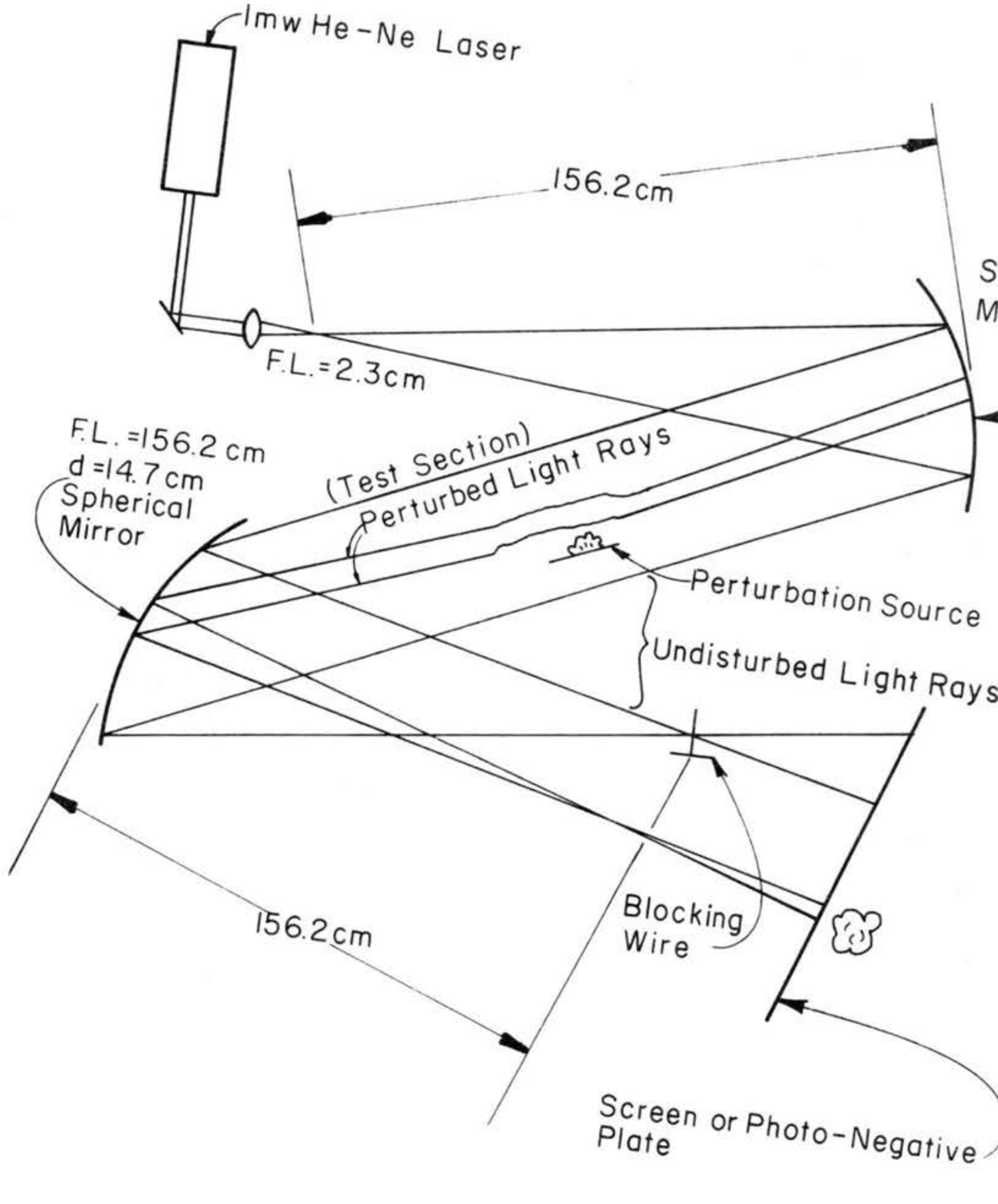

Fig. 4.5 Laser shadow-graph device.

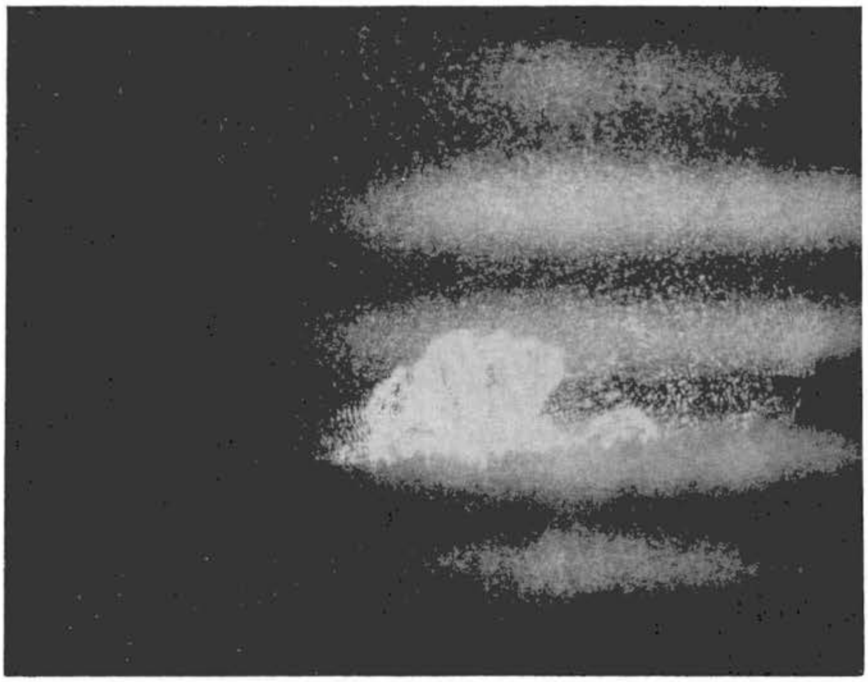

Fig. 4.6 The shadow graph picture of the burst from a freon gas bubble.

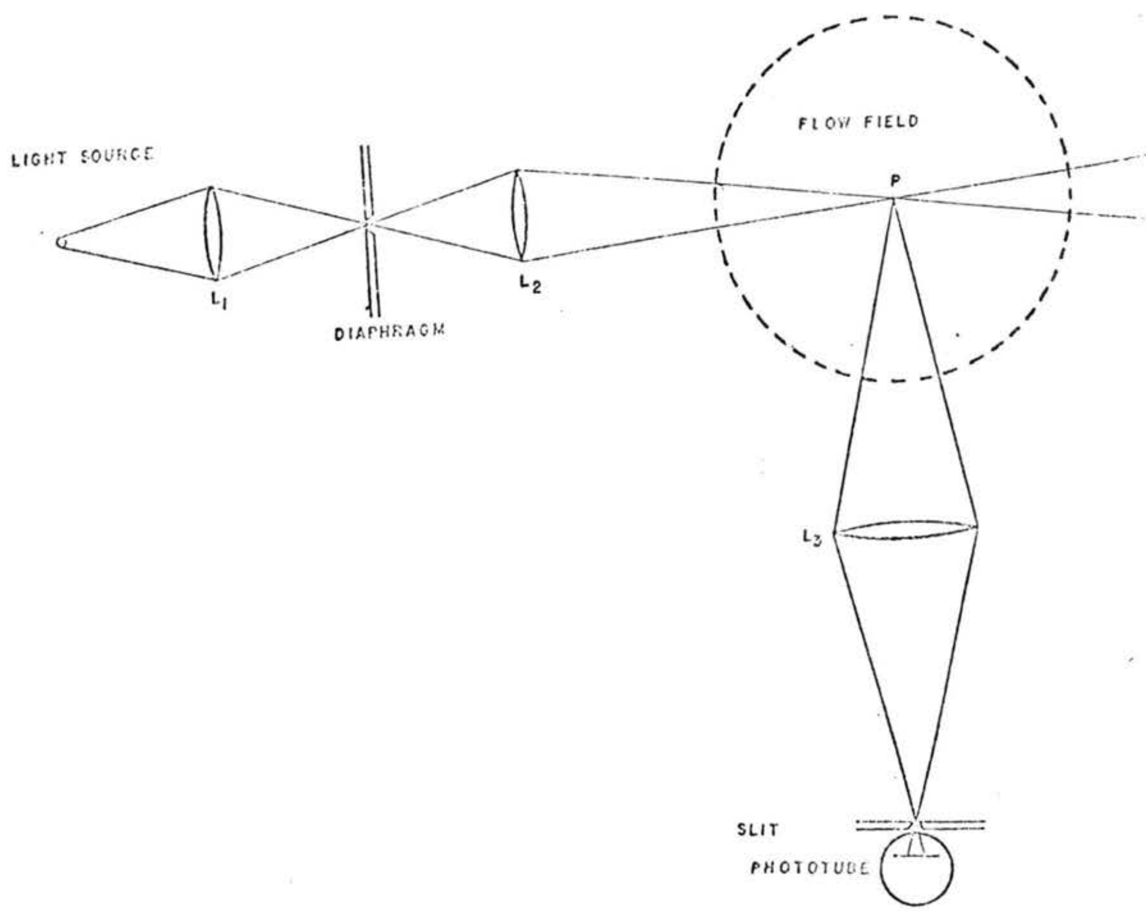

Fig. 5.1 Light scattering device after Becker et al., (1967).

Design of the optic-probe.

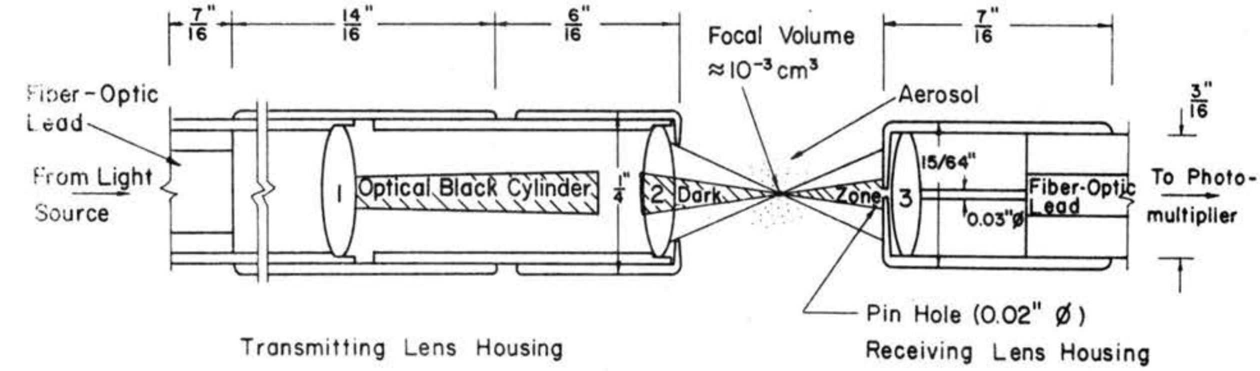

	F.L (mm)	Dia. (mm)
Lens 1	13.1	5
Lens 2	5.6	5
Lens 3	5.6	5

Fig. 5.2 Light scattering probe after Liu (1972).

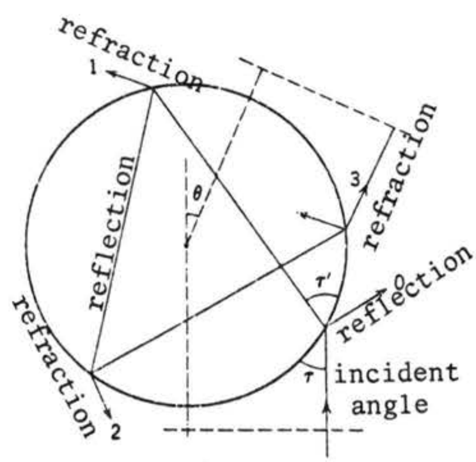

Fig. 5.3 Path of a light ray through a large spherical scatterer according to a geometrical optics.

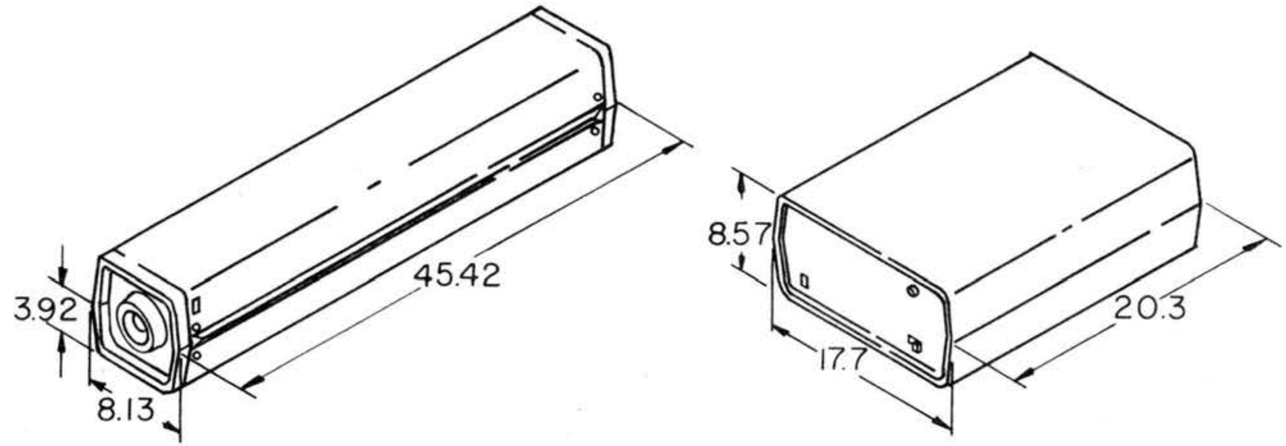

Fig. 5.4 Dimensions of the laser (Spectral Physics Model 120) and the exciter (Spectral Physics Model 256) in cm.

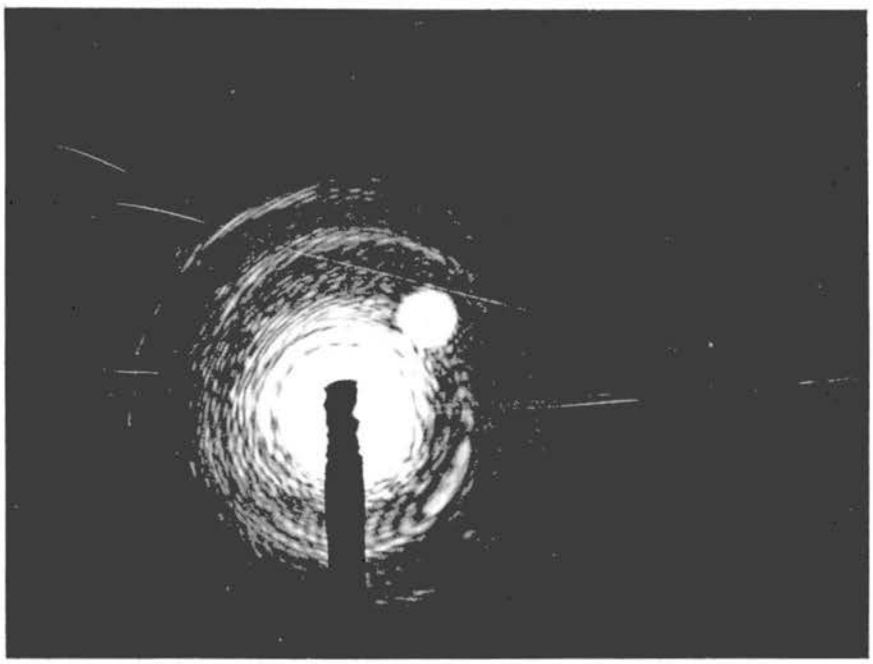

Fig. 5.5 Diffraction pattern of the laser beam.

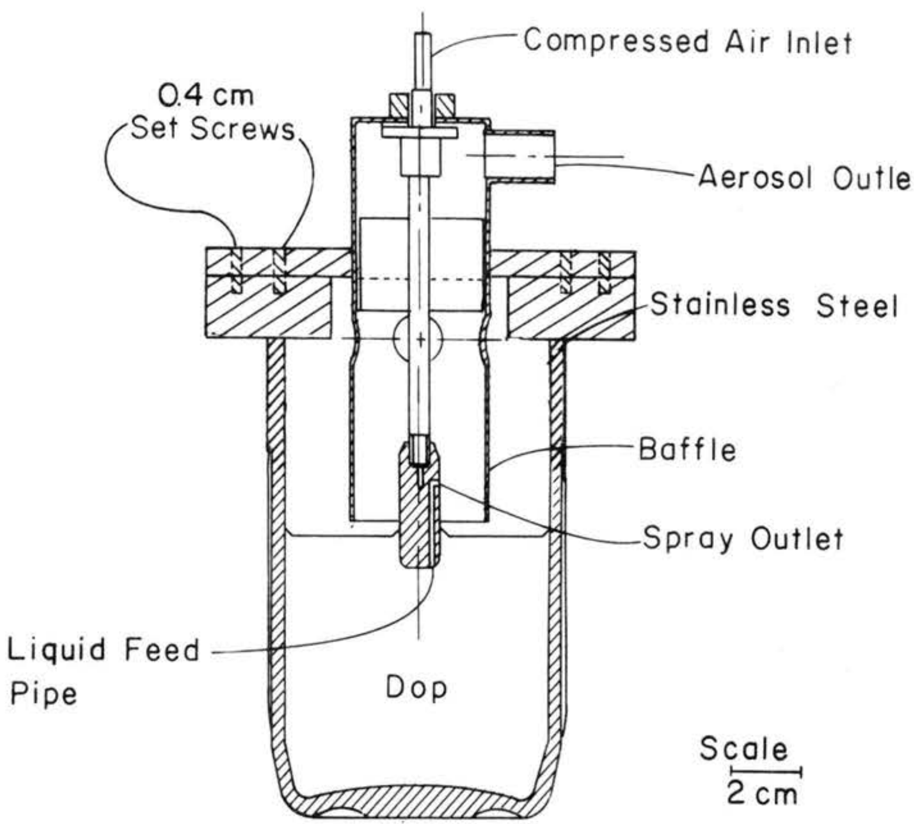

Fig. 5.6 Cross-section of the aerosol generator.

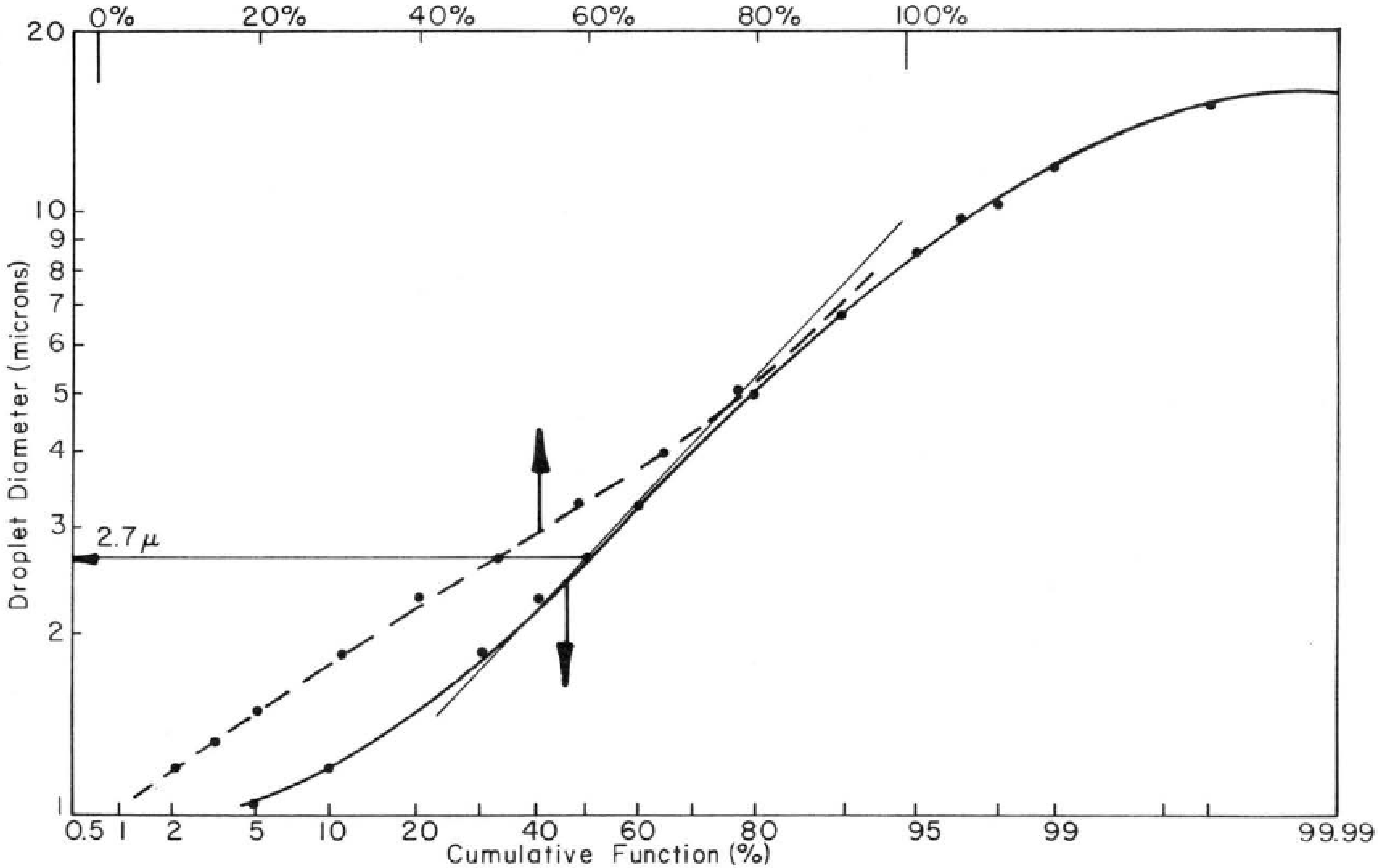

Fig. 5.7 Size distribution of BOP aerosol after Green and Lane (1964).

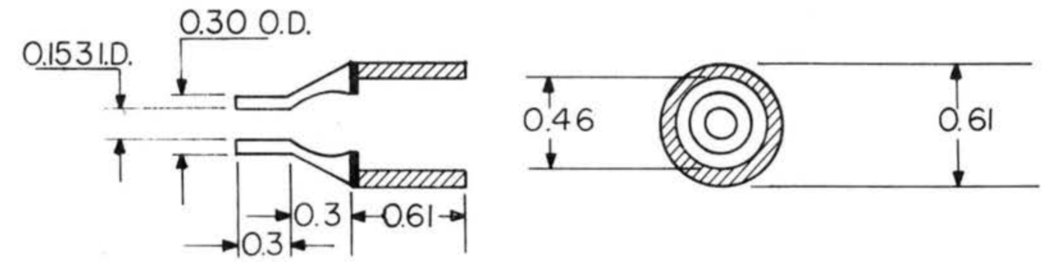

Fig. 5.8 Dimension of the optical aperture, cm.

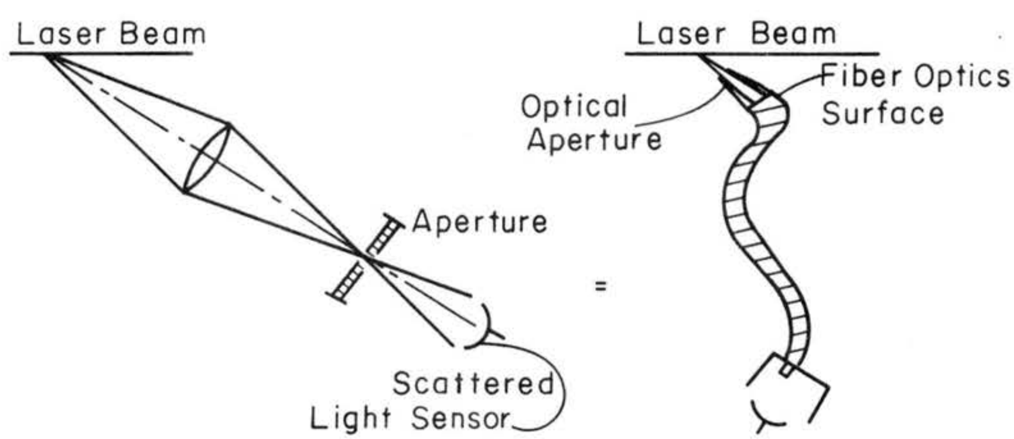

Fig. 5.9 The equivalence of an aperture-fiber optics to a conventional focusing system.

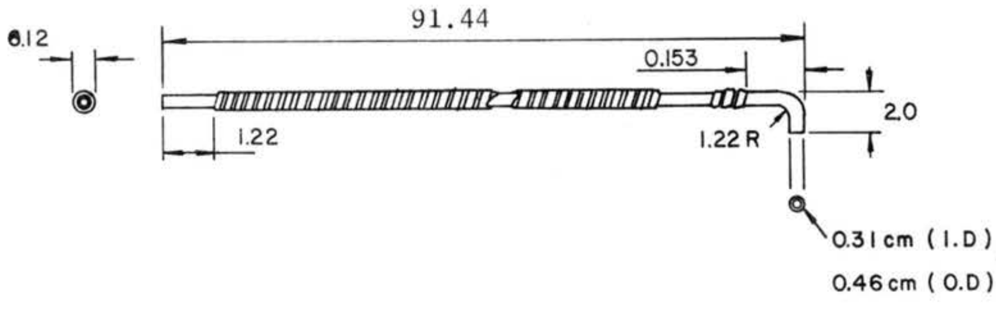

Fig. 5.10 Dimension of the fiber optics in cm.

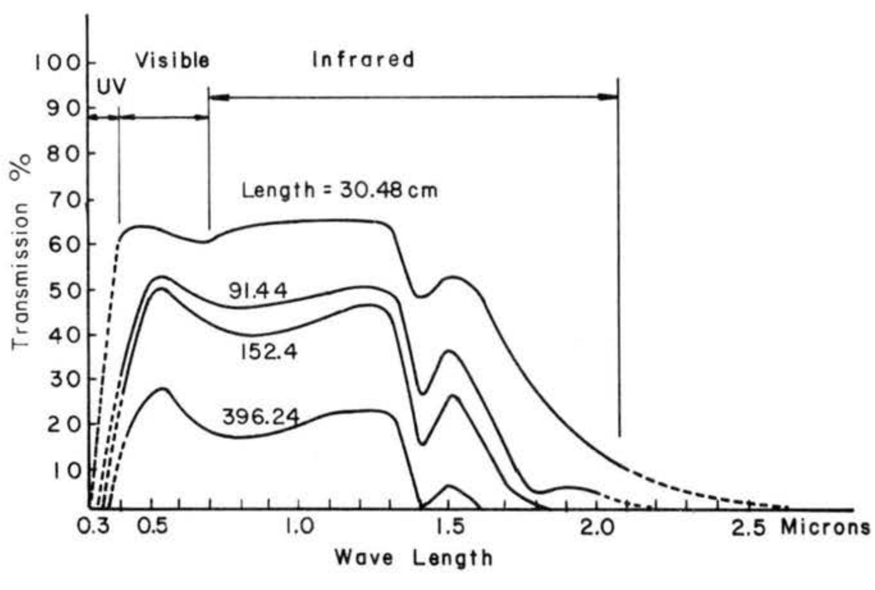

Fig. 5.11 Fiber optics light transmission characteristics.

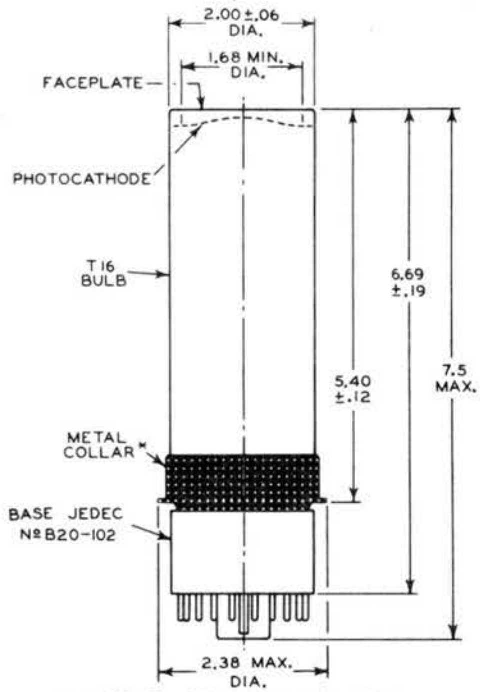

Inch Dimension Equivalents in Millimeters

Inch	mm	Inch	mm	Inch	mm
0.06	1.5	1.68	42.6	5.40	137.1
0.12	3.0	2.00	50.8	6.69	169.9
0.19	4.8	2.38	60.4	7.5	190.5

Fig. 5.12 Dimension of the PM tube.

Basing Diagram
Bottom View

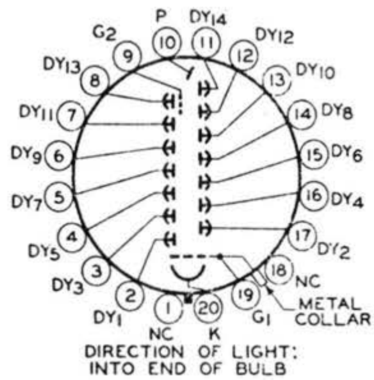

Pin 1: No Connection
Pin 2: Dynode No.1
Pin 3: Dynode No.3
Pin 4: Dynode No.5
Pin 5: Dynode No.7
Pin 6: Dynode No.9
Pin 7: Dynode No.11
Pin 8: Dynode No.13
Pin 9: Grid No.2 (Accelerating Electrode)
Pin 10: Anode
Pin 11: Dynode No.14
Pin 12: Dynode No.12
Pin 13: Dynode No.10
Pin 14: Dynode No.8
Pin 15: Dynode No.6
Pin 16: Dynode No.4
Pin 17: Dynode No.2
Pin 18: No Connection
Pin 19: Grid No.1 (Focusing Electrode)
Pin 20: Photocathode

Fig. 5.13 Basing diagram (bottom view).

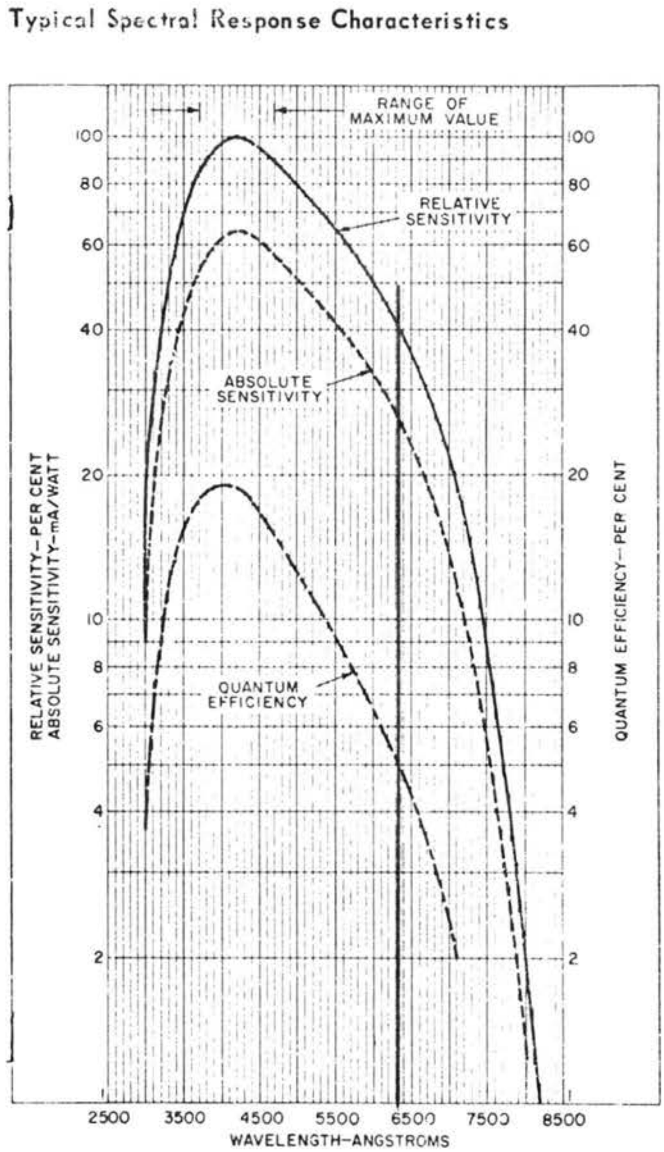

Fig. 5.14 Typical spectral response characteristics of the PM tube.

Sensitivity and Current Amplification Characteristics

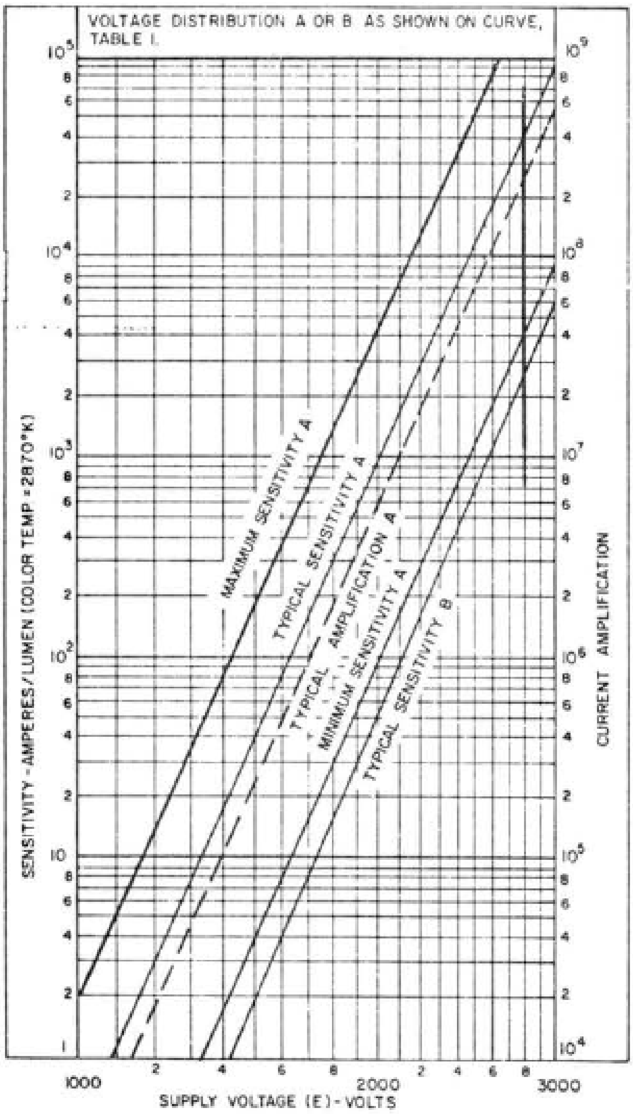

Fig. 5.15 Sensitivity and current amplification characteristics of the PM tube.

Typical Voltage-Divider Arrangement (A)

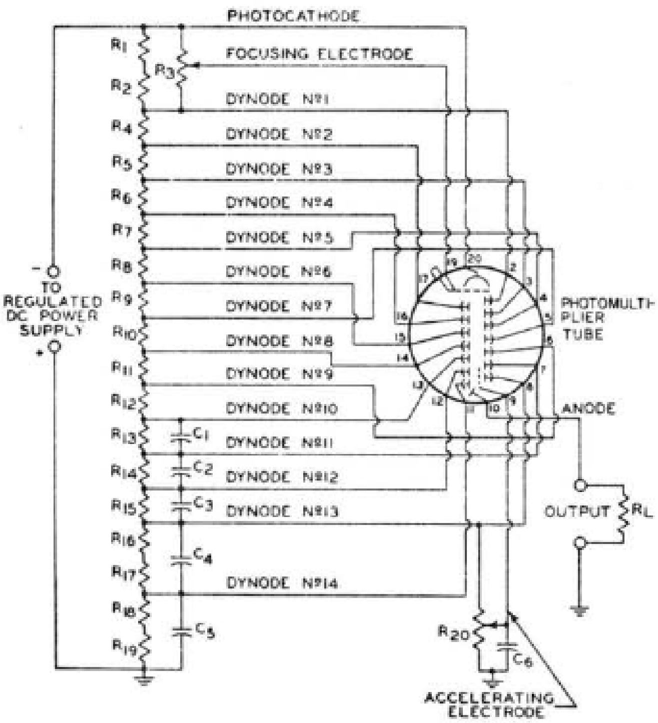

C_1: 25 pF, 20%, 600 volts (dc working), ceramic disc
C_2: 50 pF, 20%, 600 volts (dc working), ceramic disc
C_3: 100 pF, 20%, 600 volts (dc working), ceramic disc
C_4: 250 pF, 20%, 600 volts (dc working), ceramic disc
C_5: 500 pF, 20%, 600 volts (dc working), ceramic disc
C_6: 100 pF, 20%, 1000 volts (dc working), ceramic disc
R_1: 24000 ohms, 5%, 1 watt
R_2: 22000 ohms, 5%, 1 watt
R_3: 1 megohm, 20%, 2 watts, adjustable
R_4 through R_{13}: 22000 ohms, 5%, 1 watt
R_{14}: 27000 ohms, 5%, 2 watts
R_{15}: 33000 ohms, 5%, 2 watts
R_{16}: 22000 ohms, 5%, 2 watts
R_{17}: 18000 ohms, 5%, 2 watts
R_{18}: 22000 ohms, 5%, 2 watts
R_{19}: 22000 ohms, 5%, 2 watts
R_{20}: 10 megohms, 2 watts, adjustable

Fig. 5.16 Voltage-divider arrangement of the PM tube.

Typical Voltage-Divider Arrangement for Constant Voltage Between Cathode and Dynode No. 1 (B)

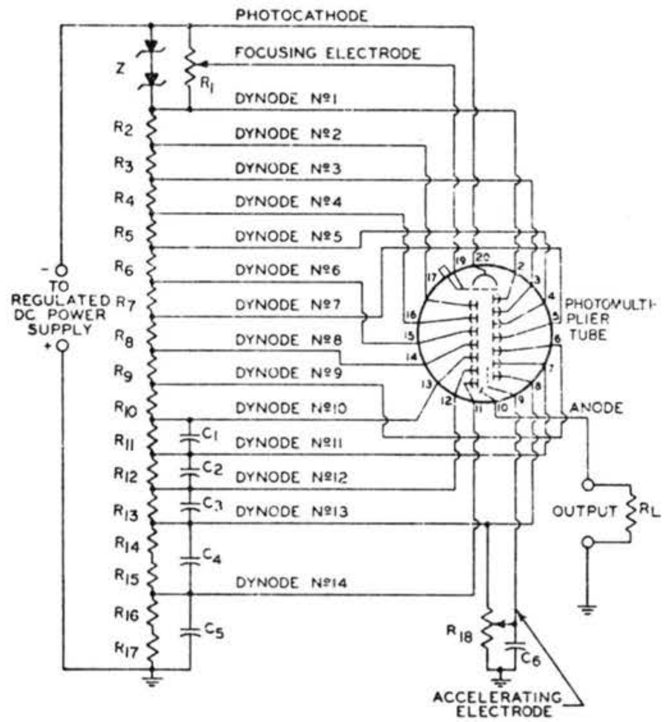

Fig. 5.17 Voltage-divider arrangement of extremely low light intensity.

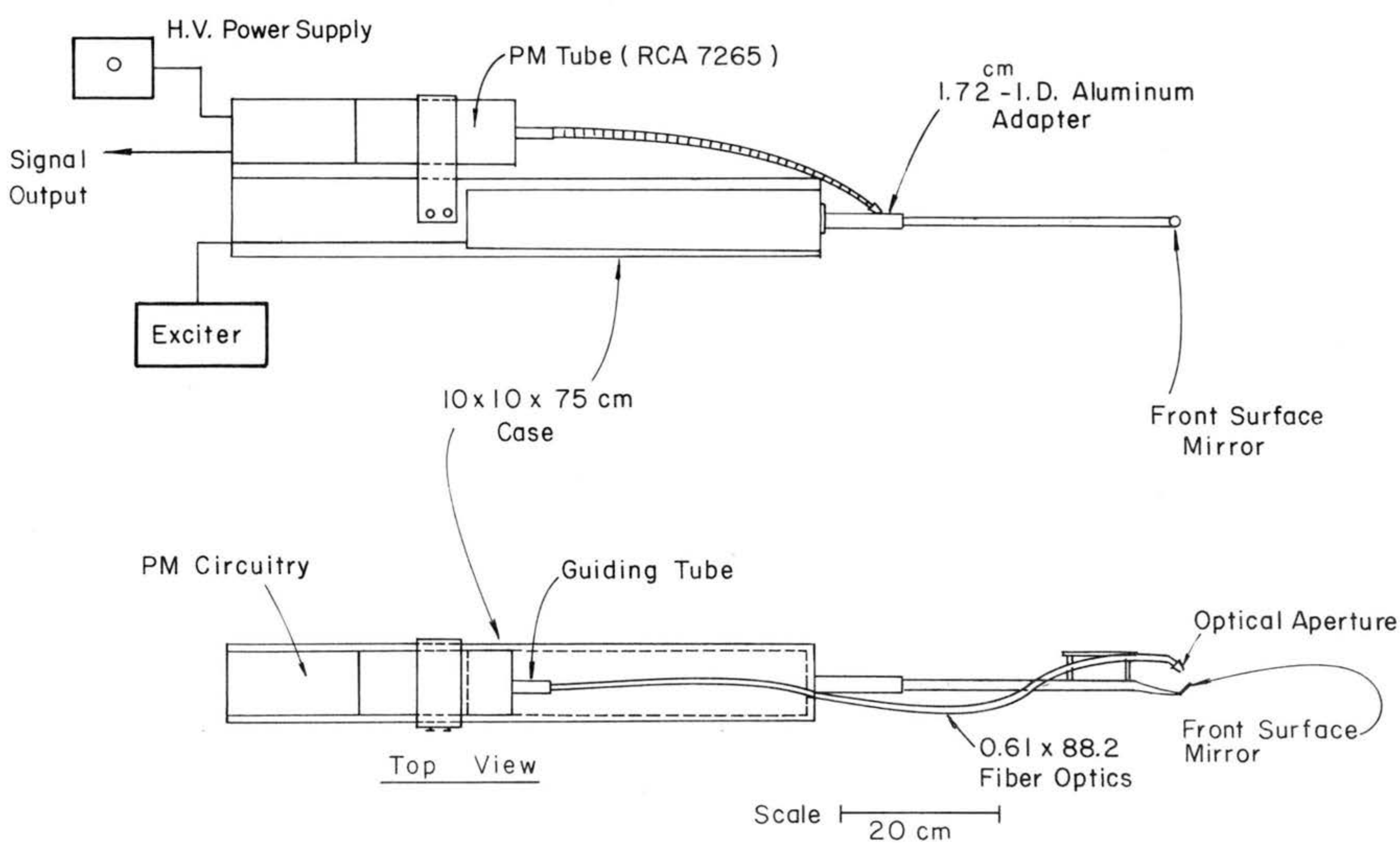

Fig. 5.18 Laser light scattering probe outline drawing.

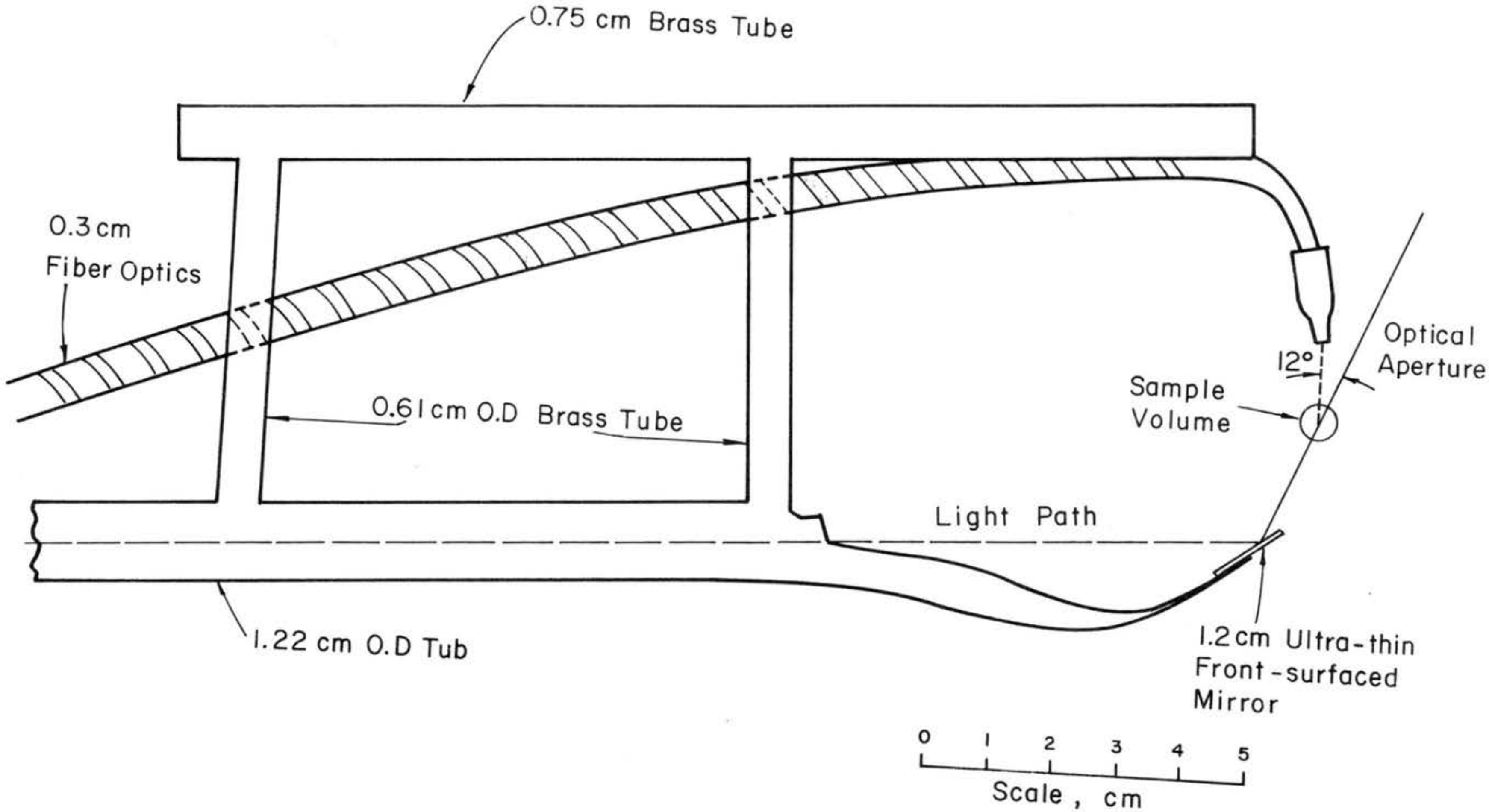

Fig. 5.19 Full scale outline of the laser light-scattering probe (L.L.S.P.).

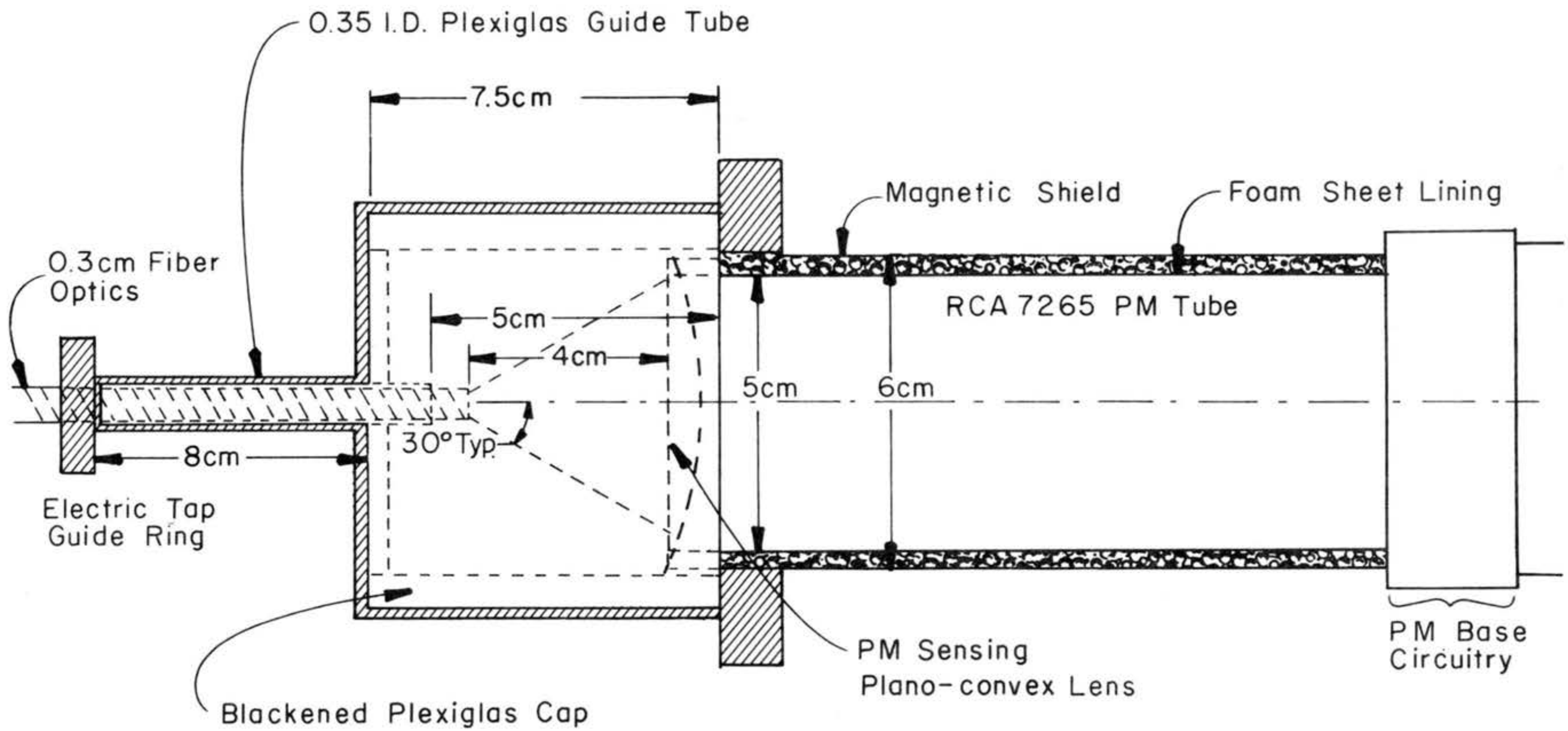

Fig. 5.20 Outline of the guiding cap connecting fiber optics and PM tube.

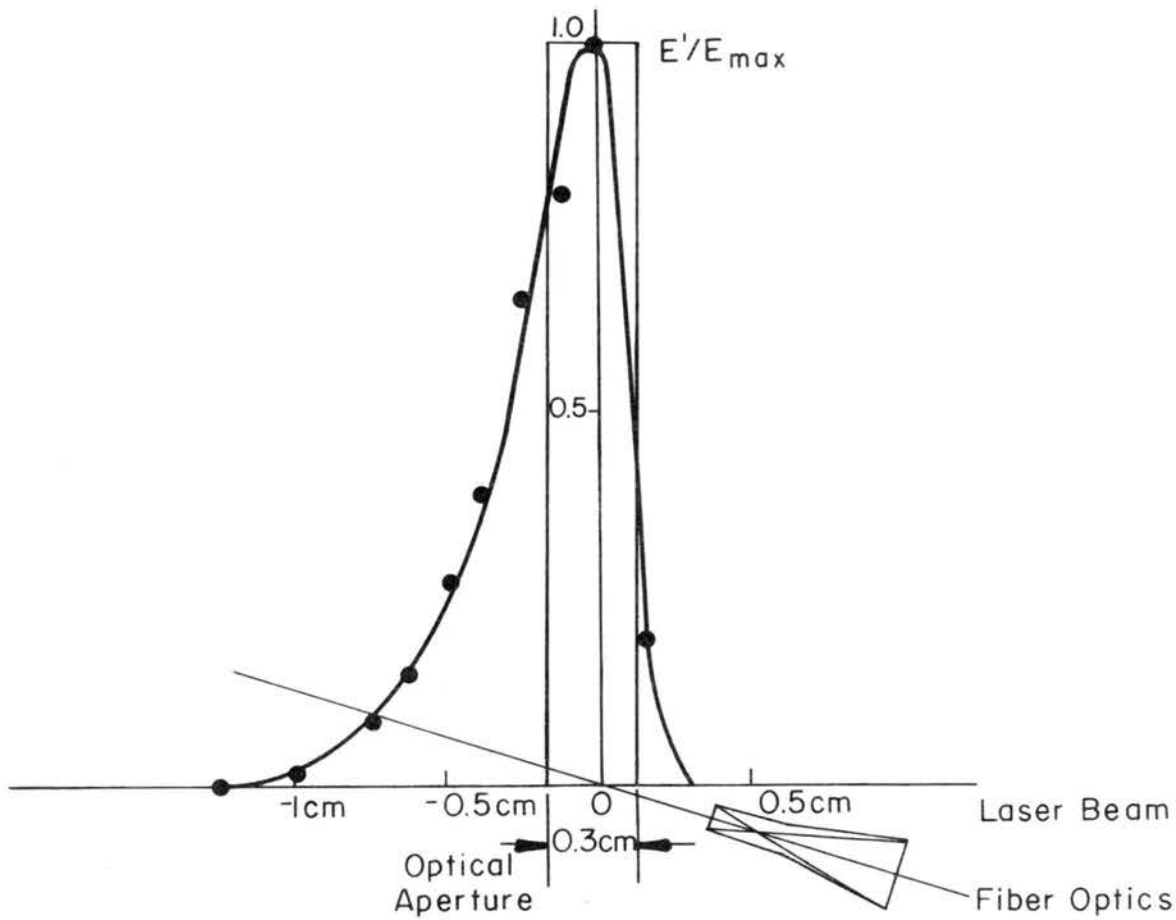

Fig. 5.21 Sample volume diagram.

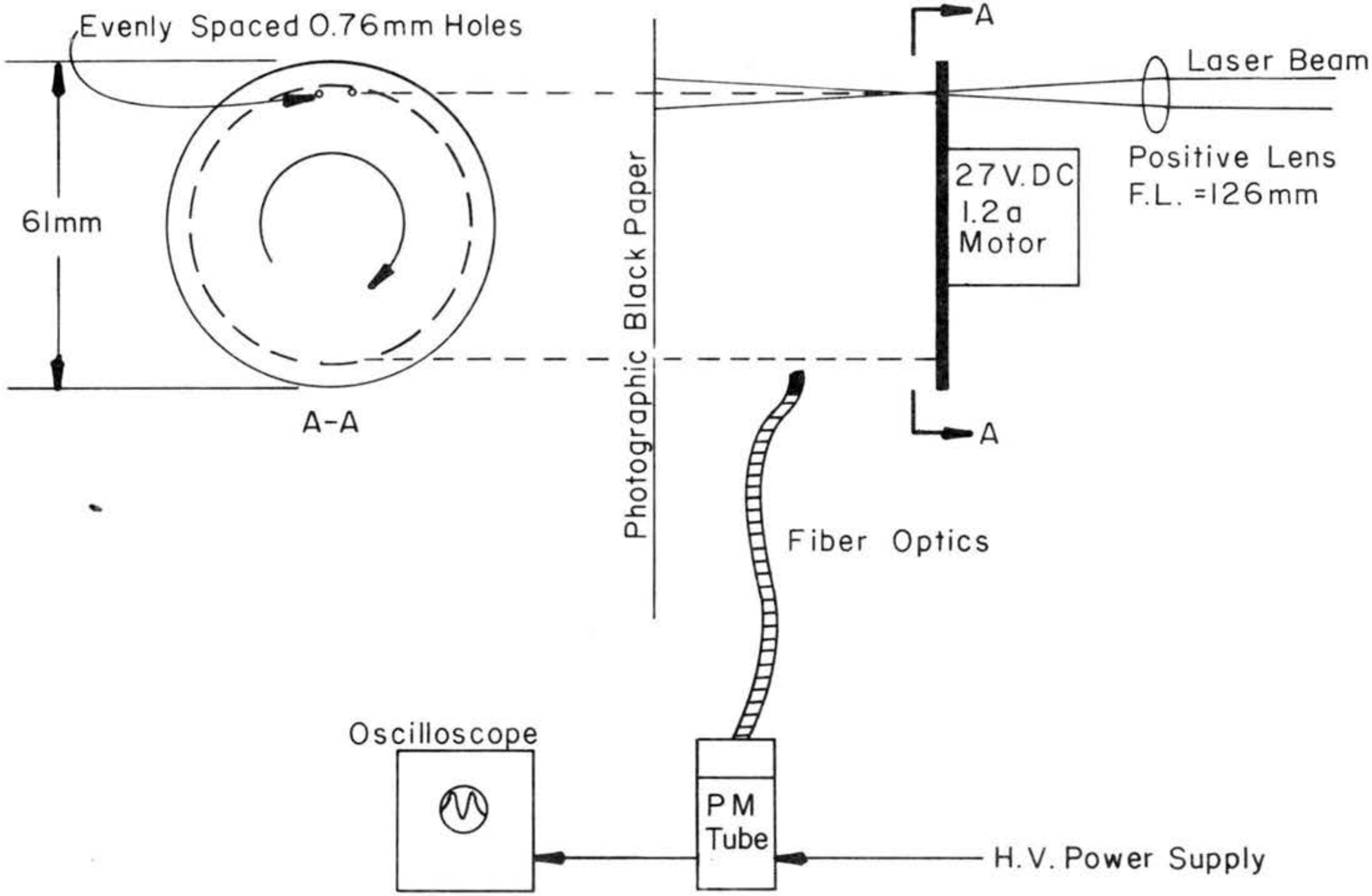

Fig. 5.22 Experimental arrangement for measuring the frequency attenuation of the optical system.

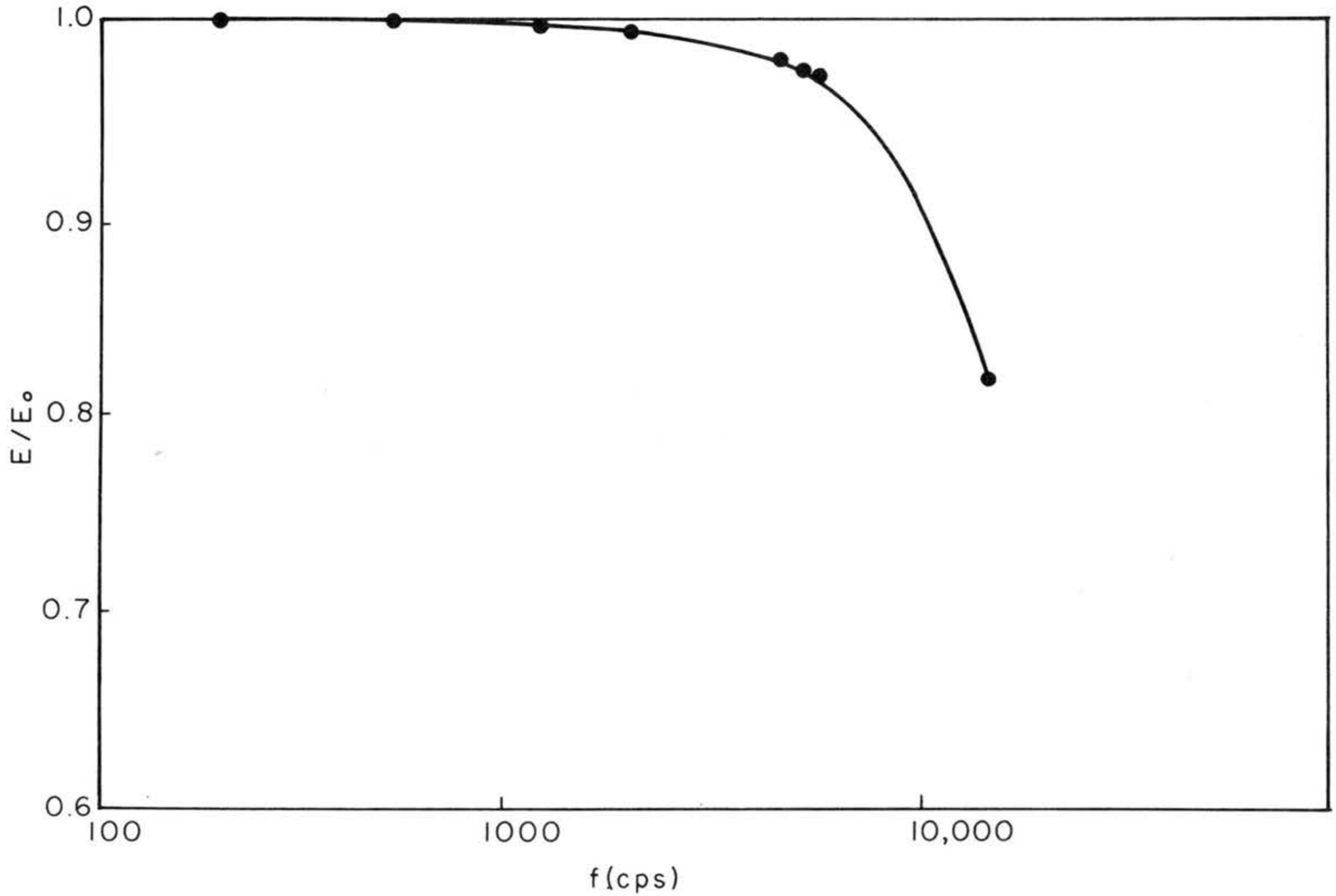

Fig. 5.23 Frequency attenuation curve of the PM tube - light filament system.

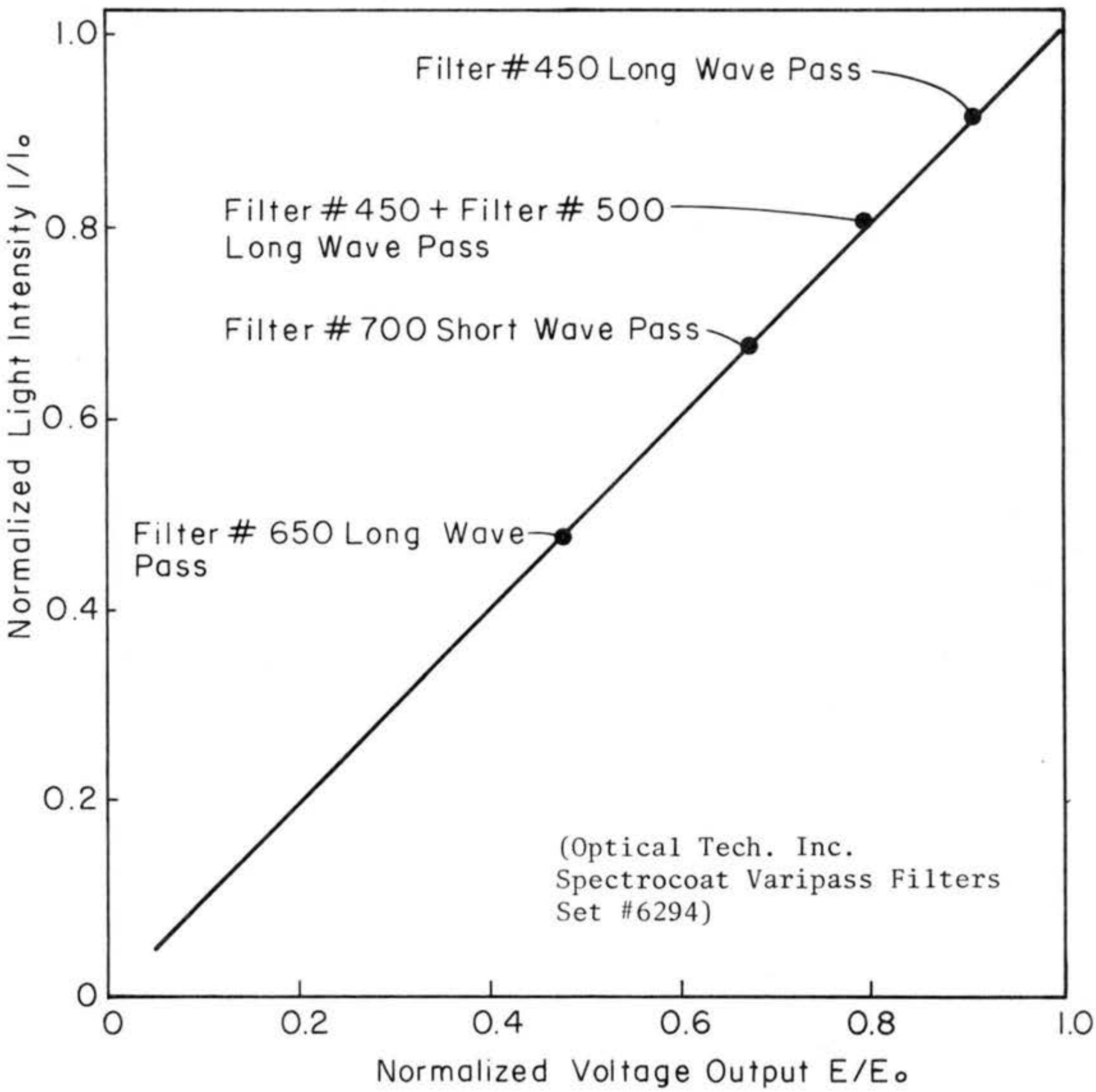

Fig. 6.1 Linearity of the PM tube output.

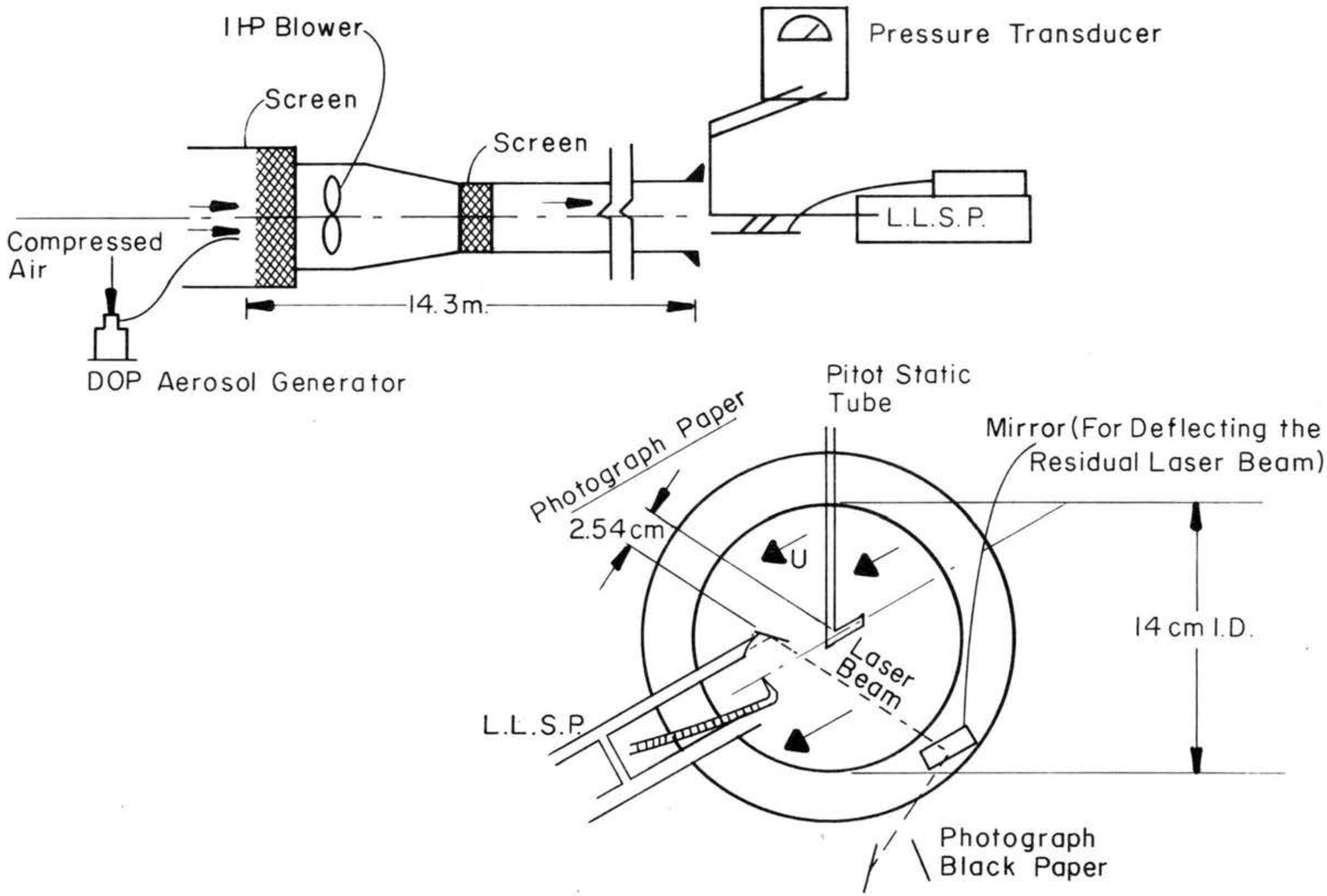

Fig. 6.2 Experimental arrangement of the PM - L.L.S.P. calibration process.

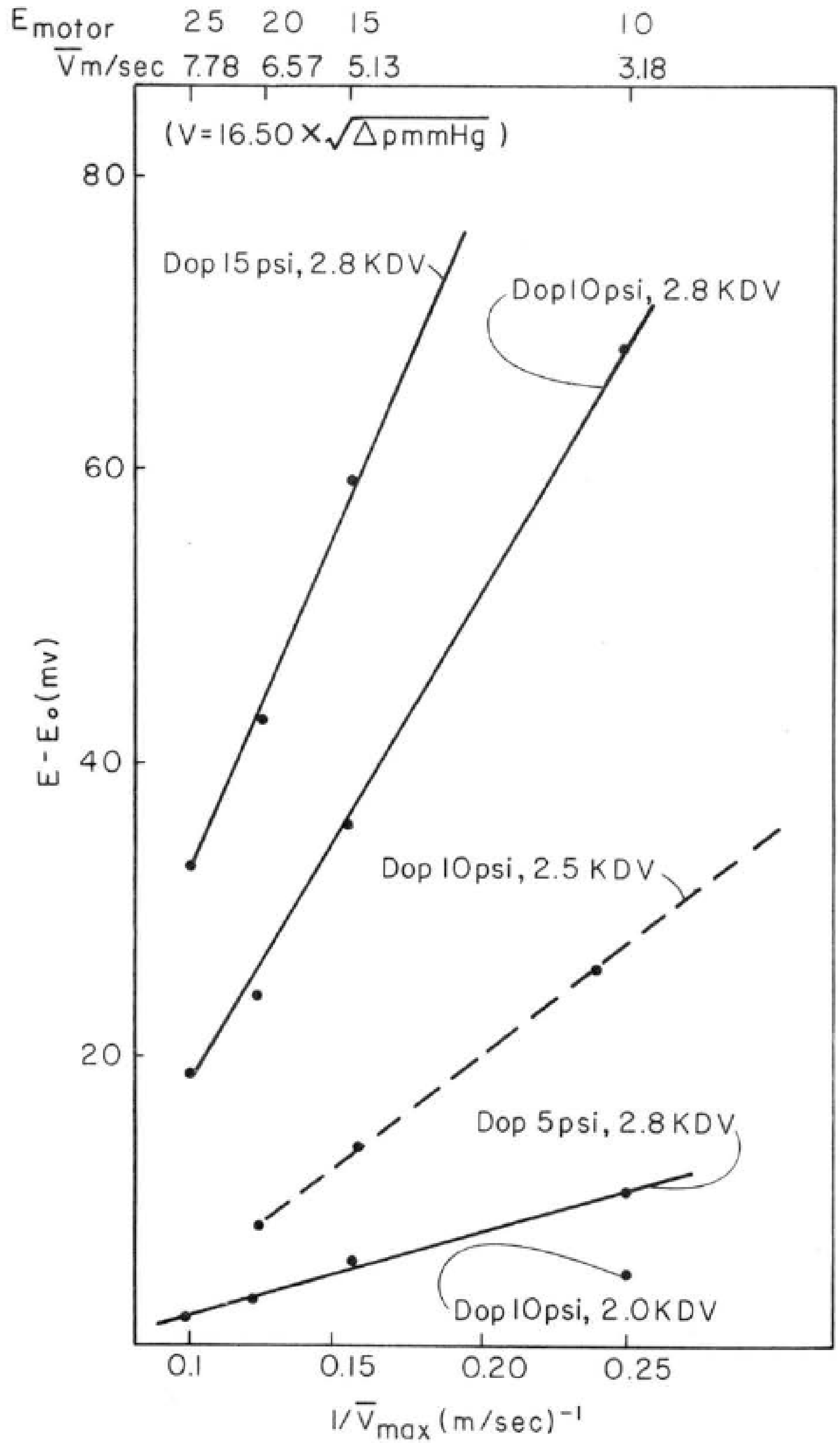

Fig. 6.3 Calibration of PM tube vs. concentration.

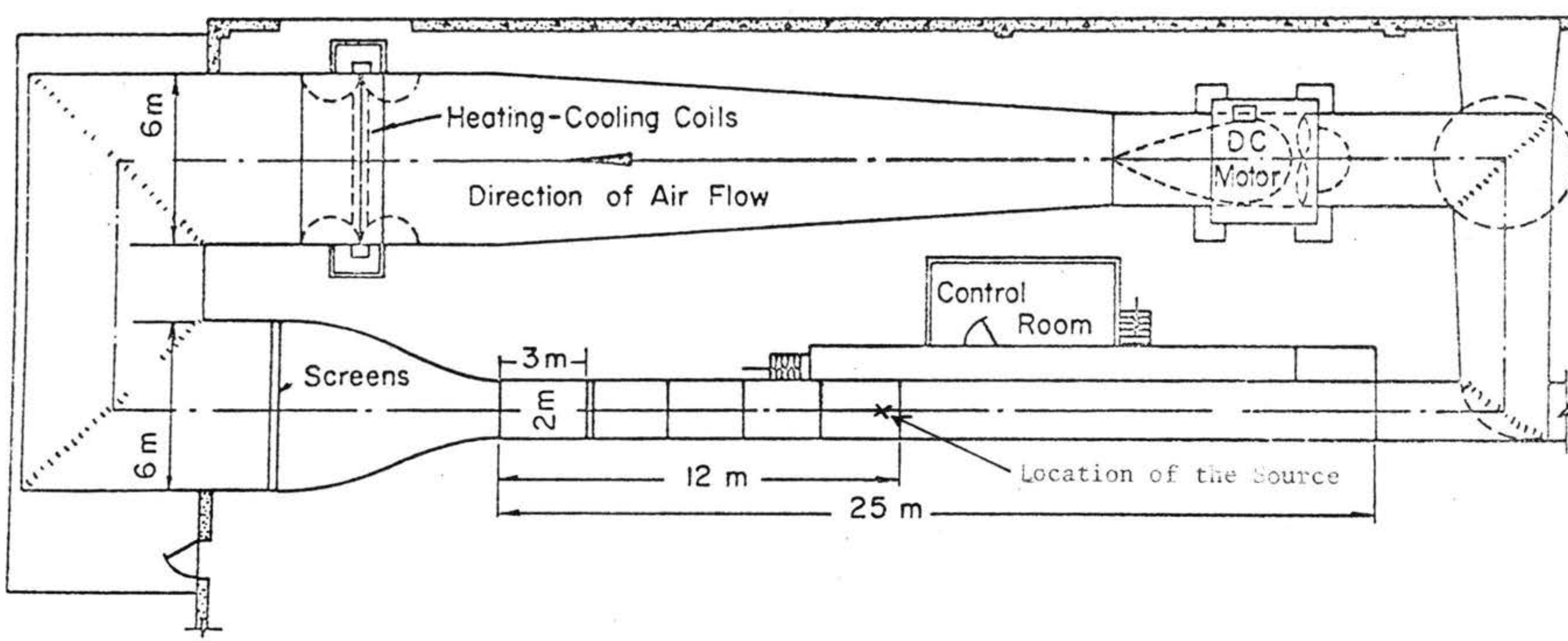

Fig. 6.4 Wind tunnel.

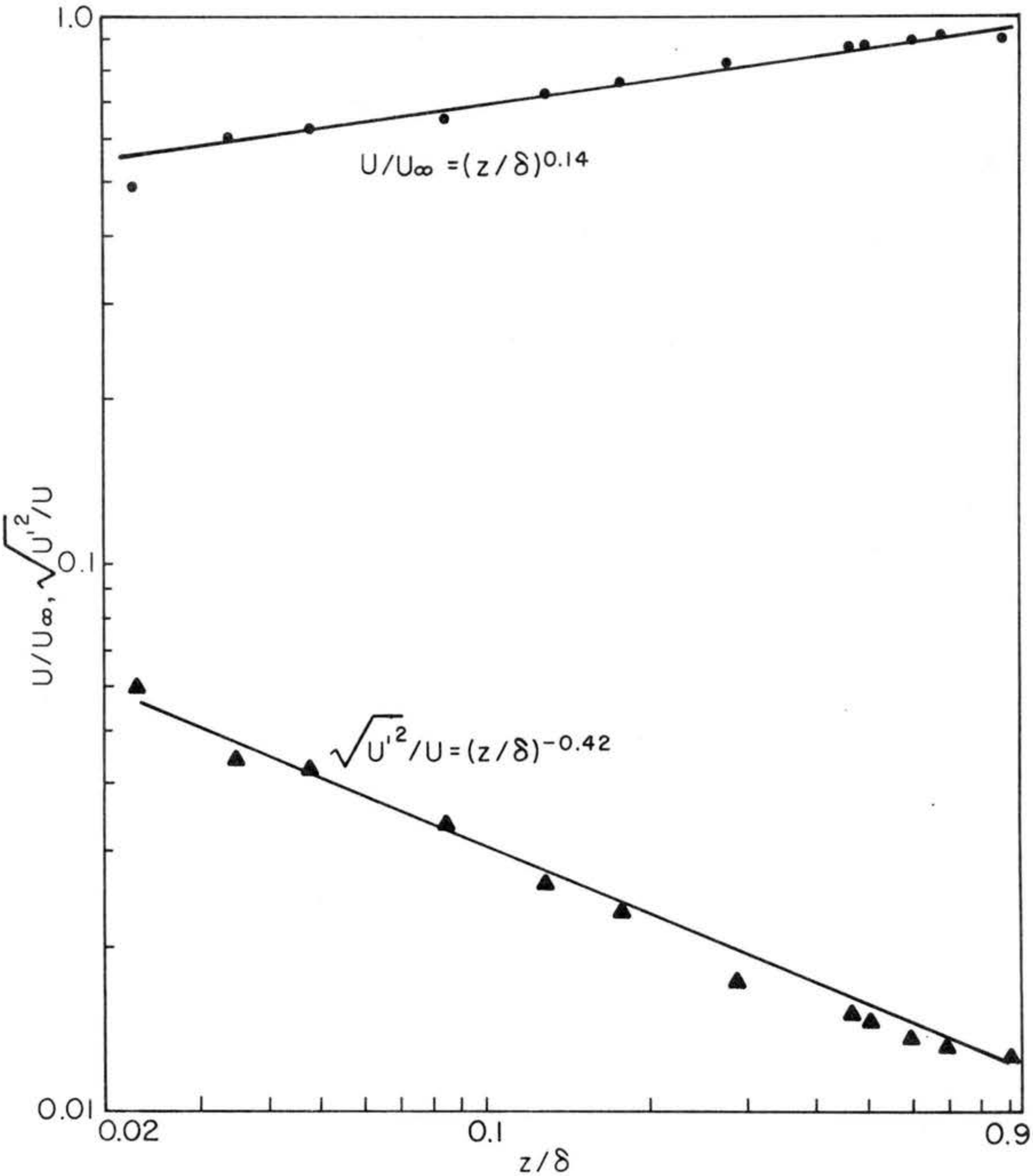

Fig. 6.5 Mean velocity profile and turbulent intensity profile.

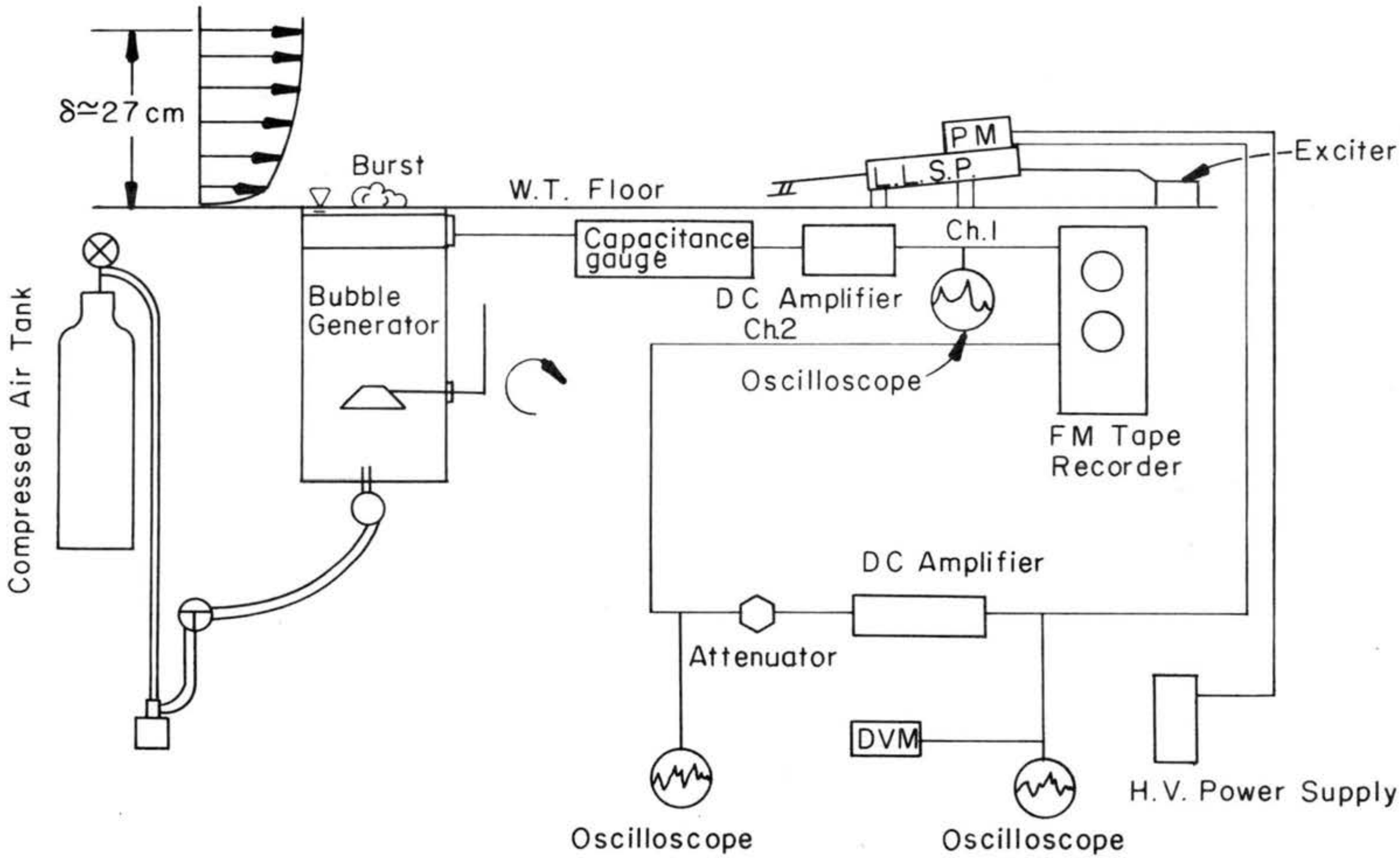

Fig. 6.6 Experimental arrangement during puff measurements.

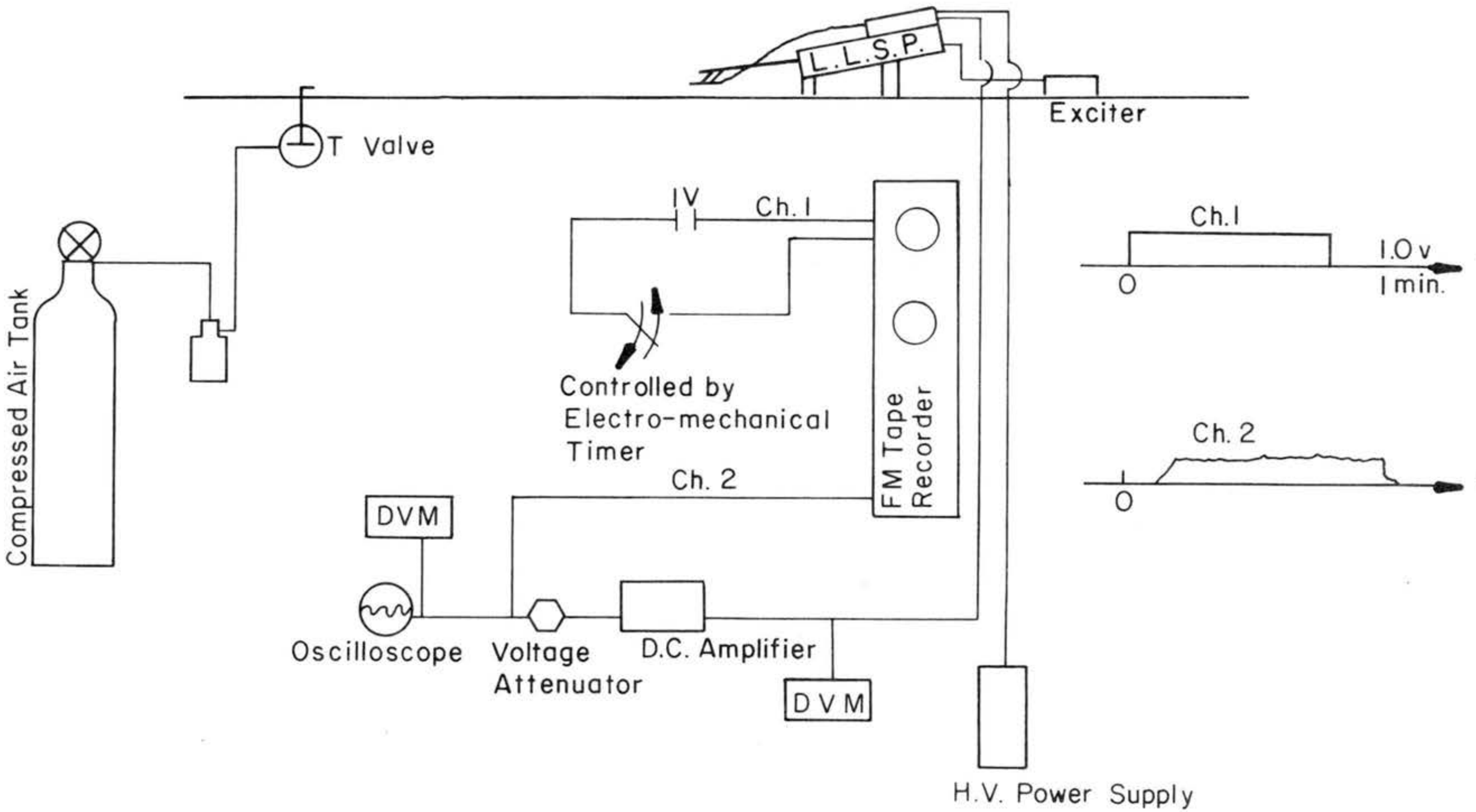

Fig. 6.7 Experimental arrangement during plume measurements.

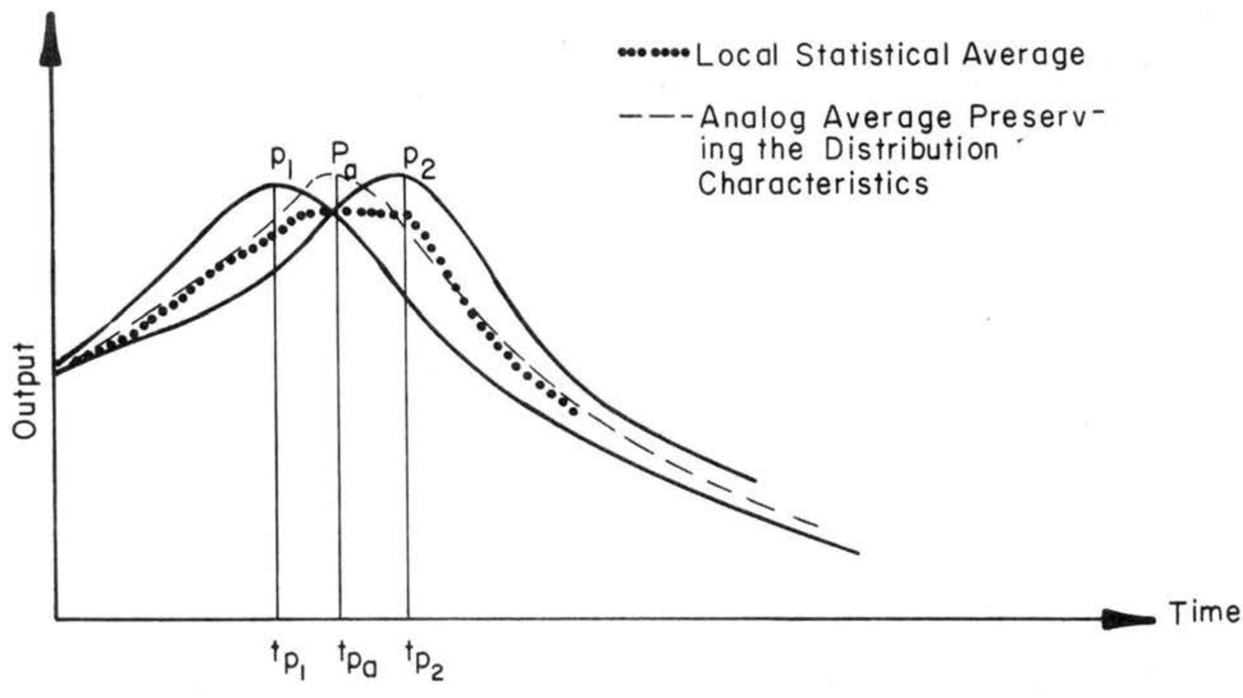

Fig. 6.8 Averaging principle for a small number of records.

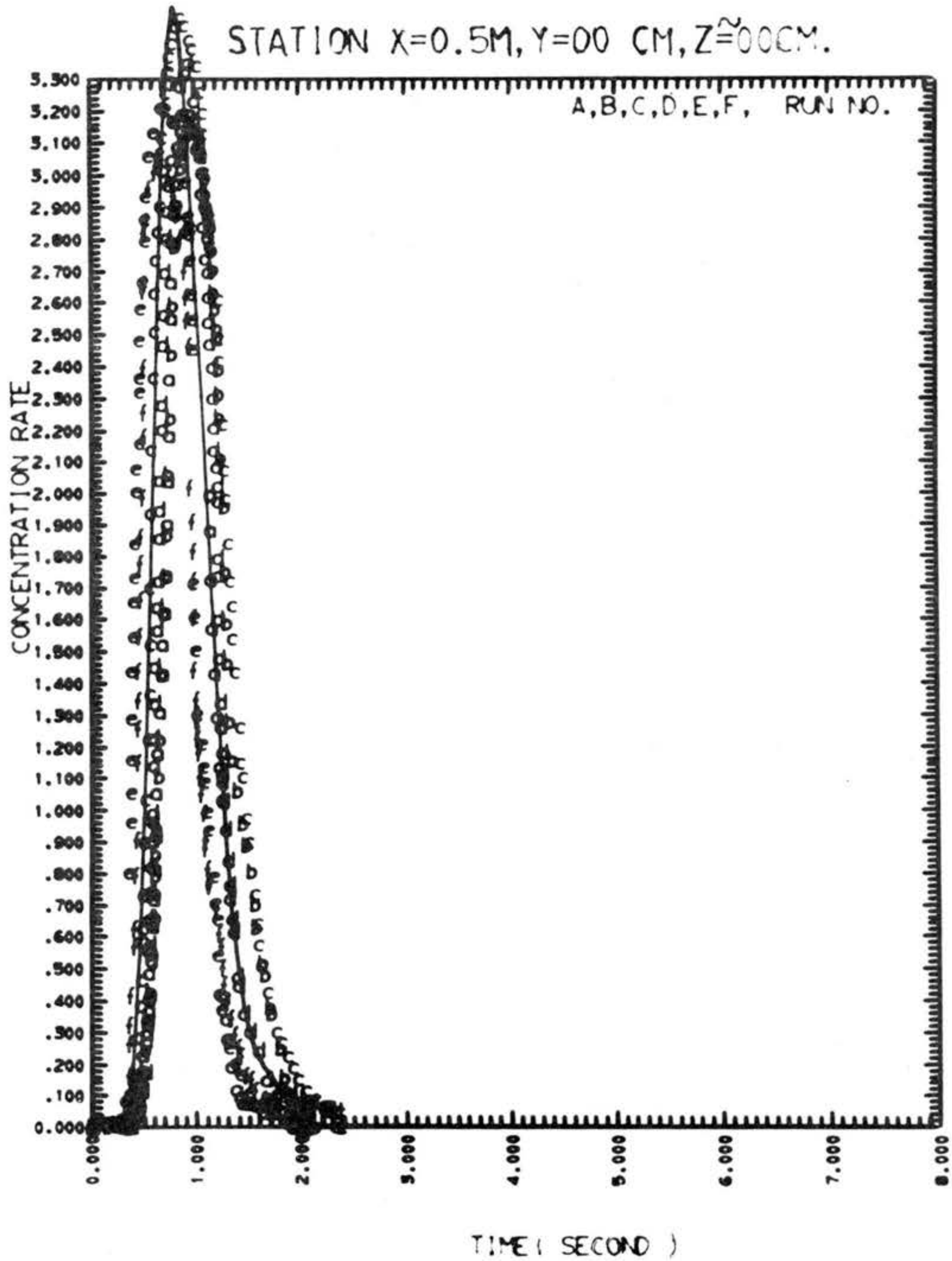

Fig. 7.1 Typical set of L.L.S.P. signals for puffs and their fit by Gram-Charlier series (I).

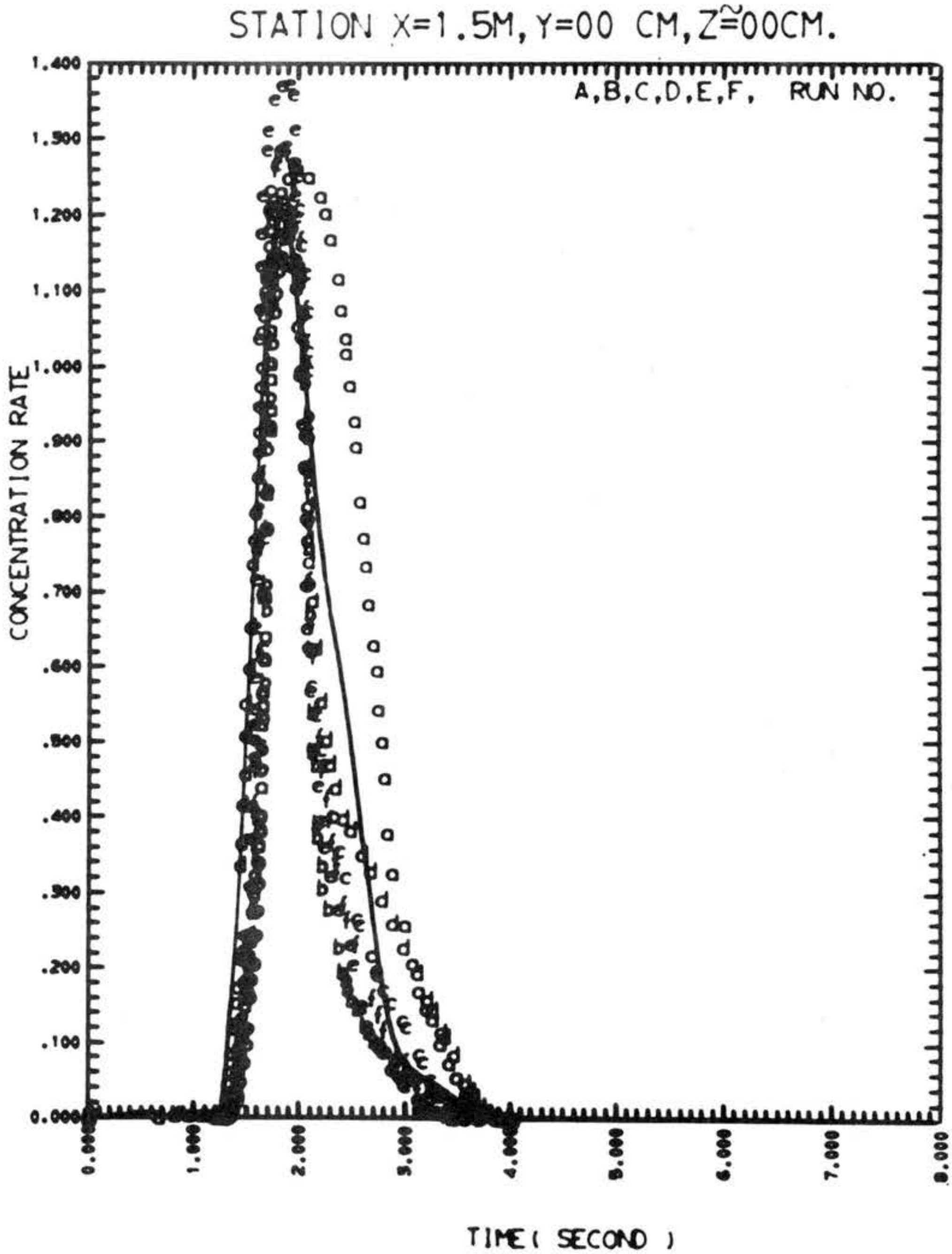

Fig. 7.2 Typical set of L.L.S.P. signals for puffs and their fit by Gram-Charlier series (II).

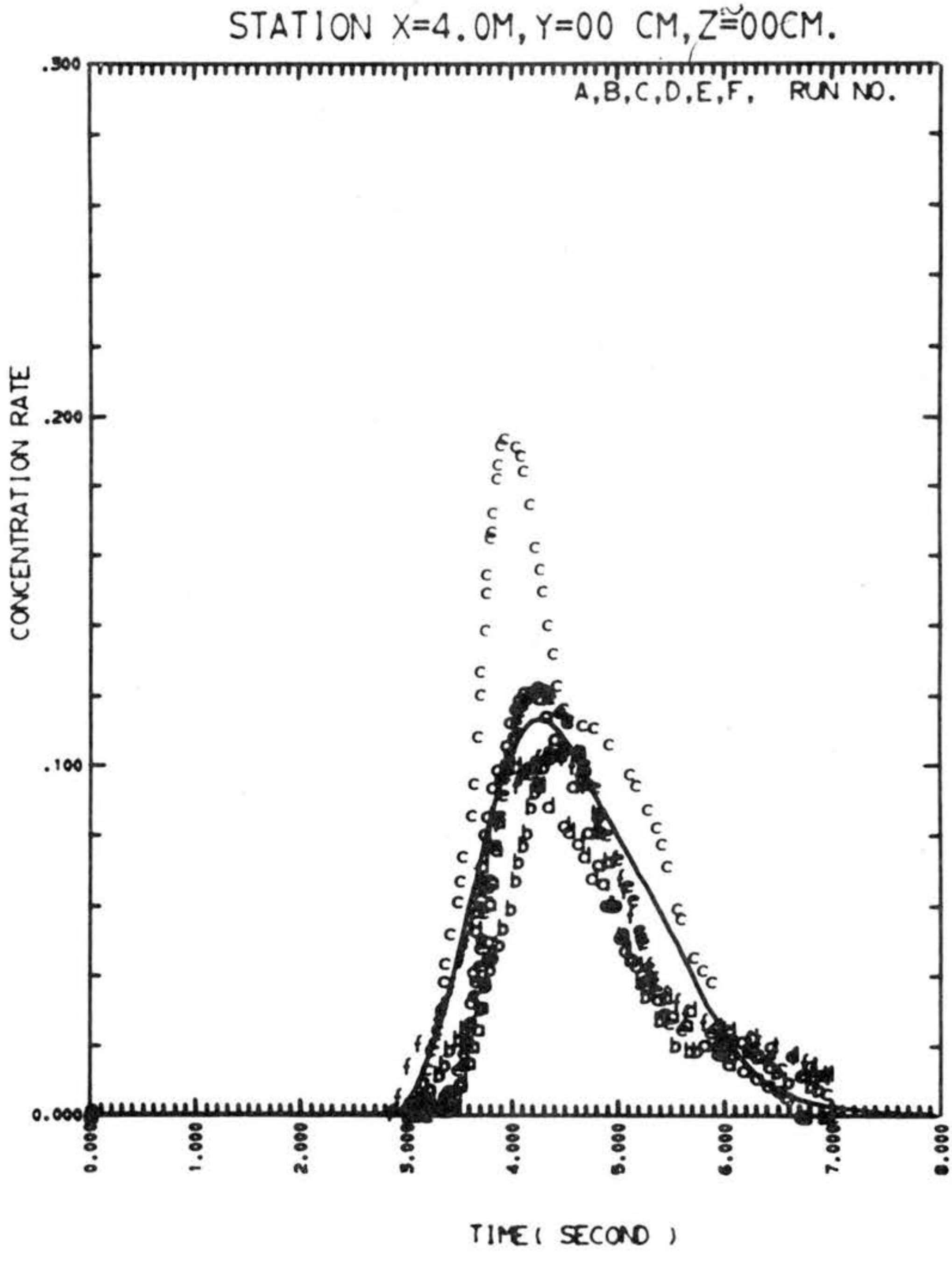

Fig. 7.3 Typical set of L.L.S.P. signals for puffs and their fit by Gram-Charlier series (III).

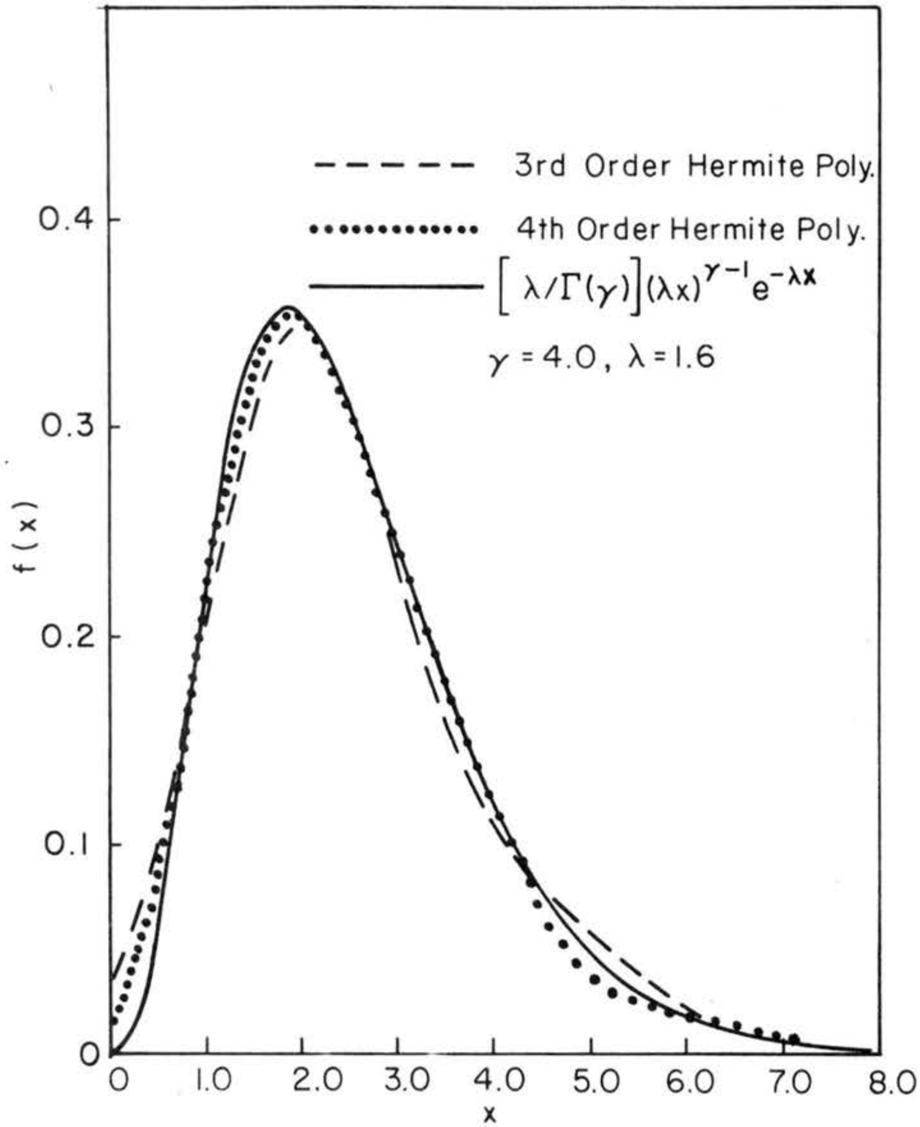

Fig. 7.4 Gram-Charlier series fit for a Gamma distribution ($\gamma = 4$, $\lambda = 1.6$).

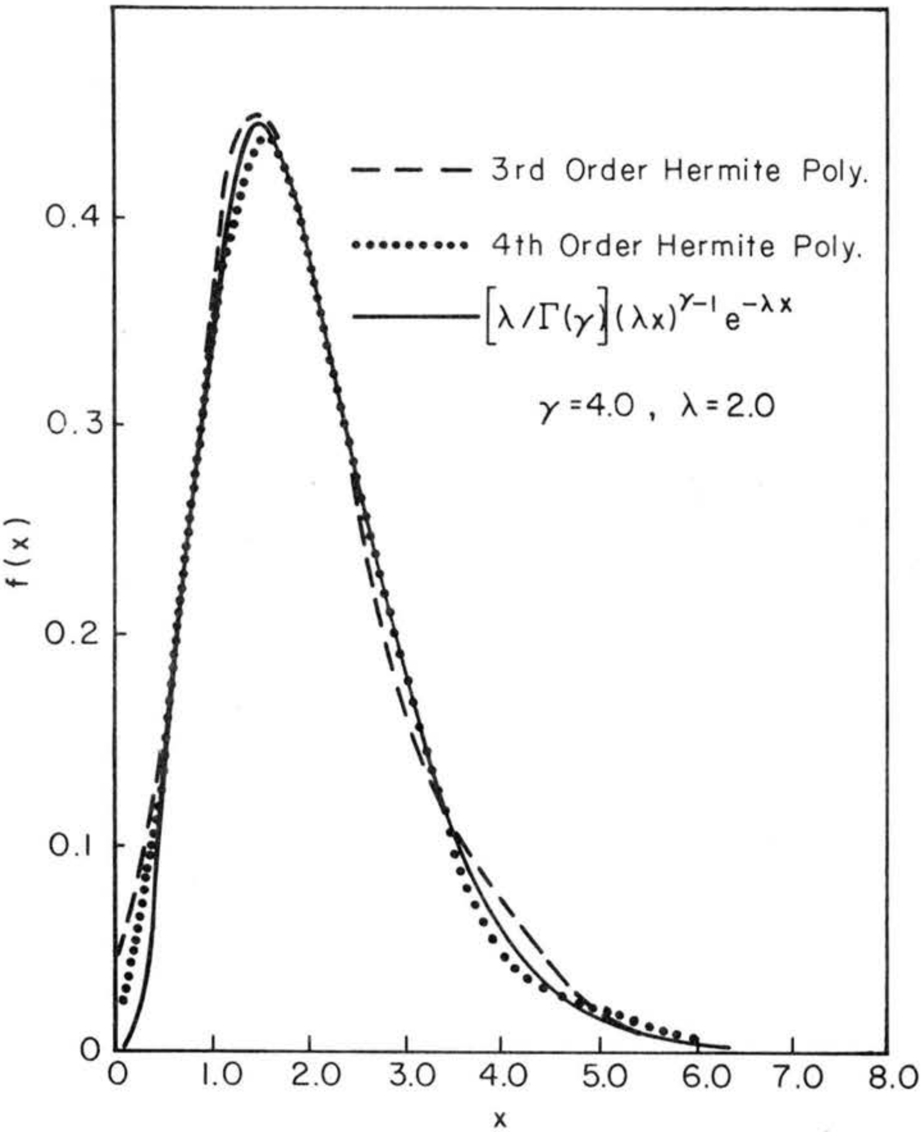

Fig. 7.5 Gram-Charlier series fit for a Gamma distribution (γ = 4, λ = 2.0).

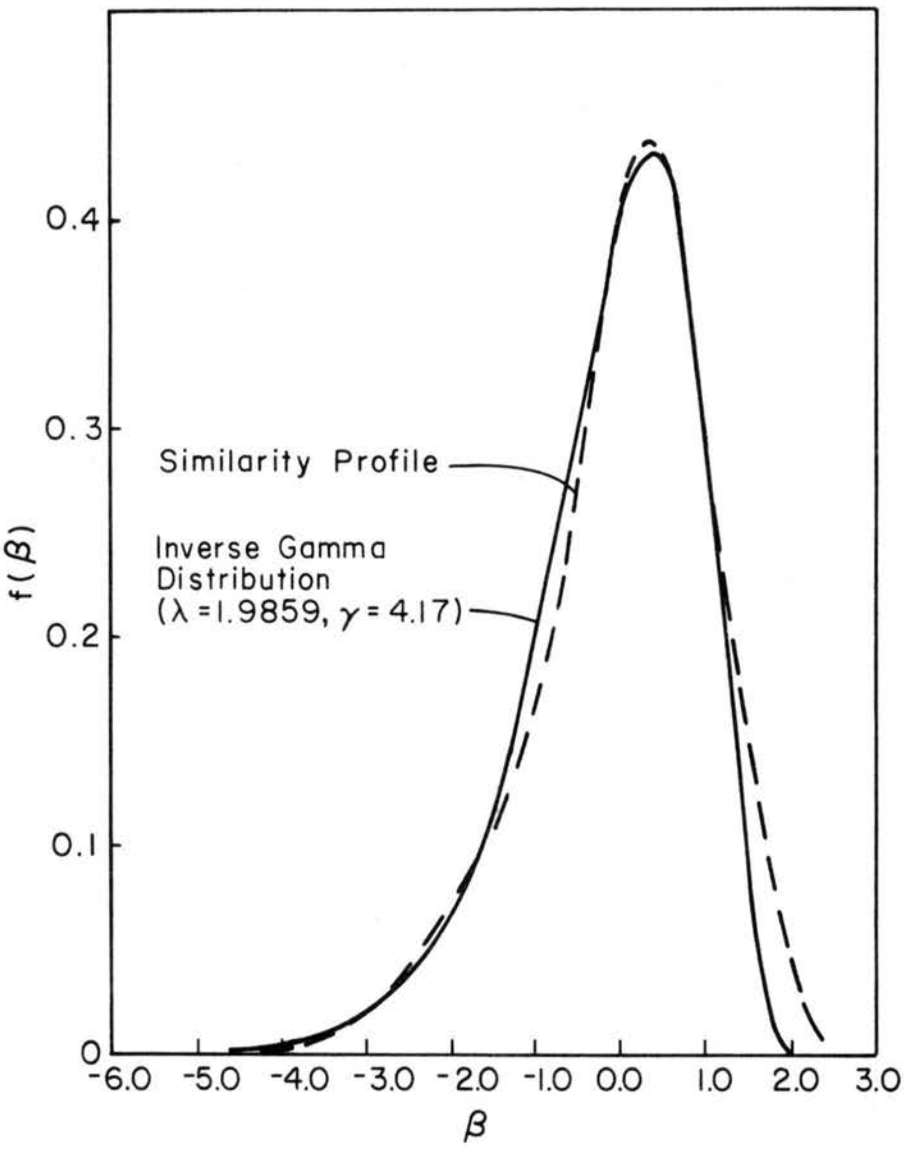

Fig. 8.1 Comparison of similarity profile and the inverse-Gamma distribution (λ = 1.9859, γ = 4.17).

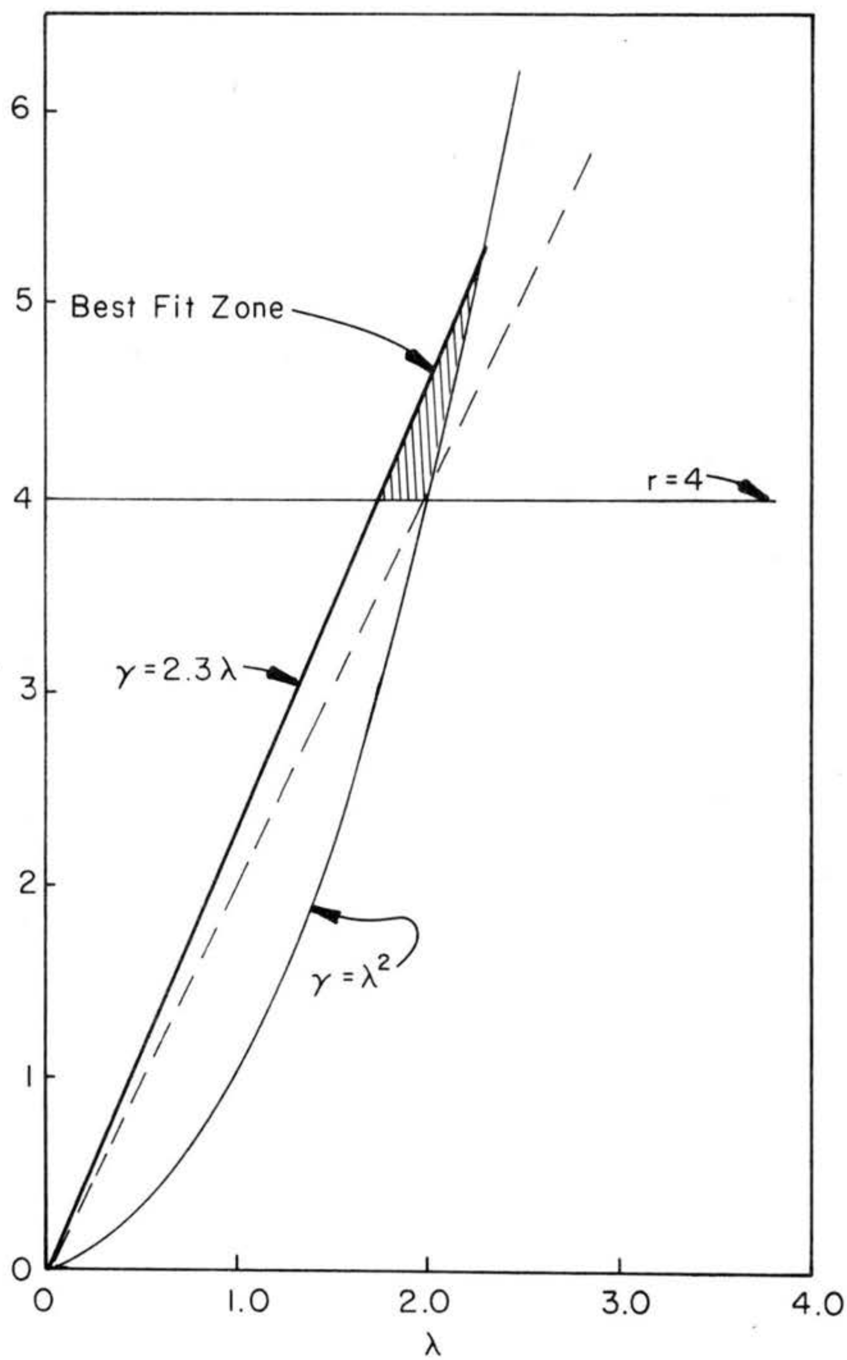

Fig. 8.2 Optimization process to find the parameters for the inverse-Gamma distribution.

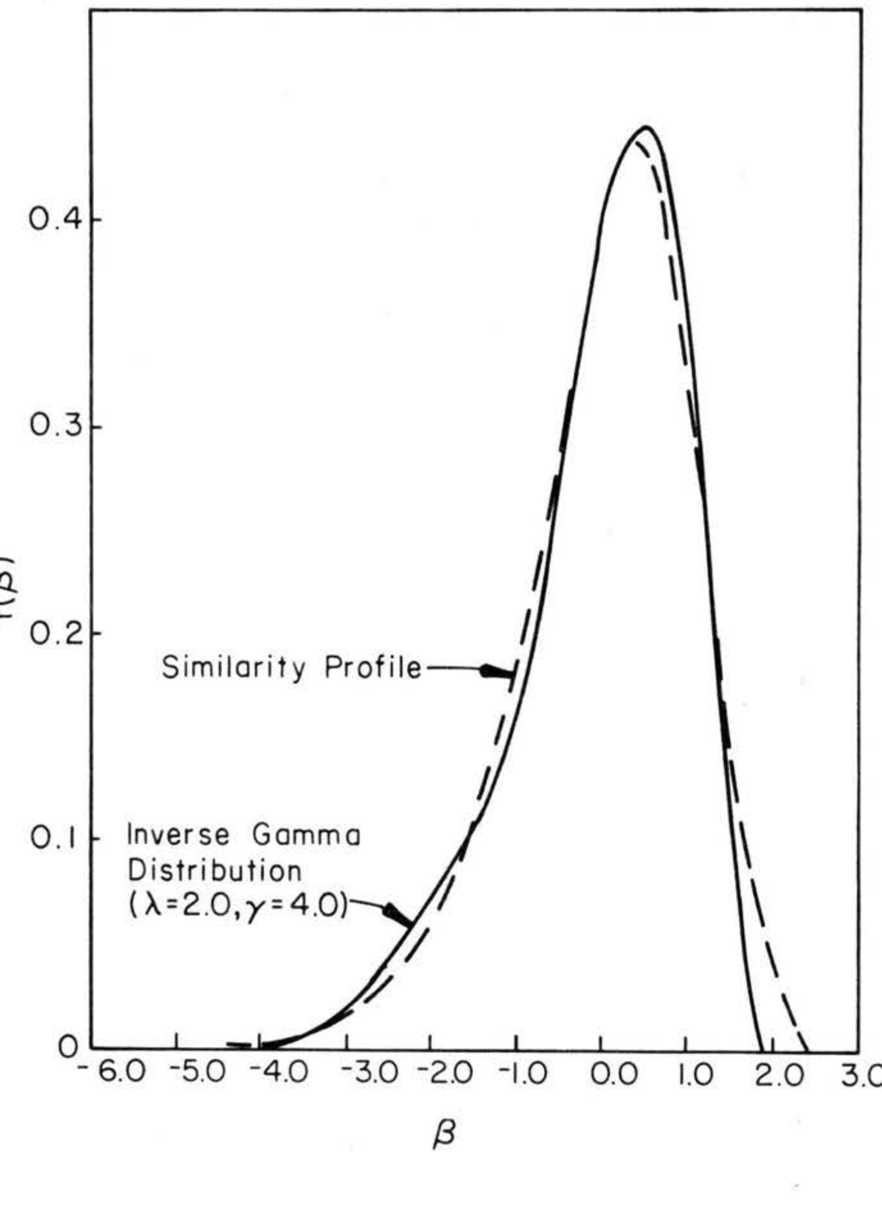

Fig. 8.3 Comparison of similarity profile and the inverse-Gamma distribution ($\lambda = 2.0$, $\gamma = 4.0$).

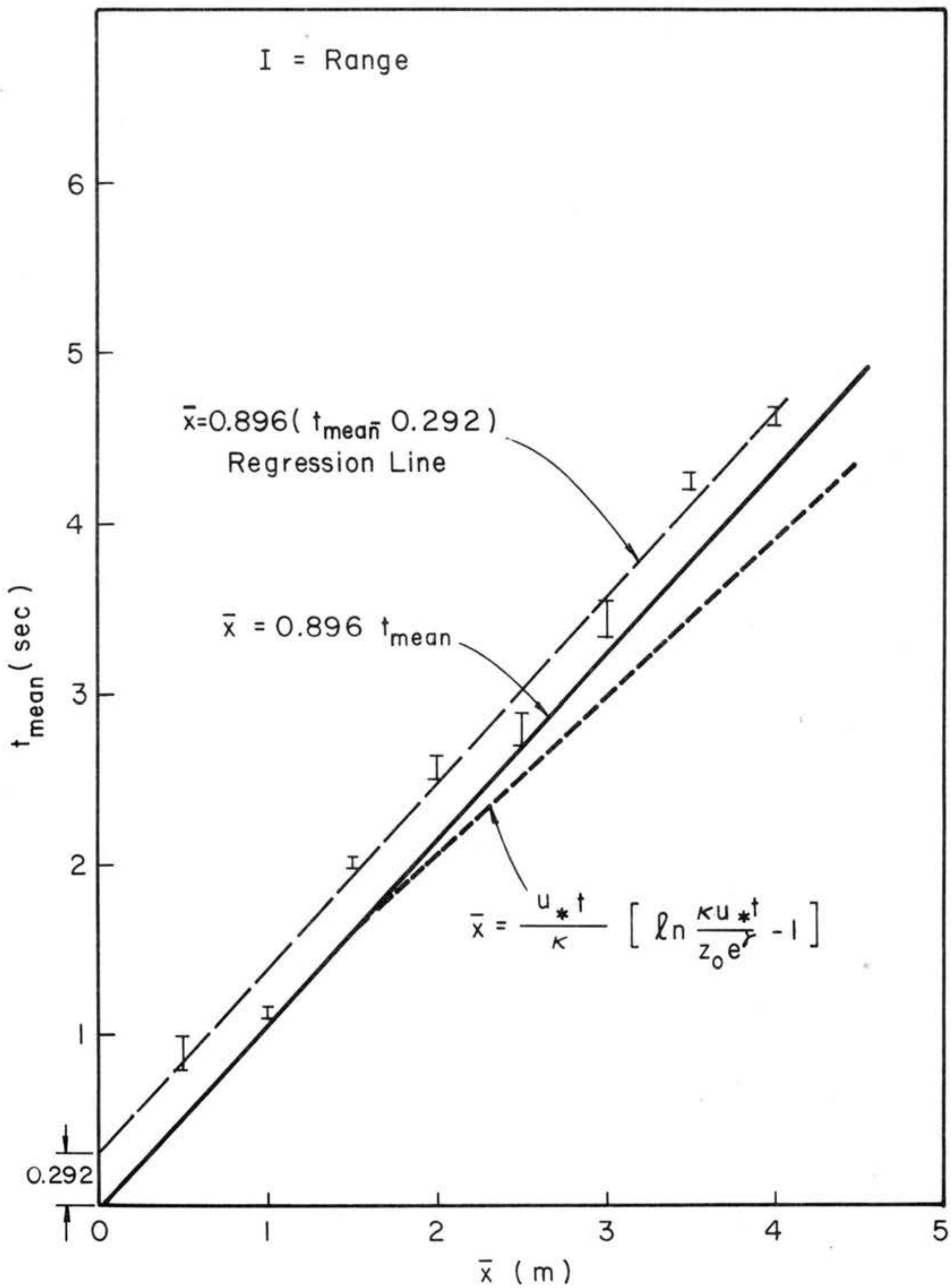

Fig. 9.1 Mean arrival time of puffs at the ground level.

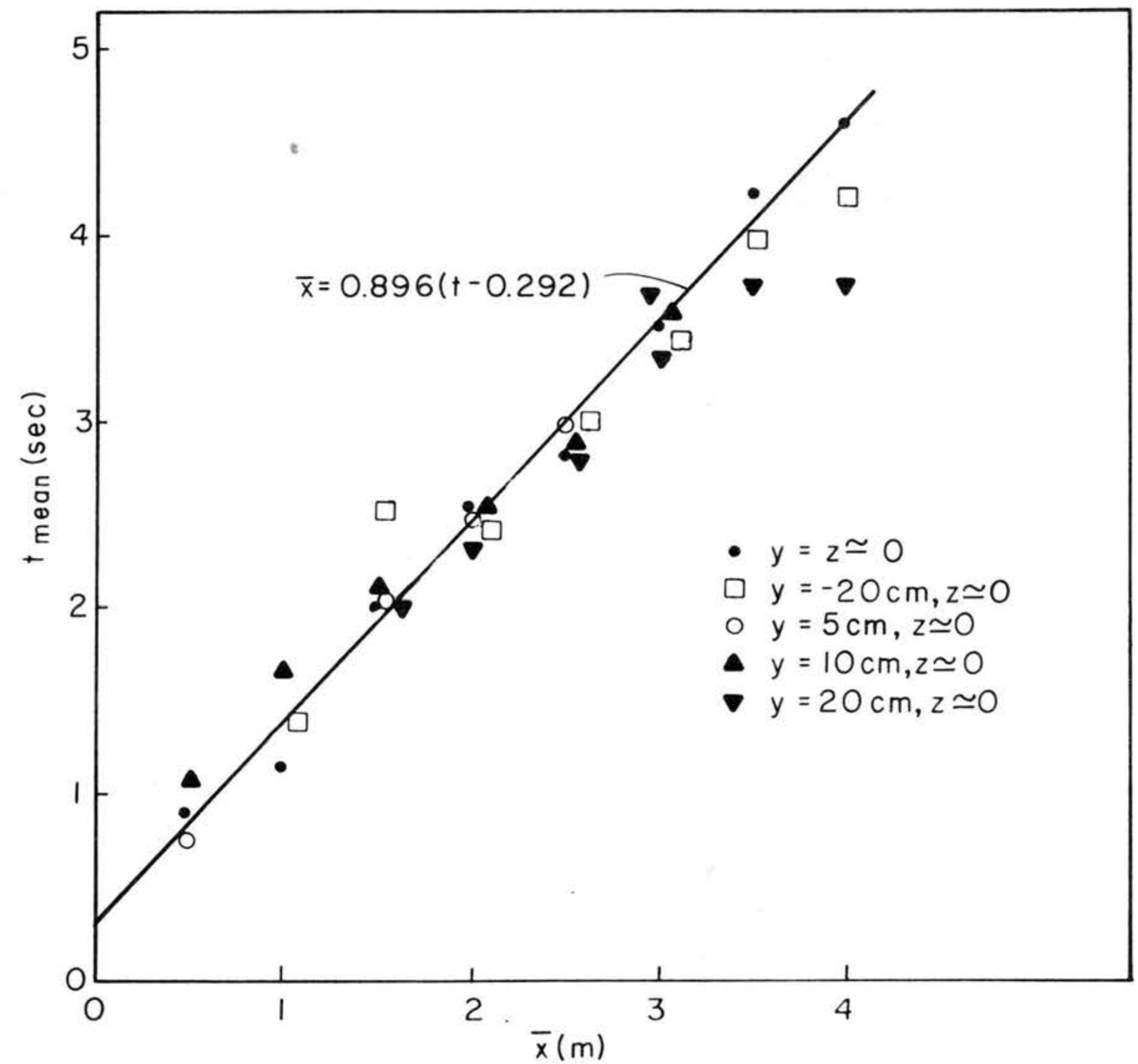

Fig. 9.2 Mean arrival time of puffs (off centerline) at the ground level.

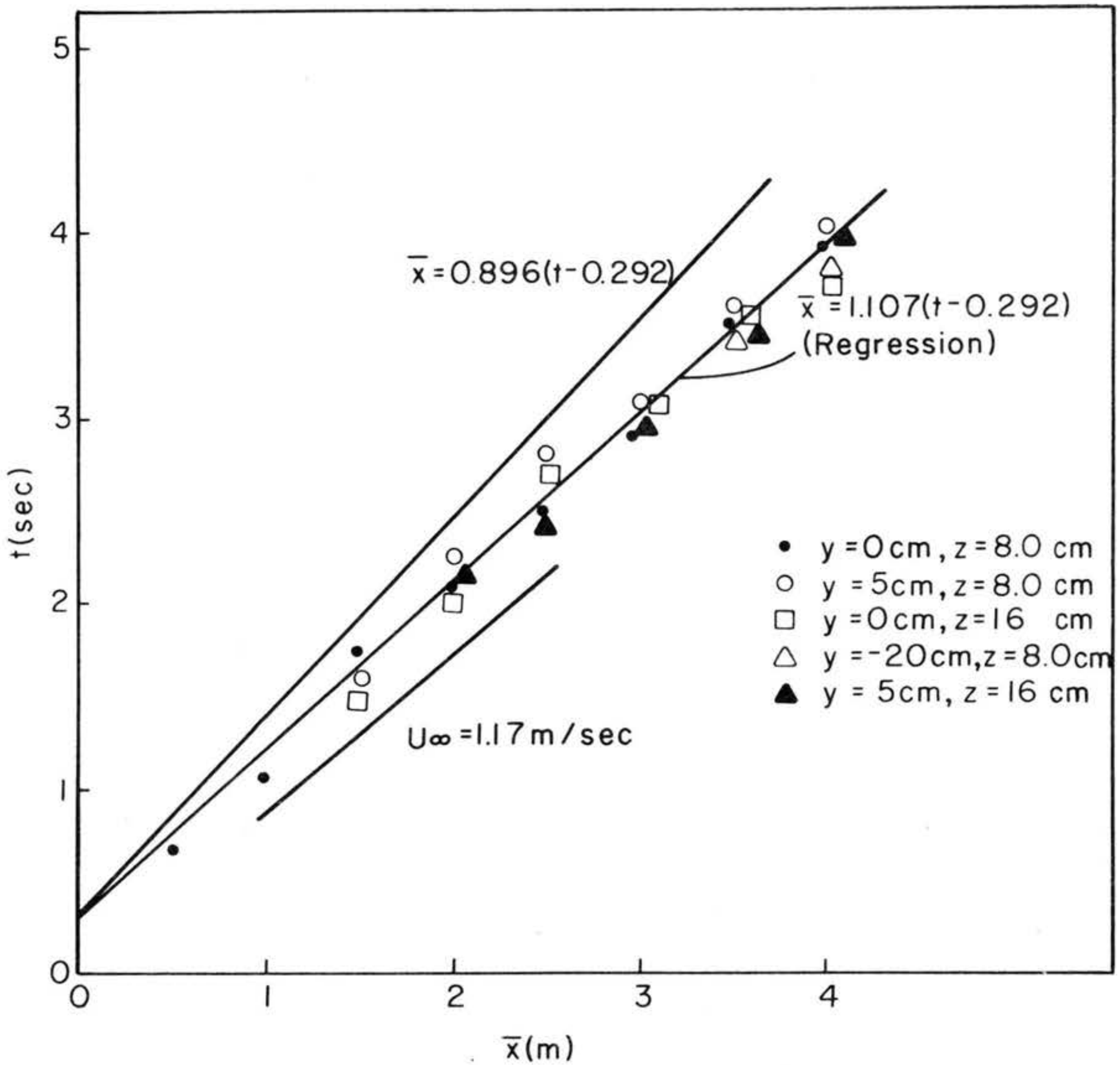

Fig. 9.3 Mean arrival time of puffs at an elevated level.

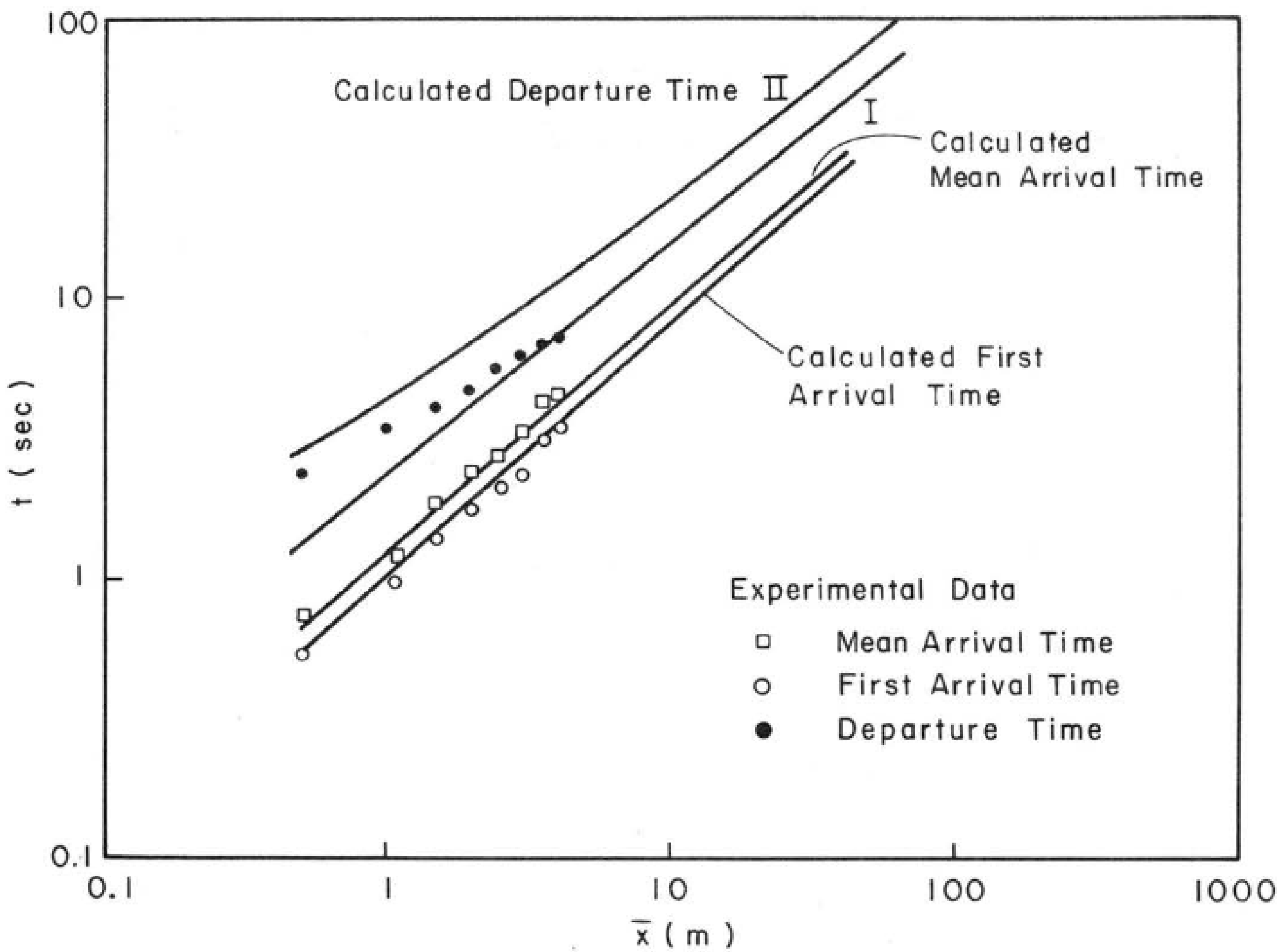

Fig. 9.4 Mean arrival time, first arrival time and departure time.

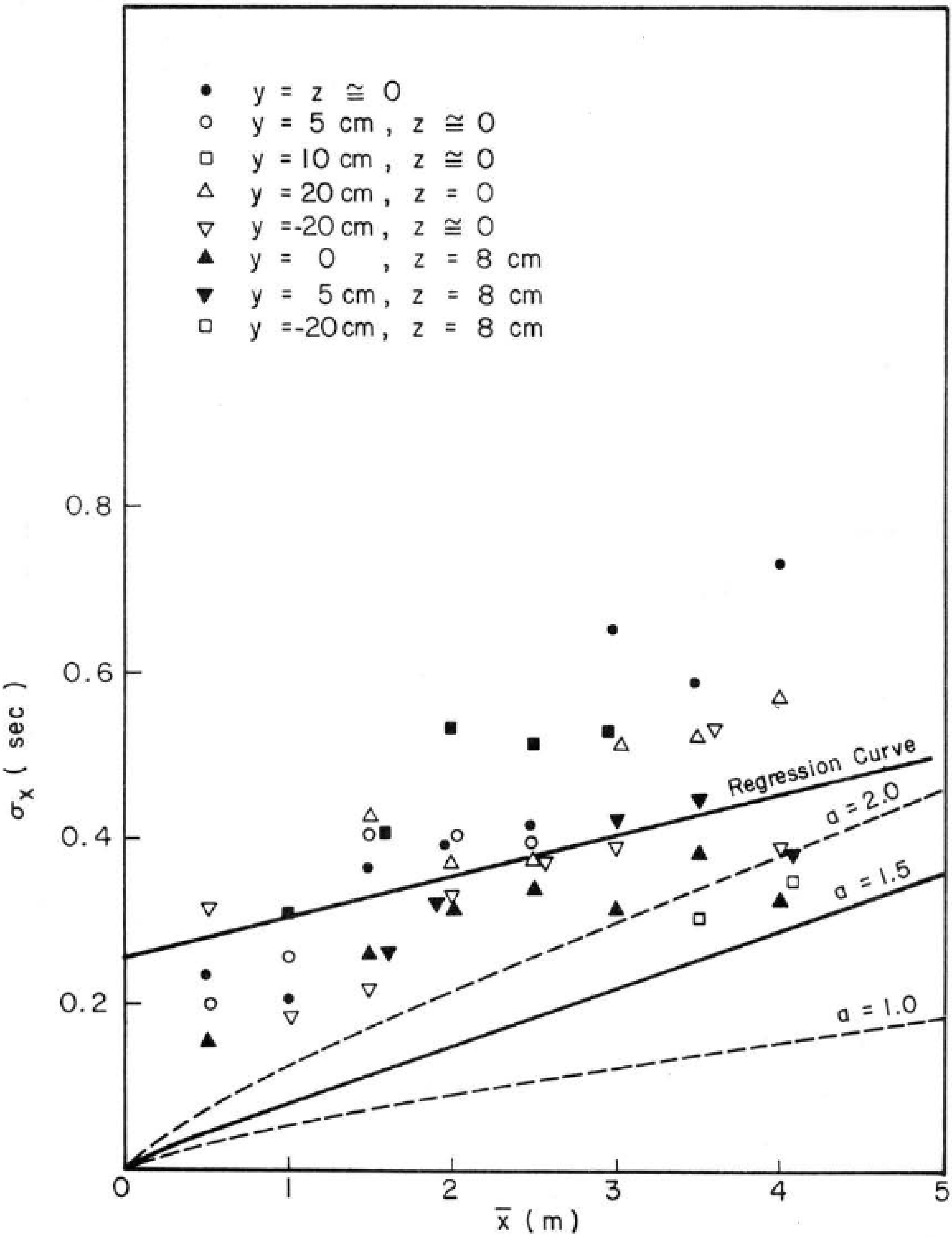

Fig. 9.5 Standard deviation of puffs.

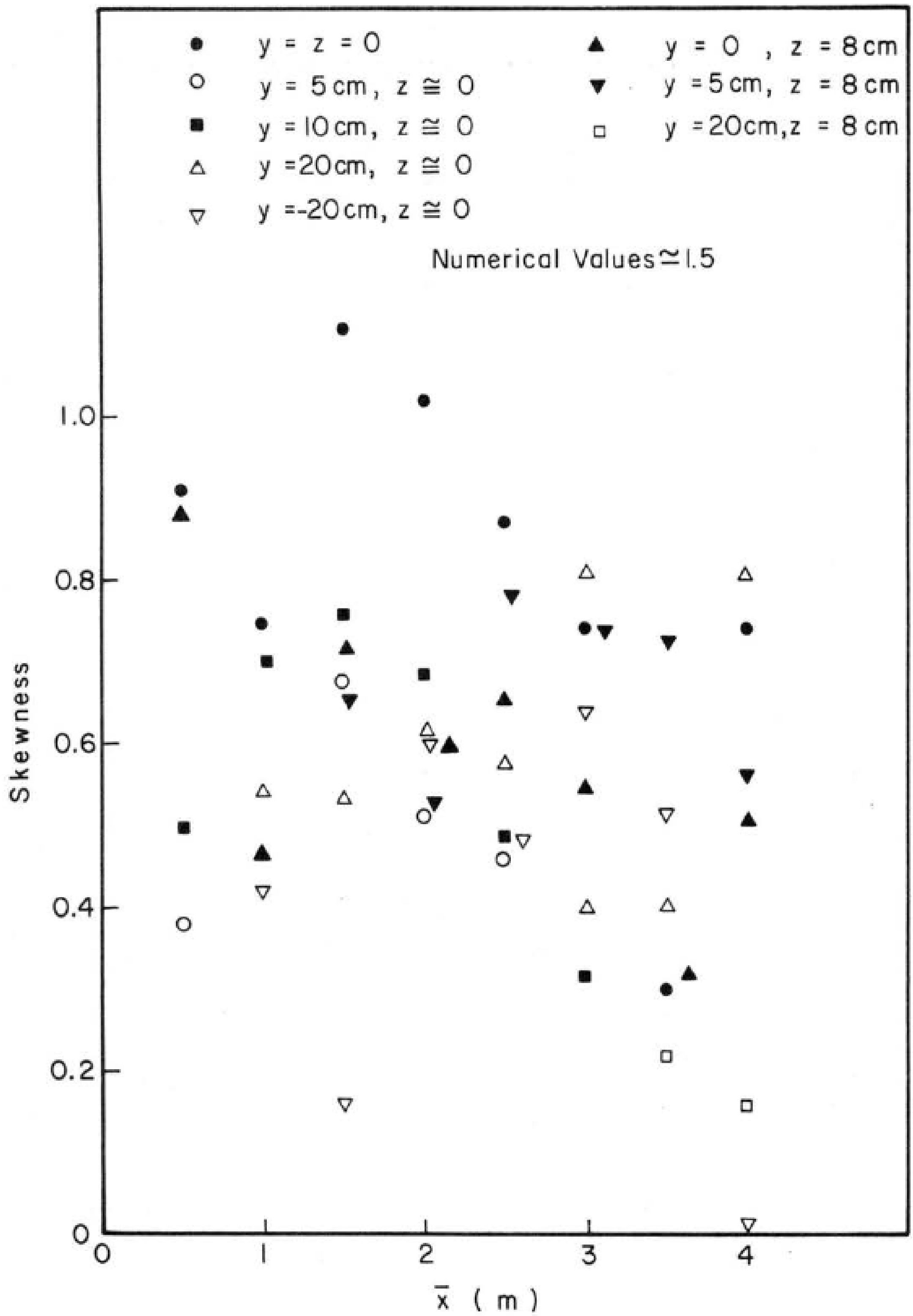

Fig. 9.6 Skewness of puffs.

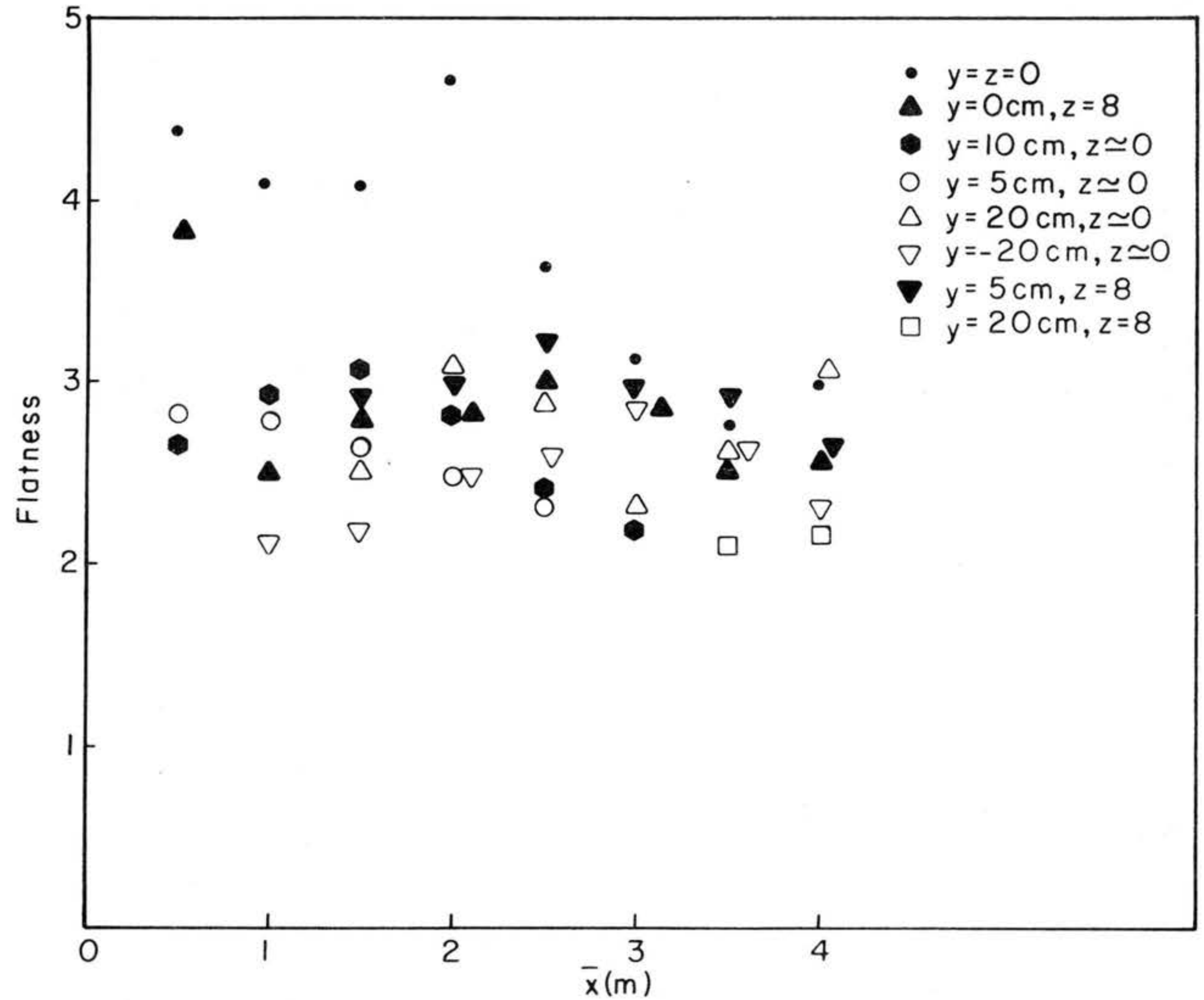

Fig. 9.7 Flatness of puffs.

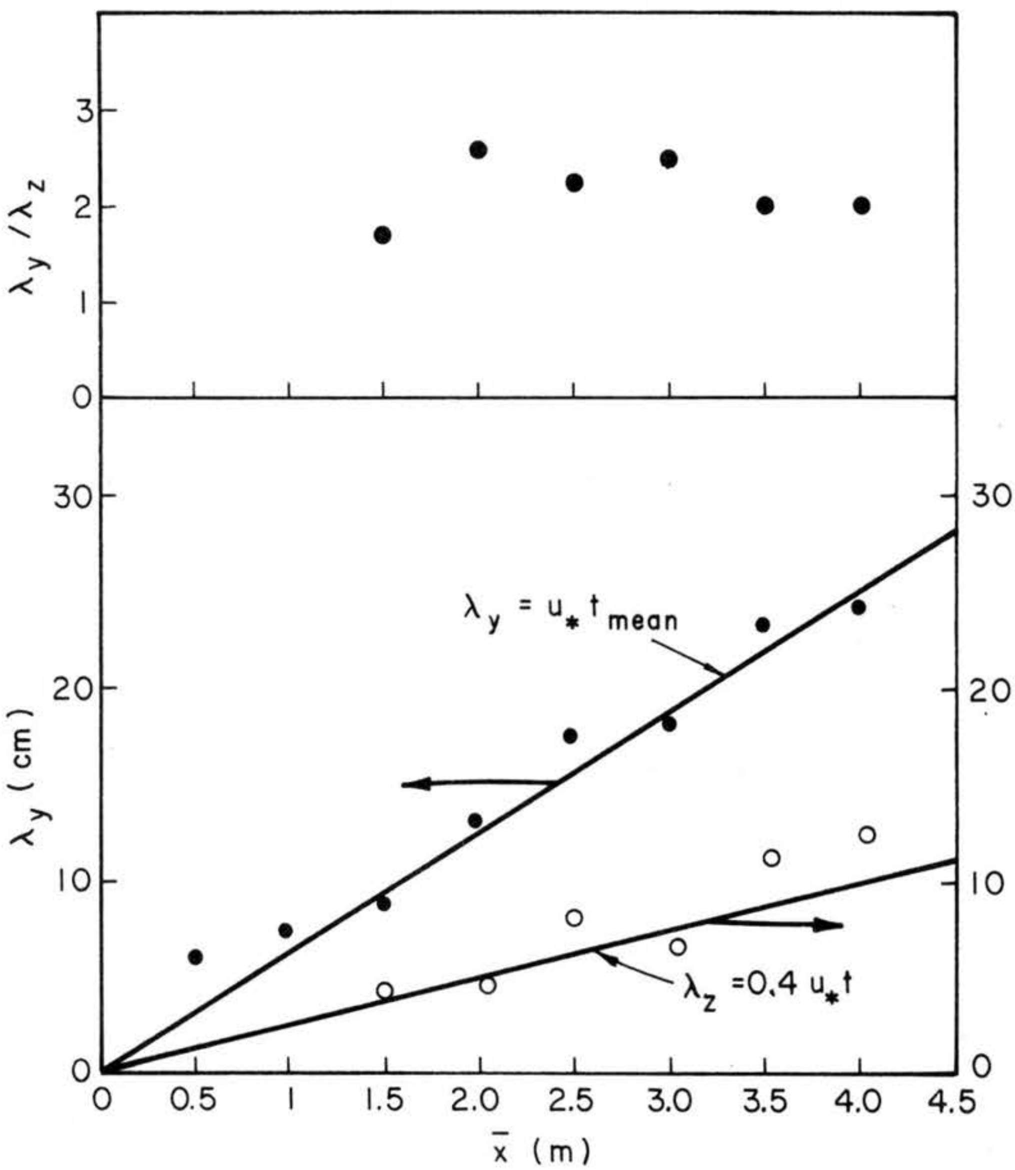

Fig. 9.8 Characteristic puff dimensions in y and z directions.

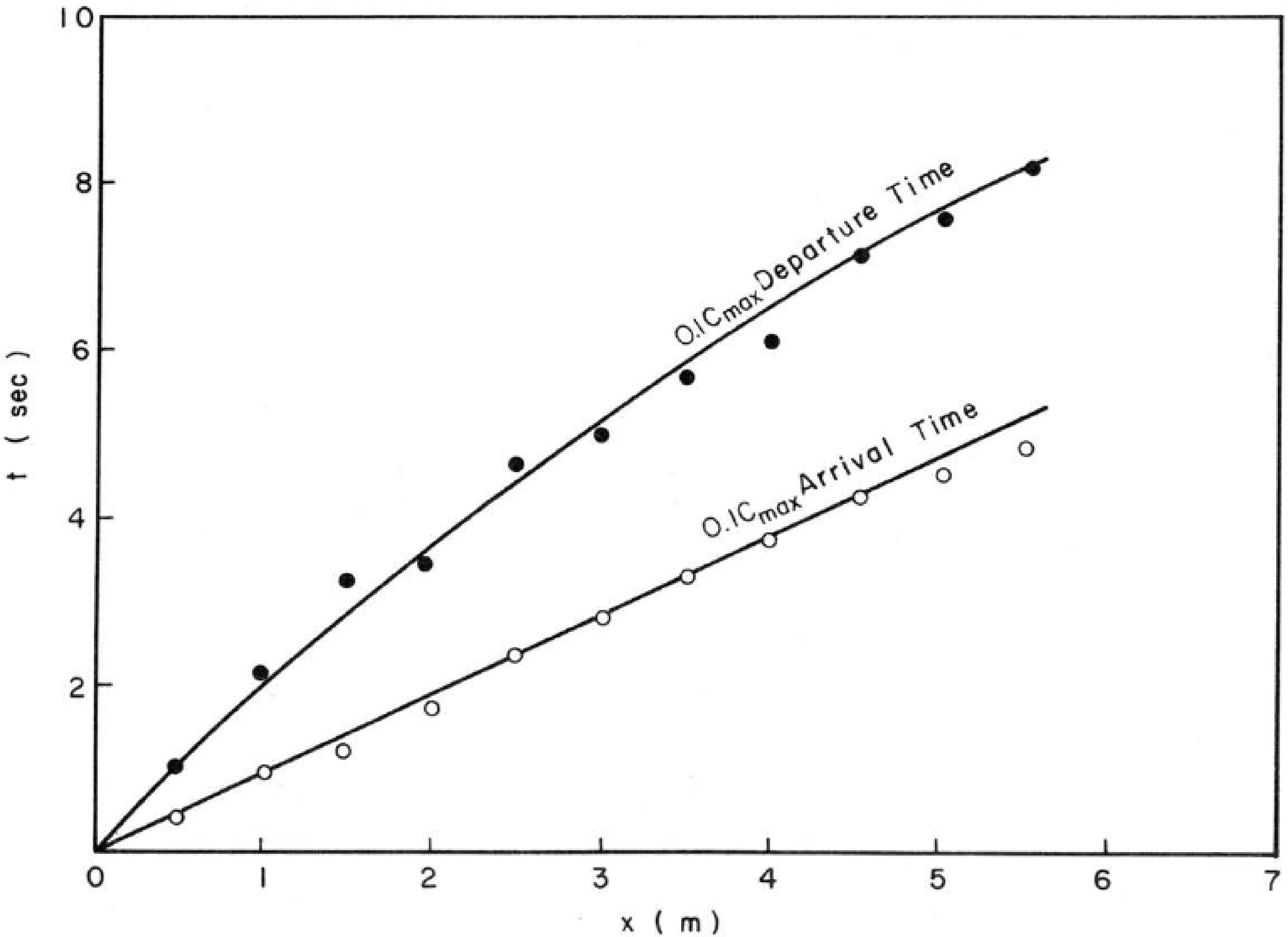

Fig. 9.9 Arrival time and departure time $(0.1\ C_{max})$ from short-release plumes.

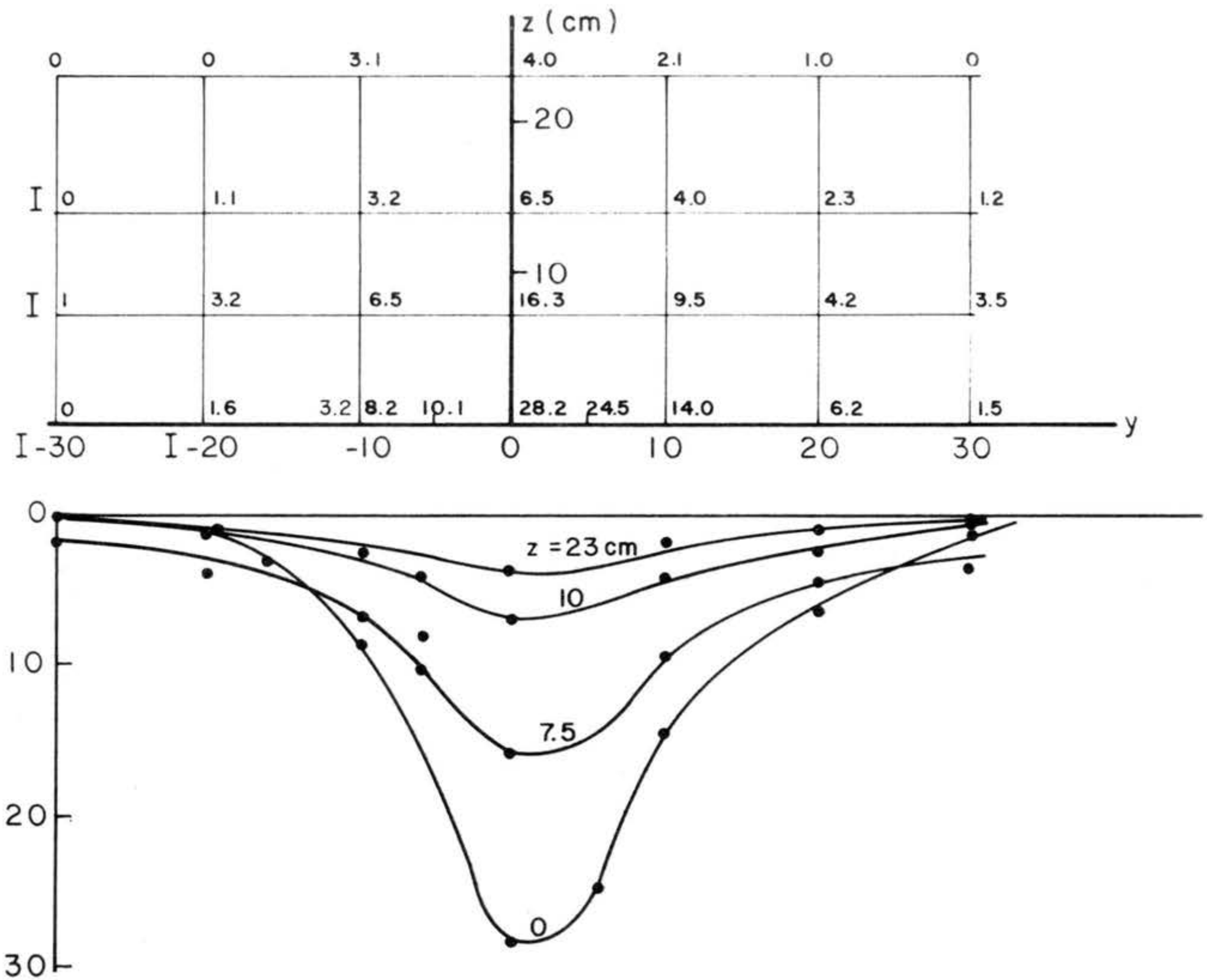

Fig. 9.10 Local mean concentration for continuous point sources at x = 4m .

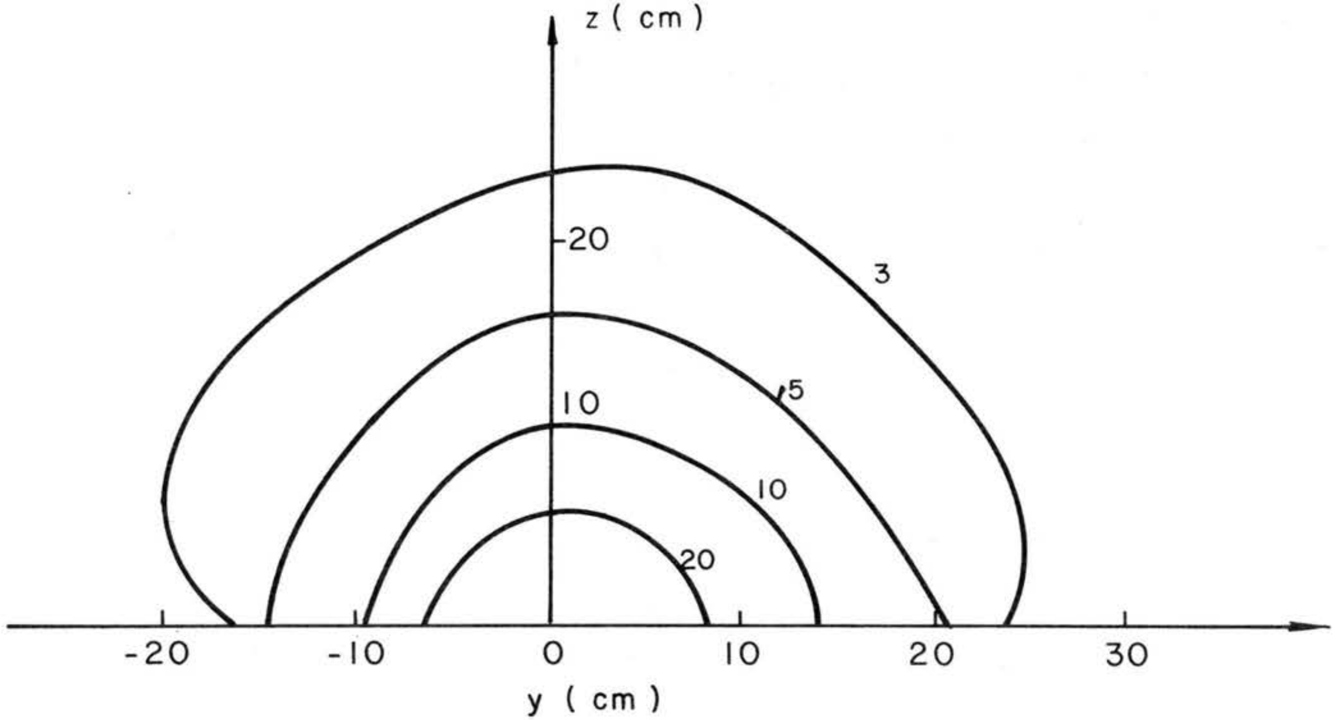

Fig. 9.11 Relative concentration iso-pleth at x = 4.0m from continuous point sources.

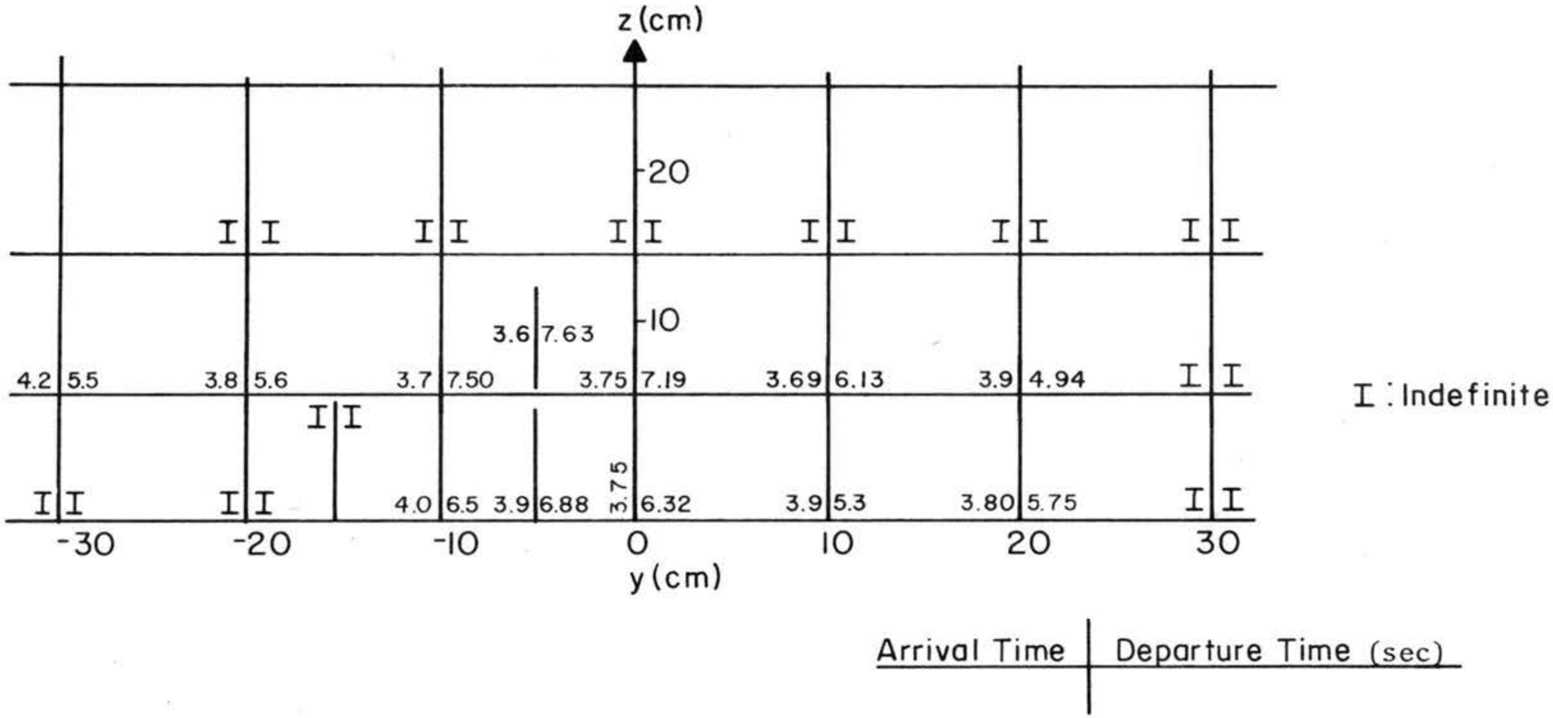

Fig. 9.12 Plume arrival time and departure time at x = 4.0m in y-z plane.

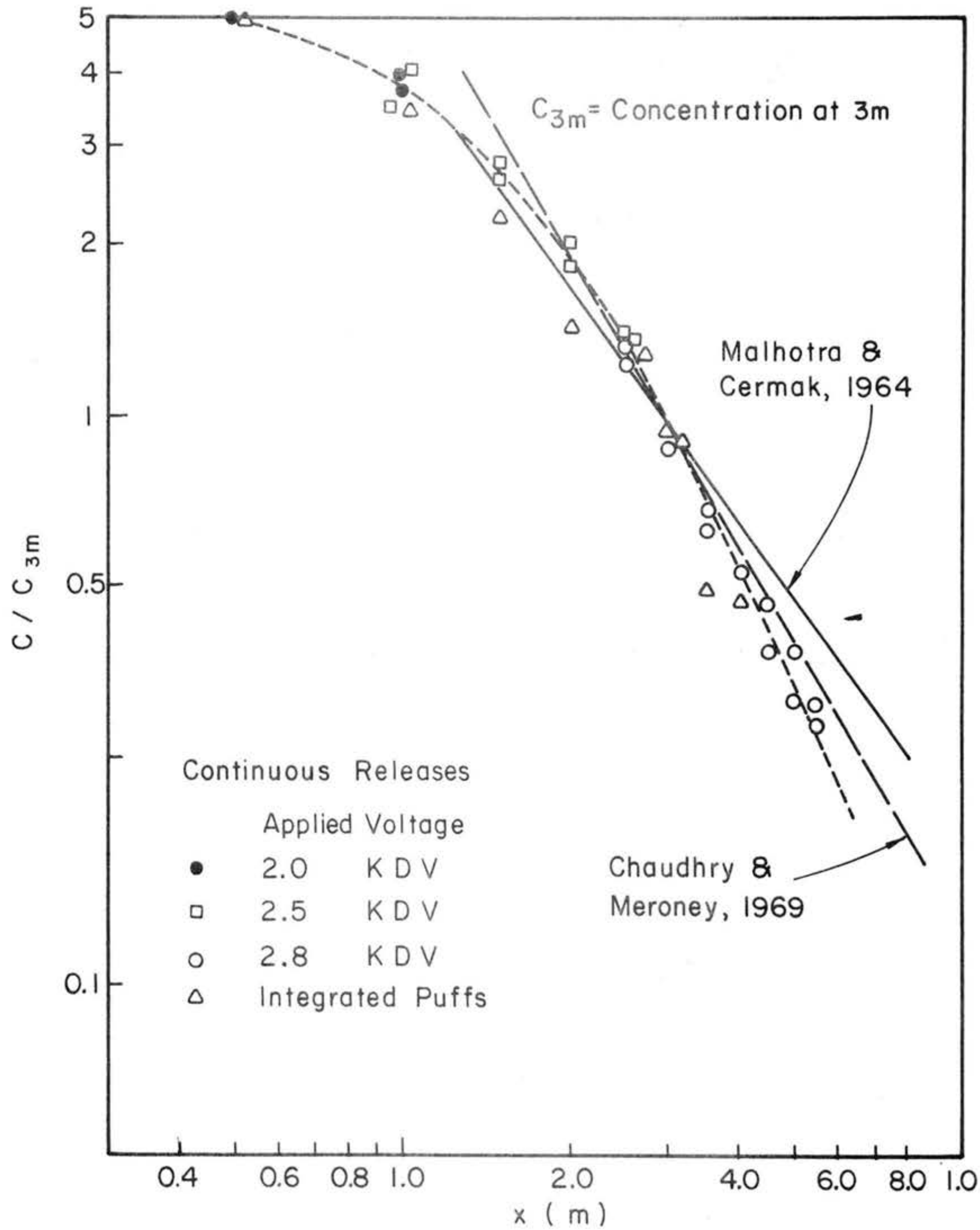

Fig. 9.13 Comparison between integrated puff concentration and previous continuous-release measurements.

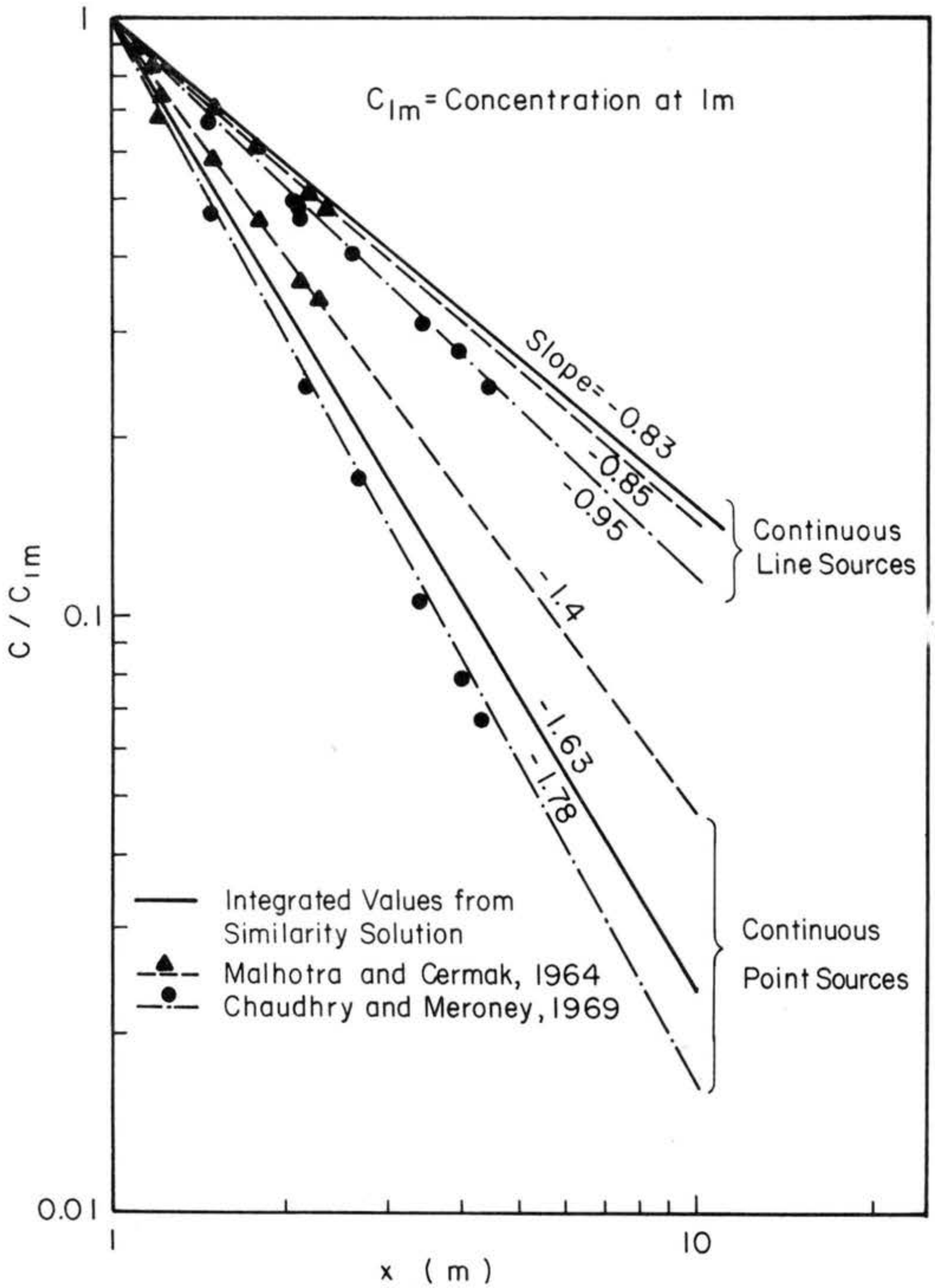

Fig. 9.14 Comparison of the concentration distribution from integrating the similarity solution and the previous measurements.

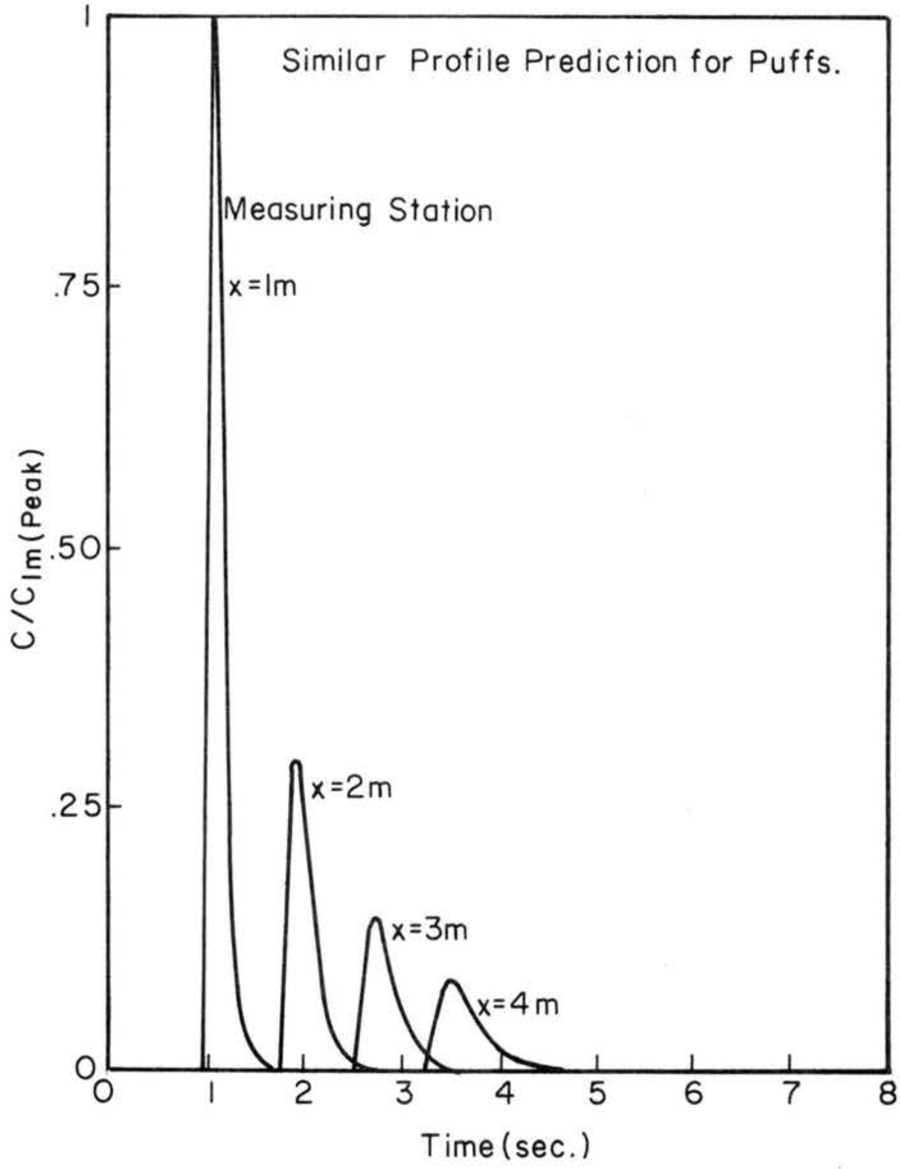

Fig. 9.15 Time trace predicted by similarity solution for puffs.

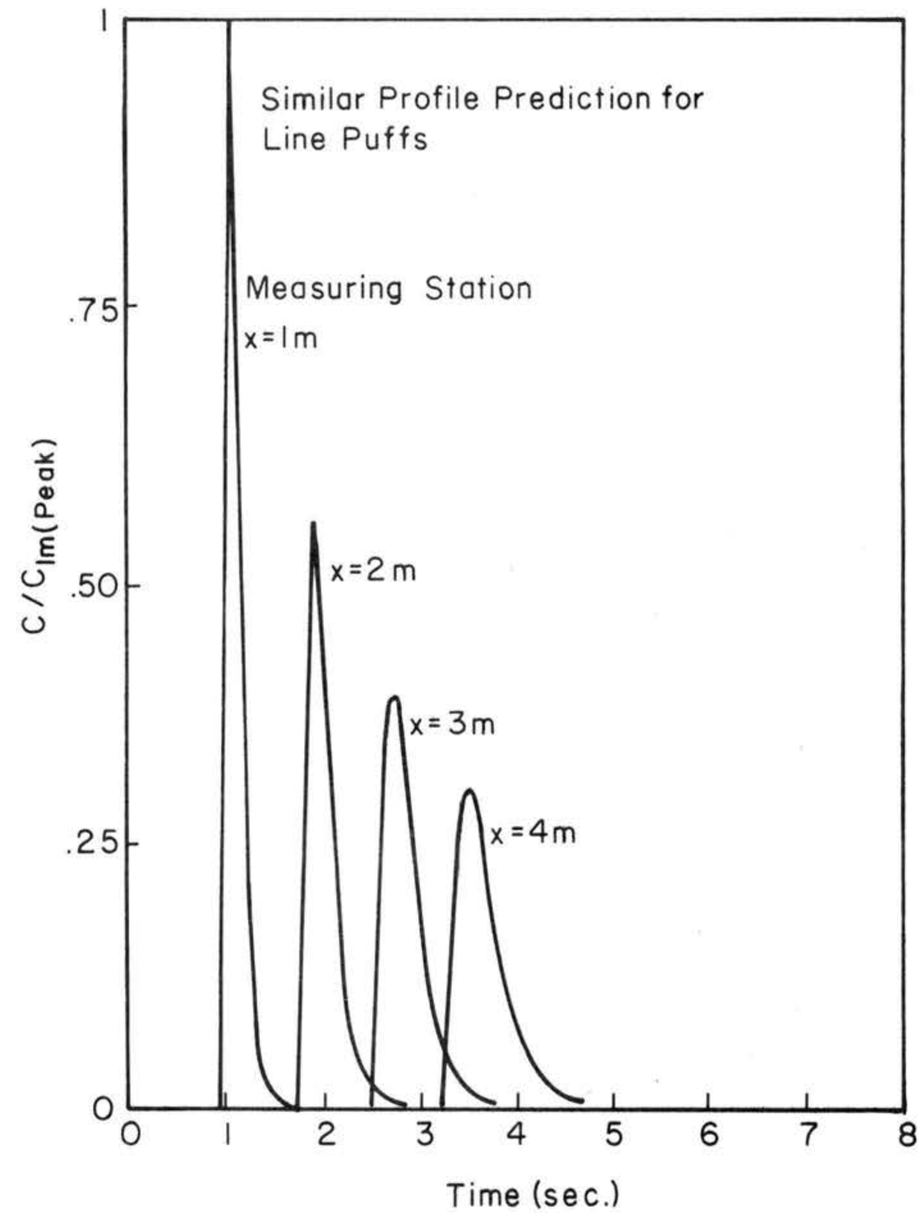

Fig. 9.16 Time trace predicted by similarity solution for line puffs.

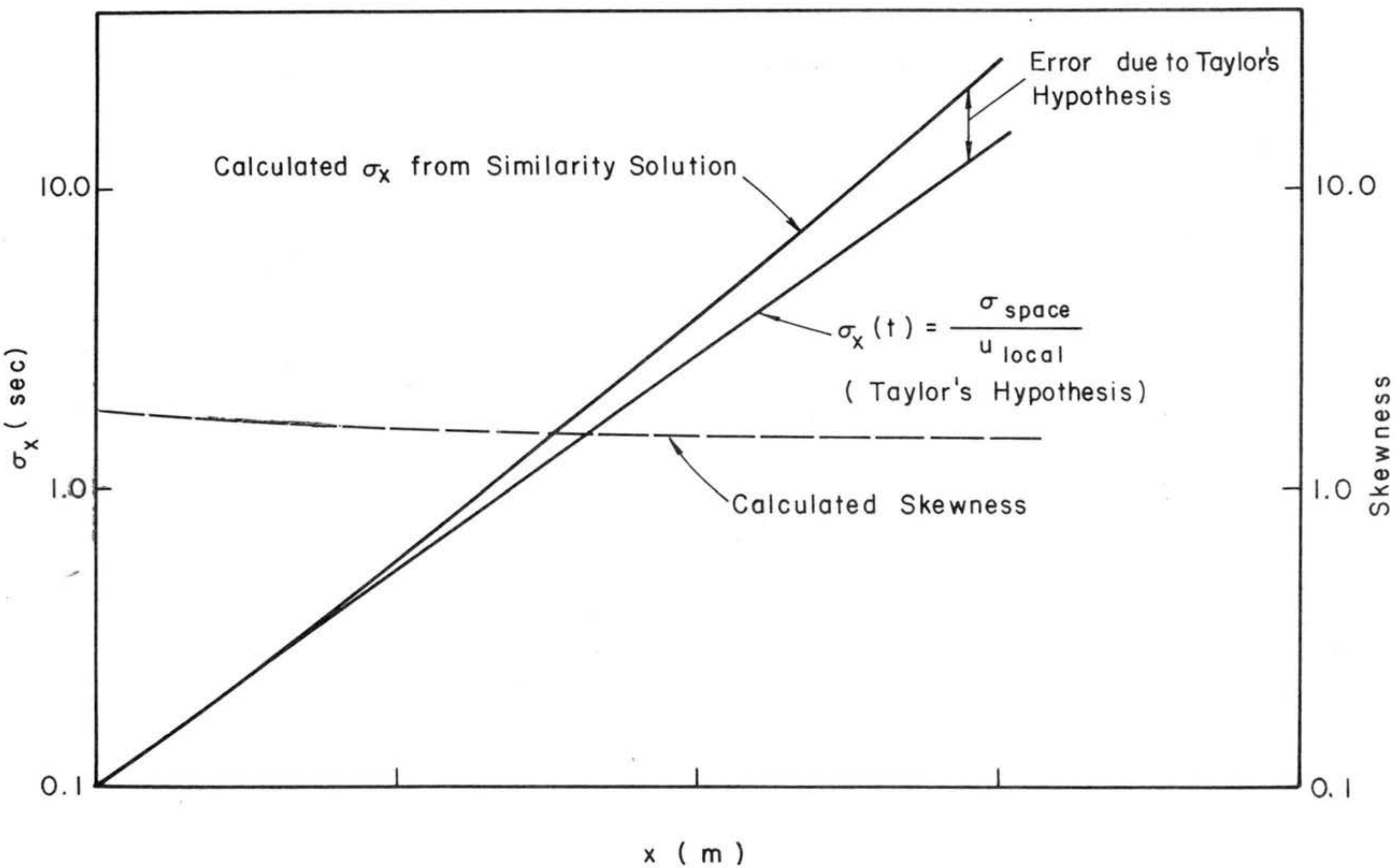

Fig. 9.17 The standard deviation in time domain and the errors due to Taylor's hypothesis.

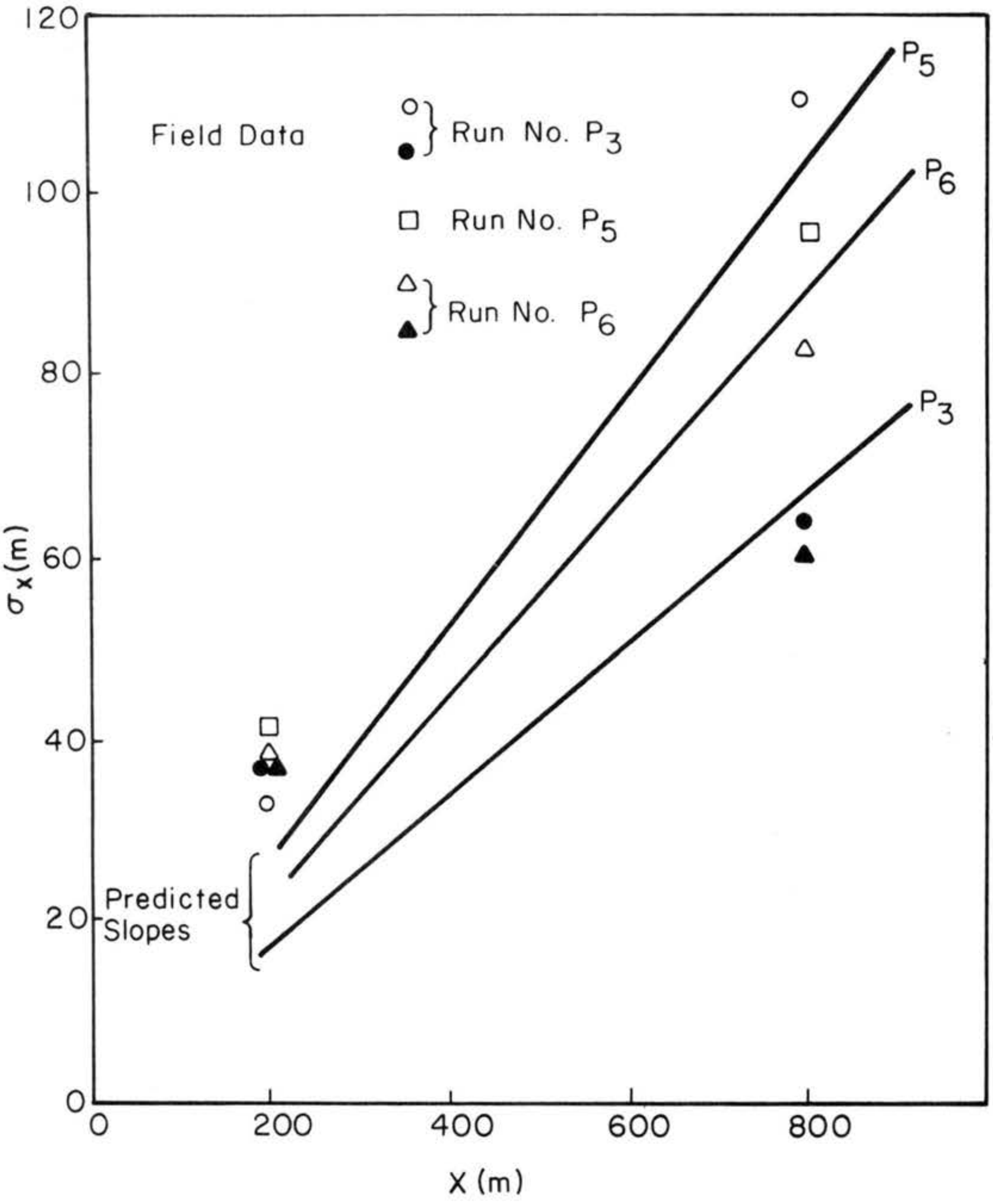

Fig. 9.18 Standard deviations of puffs in the spatial domain (field data; Nickola, 1970).

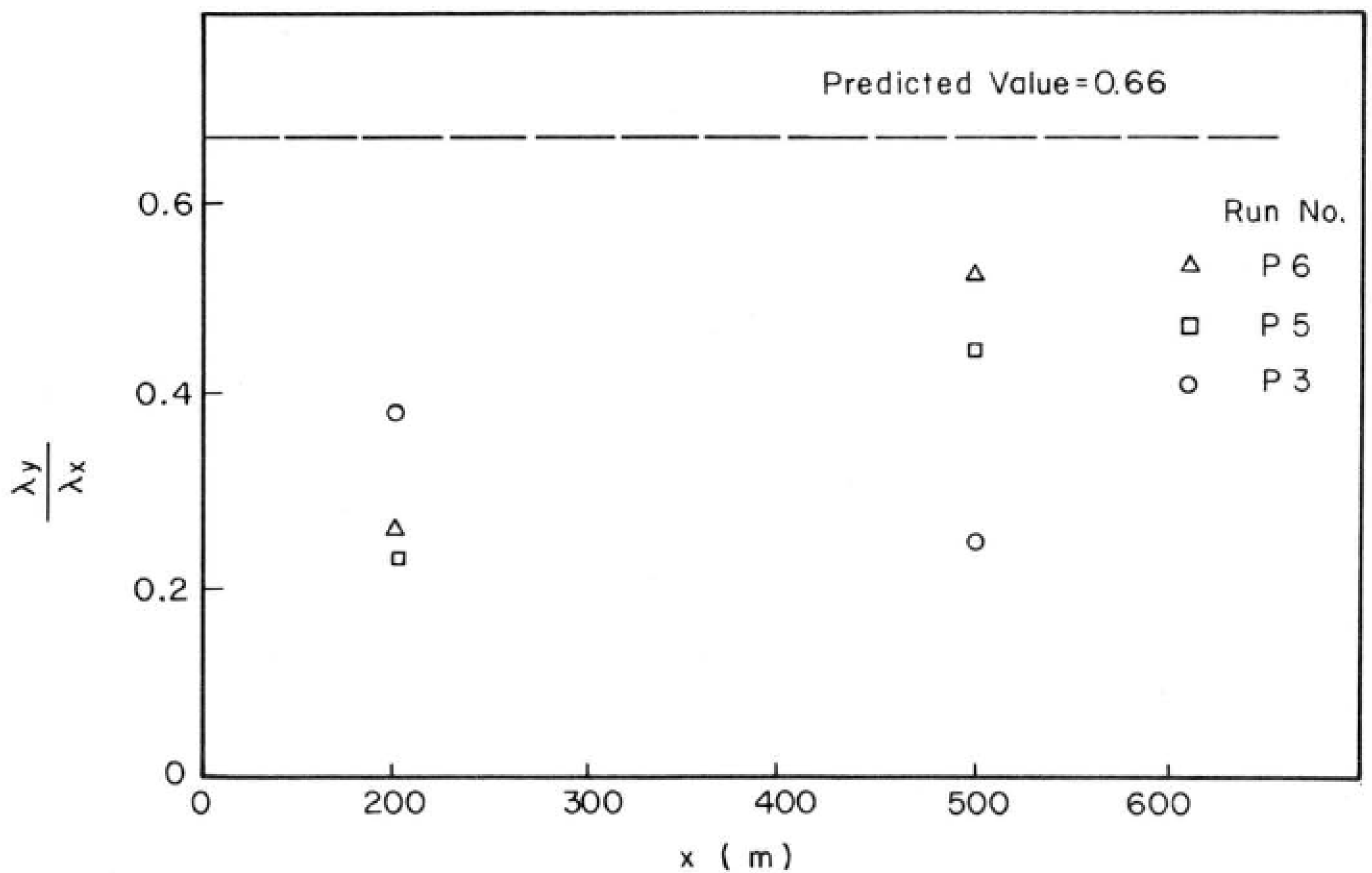

Fig. 9.19 Data of lateral to longitudinal puff widths (field data; Nickola, 1970).

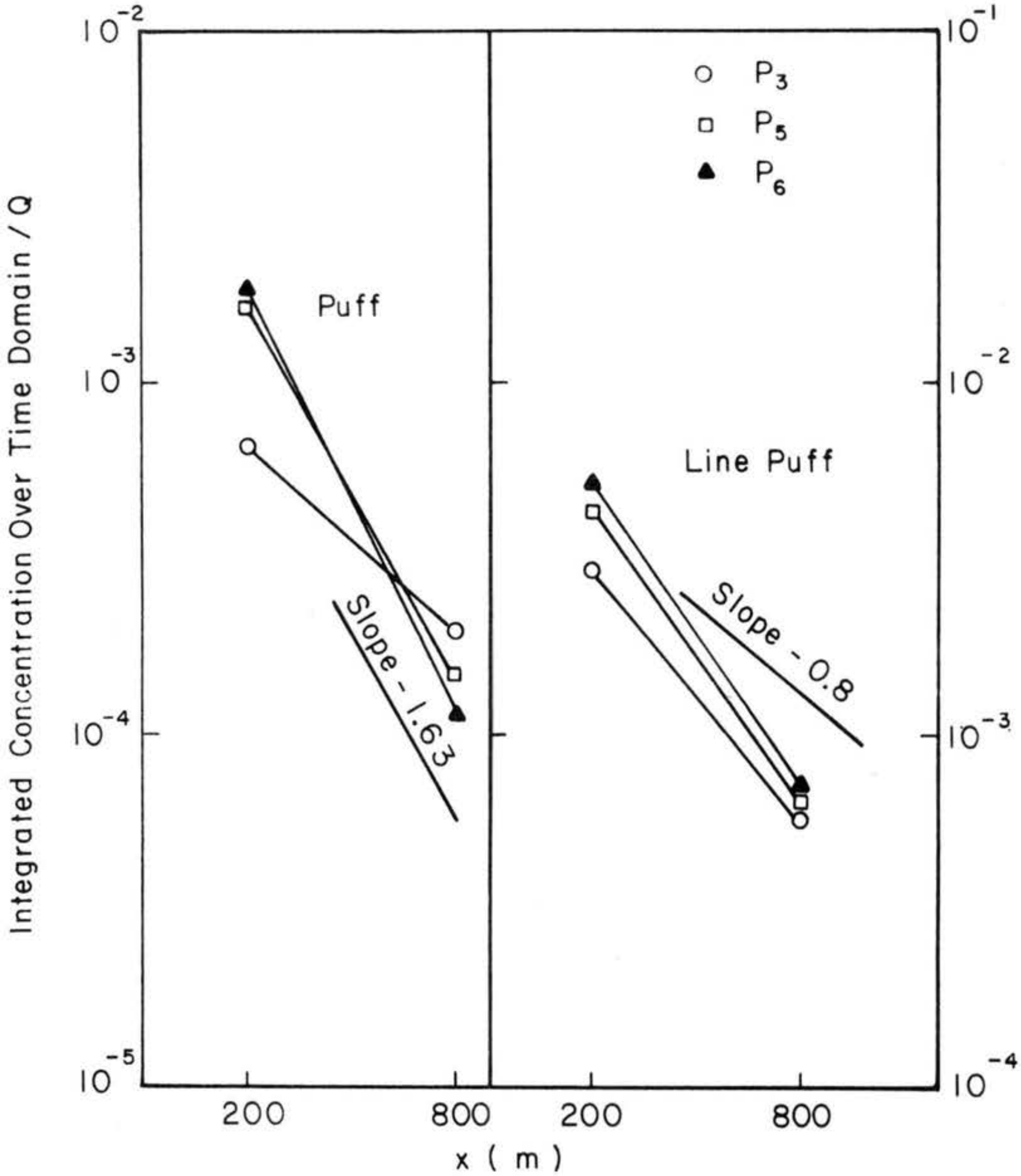

Fig. 9.20 Integrated concentration due to puffs (field data; Nickola, 1970).

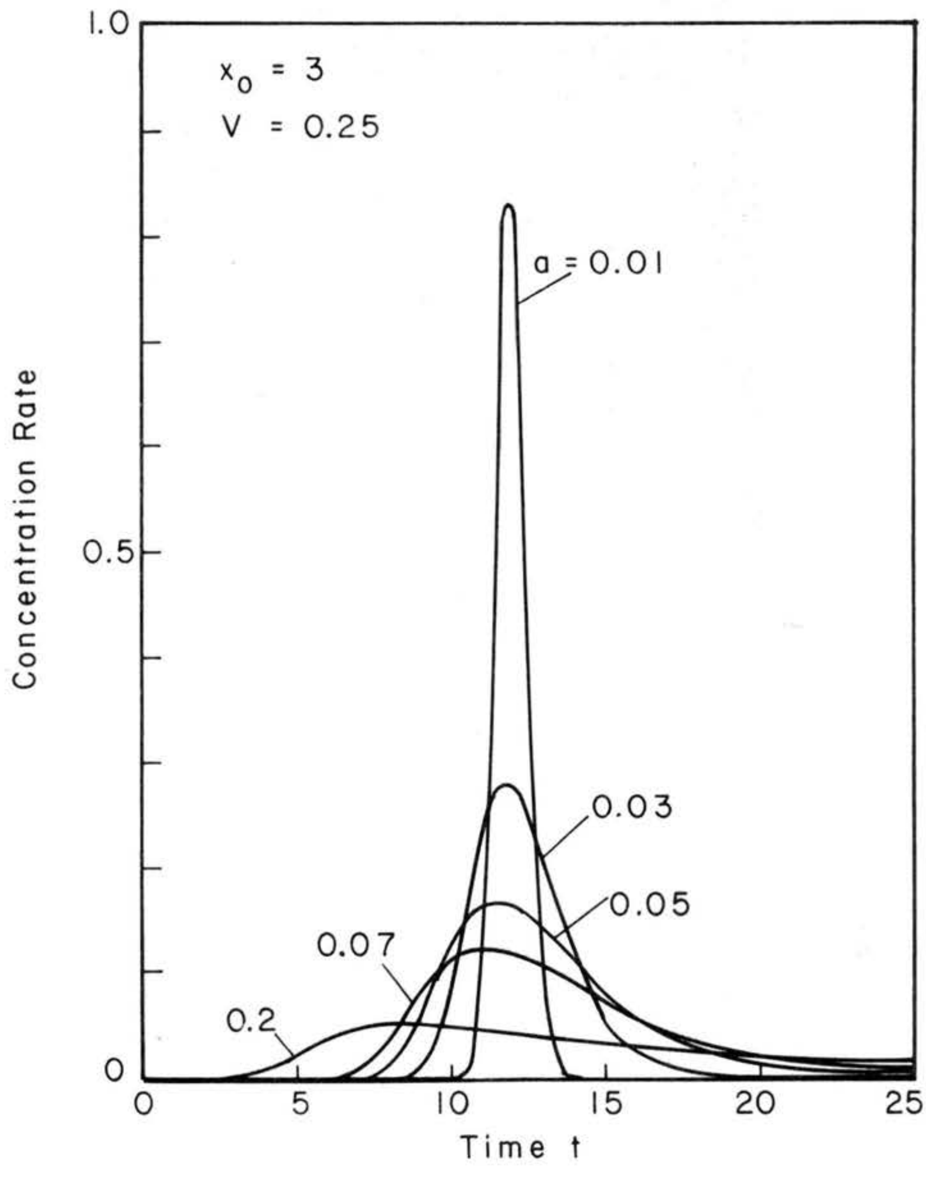

Fig. A.1 Comparison of Eulerian-Lagrangian distribution by using a simple analysis.

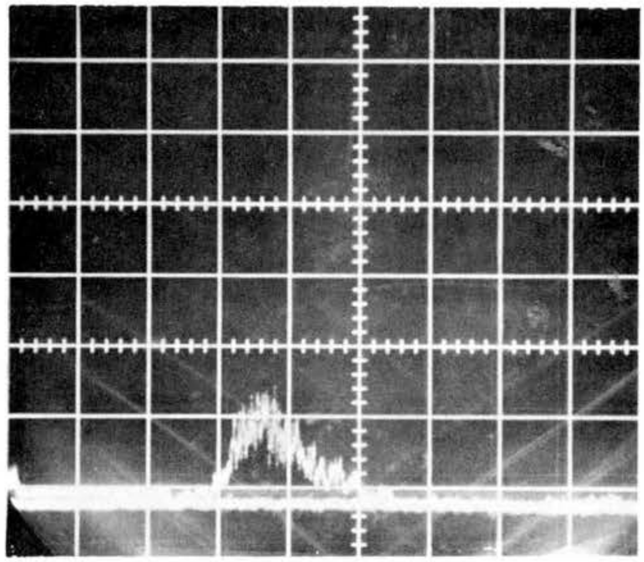

Fig. A.2 Oscillogram of typical output from a puff (x:1 sec/cm).

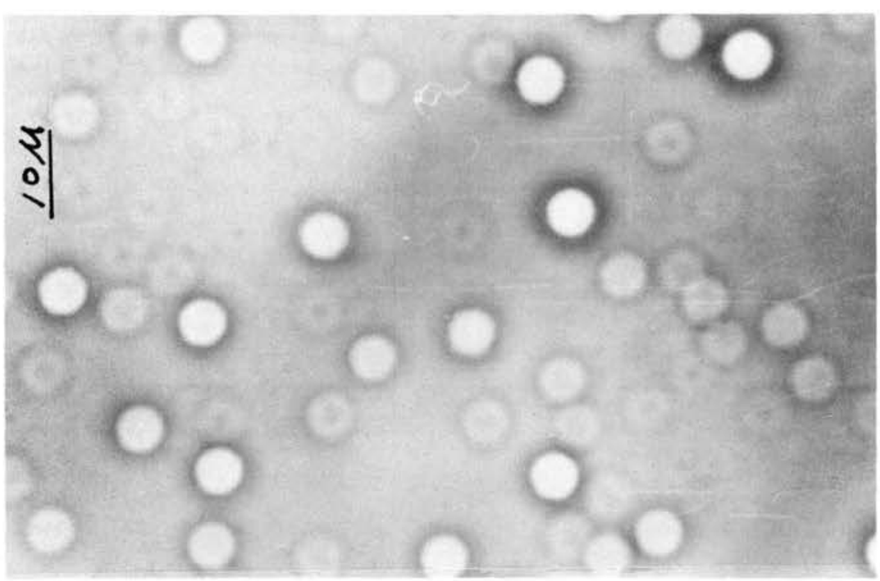

Fig. A.3 Aerosol particles under a photographic microscope.

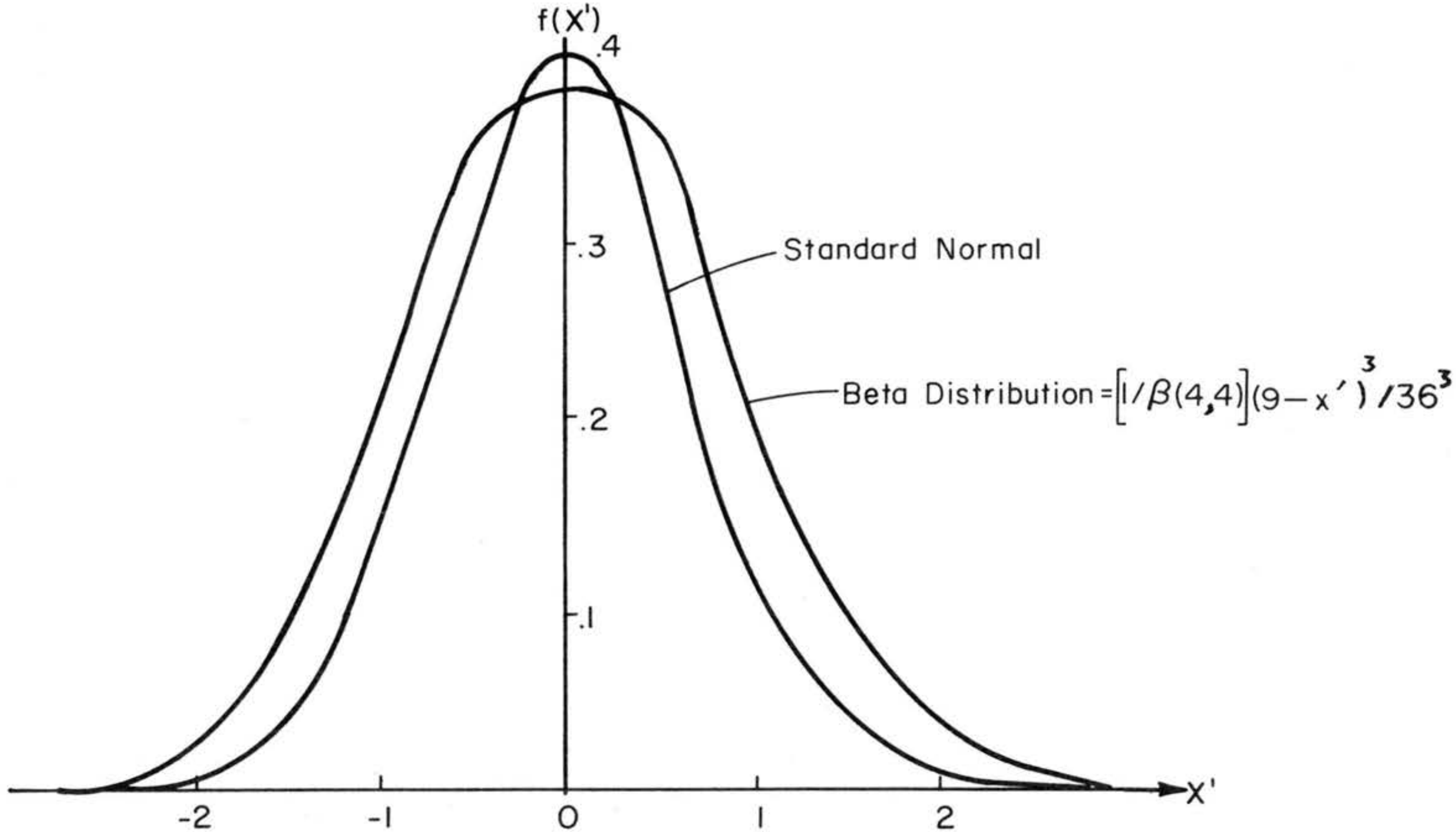

Fig. A.4 Plot of the Beta-distribution fitting to a standard normal.

Unclassified

Security Classification

DOCUMENT CONTROL DATA - R & D

(Security classification of title, body of abstract and indexing annotation must be entered when the overall report is classified)

1. ORIGINATING ACTIVITY (Corporate author) Fluid Dynamics & Diffusion Laboratory College of Engineering, Colorado State University Fort Collins, Colorado 80521	2a. REPORT SECURITY CLASSIFICATION Unclassified 2b. GROUP

3. REPORT TITLE

On Diffusion From an Instantaneous Point Source In a Neutrally Stratified Turbulent Boundary Layer with a Laser Light Scattering Probe

4. DESCRIPTIVE NOTES (Type of report and inclusive dates)

Technical Report

5. AUTHOR(S) (First name, middle initial, last name)

Yang, B. T. and Meroney, R. N.

6. REPORT DATE	7a. TOTAL NO. OF PAGES	7b. NO. OF REFS
October 1972	219	82

8a. CONTRACT OR GRANT NO. N00014-68-A-0493-0001 b. PROJECT NO.	9a. ORIGINATOR'S REPORT NUMBER(S) CER72-73BTY-RNM-17
c. d.	9b. OTHER REPORT NO(S) (Any other numbers that may be assigned this report) THEMIS Tech. Rpt. No. 20

10. DISTRIBUTION STATEMENT

Distribution of this report is unlimited.

11. SUPPLEMENTARY NOTES	12. SPONSORING MILITARY ACTIVITY U.S. Department of Defense Office of Naval Research

13. ABSTRACT

The behavior of an instantaneous point source, as it disperses in a thick, neutrally stratified, turbulent shear layer, has been examined by a laser light-scattering technique in the Meteorological Wind Tunnel. An aerosol-filled gas bubble was released in a column of water to subsequently rise and burst at the floor of the wind tunnel. This "pseudo-instantaneous" gas volume dispersed in the turbulent shear layer. Time dependent concentrations at a point were monitored by measuring the scattered light from a coherent light source by a photomultiplier-fiber optics probe. Data consisted of a series of concentration realizations downstream from the ground level source. The distribution of concentration was described by selecting coefficients empirically in a Gram-Charlier series. Puff dispersion characteristics were compared with prediction of the Lagrangian similarity diffusion theory.

Wind tunnel results were also compared with field dispersion studies conducted by Pacific Northwestern Laboratory at Hanford Reservation, Washington.

DD FORM 1 NOV 65 1473

Unclassified

Security Classification

Unclassified
Security Classification

14 KEY WORDS	LINK A		LINK B		LINK C	
	ROLE	WT	ROLE	WT	ROLE	WT
Instantaneous Point Source Lagrangian Similarity Hypothesis Gram-Charlier Series Inverse-Gamma Distribution Laser Light-Scattering Probe Zulerian-Lagrangian Relationship Arrival Times Turbulent Boundary Layer						

Unclassified
Security Classification

October 1972

DISTRIBUTION LIST FOR UNCLASSIFIED TECHNICAL REPORTS ISSUED UNDER
CONTRACT N00014-68-A-0493-0001 TASK 062-414

All addressees receive one copy unless otherwise specified

Defense Documentation Center
Cameron Station
Alexandria, Virginia 22314 (12 copies)

Technical Library
Naval Ship Research and
Development Laboratory
Annapolis, Maryland 21402

Professor Bruce Johnson
Engineering Department
Naval Academy
Annapolis, Maryland 21402

Library
Naval Academy
Annapolis, Maryland 21402

Professor W. P. Graebel
Department of Engineering Mechanics
College of Engineering
University of Michigan
Ann Arbor, Michigan 48108

Professor T. Francis Ogilvie
Department of Naval Architecture and
Marine Engineering
University of Michigan
Ann Arbor, Michigan 48108

Professor W. W. Willmarth
Department of Aerospace Engineering
University of Michigan
Ann Arbor, Michigan 48108

AFOSR (REM)
1400 Wilson Boulevard
Arlington, Virginia 22204

Professor S. Corrsin
Department of Mechanics and
Materials Science
The Johns Hopkins University
Baltimore, Maryland 21218

Professor R. B. Couch
Department of Naval Architecture
and Marine Engineering
The University of Michigan
Ann Arbor, Michigan 48105

Professor L. S. G. Kovasznay
Department of Mechanics and
Materials Science
The Johns Hopkins University
Baltimore, Maryland 21218

Professor O. M. Phillips
Department of Mechanics and
Materials Science
The Johns Hopkins University
Baltimore, Maryland 21218

Professor M. Holt
Department of Mechanical Engineering
University of California
Berkeley, California 94720

Professor E. V. Laitone
Department of Mechanical Engineering
University of California
Berkeley, California 94720

Librarian
Department of Naval Architecture
University of California
Berkeley, California 94720

Professor P. Lieber
Department of Mechanical Engineering
Institute of Engineering Research
Berkeley, California 94720

Professor J. R. Paulling
Institute of Engineering Research
Department of Naval Architecture
University of California
Berkeley, California 94720

Professor W. C. Webster
College of Engineering
Department of Naval Architecture
University of California
Berkeley, California 94720

Professor J. V. Wehausen
Institute of Engineering Research
Department of Naval Architecture
University of California
Berkeley, California 94720

Commander
Boston Naval Shipyard
Boston, Massachusetts 02129

Director
Office of Naval Research Branch
Office
495 Summer Street
Boston, Massachusetts 02210

Commander
Puget Sound Naval Shipyard
Bremerton, Washington 98314

Dr. Alfred Ritter
Cornell Aeronautical Laboratory, Inc.
P. O. Box 235
Buffalo, New York 14221

Professor G. Birkhoff
Department of Mathematics
Harvard University
Cambridge, Massachusetts 02138

Professor G. F. Carrier
Division of Engineering and
Applied Physics
Harvard University
Cambridge, Massachusetts 02139

Commanding Officer
NROTC Naval Administrative Unit
Massachusetts Institute of Technology
Cambridge, Massachusetts 02139

Professor M. A. Abkowitz
Department of Ocean Engineering
Massachusetts Institute of Technology
Cambridge, Massachusetts 02139

Professor A. T. Ippen
Department of Civil Engineering
Massachusetts Institute of Technology
Cambridge, Massachusetts 02139

Professor Phillip Mandel
Department of Ocean Engineering
Massachusetts Institute of Technology
Cambridge, Massachusetts 02139

Professor E. W. Merrill
Department of Chemical Engineering
Massachusetts Institute of Technology
Cambridge, Massachusetts 02139

Professor E. Mollo-Christensen
Department of Meteorology
Room 54-1722
Massachusetts Institute of Technology
Cambridge, Massachusetts 02139

Professor J. Nicholas Newman
Department of Ocean Engineering
Room 5-324A
Massachusetts Institute of Technology
Cambridge, Massachusetts 02139

Commander
Charleston Naval Shipyard
Naval Base
Charleston, South Carolina 29408

A. R. Kuhlthau, Director
Research Laboratories for the
Engineering Sciences
Thorton Hall, University of Virginia
Charlottesville, Virginia 22903

Director
Office of Naval Research Branch Office
536 South Clark Street
Chicago, Illinois 60605

Library
Naval Weapons Center
China Lake, California 93555

Professor R. V. Edwards
Division of Chemical Engineering
Case Western Reserve University
Cleveland, Ohio 44106

Professor J. M. Burgers
Institute of Fluid Dynamics and
Applied Mathematics
University of Maryland
College Park, Maryland 20742

Professor Pai
Institute of Fluid Dynamics and
Applied Mathematics
University of Maryland
College Park, Maryland 20742

Acquisition Director
NASA Scientific and Technical Information
P. O. Box 33
College Park, Maryland 20742

Technical Library
Naval Weapons Laboratory
Dahlgren, Virginia 22448

Computation and Analyses Laboratory
Naval Weapons Laboratory
Dahlgren, Virginia 22448

Dr. R. H. Kraichnan
Dublin, New Hampshire 03444

Commanding Officer
Army Research Office
Box CM, Duke Station
Durham, North Carolina 27706

Dr. Martin H. Bloom
Polytechnic Institute of Brooklyn
Long Island Graduate Center
Department of Aerospace Engineering and
Applied Mechanics
Farmingdale, New York 11735

Technical Documents Center
Building 315
U. S. Army Mobility Equipment Research and
Development Center
Fort Belvoir, Virginia 22060

Professor J. E. Cermak
Department of Atmospheric Sciences
Colorado State University
Fort Collins, Colorado 80521

Professor O. H. Shemdin
Coastal and Oceanographic Engineering
Department
University of Florida
Gainesville, Florida 32601

Technical Library
Webb Institute of Naval Architecture
Glen Cove, Long Island, New York 11542

Professor E. V. Lewis
Webb Institute of Naval Architecture
Glen Cove, Long Island, New York 11542

Dr. J. P. Breslin
Davidson Laboratory
Stevens Institute of Technology
Castle Point Station
Hoboken, New Jersey 07030

Mr. C. H. Henry
Stevens Institute of Technology
Davidson Laboratory
Castle Point Station
Hoboken, New Jersey 07030

Dr. D. Savitsky
Davidson Laboratory
Stevens Institute of Technology
Castle Point Station
Hoboken, New Jersey 07030

Dr. A. Strumpf
Davidson Laboratory
Stevens Institute of Technology
Castle Point Station
Hoboken, New Jersey 07030

Dr. J. P. Craven
University of Hawaii
1801 University Avenue
Honolulu, Hawaii 96822

Professor J. F. Kennedy, Director
Iowa Institute of Hydraulic Research
State University of Iowa
Iowa City, Iowa 52240

Professor L. Landweber
Iowa Institute of Hydraulic Research
State University of Iowa
Iowa City, Iowa 52240

Professor E. L. Resler
Graduate School of Aeronautical Engineering
Cornell University
Ithaca, New York 14851

Dr. Y. H. Pao
Flow Research, Inc.
1819 South Central Avenue
Suite 72
Kent, Washington 98031

Dr. D. E. Ordway
Sage Action, Incorporated
P. O. Box 416
Ithaca, New York 14850

Professor John Miles
c/o I.G.P.P.
University of California, San Diego
La Jolla, California 92038

Director
Scripps Institute of Oceanography
University of California
La Jolla, California 92037

Professor A. T. Ellis
University of California, San Diego
Department of Aerospace and
Mechanical Engineering Science
La Jolla, California 92037

Dr. Coda Pan
Mechanical Technology Incorporated
968 Albany-Shaker Road
Latham, New York 12110

Mr. P. Eisenberg, President
Hydronautics, Incorporated
8210 Pindell School Road
Laurel, Maryland 20810

Mr. M. P. Tulin
Hydronautics, Incorporated
8210 Pindell School Road
Laurel, Maryland 20810

Commander
Long Beach Naval Shipyard
Long Beach, California 90802

Professor John Laufer
Department of Aerospace Engineering
University Park
Los Angeles, California 90007

Dr. F. H. Harlow
University of California
Los Alamos Scientific Laboratory
P. O. Box 1663
Los Alamos, New Mexico 87544

Professor J. M. Killen
St. Anthony Falls Hydraulic Laboratory
University of Minnesota
Minneapolis, Minnesota 55414

Lorenz G. Straub Library
St. Anthony Falls Hydraulic Laboratory
University of Minnesota
Minneapolis, Minnesota 55414

Professor J. Ripkin
St. Anthony Falls Hydraulic Laboratory
University of Minnesota
Minneapolis, Minnesota 55414

Dr. E. Silberman
St. Anthony Falls Hydraulic Laboratory
University of Minnesota
Minneapolis, Minnesota 55414

Superintendent
Naval Postgraduate School
Attn: Library
Monterey, California 93940

Professor A. B. Metzner
Department of Chemical Engineering
University of Delaware
Newark, New Jersey 19711

Technical Library
Naval Underwater Systems Center
Newport, Rhode Island 02840

Office of Naval Research
New York Area Office
207 W. 24th Street
New York, New York 10011

Professor V. Castelli
Department of Mechanical Engineering
Columbia University
New York, New York 10027

Professor H. Elrod
Department of Mechanical Engineering
Columbia University
New York, New York 10027

Engineering Societies Library
345 E. 47th Street
New York, New York 10017

Professor J. J. Stoker
Institute of Mathematical Sciences
New York University
251 Mercer Street
New York, New York 10003

Society of Naval Architects and
Marine Engineers
74 Trinity Place
New York, New York 10006

Miss O. M. Leach, Librarian
National Research Council
Aeronautical Library
Montreal Road
Ottawa 7, Canada

Technical Library
Naval Coastal System Laboratory
Panama City, Florida 32401

Dr. J. W. Hoyt
Naval Undersea R & D Center
Pasadena Laboratory
3202 E. Foothill Boulevard
Pasadena, California 91107

Technical Library
Naval Undersea R & D Center
Pasadena Laboratory
3203 E. Foothill Boulevard
Pasadena, California 91107

Professor A. J. Acosta
Department of Mechanical Engineering
California Institute of Technology
Pasadena, California 91109

Professor H. Liepmann
Graduate Aeronautical Laboratory
California Institute of Technology
Pasadena, California 91109

Professor M. S. Plesset
Department of Engineering Science
California Institute of Technology
Pasadena, California 91109

Professor A. Roshko
California Institute of Technology
Graduate Aeronautical Laboratories
Pasadena, California 91109

Professor T. Y. Wu
Department of Engineering Science
California Institute of Technology
Pasadena, California 91109

Director
Office of Naval Research Branch Office
1030 E. Green Street
Pasadena, California 91106

Naval Ship Engineering Center
Philadelphia Division
Technical Library
Philadelphia, Pennsylvania 19112

Technical Library
Philadelphia Naval Shipyard
Philadelphia, Pennsylvania 19112

Professor R. C. MacCamy
Department of Mathematics
Carnegie Institute of Technology
Pittsburgh, Pennsylvania 15213

Dr. Paul Kaplan
Oceanics, Inc.
Technical Industrial Park
Plainview, New York 11803

Technical Library
Naval Missile Center
Point Mugu, California 93441

Technical Library
Naval Civil Engineering Laboratory
Port Hueneme, California 93041

Commander
Norfolk Naval Shipyard
Portsmouth, Virginia 23709

Dr. H. N. Abramson
Southwest Research Institute
8500 Culebra Road
San Antonio, Texas 78228

Editor
Applied Mechanics Review
Southwest Research Institute
8500 Culebra Road
San Antonio, Texas 78206

Dr. Andrew Fabula
Code 600, Building 106
Naval Undersea R & D Center
San Diego, California 92132

Office of Naval Research
San Francisco Area Office
760 Market Street, Room 447
San Francisco, California 94102

Library
Pearl Harbor Naval Shipyard
Box 400, FPO
San Francisco, California 96610

Technical Library
Hunters Point Naval Shipyard
San Francisco, California 94135

Librarian
Naval Ordnance Laboratory
White Oak
Silver Spring, Maryland 20910

Mr. J. Enig
Room 3-252
Naval Ordnance Laboratory
White Oak
Silver Spring, Maryland 20910

Fenton Kennedy Document Library
The Johns Hopkins University
Applied Physics Laboratory
8621 Georgia Avenue
Silver Spring, Maryland 20910

Professor E. Y. Hsu
Department of Civil Engineering
Stanford University
Stanford, California 94305

Dr. Byrne Perry
Department of Civil Engineering
Stanford University
Stanford, California 94305

Dr. R. L. Street
Department of Civil Engineering
Stanford University
Stanford, California 94305

Professor R. C. Di Prima
Department of Mathematics
Rensselaer Polytechnic Institute
Troy, New York 12181

Professor J. Lumley
Department of Aerospace Engineering
Pennsylvania State University
University Park, Pennsylvania 16802

Dr. J. M. Robertson
Department of Theoretical and
Applied Mechanics
University of Illinois
Urbana, Illinois 61803

Technical Library
Mare Island Naval Shipyard
Vallejo, California 94592

Code 438
Office of Naval Research
Department of the Navy
Arlington, Virginia 22217 (3 copies)

Code 461
Office of Naval Research
Department of the Navy
Arlington, Virginia 22217

Code 463
Office of Naval Research
Department of the Navy
Arlington, Virginia 22217

Code 466
Office of Naval Research
Department of the Navy
Arlington, Virginia 22217

Code 468
Office of Naval Research
Department of the Navy
Arlington, Virginia 22217

Code 473
Office of Naval Research
Department of the Navy
Arlington, Virginia 22217

Code 481
Office of Naval Research
Department of the Navy
Arlington, Virginia 22217

Code 2627
Naval Research Laboratory
Washington, D. C. 20390 (6 copies)

Library, Code 2629 (ONRL)
Naval Research Laboratory
Washington, D. C. 20390 (6 copies)

Code 6170
Naval Research Laboratory
Washington, D. C. 20390

Code 4000
Director of Research
Naval Research Laboratory
Washington, D. C. 20390

Code 8030 (Maury Center)
Naval Research Laboratory
Washington, D. C. 20390

Code 8040
Naval Research Laboratory
Washington, D. C. 20390

Code 031
Naval Ship Systems Command
Washington, D. C. 20360

Code 0341
Naval Ship Systems Command
Washington, D. C. 20360

Code 0322 (L. Benen)
Naval Ship Systems Command
Washington, D. C. 20360

Code 0321 (J. Schuler)
Naval Ship Systems Command
Washington, D. C. 20360

Code 2052
Naval Ship Systems Command
Washington, D. C. 20360

Code 6034
Naval Ship Engineering Center
Center Building
Prince George's Center
Hyattsville, Maryland 20782

Code 6101E
Naval Ship Engineering Center
Center Building
Prince George's Center
Hyattsville, Maryland 20782

Code 6110
Naval Ship Engineering Center
Center Building
Prince George's Center
Hyattsville, Maryland 20782

Code 6114
Naval Ship Engineering Center
Center Building
Prince George's Center
Hyattsville, Maryland 20782

Code 6120E
Naval Ship Engineering Center
Center Building
Prince George's Center
Hyattsville, Maryland 20782

Code 6136
Naval Ship Engineering Center
Center Building
Prince George's Center
Hyattsville, Maryland 20782

Dr. A. Powell (Code 01)
Naval Ship Research & Development Center
Bethesda, Maryland 20034

Mr. W. M. Ellsworth (Code 11)
Naval Ship Research & Development Center
Bethesda, Maryland 20034

Dr. W. E. Cummins (Code 15)
Naval Ship Research & Development Center
Bethesda, Maryland 20034

Dr. H. R. Chaplin (Code 16)
Naval Ship Research & Development Center
Bethesda, Maryland 20034

Mr. G. H. Gleissner (Code 18)
Naval Ship Research & Development Center
Bethesda, Maryland 20034

Mr. R. Wermter (Code 152)
Naval Ship Research & Development Center
Bethesda, Maryland 20034

Dr. W. B. Morgan (Code 154)
Naval Ship Research & Development Center
Bethesda, Maryland 20034

Mr. J. B. Hadler (Code 156)
Naval Ship Research & Development Center
Bethesda, Maryland 20034

Library (Code 5641)
Naval Ship Research & Development Center
Bethesda, Maryland 20034

Mr. S. F. Crump (Code 1505)
Naval Ship Research & Development Center
Bethesda, Maryland 20034

Dr. P. Pien (Code 1521)
Naval Ship Research & Development Center
Bethesda, Maryland 20034

Mr. Paul Granville (Code 1541)
Naval Ship Research & Development Center
Bethesda, Maryland 20034

Mr. J. McCarthy (Code 1552)
Naval Ship Research & Development Center
Bethesda, Maryland 20034

Dr. Nils Salvesen (Code 1552)
Naval Ship Research & Development Center
Bethesda, Maryland 20034

Dr. M. Strasberg (Code 1901)
Naval Ship Research & Development Center
Bethesda, Maryland 20034

Code 03
Naval Air Systems Command
Department of the Navy
Washington, D. C. 20360

AIR 5301
Naval Air Systems Command
Department of the Navy
Washington, D. C. 20360

AIR 604
Naval Air Systems Command
Department of the Navy
Washington, D. C. 20360

Code ORD 03
Naval Ordnance Systems Command
Department of the Navy
Washington, D. C. 20360

Code ORD 035
Naval Ordnance Systems Command
Department of the Navy
Washington, D. C. 20360

Code ORD 05413
Naval Ordnance Systems Command
Department of the Navy
Washington, D. C. 20360

Code ORD 9132
Naval Ordnance Systems Command
Department of the Navy
Washington, D. C. 20360

CNM PM-1
Strategic Systems Project Office
Department of the Navy
Washington, D. C. 20360

Technical Division (CNM PM 11-20)
Deep Submergence Systems Project Office
Department of the Navy
Washington, D. C. 20360

Oceanographer of the Navy
Washington, D. C. 20390

Commander
Naval Oceanographic Office
Washington, D. C. 20390

Dr. A. L. Slafkosky
Scientific Advisor
Commandant of the Marine Corps (CODE AX)
Washington, D. C. 20380

Librarian Station 5-2
Coast Guard Headquarters
NASSIF Building
400 7th Street, S.W.
Washington, D. C. 20591

Office of Research and Development
Maritime Administration
441 G Street, N.W.
Washington, D. C. 20235

Division of Ship Design
Maritime Administration
441 G Street, N.W.
Washington, D. C. 20235

National Science Foundation
Engineering Division
1800 G Street, N.W.
Washington, D. C. 20550

Dr. G. Kulin
National Bureau of Standards
Washington, D. C. 20234

Science & Technology Division
Library of Congress
Washington, D. C. 20540

Chief of Research & Development
Office of Chief of Staff
Department of the Army
Washington, D. C. 20310

Professor A. Thiruvengadam
Department of Mechanical Engineering
The Catholic University of America
Washington, D. C. 20017

Dr. A. S. Iberall, President
General Technical Services, Inc.
451 Penn Street
Yeadon, Pennsylvania 19050

Commander
Portsmouth Naval Shipyard
Portsmouth, New Hampshire 03801